JOURNAL OF RESEARCH

OF THE U.S. GEOLOGICAL SURVEY

MAY–JUNE 1973
VOLUME 1, NUMBER 3

Scientific notes and summaries of investigations in geology, hydrology, and related fields

U.S. DEPARTMENT OF THE INTERIOR

UNITED STATES DEPARTMENT OF THE INTERIOR
ROGERS C. B. MORTON, Secretary
GEOLOGICAL SURVEY
V. E. McKelvey, Director

For sale by the Superintendent of Documents, U.S. Government Printing Office, Washington, D.C., 20402. Order by SD Catalog No. JRGS. Annual subscription rate $8.50 (plus $2.25 for foreign mailing). Single copy $1.50. Prices valid until July 1, 1973, at which time a price increase is scheduled. Make checks or money orders payable to the Superintendent of Documents.

Send all subscription inquiries and address changes to the Superintendent of Documents at the above address.

Purchase orders should not be sent to the U.S. Geological Survey library.

Library of Congress Card No. 72-600241

The Journal of Research consists of six issues a year (January-February, March-April, May-June, July-August, September-October, November-December) published in Washington, D.C., by the U.S. Geological Survey. It contains papers by members of the Geological Survey on geologic, hydrologic, topographic, and other scientific and technical subjects.

The Journal supersedes the short-papers chapters (B, C, and D) of the former Geological Survey Research ("Annual Review") series of professional papers. The synopsis chapter (A) of the former Geological Survey Research series will be published as a separate professional paper each year.

Correspondence and inquiries concerning the Journal (other than subscription inquiries and address changes) should be directed to the Managing Editor, Journal of Research, Publications Division, U.S. Geological Survey, Washington, D.C., 20244.

Papers for the Journal should be submitted through regular Division publication channels.

The Secretary of the Interior has determined that the publication of this periodical is necessary in the transaction of the public business required by law of this Department. Use of funds for printing this periodical has been approved by the Director of the Office of Management and Budget through February 11, 1975.

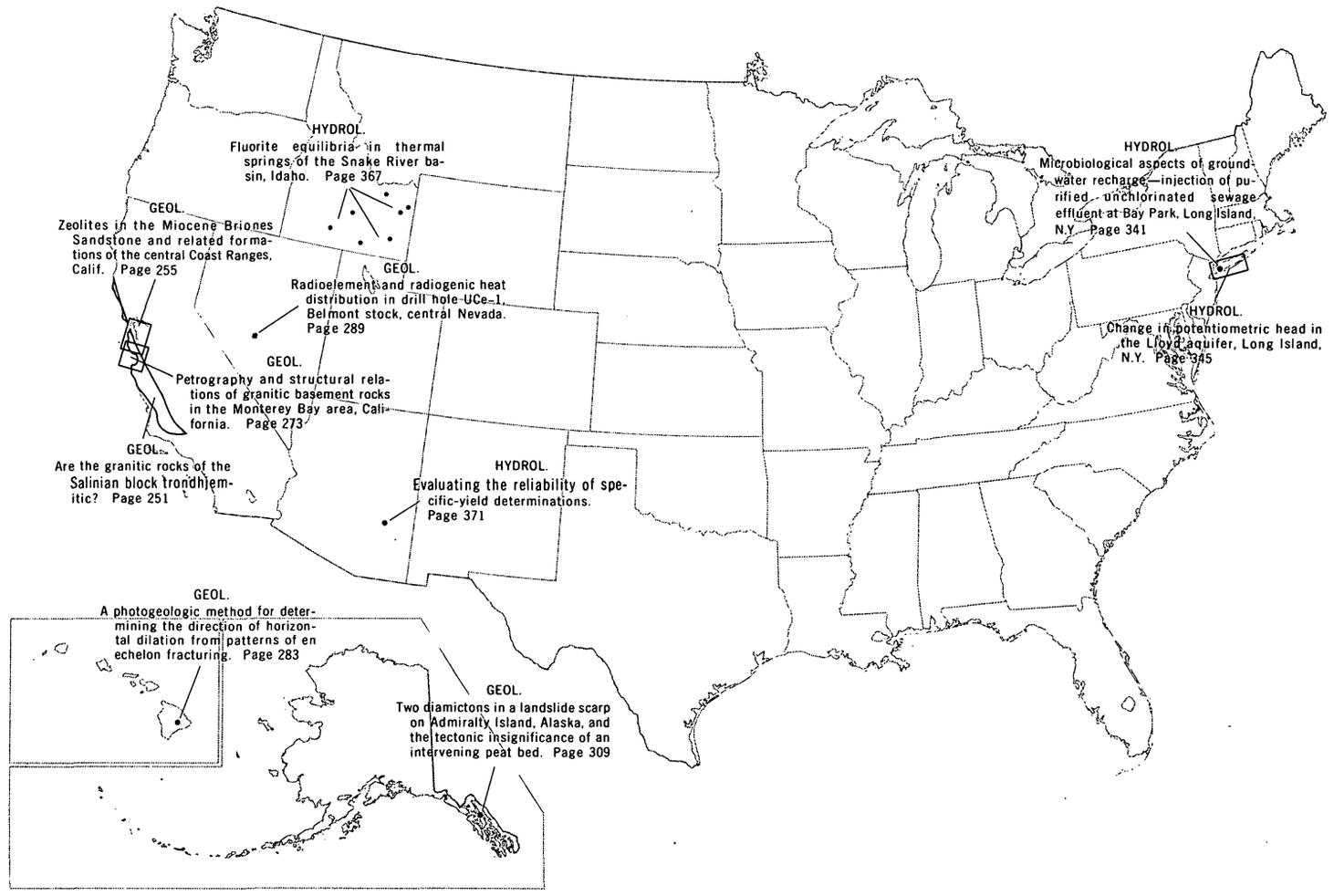

GEOGRAPHIC INDEX TO ARTICLES

[See Contents for articles concerning areas outside the United States and articles without geographic orientation]

JOURNAL OF RESEARCH

of the

U.S. Geological Survey

Vol. 1 No. 3 May-June 1973

CONTENTS

ABBREVIATIONS AND SYMBOLS

[Singular and plural forms for abbreviations of units of measure are the same]

A ..... angstrom units
A^3 ..... cubic angstroms
a-c ..... alternating current
amp ..... amperes
atm ..... atmospheres
B.P. ..... Before Present
b.y. ..... billion years
c ..... crystalline state
C_x ..... molal concentration (of substance x)
cal ..... calories
cfs ..... cubic feet per second
Ci ..... Curies
cm ..... centimeters
cm^2 ..... square centimeters
cm^3 ..... cubic centimeters
cpm ..... counts per minute
cu ft ..... cubic feet
cu mi ..... cubic miles
d-c ..... direct current
eV ..... electron volts
emu ..... electromagnetic units
ft ..... feet
g ..... grams
gal ..... gallons
gpd ..... gallons per day
gpm ..... gallons per minute
hr ..... hours
in. ..... inches
kb ..... kilobars
kg ..... kilograms
km ..... kilometers
km^2 ..... square kilometers
km^3 ..... cubic kilometers
kV ..... kilovolts
l ..... liters
lb ..... pounds
m ..... meters
m ..... molal (concentration)
m^2 ..... square meters
m^3 ..... cubic meters
M ..... molar (concentration)
me ..... milliequivalents
MeV ..... million electron volts
mg ..... milligrams
mgd ..... million gallons per day
min ..... minutes
ml ..... milliliters
mm ..... millimeters
mol ..... moles
mr ..... milliroentgens
mV ..... millivolts
m.y. ..... million years
μ ..... microns
μm ..... micrometers
μmho ..... micromhos
n ..... neutrons
N ..... normal
ng ..... nanograms
nm ..... nanometers
Oe ..... oersteds
pCi ..... picocuries
pH ..... pH (measure of hydrogen ion activity)
ppb ..... parts per billion
ppm ..... parts per million
rad ..... radiometric
rpm ..... revolutions per minute
sec ..... seconds
sq ft ..... square feet
sq mi ..... square miles
yr ..... years

Jour. Research U.S. Geol. Survey
Vol. 1, No. 3, May-June 1973, p. 251—254

ARE THE GRANITIC ROCKS OF THE SALINIAN BLOCK TRONDHJEMITIC?

By DONALD C. ROSS, Menlo Park, Calif.

Abstract.—Trondhjemitic rocks are relatively abundant in the granitic terranes of the western Sierra Nevada and the Klamath Mountains but have not been found in the granitic plutons of the Salinian block, which lies westward, across the San Andreas fault. A ternary plot of modal quartz : K-feldspar : plagioclase from more than 200 granitic samples from the Salinian block has an elongate, nearly horizontal, quartz-rich trend that appears trondhjemitic to some observers. However, petrographic and chemical comparison of these rocks with trondhjemite from the type area in Norway and with rocks called trondhjemite in the Western United States shows that the granitic rocks of the Salinian block are not trondhjemitic. The absence of trondhjemite in the Salinian block further supports the contention that this terrane is not merely a westward continuation of Sierran basement but is a displaced basement block.

Trondhjemite has been identified from various localities in the nearest granitic terranes east and north of the Salinian block of the California Coast Ranges (fig. 1)—the western Sierra Nevada (Turner, 1894; Hietanen, 1951; Larsen and Poldervaart, 1961; Olmsted, 1971; and L. D. Clark, written commun., 1972) and the Klamath Mountains (Davis, 1963; Lipman, 1963; and Hotz, 1971). Trondhjemite has also been described to the west of the Salinian block where it is associated with gabbroic intrusions in an oceanic crust sequence (Page, 1972). Recently, a reference has been made to a "hornblende-biotite trondhjemite" in the Salinian block near Point Reyes (Mattinson and others, 1971). In a rather widespread study of granitic outcrops in the Salinian block I have identified no trondhjemites. Nevertheless, a ternary plot of modal quartz : K-feldspar : plagioclase of more than 200 samples from this study (fig. 2) has an elongate, nearly horizontal, quartz-rich trend which some colleagues suggest is trondhjemitic.

In view of the possibly erroneous conclusion that can be drawn from the trend on the modal plot of the granitic rocks of the Salinian block, it seems worthwhile at this time to compare these Salinian rocks with trondhjemite as originally defined and currently used.

The term "trondhjemite" was first applied by Goldschmidt (1916) to quartz-rich tonalites from the Trondhjem (Trondheim) area of Norway. Johannsen (1932) translated Goldschmidt's definition of trondhjemite as:

> leucocratic acid plutonic rocks, whose essential constituents are soda-rich plagioclase (oligoclase or andesine) and quartz. Potash-feldspar is entirely wanting or is present only in subordinate amounts. Biotite is the most important of the mafic constituents, although it is present in small quantity. Muscovite is often present * * *.

Current usage of the term "trondhjemite" seems to correspond fairly well to the original definition. For example, Williams, Turner, and Gilbert (1955) stated that trondhjemite is "essentially an oligoclase-biotite-quartz diorite." Five representative trondhjemite modes of Goldschmidt (1916, 1921) are shown in figure 3; plagioclase is oligoclase in four specimens and andesine in the fifth. These rocks have about the same quartz content as many rocks that are now called trondhjemites. In contrast, rocks called trondhjemites from the Western United States (Klamath Mountains, western Sierra Nevada, Idaho) contain considerably more K-feldspar than those of the type area, and some have several percent of hornblende (fig. 3). Davis (1963, p. 343) has described some trondhjemites whose average plagioclase is more calcic than An_{30}, for which he suggested the name "calcic trondhjemite." These variations notwithstanding, oligoclase-biotite quartz diorite appears to describe trondhjemite generally, as commonly used in the Western United States.

The modes of numerous granitic rocks of the Salinian block determined by Ross (1972a) are plotted on figure 2. Modes of rocks chemically analyzed are identified separately, and their distribution on the diagram shows them to be representative of the entire compositional range. Geographically, the samples range from Bodega Head on the north to the La Panza Range on the south.

Feldspar-quartz ternary modal plots, such as figures 2 and 3, which indicate neither the anorthite content of the plagioclase nor the kind and amount of dark minerals, will not by themselves distinguish trondhjemites from quartz-rich tonalites. More diagnostic are chemical characteristics, such as the ratio K_2O:Na_2O:CaO, or the somewhat comparable ratio of normative Or:Ab:An shown in figures 4 and 5, respectively. On these figures, it is evident that the granitic rocks of the Salinian block are markedly different from trondhjemites. The

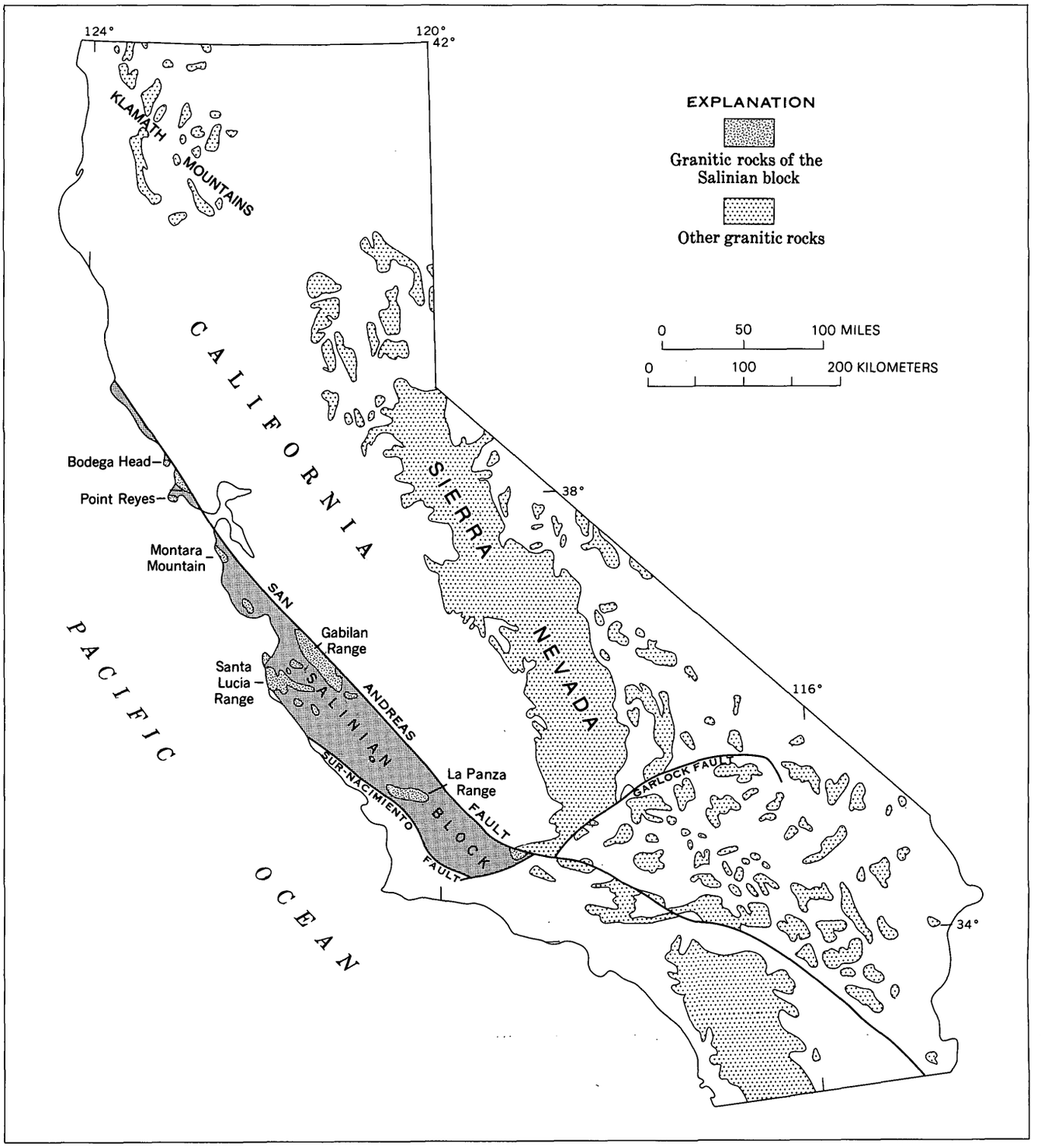

Figure 1.—Index map of Salinian block localities, California.

trondhjemite fields lie significantly closer to the Na_2O and Ab corners than the specimens from the Salinian block do.

Only one mass from the Salinian block, a gneissic quartz diorite from the southern part of the Gabilan Range (gneissic quartz diorite of Stonewall Canyon, Ross, 1972b), plots near the trondhjemite field. No chemical analyses were available from this mass, but chemical analyses were calculated from seven modes and estimated compositions of constituent minerals. These rocks contain 35 to 60 percent plagioclase (intermediate andesine), 25 to 45 percent quartz, 10 to 20 percent

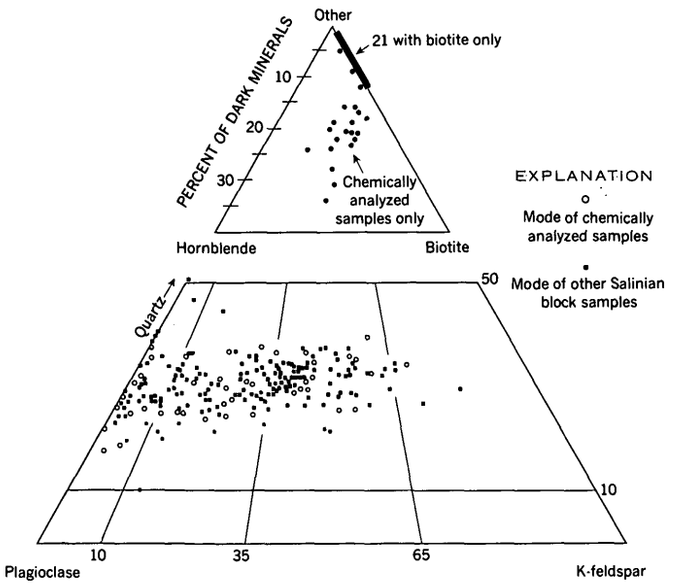

Figure 2.—Modes of granitic samples, Salinian block, California.

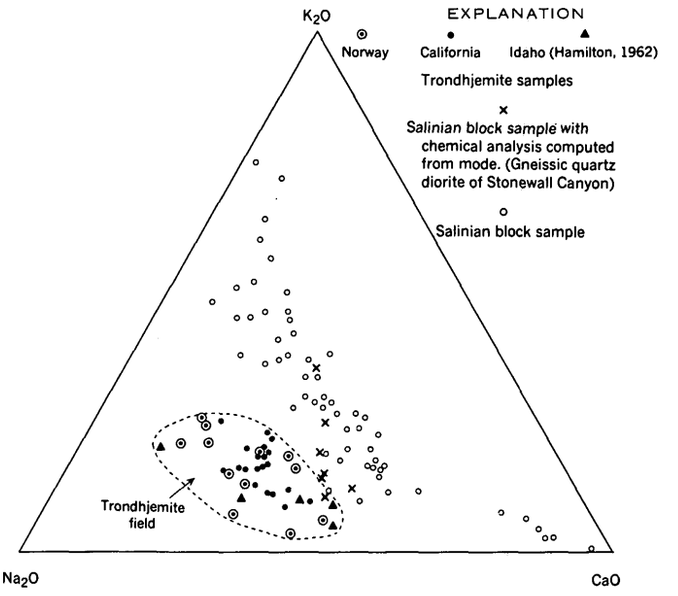

Figure 4.—Ternary K_2O – Na_2O – CaO diagram comparing trondhjemites with chemically analyzed samples from the Salinian block.

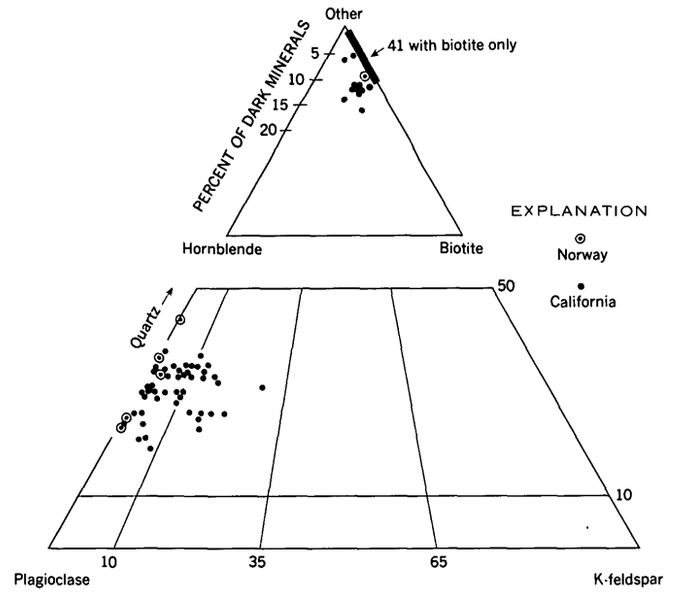

Figure 3.—Modal data on trondhjemites from California and Norway.

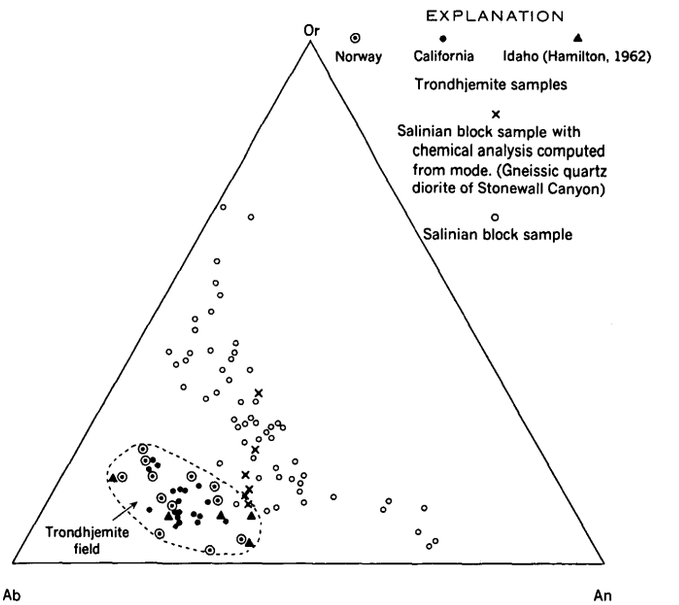

Figure 5.—Ternary diagram of normative Or–Ab–An comparing trondhjemites with chemically analyzed samples from the Salinian block.

biotite, 0 to 11 percent K-feldspar (3 percent or less in all but one specimen), and traces of hornblende and accessory minerals. Though these rocks have some of the modal character of a trondhjemite, the plagioclase, about An_{40}, seems too calcic. Also, this mass may possibly be an ultrametamorphosed metasedimentary rock that looks similar to a normal intrusive rock. Abundant gneiss, schist, and calc-hornfels are associated and mixed with the more homogeneous granitoid samples. The percentage of quartz (three samples have 40, 41, and 44 percent, respectively) is also somewhat high for a "normal" granitic rock.

One specimen from the granitic mass of Montara Mountain also plots on the edge of the trondhjemite field. This rock is strongly sheared and extensively saussuritized, which could explain why it differs from the general trend of the Salinian granitic rocks. With these exceptions, the Salinian block granitic rocks that have been analyzed are chemically distinct from analyzed trondhjemites.

The average of 37 trondhjemite analyses used in figures 4 and 5 is 3.2 percent CaO, 5.0 percent Na_2O, and 1.5 percent

K_2O. The comparable average for the normative feldspar constituents is "or," 7.5; "ab," 43.5; and "an," 15.6. The SiO_2 ranges from 66 to 76 percent and averages 70.7 percent, so that as a class, these are rather silicic rocks. In contrast, the five specimens from the gneissic body in the southern Gabilan Range that are closest to the trondhjemite field average 4.2 percent CaO, 3.8 percent Na_2O, and 1.3 percent K_2O and have normative "or" = 13, "ab" = 53, and "an" = 34; they are considerably different from trondhjemites. The saussuritized sample from Montara Mountain has almost the same K_2O, Na_2O, and CaO contents as the average for the gneissic mass from the Gabilan Range.

In conclusion, both petrographically and chemically, the granitic rocks of the Salinian block that I have studied are not trondhjemitic. It is possible that some individual specimens might qualify as "calcic trondhjemite" because they are intermediate andesine-bearing quartz diorite with biotite as their only dark mineral. However, these are all local variations from "normal" hornblende-bearing quartz diorites; in other words, none of the granitic masses in the Salinian block that have been studied are trondhjemites. Although not all the granitic masses in the Santa Lucia Range have been studied, where granitic rocks have been mapped by Compton (1966), Pearson, Hayes, and Fillo (1967), and Wiebe (1970), no trondhjemite has been noted.

The granitic terranes that are the closest to the Salinian block on the north and east, the Klamath Mountains and the western Sierra Nevada, contain significant amounts of trondhjemite. The contrasting absence of trondhjemite in the Salinian block seems to suggest that this block is not a westward continuation of the Sierran basement that has merely been differentially uplifted to expose the granitic terrane. Ross (1972a) has already suggested that the chemical character of the granitic rocks of the Salinian block does not seem to be a logical projection of the east-west chemical trends across the central Sierra Nevada, as reported by Bateman and Dodge (1970). The absence of trondhjemite in the Salinian block reinforces this chemical contrast and supports the suggestion that the Salinian block has been laterally transported to its present position.

REFERENCES CITED

Bateman, P. C., and Dodge, F. C. W., 1970, Variations of major chemical constituents across the central Sierra Nevada batholith: Geol. Soc. America Bull., v. 81, p. 409–420.

Compton, R. R., 1966, Granitic and metamorphic rocks of the Salinian block, California Coast Ranges: California Div. Mines and Geology Bull. 190, p. 277–287.

Davis, G. A., 1963, Structure and mode of emplacement of Caribou Mountain pluton, Klamath Mountains, California: Geol. Soc. America Bull., v. 74, p. 331–348.

Goldschmidt, V. M., 1916, Geologisch–petrographische studien im Hochgebirges des Südlichen Norwegens; IV, übersicht der Eruptivegesteine in Kaledonischen Gebirge zwischen Stavanger und Trondhjem: Vidensk. Selsk. Skr., Kristiana, no. 2, 140 p.

—— 1921, Geologisch–petrographische Studien im Hochgebirge des Südlichen Norwegens, V, die Injectionsmetamorphose im Stavanger–Gebiete: Vidensk. Selsk. Skr., Kristiana No. 10, p. 142.

Hamilton, Warren, 1962, Trondhjemite in the Riggins quadrangle, western Idaho: Art. 205 *in* U.S. Geol. Survey Prof. Paper 450-E, p. E98–E101.

Hietanen, Anna, 1951, Metamorphic and igneous rocks of the Merrimac area, Plumas National Forest, California: Geol. Soc. America Bull., v. 62, p. 565–608.

Hotz, P. E., 1971, Plutonic rocks of the Klamath Mountains, California and Oregon: U.S. Geol. Survey Prof. Paper 684-B, p. B1–B20.

Johannsen, Albert, 1932, A descriptive petrography of the igneous rocks, Volume II, the quartz-bearing rocks: Chicago, Chicago Univ. Press, 428 p.

Larsen, L. H., and Poldervaart, Arie, 1961, Petrologic study of Bald Rock batholith, near Bidwell Bar, California: Geol. Soc. America Bull., v. 72, p. 69–92.

Lipman, P. W., 1963, Gibson Peak pluton: A discordant composite intrusion in the southeastern Trinity Alps, northern California: Geol. Soc. America Bull., v. 74, p. 1259–1280.

Mattinson, J. M., Davis, T. E., and Hopson, C. A., 1971, U-Pb studies in the Salinian block of California: Annual Rept. of the Director, Geophys. Lab, *in* Carnegie Inst. Washington Year Book 70, p. 248–251.

Olmsted, F. H., 1971, Pre-Cenozoic geology of the south half of the Auburn 15-minute quadrangle, California: U.S. Geol. Survey Bull. 1341, 30 p.

Page, B. M., 1972, Oceanic crust and mantle fragment in subduction complex near San Luis Obispo, California: Geol. Soc. America Bull., v. 83, p. 957–972.

Pearson, R. C., Hayes, P. T., Fillo, P. V., 1967, Mineral resources of the Ventana primitive area, Monterey County, California: U.S. Geol. Survey Bull. 1261-B, 42 p.

Ross, D. C., 1972a, Petrographic and chemical reconnaissance of some granitic and gneissic rocks near the San Andreas fault from Bodega Head to Cajon Pass, California: U.S. Geol. Survey Prof. Paper 698, 92 p.

—— 1972b, Geologic map of the pre-Cenozoic basement rocks, Gabilan Range, Monterey and San Benito Counties, California: U.S. Geol. Survey Misc. Field Inv. Map MF-357, scale 1:125,000.

Turner, H. W., 1894, Rocks of the Sierra Nevada: U.S. Geol. Survey Ann. Rept. 14, pt. 2, p. 435–495.

Wiebe, R. A., 1970, Relations of granitic and gabbroic rocks, northern Santa Lucia Range, California: Geol. Soc. America Bull., v. 81, p. 105–116.

Williams, Howel, Turner, F. J., and Gilbert, C. M., 1955, Petrography, an introduction to the study of rocks in thin sections: San Francisco, W. H. Freeman and Co., 406 p.

Jour. Research U.S. Geol. Survey
Vol. 1, No. 3, May-June 1973, p. 255–265

ZEOLITES IN THE MIOCENE BRIONES SANDSTONE AND RELATED FORMATIONS OF THE CENTRAL COAST RANGES, CALIFORNIA

By K. J. MURATA and KAREN R. WHITELEY,
Menlo Park, Calif.

Abstract.—Authigenic zeolites present in the generally tuffaceous Miocene Briones Sandstone and related formations of the central Coast Ranges of California indicate three stages of diagenetic history: (1) Initial alteration of pyroclastic materials to clinoptilolite (and montmorillonite) that is widely distributed in small amounts throughout the region. (2) Subsequent crystallization of heulandite followed by stilbite in fractures at a few places. (3) Widespread development of laumontite in only the southern part of the region, where the sandstone appears to have been downfolded and faulted to greater depths than elsewhere. Laumontite occurs both as pervasive cement of sandstone and as filling of fractures, and was produced through the reaction of interstitial solutions with other zeolites and with such major constituents of the sandstone as plagioclase, montmorillonite, and calcite at temperatures of 100°C or higher. Mordenite was found at only one locality, closely associated with clinoptilolite and opal. Analcite occurs in diverse settings, and its relation to the other zeolites is obscure. Sparry calcite and coexisting stilbite, laumontite, or analcite in veins seem to make up nonequilibrium assemblages.

The widely scattered occurrences of diagenetic laumontite in Tertiary marine sandstones of California Coast Ranges were described recently by Madsen and Murata (1970). A subsequent study restricted to Miocene sandstones of the central Coast Ranges east of San Francisco Bay has clarified some of the factors that control the distribution of laumontite and has led to the discovery of several other zeolites (clinoptilolite, mordenite, heulandite, stilbite, and analcite) in these sandstones. Although most of them occur in small amounts, these zeolites merit careful study because they can provide new insights into the diagenetic history of the host sandstone.

Acknowledgments.—Paleontologic and geologic data on the several formations that we sampled were provided by W. O. Addicott, E. H. Bailey, M. D. Crittenden, T. W. Dibblee, Jr., J. W. Miller, and Julius Schlocker. Ranchers of the region and administrators of the San Francisco Water Department and the Sunol Valley Regional Park kindly granted access to lands under their control. Authenticated samples of different zeolites were made available by R. C. Erd, Robert Fournier, R. A. Gulbrandsen, W. H. Lee, and M. B. Norman II. We are also indebted to J. D. Gleason and J. R. O'Neil for isotopic analyses of calcites, to N. F. Prime for the photomicrographs of tiny zeolite crystals shown in figure 4, and to Elizabeth Murata for help with the fieldwork.

OCCURRENCE OF ZEOLITES

The stratigraphy of middle and upper Miocene rocks of the central Coast Ranges and environs was originally defined by Lawson (1914), and subsequently refined and extended by Trask (1922), Taliaferro (1943), Weaver (1949), Crittenden (1951), Page (1966), and many others. The sedimentary units that have been mapped in different parts of the region are listed below, in order of increasing geologic age.

Upper Miocene	San Pablo Group	Neroly Sandstone
		Cierbo Sandstone
		Briones Sandstone
Middle Miocene	Monterey Group	Rodeo Shale
		Hambre Sandstone
		Tice Shale
		Oursan Sandstone
		Claremont Shale
		Sobrante Sandstone

All these formations except the Rodeo Shale were sampled by us; by far the largest number of samples were collected from the widely distributed upper Miocene Briones Sandstone.

The combined outcrop areas of the middle and upper Miocene marine formations (fig. 1, table 1) delineate the broadly folded structure of the central Coast Ranges. Pyroclastic material in the form of andesitic to rhyolitic debris is a common constituent in these formations (Taliaferro, 1933; Lerbekmo, 1957) along with occasional beds of ash or bentonite. Clinoptilolite and laumontite are the most common zeolites; clinoptilolite is widely distributed, whereas laumontite is restricted to the southern area (south of lat 37°40′ and west of the Calaveras fault zone). The extensive development of laumontite in the southern area in the Briones but not in the northern area suggests that the diagenetic history of the

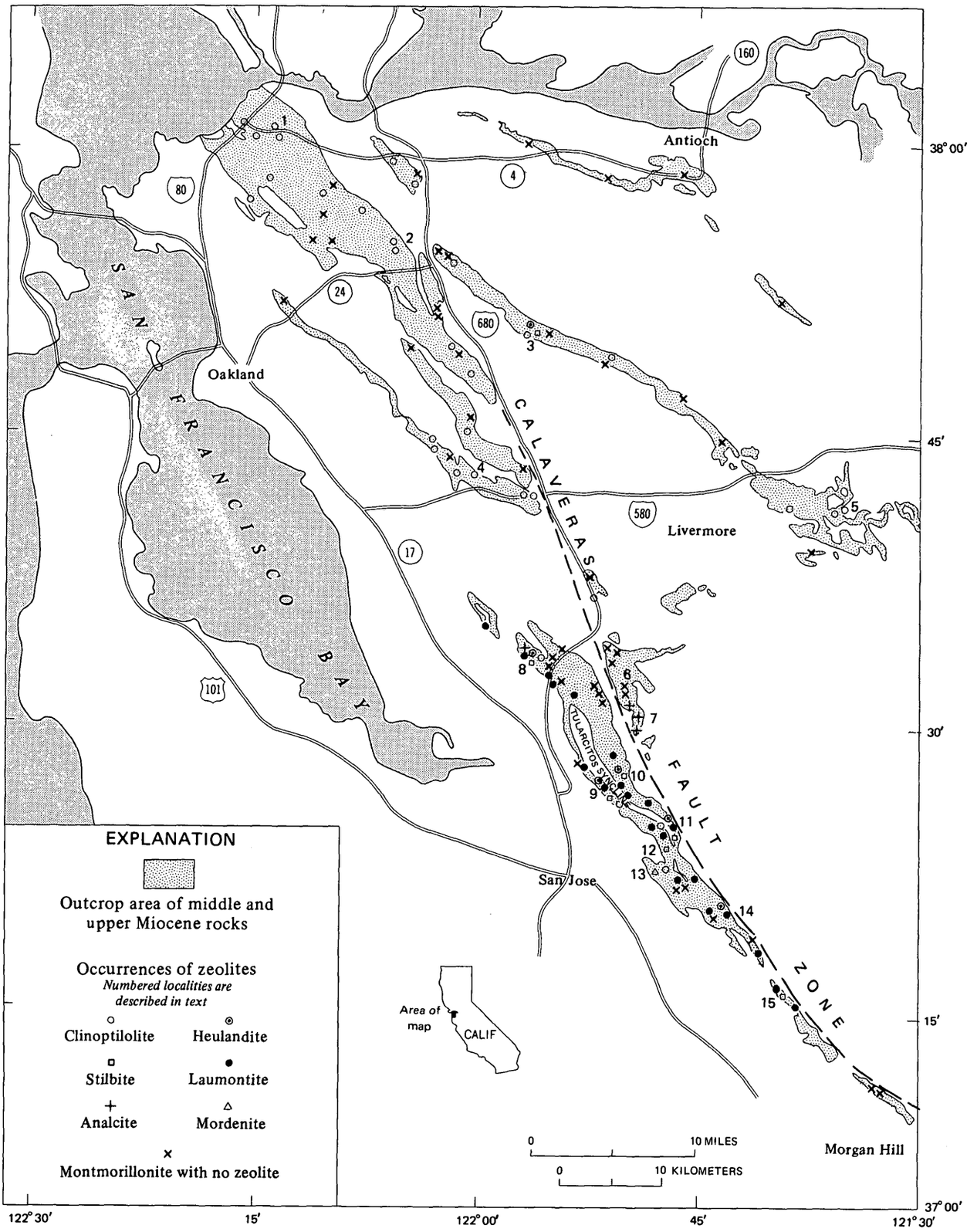

Figure 1.—Map showing outcrop areas of middle and upper Miocene formations in the central Coast Ranges east of San Francisco Bay (based on compilations by Jennings and Burnett, 1961; Koenig, 1963; Strand and Koenig, 1965; Rogers, 1966; and Brabb and others, 1971) and localities of studied samples. Zeolites from the numbered localities are discussed in the text, and the details of these localities are given in table 1. Montmorillonite is ubiquitous, and the zeolite-bearing samples also contain this common alteration product c volcanic ash.

Table 1.—*Data on numbered localities shown on figure 1*

Locality	Lat. N., long. W.	Sedimentary unit
	Contra Costa County	
1. Santa Fe RR., right-of-way.	38°01′, 122°14′	Bentonite bed in Hercules Shale Member of Briones Sandstone.
2. Briones Hills	37°57′, 122°07′	Briones Sandstone.
3. Mount Diablo	37°50′, 121°56′	Do.
	Alameda County	
4. Eden Canyon	37°43′, 122°00′	Briones Sandstone.
5. Patterson Pass	37°41′, 121°35′	Cierbo Sandstone.
6. Welch Creek	37°33′, 121°50′	Lower part of Briones Sandstone.
7. Alameda Creek	37°30′, 121°49′	Oursan Sandstone.
8. Morrison Canyon	37°34′, 121°57′	Hambre Sandstone.
	Santa Clara County	
9. Calaveras Road	37°27′, 121°51′	Briones Sandstone.
10. Weller Road	37°27′, 121°50′	Do.
11. Sierra Road	37°25′, 121°47′	Do.
12. Penitencia Creek	37°24′, 121°47′	Do.
13. Mount Hamilton Road.	37°21′, 121°46′	Do.
14. Quimby Road	37°21′, 121°43′	Do.
15. San Felipe Valley	37°16′, 121°40′	Do.

two areas differs considerably. The hardness of noncalcareous Briones Sandstone differs concomitantly in the two areas; the sandstone is dense and hard to the south and porous and friable to the north.

ZEOLITE ASSEMBLAGES AND DIAGENETIC STAGES

Field studies of zonation by depth of zeolites in sedimentary sections (for example, Coombs, 1954; Hay, 1966; Castano and Sparks, 1970; Iijima and Utada, 1971) and laboratory investigations of phase relations (for example, Coombs and others, 1959; Fyfe and Mackenzie, 1969; Thompson, 1970; Liou, 1971) suggest that different assemblages of zeolites indicate different pressure-temperature conditions of diagenesis. Pressures and temperatures involved in the zeolitic stage of diagenesis are exemplified below by data obtained from deep drill holes by Iijima and Utada (1971). The tabulated values pertain to conditions prevailing at the tops of several zeolite zones in Neogene sedimentary deposits of Niigata oil field of Japan.

Zone	*Temperature (°C)*	*Pressure (kb)*	*Depth (km)*
Clinoptilolite	41–49	.....	0.8–1.9
Mordenite	55–59	0.4–0.7	1.4–2.4
Analcite	84–91	.9–1.1	2.9–3.5
Laumontite	≈100	≈1.0	≈3.0

Similar zeolite relations are found at much shallower depths in the hydrothermal hot-spring environment, according to Steiner (1953) and Honda and Muffler (1970).

In contrast to such a zonation that is controlled mainly by physical parameters of temperature and pressure, other similar but generally shallower zonations seem to depend more on systematic variations in the chemistry of migrating solutions. Some chemical reactions or factors that are likely to affect the composition of interstitial solutions are:

1. Changing chemistry of solutions involved in hydrolysis of glassy shards (Hay, 1963, 1964; Hoover, 1968; Sheppard and Gude, 1969; and Moiola, 1970; among others).
2. Reduction in the activity of dissolved silica induced by sequential changes in the nature of deposited silica, namely, opal-cristobalite-quartz (Coombs and others, 1959; Campbell and Fyfe, 1960).
3. The dependence of the nature of the zeolite formed on the concentrations of the large cations, Na, K, Ca, and Mg; for example, the localization of laumontite in the middle part of the Briones Sandstone, where numerous shell beds constitute a rich source of calcium (Madsen and Murata, 1970).

Three main zeolite assemblages, characteristic of three successive stages of diagenesis, are apparent in the Briones and related sandstones of the Central Coast Ranges:

1. Clinoptilolite (with montmorillonite) that is pseudomorphous after glassy shards and widely distributed in small amounts throughout the studied region.
2. Heulandite together with stilbite as rare fillings of fractures in sandstone.
3. Laumontite, abundantly developed as pervasive cement or as filling of joints and other fractures, and restricted to sandstone in the southern part of the studied region. These zeolites will be described in the following sections.

Clinoptilolite

In their pioneering study of zeolitic alteration of pyroclastics, Bramlette and Posnjak (1933) identified clinoptilolite as a widespread diagenetic mineral in marine Miocene formations of California. Sheppard (1971) compiled all known American localities of this mineral and concluded that "Clinoptilolite is probably the most abundant authigenic zeolite that occurs in sedimentary rocks." The mineral is also common in Tertiary sedimentary formations of central Russia (Senderov and Khitarov, 1970) and of Japan (Utada, 1970).

Clinoptilolite is widespread among the Miocene formations of the central Coast Ranges (fig. 1), in which it is one of the earliest products of alteration of volcanic glass. Unaltered glass (fig. 2*A*) is rare in these formations.

Clinoptilolite is a common minor constituent in cores of tuffaceous Miocene deep-sea oozes drilled off the west coast of Mexico (Murata and Erd, 1964) and has been found in sediments dredged or drilled from the bottom of the Atlantic

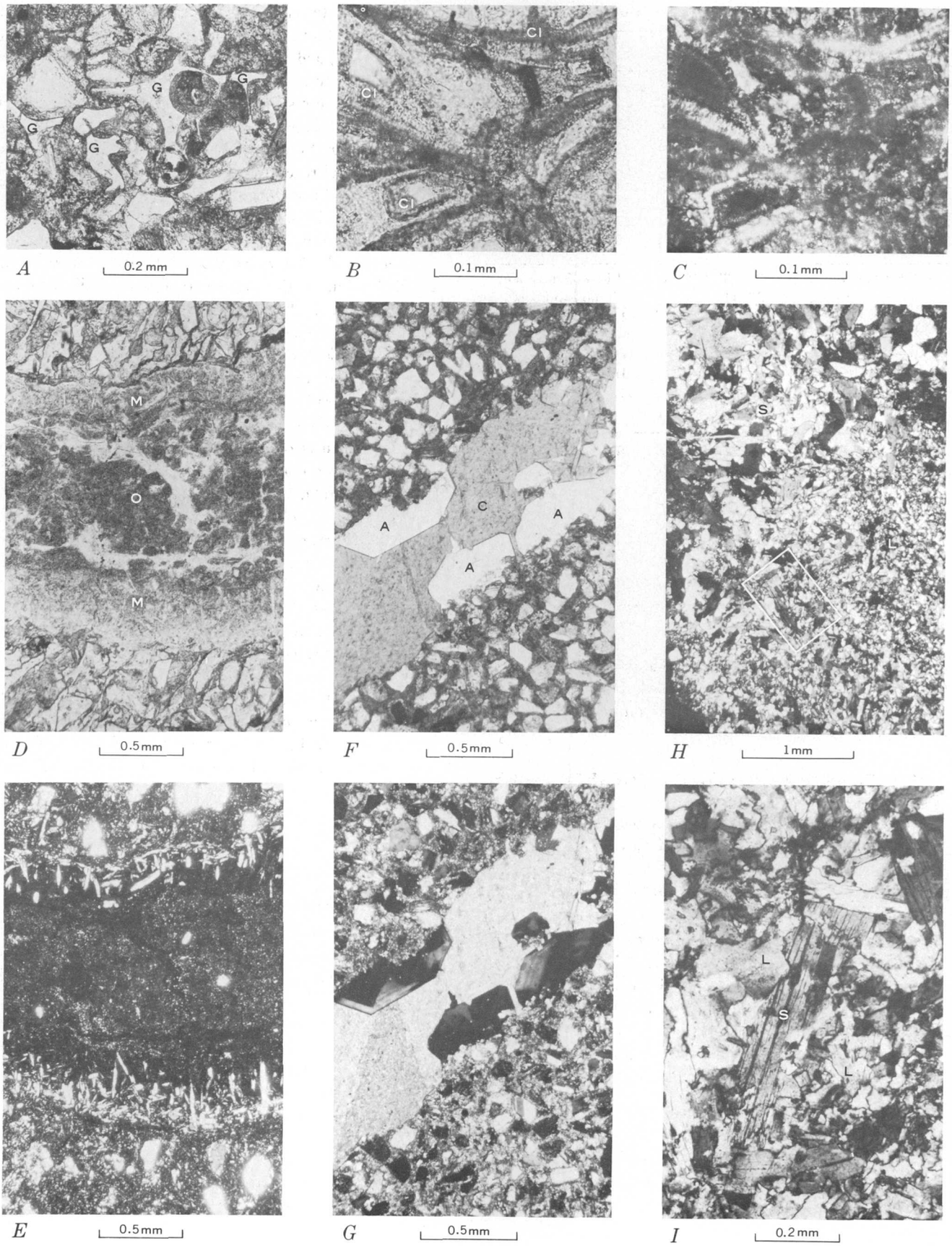
G
G
G
G
0.2 mm
A
Cl
Cl
Cl
0.1 mm
B
0.1 mm
C
M
O
M
0.5 mm
D
A
C
A
A
0.5 mm
F
S
L
1 mm
H
0.5 mm
E
0.5 mm
G
L
S
L
0.2 mm
I

Figure 2.

(Hathaway and Sachs, 1965; Peterson and others, 1970, p. 423). These occurrences suggest that clinoptilolite can be produced diagenetically at an appreciable rate even at low temperatures of the order of 10°C. The mineral is one of the more siliceous of the zeolites, and its Si/Al atomic ratio generally falls between 4 and 6 (Sheppard, 1971).

A bed of volcanic ash, which occurs in the lower part of the Briones at locality 13, was the only rock sufficiently rich in clinoptilolite to be studied directly. The mineral occurs as minutely fibrous replacement of glassy shards (figs. 2*B*,*C*). Clinoptilolite, concentrated out of sandstone from other localities (Nos. 1, 2, 4, 8, 9, 12) by means of heavy liquids, has the same fibrous replacement texture.

A heating test (400°C for 3 hours) was used to distinguish clinoptilolite from heulandite (Mumpton, 1960) on the basis of the absence of an X-ray reflection at 8.3 A in the heated sample for clinoptilolite. Upon heating, clinoptilolite from localities 1 and 4 showed very little weakening or displacement of the principal X-ray reflection at 9.0 A (exemplified by fig. 3*B*), whereas that from localities 2, 8, 9, 12, and 13 manifested an appreciable weakening of the principal reflection and a displacement to 8.7 A (fig. 3*C*). The thermal behavior of the latter type of clinoptilolite is somewhat like that of the calcium clinoptilolite described by Shepard and Starkey (1964, fig. 138.2) and by Utada (1970, fig. 10). When treated overnight with 1*M* Na_2SO_4, the sample from locality 12 released a substantial amount of calcium to solution and became appreciably more resistant to heating, though not completely so. Although differing in thermal behavior, none of the above-mentioned clinoptilolites developed a strong reflection at 8.3 A (fig. 3*A*) that is characteristic of heulandite. Also, the gamma refractive index of these clinoptilolites was determined to be less than 1.488 (Mason and Sand, 1960).

Samples separated from the vein-free sandstone of locality 3 and from the bulk sandstone of locality 5 also had the minutely fibrous habit of clinoptilolite, but many of the grains showed a gamma refractive index between 1.488 and 1.508. When heated, these two samples yielded X-ray patterns indicative of both clinoptilolite and heulandite (fig. 3*D*). This mixed type resembles the material from Nevada described by Shepard (1961), and a detailed study of it may throw light on factors that control the formation of heulandite and clinoptilolite.

Clinoptilolite, pseudomorphous after volcanic shards, formed early in the sandstones at low temperatures and shallow depths of burial. It is the characteristic zeolite in rocks of the northern half of the studied region and indicates what we shall call stage 1 of diagenesis.

Mordenite

In California, mordenite, a relatively minor zeolite most commonly associated with clinoptilolite, has been previously found with clinoptilolite in Miocene tuffs of the marine Obispo Formation of Surdam and Hall (1968) and in continental tuffaceous beds of Tertiary age in the Mojave Desert (Sheppard and Gude, 1964, 1969).

In the central Coast Ranges, small amounts of mordenite have been found only within the previously mentioned clinoptilolite-rich ash bed of locality 13, where it is localized as small stubby crystals along the borders of some opal (cristobalite) veins (figs. 2*D* and 2*E*). The close association with opal suggests that mordenite, whose Si/Al ratio is similar to that of clinoptilolite, formed from solutions with high silica activity (Coombs and others, 1959).

Heulandite

Heulandite typically grows on walls of fractures in sandstone, either as druses of minute tabular crystals (fig. 4*C*) or as sheaves of thin plates, like the sheaves of stilbite shown in figure 4*E*. The two minerals look much alike, although heulandite is generally much finer grained. Their X-ray patterns (Deer and others, 1963) are sufficiently different to distinguish one mineral from the other.

Fracture-filling heulandite has been found at localities 3, 8, 9, 10, 11, and 14, among which only locality 3 lies in the northern area characterized by the lowest stage of diagenesis. At most localities, the mineral is covered by coarse crystals of stilbite, which has a very similar crystal structure and chemical composition (Deer and others, 1963). With an average Si/Al ratio of around 3.0, heulandite and stilbite are distinctly less siliceous than clinoptilolite or mordenite (Si/Al = 5).

Figure 2.—Photomicrographs of thin sections illustrating modes of occurrence of zeolites and associated minerals.

A. Unaltered shards of rhyolitic glass (G) in lower part of Briones Sandstone of locality 6. Plane light. Such fresh glass is rare in the studied formations.

B. Zeolitized shards of a tuff bed in Briones Sandstone of locality 13. The shards may have hollow interiors (white) or centers of unaltered or altered glass. The rim of the shards has been converted to fibrous clinoptilolite (Cl). Plane light.

C. Section *B* under crossed nicols. The constant-exposure method used to obtain the photomicrographs exaggerates the apparent birefringence of the clinoptilolite fibers.

D. A vein of opal (O) in the tuff bed of preceding section *B*-*C*. The vein has a border zone rich in mordenite (M). Plane light.

E. Section *D* under crossed nicols. The opal consists mostly of specks of cristobalite, and tiny needles of mordenite are concentrated along the borders of the opal vein.

F. Cross section of the analcite-calcite vein shown in figure 4*A*. Analcite (A) grows on both walls of the fracture, and sparry calcite (C) fills the remaining space. Plane light.

G. Section *F* under crossed nicols. The analcite is birefringent and zoned.

H. The upper left half of this view of a vein from locality 9 is occupied by stilbite (S) crystals which are partly replaced by laumontite (L), the finer grained material occupying the lower right half. The marked rectangular area is shown enlarged below in photograph *I*. Crossed nicols.

I. An elongate section of a crystal of stilbite (S) that is partly replaced on all sides by laumontite (L). Crossed nicols.

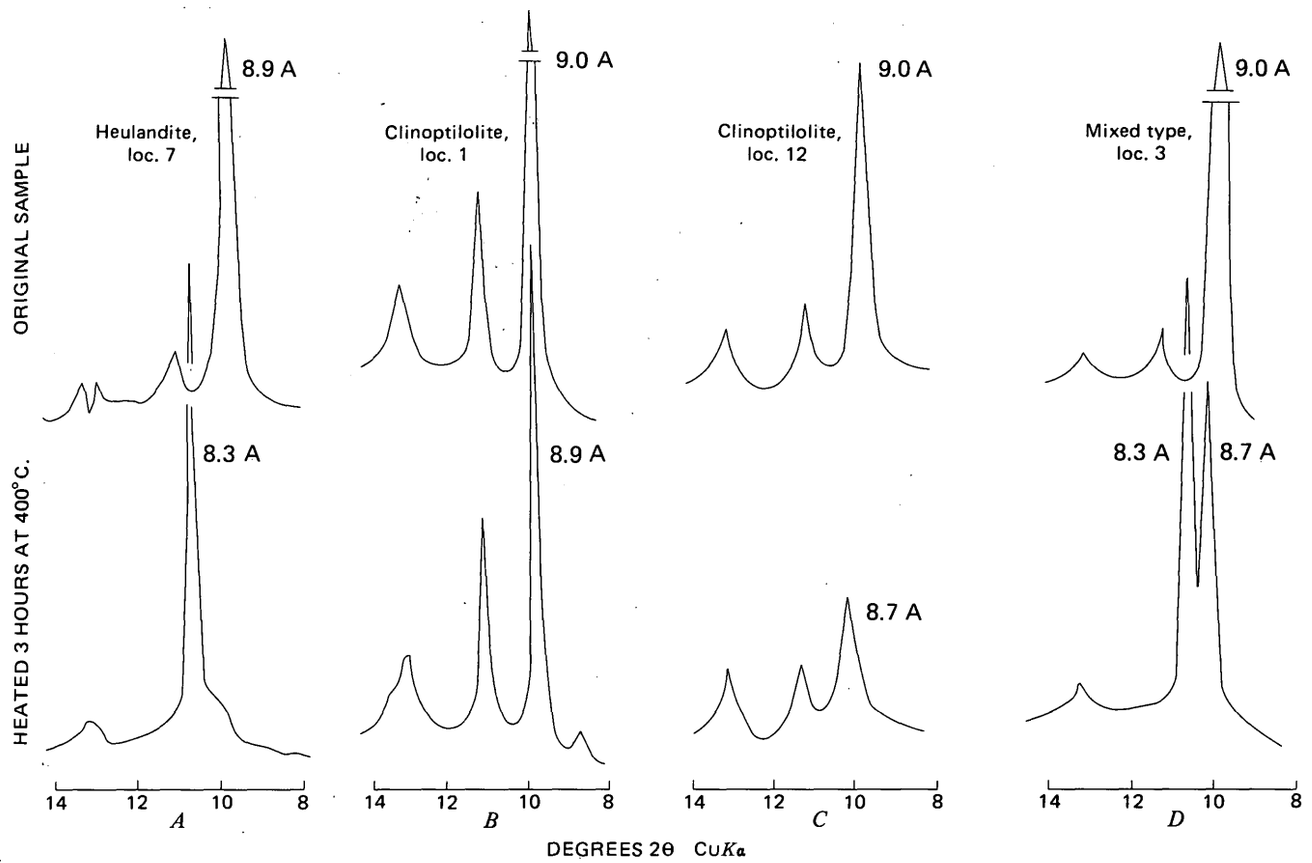

Figure 3.—X-ray diffractometer patterns of original and heated samples of heulandite-group minerals.

Stilbite

Stilbite is preeminent among fracture-filling zeolites, occurring exclusively in fractures as large and well-formed crystals. The mineral has been found at localities 3, 8, 9, 10, 11, 12, and 15, either as sheaves of glistening plates (fig. 4*E*) or as coarse druses (fig. 4*F*), commonly grown over finely crystallized heulandite. The frequent association of chemically and structurally similar stilbite and heulandite suggests that this pair of minerals represents a second stage of diagenesis, which is more advanced than the stage 1 of clinoptilolite. By the time of stage 2, the sediment probably would have been buried deeper into a hotter zone and hardened sufficiently to fracture under stress.

Locality 3 (fig. 1) is interpreted as an unusual spot where diagenetic stage 2 became developed locally in a region generally at rest in stage 1. The more numerous occurrences of stilbite-heulandite in the southern area were apparently formed while the rocks of the area were undergoing progressively more intense alteration toward diagenetic stage 3 characterized by laumontite. In the most intensely laumontized parts of the area, the stilbite-heulandite fracture fillings are replaced by laumontite.

Laumontite

Figure 5 illustrates the way in which laumontite fills joints and pervades the host sandstone throughout the southern part of the studied region. Where well developed, laumontite amounts to 5–10 percent by weight of the rock, as determined by an X-ray diffraction method that was calibrated with known mixtures of the mineral and a sandstone blank. Such percentages far exceed the percentage of clinoptilolite or other zeolites in the average Briones, so they could not have been attained solely through conversion of preexisting zeolites into laumontite. Much of the laumontite was produced through reaction of interstitial solutions with major constituents of sandstone like plagioclase, montmorillonite, and calcite (Madsen and Murata, 1970).

Stilbite, crystallized in joints at localities 9 and 12, is partially replaced by laumontite (figs. 2*H*, *I*), showing that temperature and pressure in the host rock had gone beyond those of stage 2 to those of stage 3. The temperature and pressure attained were probably similar to those observed in laumontite-bearing Miocene sandstones in the Tejon oil field of California, about 100°C and 320 bars hydrostatic pressure (Castano and Sparks, 1970). That the pressure-temperature

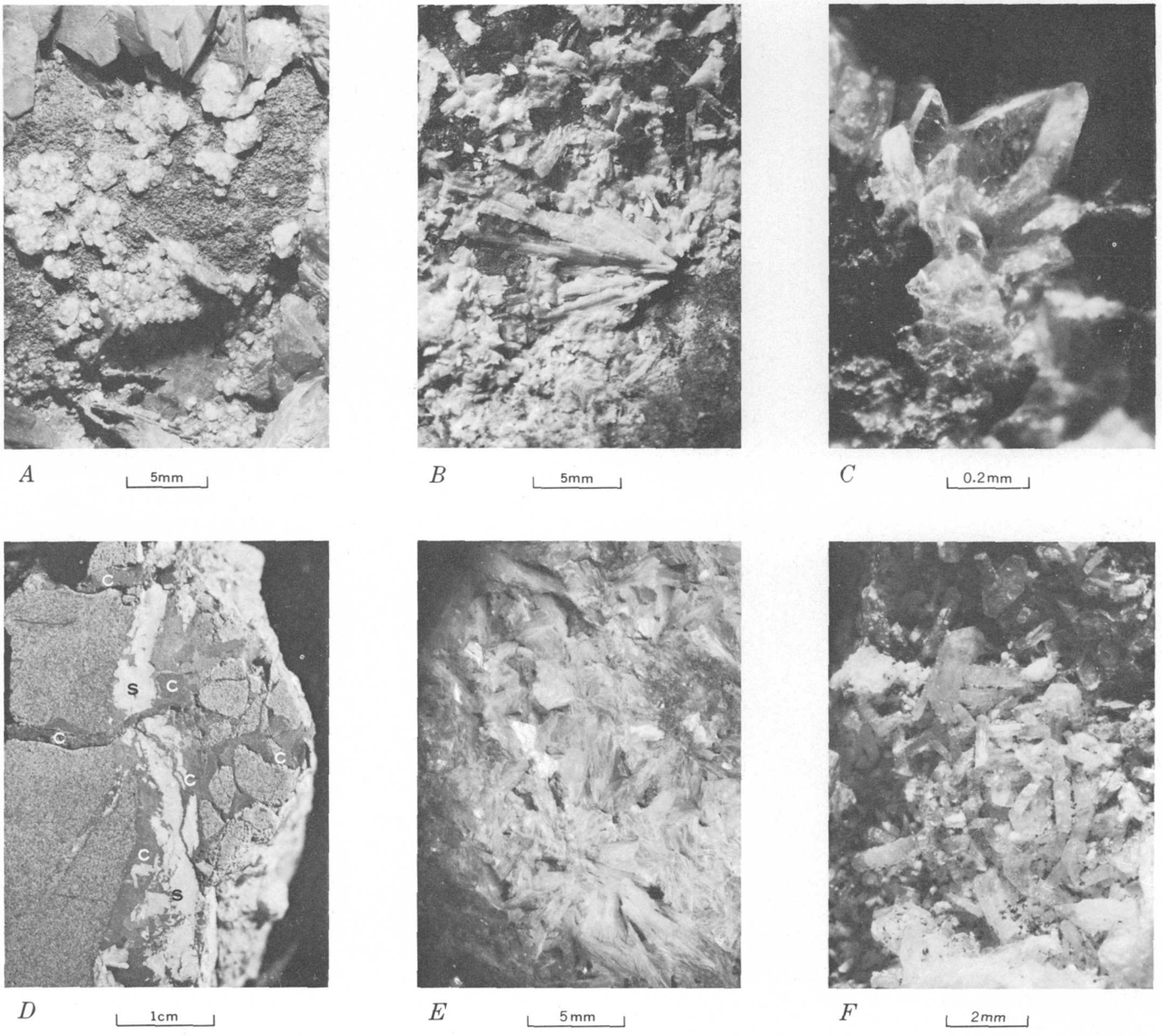

Figure 4.—Photomicrographs of zeolites and associated minerals of veins in Miocene sandstones. The direction of view, except for photographs *C* and *D*, is normal to the wall of the opened vein. Photograph *C* is an edgewise view of a heulandite druse; *D* is an edgewise view of a vein of stilbite.

A. Clusters of analcite trapezohedra (white) surrounded and overgrown by sparry calcite (gray). Oursan Sandstone of locality 7. A thin-section cut across this vein is shown in figure 2*F*.

B. A radiating group of unusually coarse prismatic crystals of laumontite in Briones Sandstone of locality 9.

C. Drusy heulandite in Briones Sandstone of locality 11. The minute crystals are tabular on (010) and elongate along the *c* axis. Commonly, they are overgrown by coarse stilbite like that of *E* below.

D. Sawed section of a fractured vein of stilbite (S) with the fractures filled by late sparry calcite (C); locality 10. Calcite is dark because it was stained with Alizarin Red S.

E. Stilbite consisting of radiating or irregularly stacked platy twin crystals in Briones Sandstone of locality 12.

F. Twin crystals of stilbite of more regular habit than those of *E*. Briones Sandstone of locality 8.

conditions did not exceed those appropriate for stage-3 laumontite is suggested by the apparent absence of higher grade minerals, such as wairakite, epidote, and lawsonite (Thompson, 1971; Liou, 1971).

The Si/Al ratio of the zeolites that characterize the three diagenetic stages decreases progressively as follows: clinoptilolite-mordenite, about 5; heulandite-stilbite, about 3; and laumontite, about 2. As noted by Kostov (1969), such a compositional progression must generally be explained in terms of an increase in temperature or a decrease in activity of

A

B

Figure 5.—Modes of occurrence of laumontite in the Briones Sandstone. *A*, white laumontite coating the walls of subparallel joints and reflecting the sunlight. The joints are nearly perpendicular to the bedding, which dips about 45° to the right. Laumontite is also dispersed throughout the sandstone. Locality 9. *B*, Laumontite dispersed through sandstone and also concentrated along bedding planes. Pencil is 14 cm long. Locality 12.

dissolved silica. The data on the geology and geography of zeolite occurrences in the central Coast Ranges favor the explanation based on increasing temperature.

Significance of laumontite occurrence

The Briones Sandstone is the principal host rock for laumontite, but only in the 30-mile stretch south of lat 37° 40′ and west of Calaveras fault zone (fig. 1). Elsewhere, the sandstone and related formations generally have clinoptilolite as a characteristic diagenetic mineral. The strikingly restricted distribution of laumontite suggests that the Briones either differs compositionally or has undergone different pressure-temperature conditions of diagenesis in its northern and southern parts. Materials such as plagioclase, volcanic debris, montmorillonite, and calcite previously noted to be involved in the formation of laumontite (Madsen and Murata, 1970) are all present in the Briones Sandstone throughout the entire region. The widespread shell beds in the generally clean sands of the middle Briones point to shallow waters of open bays as the probable depositional environment. There are no indications of heterogeneities in the depositional environment which might have led to regional differences in salinity or composition of interstitial waters or in porosity of the sands. The localization of laumontite (fig. 1) thus cannot be explained in terms of the intrinsic properties of the Briones.

From the standpoint of depth metamorphism, the localization of laumontite could be understood if the Briones Sandstone of the southern area had been buried under a greater thickness of younger sedimentary deposits than elsewhere. But according to Crittenden (1951), the cover there (excluding localized Pleistocene deposits) is at most only about 2,000 feet thick stratigraphically, and to the north, others (Ham, 1952; Robinson, 1956; Hall, 1958) have found maximum thickness of cover 3,000–12,000 feet, just the opposite of what would be expected. Although these data are somewhat uncertain because the amount of post-Briones sediments that might have been eroded away is unknown, they suggest that laumontite of the southern area did not result from burial of the Briones under a thicker cover of sediments.

T. W. Dibblee, Jr., who recently remapped a large part of the region shown in figure 1, has stressed to us (oral commun., 1972) that the Briones and related formations are more strongly deformed in the southern than in the northern area. The tightly folded, overturned, and faulted Tularcitos syncline (fig. 1) is a dominant structural feature of the southern area (Crittenden, 1951), and it stands in sharp contrast to the generally more open folds to the north. It seems highly probable that the Briones of only the southern area was downfolded and faulted to depths where temperature and pressure were appropriate for laumontite generation. This interesting relation between intensity of tectonism and metamorphic grade has been noted elsewhere (Haller, 1962; Rast, 1962).

Analcite

The few places where we found analcite have not yielded enough information to put the mineral definitely within the

three-stage scheme of diagenesis. Analcite occurs with clinoptilolite as minor cement of clasts in middle Miocene Hambre Sandstone at locality 8, and as well-formed trapezohedra (figs. 2*F*, 2*G*, and 4*A*) in fractures in the middle Miocene Oursan Sandstone of locality 7, where it is associated with no other zeolite. A third locality is in the continental Pliocene Mulholland Formation of Ham (1952) of Cull Canyon in the region of locality 4, where analcite forms tiny spherical aggregates in a thin bed of bentonite. This occurrence in bentonite seems comparable to those in the lacustrine tuffs of the Green River Formation of Wyoming (Bradley, 1928).

The refractive index of analcite from locality 7 and from Cull Canyon falls in the range 1.484–1.486, which indicates a rather siliceous composition (Saha, 1959). X-ray determinations by the method of Saha (1961) on crystals from two different places in locality 7 uniformly gave a Si/Al ratio of 2.36, compared with the 2.00 of the conventional formula $NaAlSi_2O_6 \cdot H_2O$.

Chemical, more so than physical, factors seem to have been important in the genesis of analcite. Very likely, high-sodium alkaline and saline solutions (VanHouten, 1962; Hay, 1966; Baldar and Whittig, 1968; Boles, 1971), generated by processes unrelated to the main chemistry of regional diagenesis, were involved in forming analcite in diverse settings.

ISOTOPIC COMPOSITION OF CALCITE ASSOCIATED WITH ZEOLITES IN FRACTURES

Sparry calcite commonly occurs with zeolites in both sedimentary and altered igneous rocks, and Thompson (1971) has recently discussed the significance of this association. Among our samples, an obviously late calcite fills and transects a vein of stilbite (fig. 4*D*), and calcite also fills voids in analcite-lined fractures (figs. 2*F*, 2*G*, 4*A*). Similar laumontite-calcite veins have also been collected. The possibility that calcite can coexist with zeolite, on the basis of an equilibrium reaction of the type calcite + kaolinite + 2 quartz + $2H_2O$ = laumontite + CO_2, was considered by Thompson, who concluded that most associations of calcite with zeolite are nonequilibrium assemblages.

With the hope of shedding light on the origin of calcite that coexists with zeolite, samples from four veins were submitted for isotopic analysis; the results are given in table 2.

As the last three lines of table 2 show, the ranges of carbon and oxygen isotopic compositions in calcite formed in the hydrothermal environment (exemplified by lead-zinc deposits) and those in calcite deposited from cool fresh water coincide, except that carbon can be much lighter in some fresh-water calcites. The isotopic compositions of samples 1, 2, and 4 fall in the coincident ranges, so whether these associates of zeolites were formed at low or high temperatures is unknown. The excessively light carbon (−23.9 per mil) of sample 3, however, strongly suggests very late deposition from ground water containing more than usual amounts of bicarbonate derived from soil humus.

Table 2.—*Isotopic analyses of sparry calcite associated with zeolite in the central Coast Ranges and of comparative calcites from other localities*

Locality	Sample No.	Associated mineral	δO^{18} (per mil SMOW)[1]	δC^{13} (per mil PDB)[2]	Analyst or reference
11.	1	Stilbite	+15.5	−7.5	J. D. Gleason.
9.	2	Laumontite	+12.0	−6.6	Do.
12.	3	do	+23.5	−23.9	J. R. O'Neil.
7.	4	Analcite	+22.5	+.6	J. D. Gleason.
Mexico		Pb-Zn ores	+11 to +20	−8 to −1	Ryc (1966).
Kansas		do	+15 to +23	−7 to −1	Hall and Friedman (1969).
Worldwide		Fresh-water calcite	+9 to +24	−18 to −3	Clayton and Degens (1959); Graf (1960); O'Neil and Barnes (1971).

[1] SMOW, standard mean ocean water.
[2] PDB, Pee Dee Belemnite standard.

A similar late origin for the other samples of calcite is not excluded by the isotopic data. Elementary considerations, such as the median position of calcite in the veins (fig. 2*F*), the cutting of some zeolite veins by calcite (fig. 4*D*), and the occurrence of zeolites in some veins devoid of calcite, also suggest that zeolite and calcite formed successively, not simultaneously, and were not in equilibrium with each other.

REFERENCES CITED

Baldar, N. A., and Whittig, L. D., 1968, Occurrence and synthesis of soil zeolites: Soil Sci. Soc. Am. Proc., v. 32, p. 235–240.

Boles, J. R., 1971, Synthesis of analcime from natural heulandite and clinoptilolite: Am. Mineralogist, v. 56, nos. 9–10, p. 1724–1734.

Brabb, E. E., Sonneman, H. S., and Switzer, J. R., Jr., compilers, 1971, Geologic map of the Mount Diablo-Byron area, Contra Costa, Alameda, and San Joaquin Counties, California: U.S. Geol. Survey open-file rept., scale 1:62,500.

Bradley, W. H., 1928, Zeolite beds in the Green River Formation: Science, v. 67, p. 73–74.

Bramlette, M. N., and Posnjak, Eugen, 1933, Zeolitic alteration of pyroclastics: Am. Mineralogist, v. 18, no. 4, p. 167–171.

Campbell, A. S., and Fyfe, W. S., 1960, Hydroxyl-ion catalysis of the hydrothermal crystallization of amorphous silica; a possible high-temperature indicator: Am. Mineralogist, v. 45, nos. 3–4, p. 464–468.

Castano, J. R., and Sparks, D. M., 1970, Interpretation of vitrinite reflectance measurements in sedimentary rocks and determination of burial history using vitrinite reflectance and authigenic minerals: Geol. Soc. America Abs. with Programs, v. 2, no. 7, p. 516–517.

Clayton, R. N., and Degens, E. T., 1959, Use of carbon isotope analysis of carbonates for differentiating fresh-water and marine sediments: Am. Assoc. Petroleum Geologists Bull., v. 43, no. 4, p. 890–897.

Coombs, D. S., 1954, The nature and alteration of some Triassic sediments from Southland, New Zealand: Royal Soc. New Zealand Trans., v. 82, pt. 1, p. 65–109.

Coombs, D. S., Ellis, J. A., Fyfe, W. S., and Taylor, A. M., 1959, The zeolite facies, with comments on the interpretation of hydrothermal synthesis: Geochim. et Cosmochim. Acta, v. 17, nos. 1–2, p. 53–107.

Crittenden, M. D., 1951, Geology of the San Jose-Mount Hamilton Area, California: California Div. Mines and Geology Bull. 157, 74 p.

Deer, W. A., Howie, R. A., and Zussman, J., 1963, Rock-forming minerals, v. 4, Framework silicates: London, Longmans, Green, and Co., 435 p.

Fyfe, W. S., and Mackenzie, W. S., 1969, Aspects of experimental petrology: Earth-Sci. Rev., v. 5, no. 3, p. 185–215.

Graf, D. L., 1960, Geochemistry of carbonate sediments and sedimentary carbonate rocks–Pt. 4A, Isotopic composition, chemical analysis: Illinois Geol. Survey Circ. 308, 42 p.

Hall, C. A., Jr., 1958, Geology and paleontology of the Pleasanton Area, Alameda and Contra Costa Counties, California: California Univ. Pubs. Geol. Sci., v. 34, no. 1, p. 1–90.

Hall, W. E., and Friedman, Irving, 1969, Oxygen and carbon isotopic composition of ore and host rock of selected Mississippi Valley deposits, *in* Geological Survey Research 1969: U.S. Geol. Survey Prof. Paper 650-C, p. C140–C148.

Haller, J., 1962, Structural control of regional metamorphism in East Greenland Caledonides: Geol. Soc. London Proc., no. 1594, p. 21–25.

Ham, C. K., 1952, Geology of Las Trampas Ridge, Berkeley Hills, California: California Div. Mines and Geology Spec. Rept. 22, 26 p.

Hathaway, J. C., and Sachs, P. L., 1965, Sepiolite and clinoptilolite from the Mid-Atlantic Ridge: Am. Mineralogist, v. 50, nos. 7–8, p. 852–867.

Hay, R. L., 1963, Stratigraphy and zeolitic diagenesis of the John Day Formation of Oregon: California Univ. Pubs. Geol. Sci., v. 42, p. 199–262.

—— 1964, Phillipsite of saline lakes and soils: Am. Mineralogist, v. 49, nos. 9–10, p. 1366–1387.

—— 1966, Zeolites and zeolitic reactions in sedimentary rocks: Geol. Soc. America Spec. Paper 85, 130 p.

Honda, Sakuro, and Muffler, L. J. P., 1970, Hydrothermal alteration in core from research drill hole Y-1, Upper Geyser Basin, Yellowstone National Park, Wyoming: Am. Mineralogist, v. 55, nos. 9–10, p. 1714–1737.

Hoover, D. L., 1968, Genesis of zeolites, Nevada Test Site, *in* Eckel, E. B., ed., Nevada Test Site: Geol. Soc. America Mem. 110, p. 275–284.

Iijima, Azuma, and Utada, Minoru, 1971, Present-day zeolitic diagenesis of the Neogene geosynclinal deposits in the Niigata oilfield, Japan, *in* Molecular sieve zeolites [Pt.] 1: Am. Chem. Soc. Advances in Chemistry Ser., no. 101, p. 342–349.

Jennings, C. W., and Burnett, J. L., 1961, Geologic map of California, San Francisco sheet: California Div. Mines and Geology Map Sheet, scale 1:250,000.

Koenig, J. B., 1963, Geologic map of California, Santa Rosa sheet: California Div. Mines and Geology Map Sheet, scale 1:250,000.

Kostov, Ivan, 1969, Zoning in the development of the volcanogenic zeolites: Neues Jahrb. Mineralogie Abh., v. 3, p. 264–278.

Lawson A. C., 1914, Description of the San Francisco district; Tamalpais, San Francisco, Concord, San Mateo, and Hayward quadrangles: U.S. Geol. Survey Geol. Atlas, Folio 193, 24 p.

Lerbekmo, J. F., 1957, Authigenic montmorillonoid cement in andesitic sandstones of central California: Jour. Sed. Petrology, v. 27, no. 3, p. 298–305.

Liou, J. G., 1971, Stilbite-laumontite equilibrium: Contr. Mineralogy and Petrology, v. 31, p. 171–177.

Madsen, B. M., and Murata, K. J., 1970, Occurrence of laumontite in Tertiary sandstones of the central Coast Ranges, California, *in* Geological Survey Research 1970: U.S. Geol. Survey Prof. Paper 700-D, p. D188–D195.

Mason, B. H., and Sand, L. B., 1960, Clinoptilolite from Patagonia–The relationship between clinoptilolite and heulandite: Am. Mineralogist, v. 45, nos. 3–4, p. 341–350.

Moiola, R. J., 1970, Authigenic zeolites and K-feldspar in the Esmeralda Formation, Nevada: Am. Mineralogist, v. 55, nos. 9–10, p. 1681–1691.

Mumpton, F. A., 1960, Clinoptilolite redefined: Am. Mineralogist, v. 45, nos. 3–4, p. 351–369.

Murata, K. J., and Erd, R. C., 1964, Composition of sediments from the experimental Mohole project (Guadalupe site): Jour. Sed. Petrology, v. 34, no. 3, p. 633–655.

O'Neil, J. R., and Barnes, Ivan, 1971, C^{13} and O^{18} compositions in some fresh-water carbonates associated with ultramafic rocks and serpentinites: Geochim. et Cosmochim. Acta, v. 35, no. 7, p. 687–697.

Page, B. M., 1966, Geology of the Coast Ranges of California, *in* Bailey, E. H., ed., Geology of northern California: California Div. Mines and Geology Bull. 190, p. 255–276.

Peterson, N. M. A., and others, 1970, Deep Sea Drilling Project–Initial Rept., v. 2: Washington, U.S. Govt. Printing Office, 501 p.

Rast, Nicholas, 1962, The relationship between tectonic deformation and regional metamorphism. Geol. Soc. London Proc., no. 1594, p. 25–26.

Robinson, G. D., 1956, Geology of the Hayward quadrangle, California: U.S. Geol. Survey Geol. Quad. Map GQ-88.

Rogers, T. H., 1966, Geologic map of California, San Jose sheet: California Div. Mines and Geology Map Sheet, scale 1:250,000.

Rye, R. O., 1966, The carbon, hydrogen, and oxygen isotopic composition of the hydrothermal fluids responsible for the lead-zinc deposits at Providencia, Zacatecas, Mexico: Econ. Geology, v. 61, no. 8, p. 1399–1427.

Saha, Prasenjit, 1959, Geochemical and X-ray investigation of natural and synthetic analcites: Am. Mineralogist, v. 44, nos. 3–4, p. 300–313.

—— 1961, The system $NaAlSiO_4$ (nepheline)–$NaAlSi_3O_8$ (albite)–H_2O: Am. Mineralogist, v. 46, nos. 7–8, p. 859–884.

Senderov, E. E., and Khitarov, N. I., 1970, Zeolites, their synthesis and conditions of formation in nature: Moscow, Nauka Publishing House, 283 p. [In Russian].

Shepard, A. O., 1961, A heulandite-like mineral associated with clinoptilolite in tuffs of Oak Springs Formation, Nevada Test Site, Nye County, Nevada: Art. 264 *in* U.S. Geol. Survey Prof. Paper 424-C, p. C320–C322.

Shepard, A. O., and Starkey, H. C., 1964, Effect of cation exchange on the thermal behavior of heulandite and clinoptilolite: Art. 138 *in* U.S. Geol. Survey Prof. Paper 475-D, p. D89–D92.

Sheppard, R. A., 1971, Clinoptilolite of possible economic value in sedimentary deposits of the conterminous United States: U.S. Geol. Survey Bull. 1332-B, p. B1–B15.

Sheppard, R. A., and Gude, A. J., 1964, Reconnaissance of zeolite deposits in tuffaceous rocks of the western Mojave Desert and vicinity, California, *in* Geological Survey Research 1964: U.S. Geol. Survey Prof. Paper 501-C, p. C114–C116.

—— 1969, Diagenesis of tuffs in the Barstow Formation, Mud Hills, San Bernardino County, California: U.S. Geol. Survey Prof. Paper 634, 35 p.

Steiner, Alfred, 1953, Hydrothermal rock alteration at Wairakei, New Zealand: Econ. Geology, v. 48, no. 1, p. 1–13.

Strand, R. G., and Koenig, J. B., 1965, Geologic map of California, Sacramento sheet: California Div. Mines and Geology Map Sheet, scale 1:250,000.

Surdam, R. C., and Hall, C. A., 1968, Zeolitization of the Obispo Formation, Coast Ranges of California [abs.]: Geol. Soc. America Spec. Paper 101, p. 338.

Taliaferro, N. L., 1933, The relation of volcanism to diatomaceous and associated siliceous sediments: California Univ. Pubs. Geol. Sci., v. 23, no. 1, p. 1–56.

—— 1943, Geologic history and structure of the central Coast Ranges of California: California Div. Mines and Geology Bull. 118, p. 119–163.

Thompson, A. B., 1970, Laumontite equilibria and the zeolite facies: Am. Jour. Sci., v. 269, p. 267–275.

—— 1971, PCO_2 in low-grade metamorphism; zeolite, carbonate, clay mineral, prehnite relations in the system $CaO–Al_2O_3–SiO_2–CO_2–H_2O$: Contr. Mineralogy and Petrology, v. 33, p. 145–161.

Trask, P. D., 1922, The Briones formation of Middle California: California Univ. Pubs. Geol. Sci., v. 13, p. 133–174.

Utada, Minoru, 1970, Occurrence and distribution of authigenic zeolites in the Neogene pyroclastic rocks in Japan: Tokyo Univ., Coll. Gen. Educ., Sci. Paper, v. 20, no. 2, p. 191–262.

VanHouten, F. B., 1962, Cyclic sedimentation and the origin of analcime-rich Upper Triassic Lockatong Formation, west-central New Jersey and adjacent Pennsylvania: Am. Jour. Sci., v. 260, p. 561–576.

Weaver, C. E., 1949, Geology of the Coast Ranges immediately north of the San Francisco Bay region, California: Geol. Soc. America Mem. 35, 242 p.

Jour. Research U.S. Geol. Survey
Vol. 1, No. 3, May-June 1973, p. 267–272

THE CHEMISTRY OF FIVE ACCESSORY ROCK-FORMING APATITES

By DONALD E. LEE, ELAINE L. MUNSON BRANDT,
RICHARD E. VAN LOENEN; and HARRY J. ROSE, JR.,
Denver, Colo.; Washington, D.C.

Abstract.—Chemical and physical data are given for five samples of rock-forming apatite from diverse geologic environments in Nevada and Colorado. Four of these apatites contain rare-earth assemblages in which the cerium group is well represented but the yttrium group predominates. The fifth apatite contains a highly fractionated assemblage of the lighter (cerium group) rare earths similar to the assemblage typical of alkalic rocks.

Before the advent of modern techniques of mineral purification many minerals being considered for analysis were selected on the basis of their easy availablity, and thus many of the early analyses were performed on minerals from pegmatites, tactites, or drusy cavities, from which large crystals could be handpicked with minimal effort. Fewer analyses were performed on minerals from some of the more common igneous and metamorphic rocks, especially rather fine-grained rocks. During the past 20 years or so, many analyses of the more common rock-forming minerals have been published. However, for some of the accessory (as opposed to essential) minerals—including apatite—there still is a dearth of chemical data on samples recovered from some of the more common rock types. This paper presents chemical data for four samples of accessory apatite and one sample of placer apatite.

The apatites described here were purified by the same methods used on accessory apatites from the southern Snake Range, Nev. (Lee and others, 1973). Indices of refraction were determined by the immersion method, using a spindle stage (Wilcox, 1959) and focal masking technique (Wilcox, 1962). Cell parameters were obtained by least-squares refinement of powder diffractometer data, using an internal standard of CaF_2 and a self-indexing computer program developed by Evans, Appleman, and Handwerker (1963).

Semiquantitative spectrographic results are based on their identity with geometric brackets whose boundaries are 1.2, 0.83, 0.56, 0.38, 0.26, 0.18, 0.12, and so forth, and are reported arbitrarily as midpoints of these brackets, 1., 0.7, 0.5, 0.3, 0.2, 0.15, and 0.1, respectively. The precision of a reported value is approximately one bracket at 68-percent confidence, or two brackets at 95-percent confidence.

FIELD SETTING OF APATITES

Apatite 244-MW-60 was recovered from a muscovite-rich granitoid rock collected at lat 39°35′55″ N.; long 114°7′55″ W., in the Kern Mountains of White Pine County, Nev. This granitoid rock is almost identical with the (southern Snake Range) Pole Canyon—Can Young Canyon intrusive type described in detail by Lee and Van Loenen (1971, p. 5, 38, 39), who ascribed its distinctive nature to assimilation of argillite. According to R. K. Hose and M. C. Blake, Jr. (oral commun., 1971), who prepared the geologic map of White Pine County, the distinctive nature of the granitoid rock from which apatite 244-MW-60 was recovered might also result from assimilation of argillite. Whatever the origin, the great similarity of these two granitoid rocks extends to the peculiar apatite-zircon relation described by Lee and Van Loenen (1971, p. 5, 39) and illustrated by Lee and others (1973, fig. 2). In each rock almost all the zircon is present as tiny, acicular inclusions in large, equant, rather poorly formed, and sparsely distributed apatite crystals.

Apatite 300-DL-64 was recovered from a placer concentrate collected at the mouth of Hampton Creek at lat 39°14′45″ N.; long 114°3′50″ W., in White Pine County, Nev. Except for some Middle Cambrian limestones resting above a thrust surface, all the Hampton Creek drainage is underlain by Lower Cambrian metaquartzites and metashales, as shown on the geologic map of White Pine County, Nev. (Hose and Blake, 1970). The ultimate environment(s) in which the crystals of apatite 300-DL-64 may have formed is problematical. However, the sample analyzed appeared to be homogeneous, for it gave an X-ray diffraction pattern with sharp peaks which in turn gave a good refinement of the unit cell parameters (table 1). Moreover, the Lower Cambrian metasedimentary rocks were the source of most or perhaps almost all of this placer apatite. In connection with potassium-argon age studies in the area (Lee and others, 1970; and unpub. data), we have done mineral separation work on several samples of these metasedimentary rocks. Minor amounts of apatite were commonly recovered, and petrographic study shows the apatite to be present as well-formed crystals that appear to be part of the metamorphic assemblage.

Table 1.—*Analytical data for five apatites*

[Descriptions of sample localities, methods of determination of physical properties, and general limitations of the semiquantitative method are given in text. Chemical analyses by E. L. Munson Brandt; semiquantitative analyses by L. D. Forshey]

Area of collection	White Pine County, Nev.			Elko County Nev.	Gilpin County, Colo.
Sample No.	244-MW-60	300-DL-64	301-DL-65	363-DL-66	1-CC
Physical properties					
Indices of refraction:					
ϵ (±0.001)	1.630	.....	1.630	1.634	1.630
ω (±0.001)	1.632	.....	1.632	1.640	1.632
$\omega-\epsilon$	.002	.....	.002	.006	.002
Specific gravity:					
Observed	3.20±.01	3.20±.01	3.20±.01	[1]3.226±.005	3.20±.01
Calculated	3.21	3.22	3.22	3.227	.....
Unit cell parameters:					
a (±0.001 A)	9.367	9.373	9.366	9.407	9.376
c (±0.001 A)	6.880	6.875	6.880	6.876	6.877
c/a	.734	.733	.734	.731	.733
Cell volume:					
Measured (±0.2 A^3)	522.9	523.1	522.6	527.0	523.6
Calculated	523.7	525.6	525.6	527.2	.....
Chemical analyses (weight percent)					
SiO_2	0.06	0.04	0.24	0.55	0.11
Al_2O_3	.07	.06	.09	.04	.....
Fe_2O_3	.06	.02	.05	.14	.05
FeO	.03	.12	.04	.24	.04
MgO	.....	.05	.....	.....	.....
CaO	54.54	54.97	54.21	53.91	55.09
Na_2O	.07	.05	.....	.10	.....
K_2O	.01	.01	.....	.01	.....
H_2O+	.....	.00	.....	.....	.....
H_2O-	.....	.00	.....	.....	.....
P_2O_5	42.22	42.21	41.78	41.13	.....
MnO	.11	.08	.15	.08	.....
Cl	.....	.02	.....	.71	.....
F	3.64	2.98	3.49	2.93	2.92
[2]R_2O_3	.41	.29	.88	1.69	.39
Insoluble residues[3]	.59	.22	.36	.13	.07
Subtotal	101.81	101.06	101.29	101.66	.....
Less O≡Cl,F	1.53	1.25	1.47	1.23	.....
Total	100.28	99.81	99.82	100.43	.....
Ions on basis of 26(O,OH,F,Cl)					
P	6.024	6.048	5.996	5.930	.....
Si	.010 } 6.034	.007 } 6.055	.041 } 6.037	.094 } 6.024	.....
Al	.014	.012	.018	.008	.....
Fe^{3+}	.008	.003	.006	.018	.....
Fe^{2+}	.004	.017	.006	.034	.....
Mg	.....	.013	.....	.....	.....
Mn	.016 } 9.940	.012 } 10.061	.022 } 9.954	.012 } 10.048	.....
Ca	9.848	9.968	9.847	9.836	.....
Na	.023	.016	.....	.033	.....
K	.002	.002	.....	.002	.....
[4]Ce^{3+}	.025	.018	.055	.105	.....
F	1.940 } 1.940	1.595 } 1.601	1.871 } 1.871	1.578 } 1.783	.....
Cl	.....	.006	.....	.205	.....

Table 1.—*Analytical data for five apatites*—Continued

[Descriptions of sample localities, methods of determination of physical properties, and general limitations of the semiquantitative method are given in text. Chemical analyses by E. L. Munson Brandt; semiquantitative analyses by L. D. Forshey]

Area of collection	White Pine County, Nev.			Elko County Nev.	Gilpin County, Colo.
Sample No.	244-MW-60	300-DL-64	301-DL-65	363-DL-66	1-CC
Semiquantitative spectrographic analyses (weight percent)					
Ba	0.0002	0.0002	0.0003	0.0005	0.0002
Cu	.0005	.0003	.0005	.005	.0007
Pb	.001	.0015	.0015	.0015	.001
Sr	.05	.05	.03	.15	.03
Ti	.005	.007	.01	.0002	.002
V	0	0	.0015	.007	.0007
Zr	.15	.01	.005	0	.003

[1] Specific gravity of sample 363-DL-66 was determined with greater precision than others.
[2] Rare-earth oxide precipitates. See table 2 for analyses.
[3] Insoluble in 1:1 HCl at 100°C. Results of X-ray diffraction work on these insoluble residues are given in text.
[4] Each rare-earth oxide precipitate calculated as Ce_2O_3 for sake of simplicity.

Apatite 301-DL-65 was recovered from a xenolith (of shaly quartzite?) collected at lat 38°56′49″ N.; long 114°16′26″ W., within the area of a detailed field and laboratory study by Lee and Van Loenen (1971).

Apatite 363-DL-66 was recovered from a granitoid rock collected at lat 40°20′55″ N.; long 114°34′ W., in the upper drainage of Cougar Canyon of the Dolly Varden Mountains, Elko County, Nev. This rock is the "augite monzonite" of Snow (1964, p. 69, 78), who described the various igneous rock types exposed in the area. On the basis of our mineral separation work we estimate that this apatite makes up more than 1 percent of the rock from which it was recovered.

Apatite 1-CC was recovered from a Precambrian metamorphic rock collected at lat 39°47′49″ N.; long 105°30′25″ W., about 1 mile south-southeast of Central City in Gilpin County, Colo. The rock is a fine-grained biotite-rich schist that occurs as a layer about 3 inches thick within a migmatitic biotite gneiss.

APATITE ANALYSES

Chemical analyses of the apatites (table 1) are calculated on the basis of 26(O,OH,F,Cl) to the apatite formula $Ca_5(PO_4)_3$ (F,Cl,OH), using the computer program described by Jackson, Stevens, and Bowen (1967).

Each analysis includes the weight percent of material insoluble in 1:1 HCl at 100°C., giving a good indication of the degree of purity of the apatites analyzed. Amount of impurity (insoluble material) ranges from 0.07 weight percent of apatite 1-CC to 0.54 weight percent in apatite 244-MW-60, and in each apatite probably all the insoluble material was present as inclusions in the apatite grains.

Each analysis also includes weight percent of the rare-earth oxide precipitate recovered. X-ray spectrographic analyses of these precipitates are calculated to atomic percent of total rare earths in each of the apatites (table 2) and discussed in some detail later in this paper.

The compositions (table 1) range from about 79 to 92 mole percent end-member fluorapatite. Sample 363-DL-66 is about 10 mole percent chlorapatite; the other four minerals are for the most part hydroxyfluorapatites, as indicated by the indices of refraction and unit cell parameters listed in table 1 (See Deer, Howie, and Zussman, 1962, p. 324, 331). There was enough material for determination of $H_2O(+)$ in only sample 300-DL-64. Each apatite in table 1 completely lacked effervescence when immersed in 1:1 HCl at 100°C., indicating absence of the carbonate ion.

Aside from rare earths, only minor amounts of other cations proxy for Ca^{2+} in the structural formulas (table 1). There is very nearly a straight-line relation between amounts of Si and rare earths present in the structural formulas, owing probably to the coupled $Si^{4+}RE^{3+,4+} \rightleftharpoons P^{5+}Ca^{2+}$ substitution.

The insoluble residues (table 1) were identified by means of X-ray diffraction study as follows: 244-MW-60, predominantly zircon; 300-DL-64, subequal amounts of quartz and zircon; and the other three, predominantly quartz. We attribute the zirconium values (table 1) to zircon inclusions in the apatite (0.02 weight percent zircon about equivalent to 100 ppm zirconium). The tiny amounts of the other minor elements listed most probably are present in the crystal structures of the apatites.

There are several methods of assessing the degree of fractionation of rare earths included in the structures of minerals from various geologic environments, a subject of considerable interest. Murata, Rose, and Carron (1953) pro-

Table 2.—*Analyses of rare-earth precipitates and calculation of* Σ(La+Ce+Pr) *for apatites in table 1*

Sample No.	244-MW-60	300-DL-64	301-DL-65	363-DL-66	1-CC
Weight percent of rare-earth precipitate[1]					
Y_2O_3	36.7	28.9	40.5	2.95	34.7
La_2O_3	3.11	1.85	2.53	21.3	1.76
CeO_2	11.0	6.71	9.16	41.6	7.06
Pr_2O_3	1.98	1.34	1.93	5.11	1.71
Nd_2O_3	10.5	7.73	10.4	14.3	9.47
Sm_2O_3	5.65	4.40	5.54	3.80	5.00
Eu_2O_3	1.13	1.85	1.20	1.69	1.47
Gd_2O_3	5.31	4.86	5.04	1.52	4.53
Tb_2O_3	1.69	1.62	1.45	.42	1.47
Dy_2O_3	6.79	7.27	6.39	.51	7.47
Ho_2O_3	2.26	2.18	2.17	.0	1.88
Er_2O_3	2.88	2.31	2.84	.21	3.00
Tm_2O_3	.62	.60	.77	.08	.71
Yb_2O_3	1.75	1.53	2.34	.0	2.76
Lu_2O_3	.90	.83	1.01	.0	.94
Total	92.27	73.98	93.27	93.40	83.88
Atomic percent of total rare earths in apatite					
Y	50.81	50.25	54.43	4.65	52.63
La	2.98	2.23	2.36	23.31	1.85
Ce	10.00	7.65	8.40	43.11	7.03
Pr	1.88	1.60	1.77	5.53	1.78
Nd	9.75	9.02	9.38	15.16	9.64
Sm	5.06	4.95	4.85	3.89	4.91
Eu	1.01	2.06	1.04	1.71	1.43
Gd	4.57	5.27	4.22	1.50	4.28
Tb	1.44	1.74	1.20	.40	1.38
Dy	5.68	7.64	5.20	.48	6.86
Ho	1.87	2.27	1.73	.0	1.70
Er	2.36	2.37	2.25	.19	2.68
Tm	.50	.61	.60	.07	.63
Yb	1.39	1.52	1.80	.0	2.39
Lu	.70	.82	.77	.0	.81
Total	100.00	100.00	100.00	100.00	100.00
Σ(La+Ce+Pr)	14.86	11.48	12.53	69.95	10.66

[1] X-ray spectrographic analysis by Frank Cuttitta, Ralph Christian, and Harry J. Rose, Jr. Sc_2O_3 not detected. Low totals probably due to presence of filter-paper ash in precipitate.

posed the quantity Σ(La+Ce+Pr) in atomic percent of total rare-earth elements as a numerical index of the composition and stage of fractionation attained by the rare-earth elements. Thus higher values of Σ(La+Ce+Pr) represent greater enrichment of the lighter, more basic rare-earth elements. Apatite 363-DL-66 has a sigma value of about 70, representing a much lighter assemblage of rare earths than any of the other four (with sigmas of 10.7–14.9, table 2).

Fleischer and Altschuler (1969, p. 729) based their discussion of the fractionation of lanthanides (excluding yttrium) on a triangular diagram with corners featuring (in atomic percent) the groups La–Nd, Sm–Ho, and Er–Lu. If the results in table

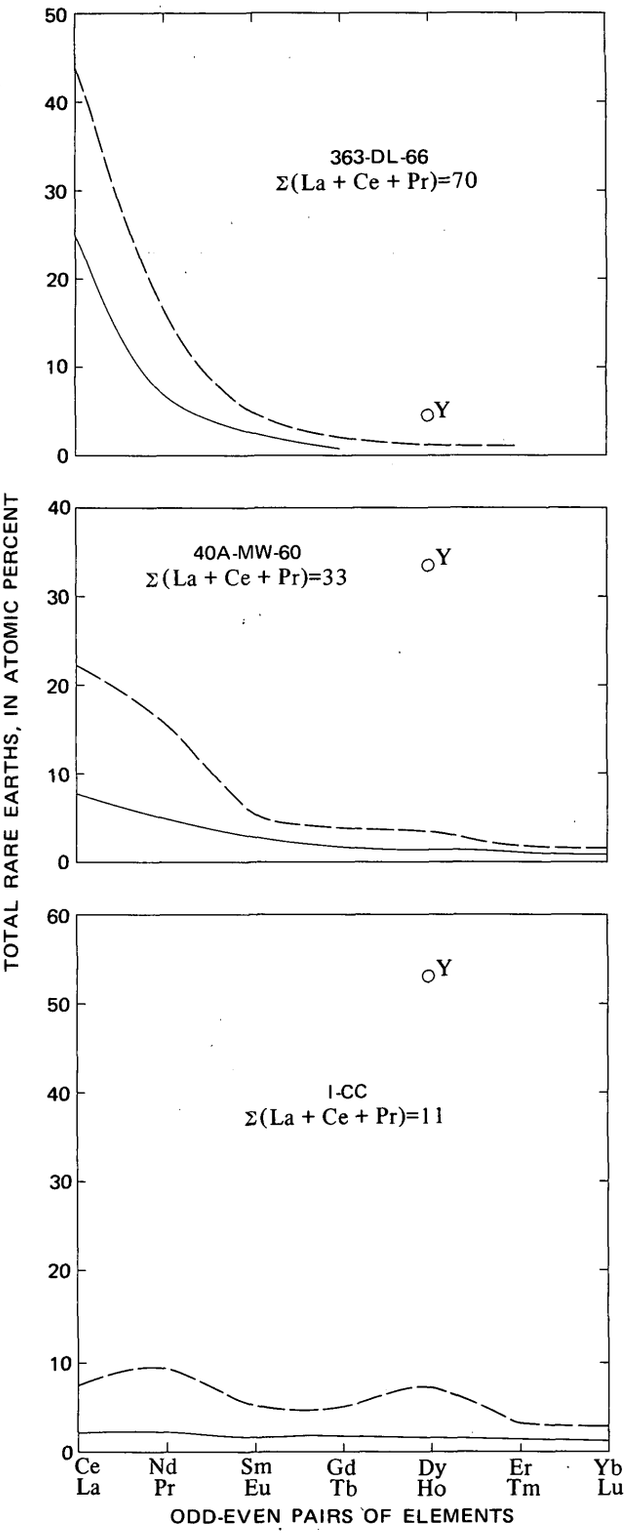

Figure 1.—Range of distribution of rare earths shown by three apatites, with Σ(La+Ce+Pr) value for each. Data for apatite 40A-MW-60 from Lee, Van Loenen, and Mays (1973); data for other two from table 2, this report. The relationship of yttritum (Y) to the other rare earths is indicated. Odd-even pairs of elements are arranged, left to right, in order of increasing atomic number.

2 are plotted on such a diagram, they include nearly the whole range of lanthanide compositions published for apatites from various environments, excluding a few apatites from pegmatites that show an extreme concentration of the heavier rare earths.

Adams (1969) summarized the several mechanisms (ionic radii differences, basicity, and accommodation in crystal lattices) that may contribute to fractionation of the lanthanide group of elements in rare-earth-bearing minerals. He illustrated lanthanide assemblages found in various minerals by means of graphs plotted in the form suggested by Semenov and Barinskii (1958), in which odd-even pairs of elements are arranged in order of increasing atomic number along the abscissa, and abundance in atomic percent along the ordinate.

The rare-earth assemblages of apatites 363-DL-66 and 1-CC are plotted in this way (fig. 1). Graphs for the other three apatites (table 2) are very similar to the one for 1-CC. A plot of the rare-earth assemblage present in apatite 40A-MW-60, from a hybrid granitoid rock (Lee and others, 1973), is included in figure 1. Fractionation of lanthanides in apatite 363-DL-66 is similar to that found in allanite, or even in bastnaesite (Adams, 1969, figs. 4*C* and 1*C*, respectively), while the assemblage in apatite 1-CC is similar to that found in gadolinite (Adams, 1969, fig. 1*E*). The plot for 40A-MW-60 does not resemble very closely any of the plots for various minerals featured by Adams (1969). As Fleischer and Altschuler (1969, p. 729) stated, "* * * the lanthanides in apatite * * * vary greatly in composition." Adams (1969, p. C43) also mentioned apatite as a mineral with a tolerance for all the rare earths, and a mineral which may therefore be a valuable guide "to changes in rare-earth composition that have taken place during the development of the rocks in which they are found."

The changes in rare-earth composition that took place during the development of the rock from which apatite 363-DL-66 was recovered may be similar to processes that lead to the formation of alkalic rocks and carbonatites. Goldschmidt, Hauptmann, and Peters (1933) and Goldschmidt (1937) first recognized the unusual abundance of rare-earth elements and the predominance of the most basic (lightest) of these elements in alkalic rocks, and Murata, Ross, Carron, and Glass (1957) emphasized the fact that cerium-earth minerals from alkalic rocks and carbonatites are rich in the most basic rare earths. Moreover, apatite is commonly well developed in alkalic rocks and carbonatites (see for example Deer, Howie, and Zussman, 1962, p. 333), and apatite 363-DL-66 makes up more than 1 percent of the host rock, as well as being unusually rich in total rare earths (table 1). Finally, the highest barium and strontium values were found in apatite 363-DL-66 (table 1), and these two elements are commonly enriched in alkalic rocks and carbonatites (Pecora, 1956).

Although it would be unwise to overinterpret data for a single mineral, we note finally that the granitoid rock containing apatite 363-DL-66 is exposed in contact with thinly interbedded limestones and sandstones (the Permian Pequop Formation of Steele, 1959; Snow, 1964, pl. 1). In a study of hybrid granitoid rocks from the southern Snake Range, Nev., Lee and Bastron (1967) found accessory allanite to contain a more basic assemblage of rare earths where the granitoid rock is in contact with limestone; and the rare-earth assemblages in accessory apatites from the same rocks show the same trend (Lee and others, 1973).

REFERENCES CITED

Adams, J. W., 1969, Distribution of lanthanides in minerals, *in* Geological Survey Research 1969: U.S. Geol. Survey Prof. Paper 650-C, p.C38–C44.

Deer, W. A., Howie, R. A., and Zussman, J., 1962, Non-silicates, v. 5 *of* Rock-forming minerals: New York, John Wiley and Sons, Inc., 371 p.

Evans, H. T., Jr., Appleman, D. E., and Handwerker, D. S., 1963, The least squares refinement of crystal unit cells with powder diffraction data by an automatic computer indexing method [abs.]: Am. Cryst. Assoc. Program and Abs., Ann. Mtg., 1963, no. E-10, p. 42–43.

Fleischer, Michael, and Altschuler, Z. S., 1969, The relationship of the rare-earth composition of minerals to geologic environment: Geochim. et Cosmochim. Acta, v. 33, p. 725–732.

Goldschmidt, V. M., 1937, The principles of distribution of chemical elements in minerals and rocks: Jour. Chem. Soc. London, 1937, p. 655.

Goldschmidt, V. M., Hauptmann, H., and Peters, C., 1933, Über die Berücksichtigung "seltener" Elemente bei Gesteins-Analysen: Naturwissenschaften, v. 21, p. 362–365.

Hose, R. K., and Blake, M. C., Jr., 1970, Geologic map of White Pine County, Nevada: U.S. Geol. Survey open-file map, scale 1:150,000.

Jackson, E. D., Stevens, R. E., and Bowen, R. W., 1967, A computer-based procedure for deriving mineral formulas from mineral analyses, *in* Geological Survey Research 1967: U.S. Geol. Survey Prof. Paper 575-C, p. C23–C31.

Lee, D. E., and Bastron, Harry, 1967, Fractionation of rare-earth elements in allanite and monazite as related to geology of the Mount Wheeler mine area, Nevada: Geochim. et Cosmochim. Acta, v. 31, p. 339–356.

Lee, D. E., Marvin, R. F., Stern, T. W., and Peterman, Z. E., 1970, Modification of potassium-argon ages by Tertiary thrusting in the Snake Range, White Pine County, Nevada, *in* Geological Survey Research 1970: U.S. Geol. Survey Prof. Paper 700-D, p. D92–D102.

Lee, D. E., and Van Loenen, R. E., 1971, Hybrid granitoid rocks of the southern Snake Range, Nevada: U.S. Geol. Survey Prof. Paper 668, 48 p.

Lee, D. E., Van Loenen, R. E., and Mays, R. E., 1973, Accessory apatite from hybrid granitoid rocks of the southern Snake Range, Nevada: U.S. Geol. Survey Jour. Research, v. 1, no. 1, p. 89–98.

Murata, K. J., Rose, H. J., Jr., and Carron, M. K., 1953, Systematic variation of rare-earths in monazite: Geochim. et Cosmochim. Acta, v. 4, p. 292–300.

Murata, K. J., Rose, H. J., Jr., Carron, M. K., and Glass, J. J., 1957, Systematic variation of rare-earth elements in cerium-earth minerals: Geochim. et Cosmochim. Acta, v. 11, p. 141–161.

Pecora, W. T., 1956, Carbonatites—A review: Geol. Soc. America Bull., v. 67, p. 1537–1555.

Semenov, E. J., and Barinskii, R. L., 1958, The composition characteristics of the rare earths in minerals: Geokhimiya, 1958, no. 4, p. 314–333 [In Russian]; translation in Geochemistry 1958, no. 4, p. 398–419.

Snow, G. G., 1964, Mineralogy and geology of the Dolly Varden Mountains, Elko County, Nevada: Utah Univ. Ph. D. thesis, 153 p., University Microfilms, Inc., Ann Arbor, Mich.

Steele, Grant, 1959, Basin and Range structure reflects Paleozoic tectonics and sedimentation [abs]: Am. Assoc. Petroleum Geologists Bull., v. 43, no. 5, p. 1105.

Wilcox, R. E., 1959, Use of the spindle stage for determination of principal indices of refraction of crystal fragments: Am. Mineralogist, v. 44, p. 1272–1293.

—— 1962, Cherkasov's "focal screening" for determination of refractive index by the immersion method, *in* McCrone, W. C., ed., Proceedings of the International Microscopy Symposium, Chicago, 1960–1962: Chicago, McCrone Associates, p. 160–165.

Jour. Research U.S. Geol. Survey
Vol. 1, No. 3, May-June 1973, p. 273–282

PETROGRAPHY AND STRUCTURAL RELATIONS OF GRANITIC BASEMENT ROCKS IN THE MONTEREY BAY AREA, CALIFORNIA

By DONALD C. ROSS and EARL E. BRABB, Menlo Park, Calif.

Abstract.—In the past, the granitic basement of the Coast Ranges has been thought to be dominantly quartz diorite and low in K-feldspar. However, a study of outcrops around Monterey Bay, basement well samples, and dredge samples from Monterey Bay shows that the granitic basement averages about 15 to 20 percent K-feldspar. Therefore, as a sedimentary provenance, the basement around Monterey Bay could have contributed abundant K-feldspar to the Cenozoic sedimentary deposits of the region; that is, in the Monterey Bay area the local basement is an adequate source for the abundant K-feldspar in the sedimentary units. The distribution of basement rocks and mapped faults, coupled with gravity-geophysical data, suggests that the area between the San Andreas and Sur-Nacimiento fault zones (the Salinian block) near Monterey Bay is broken into several discrete structural blocks. Some of these blocks juxtapose not only different basement rocks, but also different contour patterns on the buried basement surface. These features suggest large strike-slip movements along some faults within the Salinian block in the Monterey Bay area.

The Monterey Bay area (fig. 1) appears to be underlain by a dominantly granitic basement of Mesozoic age containing inclusions and roof pendants of older marble, schist, quartzite, and other metamorphic types (fig. 2). The granitic rocks range in composition from very felsic alaskites to dark gabbros, but the bulk of the outcrops is intermediate between these end types. Outcrops are mainly in the Ben Lomond area on the north, the Gabilan Range on the east, and the Monterey Peninsula and adjacent Monterey Bay on the south; farther south, the Santa Lucia Range is underlain by a mixture of metamorphic and granitic types.

This summary report provides a general picture of the composition and areal distribution of the granitic basement rocks in the Monterey Bay area. From this it may be possible to determine the provenance of Late Cretaceous and Tertiary sedimentary rocks in this area. Although in the past the granitic rocks of the Coast Ranges have been considered to be dominantly quartz diorite and low in K-feldspar, some of the Tertiary sedimentary units in this area contain abundant K-feldspar, which raises the question of whether or not there are suitable K-feldspar-rich rocks in this area to supply this Tertiary debris. Also, discontinuities in the present distribution and structural trends of the various basement types may reveal the presence of possible large faults.

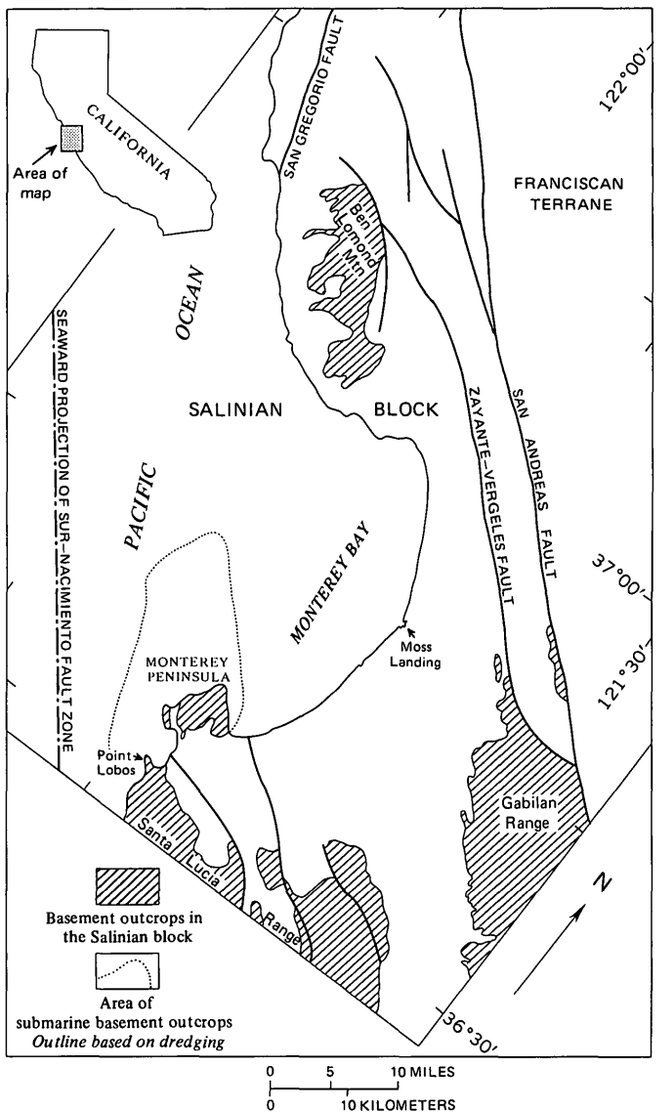

Figure 1.—Map of the Monterey Bay area, California.

Acknowledgments.—Texaco, Inc., and Union Oil Co. of California kindly provided cores of basement rocks in the Monterey Bay area. H. G. Greene, of the U.S. Geological

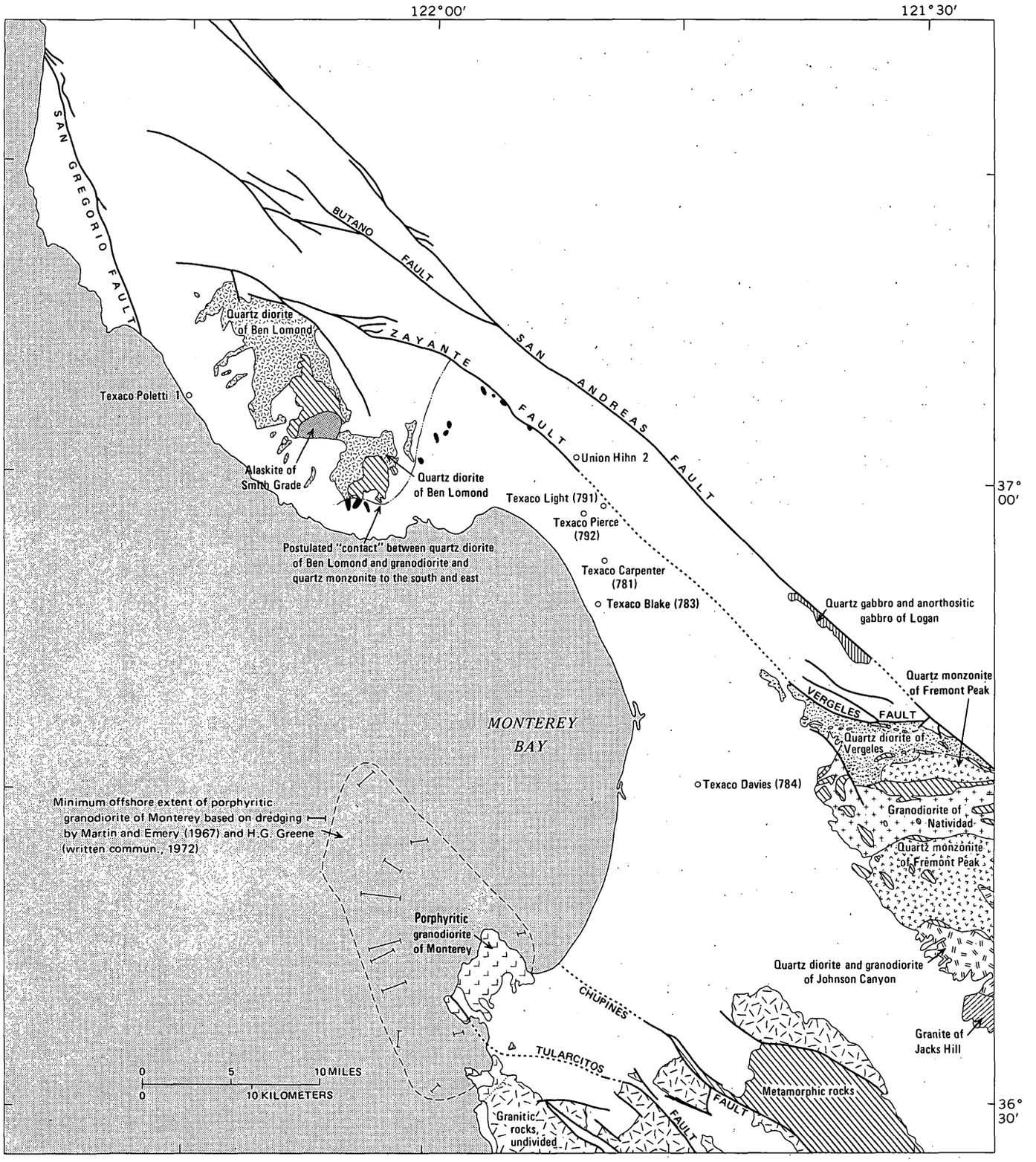

Figure 2.—Basement rock exposures in and around Monterey Bay, Calif. Open circles, locations of wells from which basement rock samples were studied.

Survey, furnished dredge samples from Monterey Bay. We also wish to thank D. L. Durham and T. W. Dibblee for their helpful reviews.

BEN LOMOND MOUNTAIN AREA

About 40 sq mi (104 km^2) of basement rocks is exposed in the Ben Lomond Mountain area. The dominant rock type, the hornblende-biotite quartz diorite of Ben Lomond Mountain, engulfs and intrudes a pendant composed of mica schist, marble, and quartzite several square miles in area. The alaskite of Smith Grade and several smaller alaskitic masses also cover a few square miles (fig. 2). The modal and petrographic data on the Ben Lomond rocks are taken in part from Leo (1967) and are supplemented by additional data from Ross (1972a).

Figure 3 shows the general modal distribution of the two main granitic masses. The alaskite of Smith Grade is a medium- to coarse-grained rock composed of nearly equal amounts of sodic plagioclase, K-feldspar, and quartz, together with a couple percent of biotite and trace amounts of garnet. There is some controversy about the relative age of this unit. Compton (1966, p. 285) thinks that it predates the main Ben Lomond mass, and Ross (1972) thinks it is a late plug related to garnet-bearing dikes that cut the Ben Lomond mass. Nonetheless, the largest body of alaskite is almost completely surrounded by the quartz diorite of Ben Lomond (fig. 2) and probably extends for no more than twice its exposed size under the overlying sediments to the south. Judging from the exposed basement sample of the Ben Lomond area, which contains only a few small alaskite plugs and dikes, we do not think that there are any very large alaskite masses in the buried basement nearby.

The more important basement unit, and the one that is more likely to have substantial subsurface extent, is the quartz diorite of Ben Lomond. This rock consists of about one-half andesine, one-quarter quartz, and one-quarter biotite and hornblende. K-feldspar normally is only a few percent, but Leo (1967) reported as much as 12 percent locally. The ternary plot of feldspar and quartz (fig. 3) shows that most specimens from the main mass fall in the quartz diorite field, but that isolated masses to the east stretch the composition well over into the quartz monzonite field. East of the main mass, the K-feldspar content of the granitic rocks is considerably higher over a rather large area. Leo (1967, p. 37) described the granodiorite of Wilder Creek at the south end of the main mass and suggested that this rather felsic biotite-bearing rock may be a gradational phase of the Ben Lomond mass. It is interesting to note that the modes of the Wilder Creek rocks recorded by Leo (fig. 3) are in the same general range as those of the isolated masses east of the main Ben Lomond body. J. C. Clarke, who was able to study several well cores, in addition to outcrops, in the area of Wilder Creek, reported gradations of rock types from quartz diorite to quartz monzonite (oral commun., 1970). It appears that both to the south and east the Ben Lomond basement becomes considerably richer in K-feldspar. A "contact" on figure 2 emphasizes this relation; however, limited examination of some of the small, isolated bodies east of Ben Lomond suggests that these are variations of the quartz diorite, rather than a separate intrusive mass.

GABILAN RANGE

The Gabilan Range is a dominantly granitic massif covering more than 300 sq mi. At the northern end of the range, which is of most interest in this report, the main rock types are the quartz diorite of Vergeles, the granodiorite of Natividad, and the quartz monzonite of Fremont Peak (fig. 2). The metamorphic rocks in the northern part of the range are dominantly marble and mica schist, with lesser calc-hornfels and tactite, and rare quartzite. Additional petrographic and modal data on these rocks are given by Ross (1972a).

The quartz diorite of Vergeles ranges to granodiorite (fig. 3), and the modal average is probably close to the boundary between these two types. The Vergeles mass is a normal granitic-looking rock composed of about 50 percent plagioclase, 20 to 30 percent quartz, about 20 percent biotite and hornblende, and as much as 15 percent K-feldspar. The Vergeles mass seems to be abruptly cut off to the northeast by the Vergeles fault. Ross (1972a, p. 33) has suggested that this mass may be correlative with the quartz diorite of Ben Lomond.

The granodiorite of Natividad is finer grained and physically distinguishable from the Vergeles unit, but the two rocks have somewhat similar modal compositions. Some question exists as to whether these are two separate intrusives or two facies of one mass, but nevertheless both units could contribute about the same sort of debris to sedimentary deposits.

The quartz monzonite of Fremont Peak is coarse-grained felsic granitic rock composed of about equal amounts of sodic plagioclase, K-feldspar, and quartz, and a few percent of biotite. This mass, which intrudes the Vergeles and Natividad units, underlies two large areas in the northern part of the range.

North of the Gabilan Range (fig. 2) is a thin sliver of basement rocks along the San Andreas fault. These rocks, quartz gabbro and anorthositic gabbro, are quite distinct from any of the granitic basement units in this region (Ross, 1970). They are composed of calcic plagioclase, hornblende, pyroxene, and less quartz and are virtually devoid of K-feldspar, except for some minor pegmatitic dikes.

MONTEREY PENINSULA AND BAY

The Monterey Peninsula and the Point Lobos areas to the south are both underlain by coarse-grained porphyritic granodiorite. Present outcrops span some 20 sq mi, and these rocks almost certainly extend some as yet unkown distance to the south and east. For example, nearly 20 miles to the southeast in the Santa Lucia Mountains, similar granitic rocks are

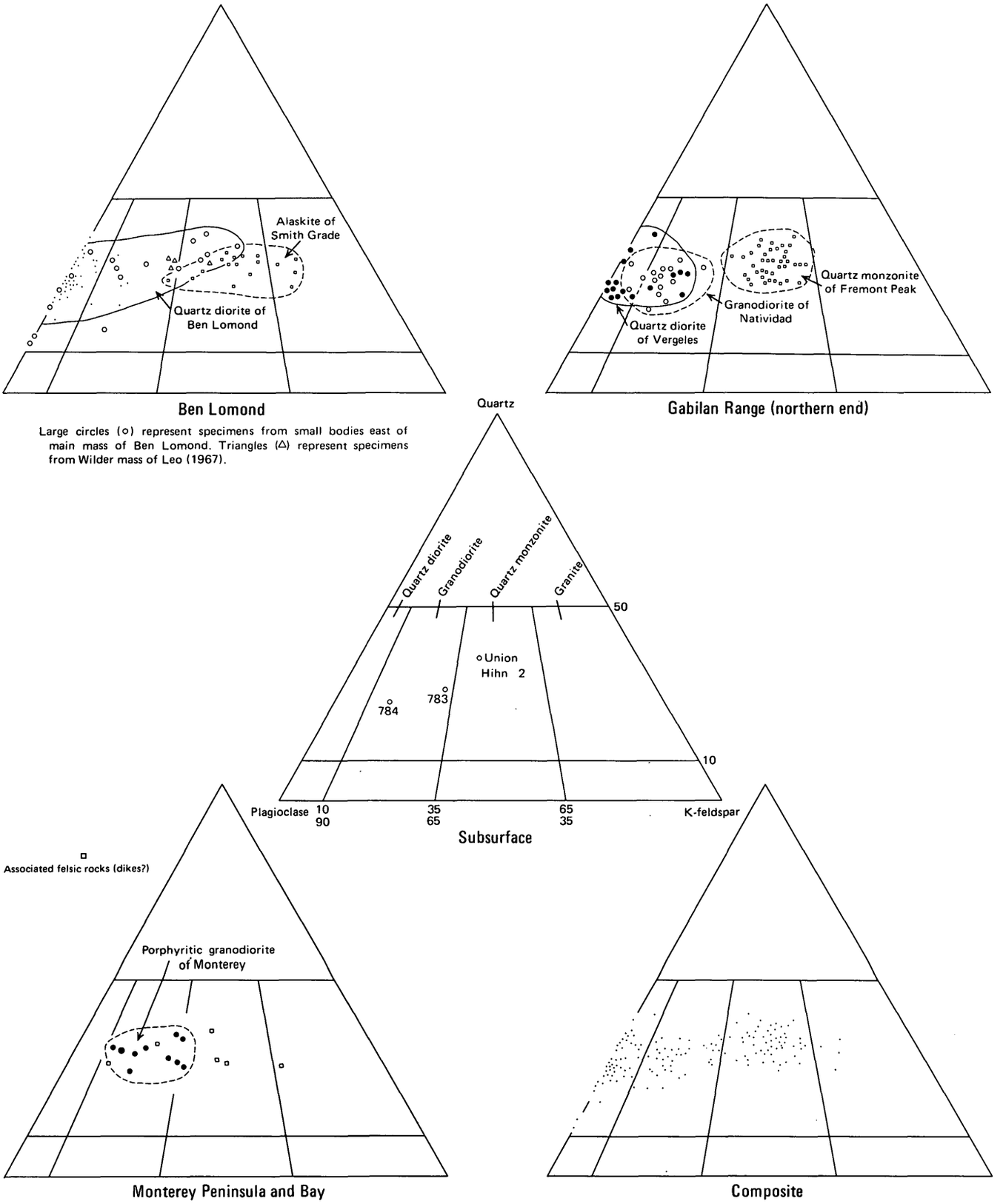

Figure 3.–Ternary diagrams showing modal data for the Monterey Bay area, California.

exposed (Alf Piwinskii, oral commun., 1969). The detailed granitic geology has not yet been worked out for the area of figure 2 labeled "granitic rocks, undivided." However, from the work of Compton (1966) and Wiebe (1970), we know that the granitic basement of the Santa Lucia Range encompasses a wide range of compositions and includes abundant quartz monzonite and granodiorite.

According to the few samples analyzed, the Monterey mass is a granodiorite having a modal composition of about 50 percent sodic plagioclase, 30 percent quartz, 15 to 20 percent K-feldspar, and 5 to 10 percent biotite. Primary muscovite is also present in this body. K-feldspar phenocrysts as large as 30 mm in longest dimension are distinctive in this rock. Rocks as coarsely porphyritic as the Monterey mass do not lend themselves to accurate modal analysis, but the overall abundance of K-feldspar in this mass is nevertheless indisputable, judging from the abundance of K-feldspar phenocrysts in many outcrops.

The extension of this mass offshore from the Monterey Peninsula has been confirmed by dredging. Martin and Emery (1969, p. 2288) briefly described dredged specimens in which they noted that, though mineral percentages varied, a typical sample was 35 percent quartz, 30 percent K-feldspar, 20 percent oligoclase, 10 percent biotite, and 5 percent chlorite. Further dredging in 1971 and 1972 by H. G. Greene extended the area of known granitic outcrop in the bay both north and south of the area of Martin's and Emery's work. The present known extent of offshore granitic outcrops is shown by the dashed line on figure 2. Greene kindly furnished us with specimens from these dredge hauls; the dominant material was found to be porphyritic granodiorite that was similar to the exposures on Monterey Peninsula. Associated with the porphyritic rocks were finer grained rocks, rich in K-feldspar, that may be from satellitic bodies or dikes. Thus it seems highly likely that an offshore area of more than 100 sq mi is underlain by rocks rich in K-feldspar and generally similar to the rocks on the Monterey Peninsula. These rocks almost surely also extend some distance farther north under the sediments of the bay. They do not appear to extend very far south, however, at least along the coast. One of the samples from the southernmost dredge line is a quartz diorite containing pseudomorphs of hornblende as well as abundant biotite; quartz diorite containing abundant hornblende and biotite is also found along State Highway 1 about 4 miles south of Point Lobos.

DATA ON SUBSURFACE GRANITIC BASEMENT ROCKS

The outcrop data have been supplemented by the acquisition of basement samples from cores of six wells drilled for oil between Ben Lomond Mountain and Gabilan Range and another sample core west of Ben Lomond. The locations of these wells are plotted on figure 2. These widely isolated core samples are particularly valuable to help determine the types of basement rock between the exposures of Ben Lomond and the Gabilan Range and therefore deserve individual description. The limitation on drawing conclusions from these scattered cores is, we trust, readily obvious to readers.

Union Hihn Well 2.—From this well we have four samples from 3,436 feet, where basement was first found, to 3,507 feet, and a fifth sample from the interval 3,565 to 3,569 feet, the total depth of the well. An additional sample of arkosic sand, rich in K-feldspar, from the interval 3,413 to 3,436 feet appears to overlie the basement immediately. All the quartz-rich, felsic granitic samples are very similar. They are quartz monzonite with an average mode of 35 percent andesine, 26 percent K-feldspar, 36 percent quartz, and 3 percent medium-brown biotite. Zircon is present in all samples; metallic opaque grains are extremely rare, and at least some of them are pyrite. Modally, these rocks resemble some of those exposed east of the main Ben Lomond basement outcrops. Texturally, they are somewhat finer grained, aplitic in part, and contain lacy, irregular growths of K-feldspar; but they bear textural resemblance to some of the finer grained and less felsic rocks east of Ben Lomond. These rocks are very tenuously considered to be a continuation of the quartz diorite of Ben Lomond; but even if the correlation is erroneous, they still provide another sample point of granitic basement relatively rich in K-feldspar.

The plotted position of Union Hihn well 2 is about 1,000 feet east of the mapped trace of the Zayante fault; yet the granitic material at the bottom of the hole seems to be related to the basement rocks west of the fault in the Ben Lomond-Gabilan block, which crop out only 3 miles to the northwest. A short distance northeast of the Hihn well 2, Union Hihn 1 went down 7,747 feet and was still in Miocene rocks, which suggests that there is a basement break (the Zayante fault) between the bottoms of Hihn wells 1 and 2. A dip of 70° or less to the east on the Zayante fault would permit the Union Hihn 2 to bottom on the west side of the fault; a southwestward deflection of the well would also produce the same effect. With the present limited data, it seems most logical to speculate that the Hihn 2 basement rocks belong to the Ben Lomond-Gabilan block.

Texaco Light (791).—Two samples are available from this well. One from 3,240 feet is a "granitic breccia" that could represent either fragmental material near the contact with the basement rocks or tectonic breccia; it is probably the former. The other sample from 3,620 feet is extensively weathered but appears to be quartz diorite containing abundant black biotite. Both specimens contain little K-feldspar. It is impossible to relate these samples adequately to any granitic basement of the region. General composition and appearance make correlation with the Ben Lomond rocks permissible; little more can be said.

Texaco Pierce (792).—Three samples from intervals 2,633 to 2,637, 2,637 to 2,642, and 2,642 to 2,655 feet are light-gray aplitic rocks that are liberally sprinkled with small flakes of yellowish-orange biotite, grains of sphene, and as much as 2 percent small pyrite crystals. Thin-section appearance definitely suggests that these rocks are aplite, but it is possible that

they are fine-grained hornfelses.

Texaco Carpenter (781).—Samples from 3,050 and 3,096 feet are both dark-gray medium- to fine-grained quartz-bearing diorite containing small plagioclase phenocrysts as long as 3 mm. In general appearance the specimens resemble inclusion material that is common in granitic rocks, but the fact that the hole passed through at least 46 feet of this material and that no other basement rock type was recovered suggests that a diorite body was penetrated. The mode of this rock is 41 percent intermediate andesine, 5 percent quartz, 43 percent pale-greenish-yellow to pale-olive hornblende, and 11 percent yellowish-orange to moderate-reddish-brown biotite. Accessory apatite, zircon, and magnetite are also present.

Texaco Blake (783).—Samples were obtained from the basement rocks at 2,426, 2,458, and 2,462 feet. The upper and lower samples are light-gray aplites that are somewhat banded by variation in grain size and K-feldspar content and somewhat streaked with yellowish-orange to brown biotite. These samples look much like those from the Texaco Pierce (792) hole. The sample from 2,458 feet, however, is a medium- to coarse-grained, weakly porphyritic granitic rock. It is composed of 40 percent zoned sodic to intermediate andesine, 20 percent K-feldspar, 24 percent moderately strained quartz, and 16 percent brown biotite. Trace amounts of grayish-green hornblende are present, as are sphene, allanite, epidote, apatite, and zircon. No metallic opaque grains were seen in the specimen studied. This biotite granodiorite bears a striking resemblance to much of the rock in the isolated outcrops east of the main Ben Lomond mass and is considered here to be correlative of those rocks. The aplites are presumably dikes or small masses, which are also present in the Ben Lomond area.

Texaco Davies (784).—One basement sample from 2,194 feet is a relatively fresh, medium-light-gray granitic rock containing abundant dark minerals in fairly large crystals. This rock is a granodiorite that is hypautomorphic granular and is composed of 51 percent sodic andesine, 10 percent K-feldspar, 21 percent quartz, 11 percent dark-yellowish-brown biotite, and 7 percent grayish- to medium-green hornblende. Some of the dark mineral plates are as much as 5 mm across. Sphene crystals as large as 3 mm across are most abundant as an accessory mineral; minor apatite, zircon, allanite, and the merest traces of metallic opaque minerals are also seen. The K-feldspar tends to occur in large, lacy, interstitial masses rather than in discrete crystals.

The general appearance of this rock as well as its modal composition suggest that it is a correlative of the Vergeles mass of the Gabilan Range. Rocks with abundant, large, discrete dark-mineral plates like those in this specimen are not only characteristic of the Vergeles mass but also are present in the Ben Lomond mass, as well as in other Coast Ranges granitic outcrops farther north. This recurring, rather distinctive texture has led Ross (1972a) to suggest that the Vergeles mass and the rest of the granitic basement north to Bodega Head are a comagmatic, closely related granodiorite-quartz diorite terrane, or possibly even one large pluton, into which numerous, younger, more felsic masses have been intruded.

Texaco Poletti 1.—In this well near the coast west of Ben Lomond, basement was hit at about 9,000 feet, and three samples were examined from 9,163, 9,191, and 9,193 feet. Another basement sample is available from an unknown depth below 9,000 feet, and still another sample was examined briefly and subsequently lost. The sample from an unknown depth is a massive medium-grained biotite quartz monzonite to granodiorite with schistose to gneissose layers. Some concentrations of pinkish K-feldspar are present but not quite discrete enought to be phenocrysts; K-feldspar crystals about 55 mm long were observed in the core that was lost. The schistose-gneissose layers are composed of quartz, sodic plagioclase, and olive-brown biotite, as well as abundant secondary calcite. The layered part of the specimen appears to lack K-feldspar, in sharp contrast to its abundance in the adjoining granitic rock. This rock somewhat resembles the porphyritic granodiorite of Monterey and, probably more importantly, does not seem to resemble the nearby surface outcrops of the Ben Lomond mass.

The three basement samples from near the top of the basement in this well are all brecciated to some extent with anastomosing shear zones rich in chloritic material. There is no mylonite, but crushing and shearing are suggested from the specimens. The original rock in all three samples was a relatively quartz-rich biotite granodiorite. None of these samples resemble the nearby Ben Lomond basement rocks.

REGIONAL CONSIDERATIONS

The new well-core data allow us to extend the Ben Lomond granitic basement tentatively some 12 miles farther southeast. But more significantly they allow us to enlarge the area of granitic rocks relatively rich in K-feldspar east and south of the Ben Lomond mass. Well 784 permits us to extend the Vergeles mass of the Gabilan Range some 7 miles farther west. Even with these new data, however, there is still a 10-mile gap between the Gabilan outcrops and the nearest well with granitic rock like that in the Ben Lomond area.

Figure 4 is a highly speculative interpretation of the configuration of granitic basement rocks beneath the cover of Mesozoic and Cenozoic sedimentary and volcanic rocks and sediments. It was constructed partly from oil test-well data, partly from gravity data or profiles by Clark (1970), H. C. Sieck (unpub. data), and J. W. Fairborn (unpub. data), and partly from an analysis of geologic maps by Clark (1970), Bowen (1965), and Brabb (1970). Even though the data points are few and scattered, the abrupt change in depth to granitic basement rocks across inferred faults is well established. Some of the irregularities in the surface of these granitic basement rocks, such as the reentrant in the Moss Landing area, could be due to erosion by fluvial process prior to submergence, as suggested by Starke and Howard (1968), but other irregularities seem related to folding or warping of the basement rocks.

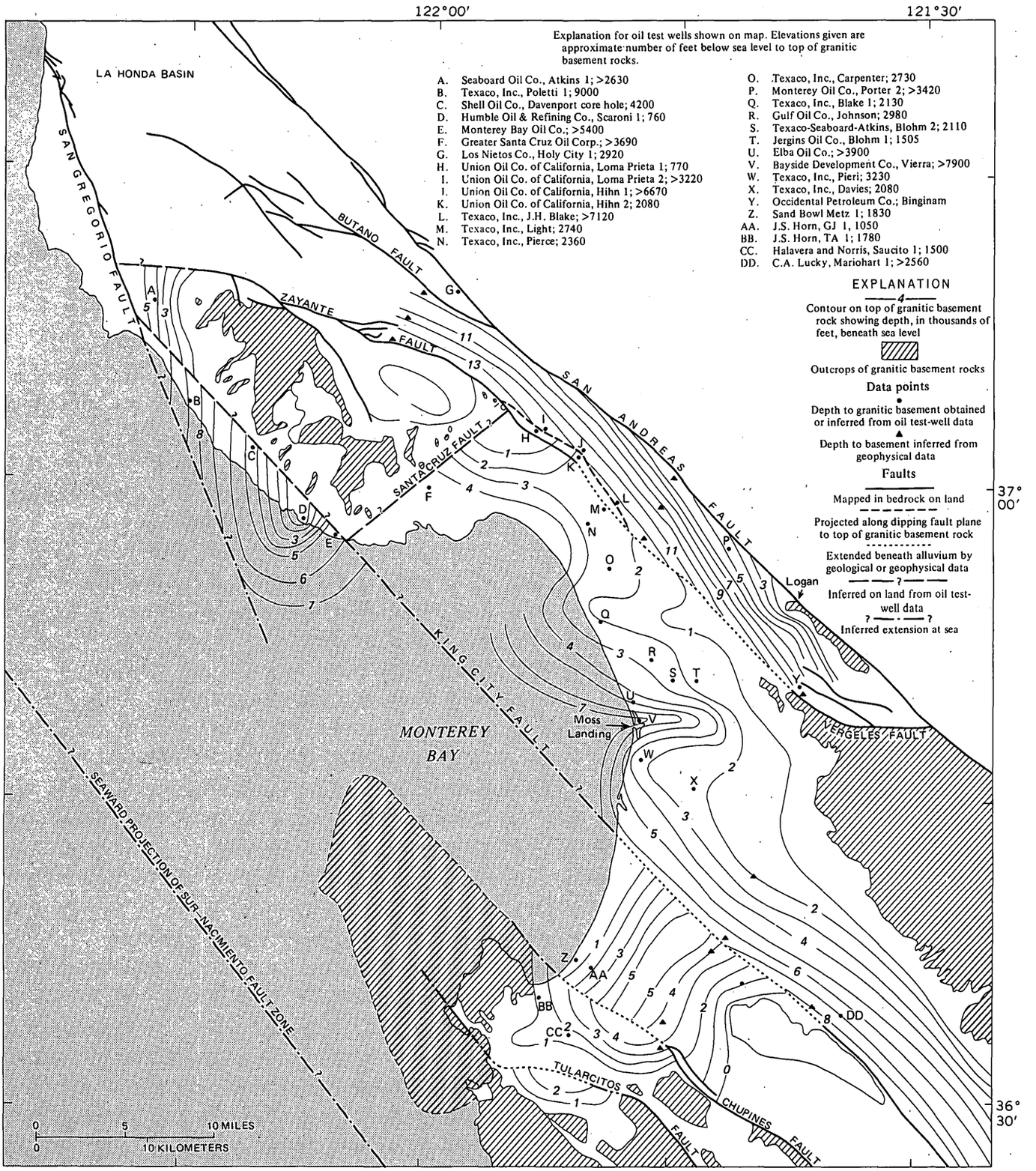

Figure 4.—Map showing depth to granitic basement rocks and major fault systems in the Monterey Bay area, California. The map is highly speculative and is based on relatively few data points.

Such deformation was postulated many years ago, mainly on geomorphic evidence, by Rode (1930), and more recently by Cummings, Touring, and Brabb (1962, p. 214) and Gribi (1957, fig. 6). Termination of the folded surfaces at faults and the abrupt change in strike of these surfaces across faults suggest that the deformation was not related to simple up-and-down movement of the faults or simple compression of the blocks, but rather that it was complex and associated with extensive strike-slip movement. In support of this argument, Bowen (1965, p. 66) has postulated at least some right-lateral movement on the Tularcitos and Chupines faults, largely on the basis of offset of a middle Miocene formation. If so, then the granitic rocks in the Monterey area may be juxtaposed from terranes that were once widely separated.

Two new faults are proposed to explain abrupt changes in depth to basement rocks reached by oil test wells. Neither fault has any known surface expression, and both seem to be older than late Miocene. The Santa Cruz fault seems to extend northeastward from Santa Cruz at least to the Zayante fault. A slight deflection in the San Andreas fault along the extension of the Santa Cruz fault may or may not be coincidental. The King City fault, as mapped originally by Clark (1929) and later by Bowen (1965) in the Salinas River area, is extended across Monterey Bay and northwestward from Santa Cruz at least to the San Gregorio fault. The extension of the King City fault was also recognized but not mapped or named by Starke and Howard (1968, p. 822–823) on the basis of the same oil test-well data. Directly on strike to the south of the King City fault is the Reliz-Espinosa-San Marcos-Rinconada fault zone, a regionally significant feature that is probably continuous with the King City fault in the Monterey Bay area. Dibblee (1972, p. 145–146) has noted that drag folding associated with this fault zone indicates right-lateral movement. He postulates that strata of Late Cretaceous to early Tertiary age have been offset in a right-lateral sense nearly 40 miles along this zone.

On the basis of the distribution of basement rock types, we can speculate that the striking contrasts in basement rocks across both the Zayante-Vergeles and King City faults (fig. 4) require some lateral movement, whereas the distribution of basement across the Santa Cruz fault requires only moderate dip-slip movement. At both the north and south ends of the Zayante-Vergeles fault zone, petrographically similar granitic rocks abut the west side of the fault. In between those larger outcrop areas, isolated granitic outcrops and well and gravity data suggest a relatively shallow movement along the west side of the fault. East of the fault there are no exposures of Salinian block-type granitic rocks. The only basement exposed is the unusual gabbro of Logan, which Ross (1970) has suggested may be exotic and unrelated to the granitic rocks of the Salinian block to the west. The contrast in basement contours across the fault (fig. 4) could possibly result solely from vertical fault movement, but the markedly different basements across the fault suggest that lateral movement has juxtaposed these different rocks. From the present data, we must also entertain the possibility that the Zayante-Vergeles block is underlain by Franciscan basement, rather than Salinian granitic basement.

The Santa Cruz fault, in contrast, has similar, possibly correlative granitic basement rocks on both sides. Basement evidence suggests that this may be a dip-slip fault of moderate displacement that has had little effect on distribution of the basement rocks.

The King City fault, however, appears to have had significant effect on the distribution of the basement rocks. The core material from the Texaco Poletti well 1 has some resemblance to the basement of Monterey Peninsula, but none to the nearby exposures of granitic rocks of the Ben Lomond area. Also, Ross (1972a) has suggested that the basement of the Gabilan Range is different from the basement of the Santa Lucia Range of the Monterey block west of the King City fault. Preliminary study suggests that the dominantly granitic Gabilan basement has little in common with the largely metamorphic Santa Lucia basement, although many areas in the Santa Lucia Range have not yet been examined in detail. The contrast in basement rocks across the proposed King City fault seems to require more than dip-slip fault movement. It seems more probable that strike-slip movement on the King City fault has juxtaposed these contrasting basement terranes.

From the surface and subsurface data around and under Monterey Bay, we can make some generalizations about the overall composition of the basement rocks. More specifically, for the purposes of this report, we can generalize about the K-feldspar content of the basement rocks in this area. From the preceding discussion of modal composition and structural blocks in this region, a generalized basement map can be constructed (fig. 5). Within the outlined semicircular area, an average K-feldspar content can be estimated for each postulated basement block. Weighting each area according to size, an average K-feldspar content of 15 percent is obtained for the approximately 1,000-sq-mi area. It is also possible to estimate an average granitic composition for this area by assuming that the Monterey Bay area is representative of the granitic basement of the entire Coast Ranges. For the 450 sq mi of granitic rocks exposed in the Coast Ranges (excluding the Santa Lucia Range), Ross (1972a) has estimated that they consist of 40 percent quartz monzonite, 36 percent granodiorite, 23 percent quartz diorite, and 1 percent diorite and gabbro. It should be remembered, however, that the Monterey Bay area is between the central Coast Ranges with a generally higher proportion of quartz diorite and the southern Coast Ranges (Gabilan Range and to the south) where granodiorite and quartz monzonite greatly predominate. Nevertheless, if we use these average amounts, we could postulate about 20 to 25 percent K-feldspar as a general amount for the Monterey Bay area. However, considering all the uncertainties that result from both these methods based on limited data, 15 to 20 percent of K-feldspar is probably a fair estimate of overall content in the granitic rocks of the Monterey Bay area. The composite plot of all the modal data from the Monterey Bay area (fig. 3) shows that there is a wide range of composition

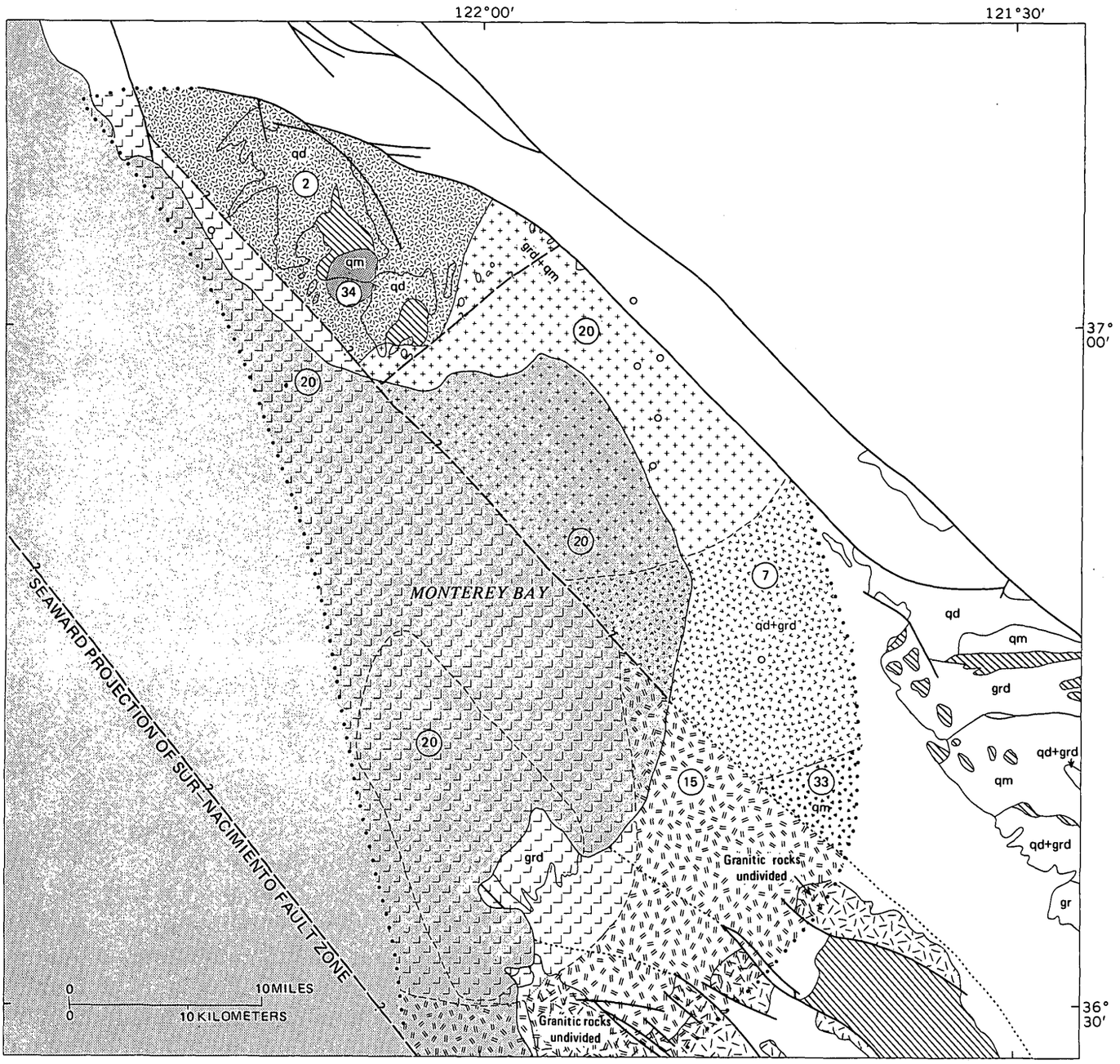

Figure 5.—Estimated percentage of K-feldspar (circled numbers in patterned areas) in granitic basement in and around Monterey Bay, Calif., within area enclosed by heavy dotted line. Generalized granitic type shown for each basement segment by letter symbols: qd, quartz diorite; grd, granodiorite; qm, quartz monzonite; gr, granite. Metamorphic rocks (diagonal line pattern) are presumed to occupy only a small part of the area outlined by the heavy dotted line. Open circles, locations of wells (see fig. 2).

and relatively abundant source material for significant amounts of K-feldspar in the sedimentary section derived from this basement, even though the plot is somewhat weighted in favor of the K-feldspar-rich rocks, which were more densely sampled in the Ben Lomond area.

Generally, the Monterey Bay area rocks have 20 to 30 percent quartz and from 10 to 25 percent dark minerals, so we can predict an overall range of plagioclase from 25 to 50 percent. Thus sedimentary units that received granitic debris might be expected to receive about twice as much plagioclase as K-feldspar. However, a relative enrichment of K-feldspar over plagioclase may take place during the weathering process because much of the plagioclase in the granitic rocks is to some extent altered, whereas K-feldspar is generally much

fresher. The plagioclase of these granitic rocks is much more likely to break down during mechanical weathering than is the K-feldspar because much of it is already partly saturated with micaceous and clayey alteration material. Also these somewhat altered plagioclase crystals should be much more receptive to additional chemical alteration during the weathering process.

Some of the Tertiary sedimentary rocks that could have been derived from granitic basement rocks surrounding Monterey Bay have been described by Cummings, Touring, and Brabb (1962). These sedimentary rocks occur in the La Honda basin, north of Ben Lomond Mountain (fig. 2). Cummings and his colleagues found that sandstones of Eocene and Oligocene age have about 30 percent K-feldspar and 10 percent plagioclase, whereas sandstones of Miocene age, according to Brabb (1960, p. 72), contain as much as 92 percent plagioclase and only 5 percent K-feldspar. The change in ratio of feldspar is attributed to a significant change in source areas during early or Middle Miocene time. The source for the Eocene and Oligocene sediments was thought by these authors to be south and west of the present outcrops of predominantly quartz diorite on Ben Lomond Mountain, in what is now the Pacific Ocean, whereas the Miocene sediments were thought to come directly from the Ben Lomond Mountain area. Corroboration for at least the southern source during the Eocene has been provided by Nilsen (1971).

These data provide additional clues to understanding the structural framework of granitic basement rocks in the Monterey Bay area. If major strike-slip dislocations have occurred, then movement of the Monterey block away from the La Honda basin probably occurred in early or middle Miocene time.

REFERENCES CITED

Bowen, O. E., 1965, Stratigraphy, structure and oil possibilities in Monterey and Salinas quadrangles, California: Am Assoc. Petroleum Geologists, 40th Ann. Mtg., Pacific Sec., Bakersfield, Calif., 1965, p. 48–67.

Brabb, E. E., 1960, Geology of the Big Basin area, Santa Cruz Mountains, California: Stanford Univ., Stanford, Calif., Ph. D. thesis, 197 p.

—— compiler, 1970, Preliminary geologic map of the central Santa Cruz Mountains, California: U.S. Geol. Survey open-file rept.

Clark, B. L., 1929, Tectonics of the Valle Grande of California: Am. Assoc. Petroleum Geologists Bull., v. 13, no. 3, p. 199–238.

Clark, J. C., compiler, 1970, Preliminary geologic and gravity maps of the Santa Cruz–San Juan Bautista area, Santa Cruz, Santa Clara, Monterey, and San Benito Counties, California: U.S. Geol. Survey open-file rept.

Compton, R. R., 1966, Granitic and metamorphic rocks of the Salinian block, California Coast Ranges: California Div. Mines and Geology Bull. 190, p. 277–287.

Cummings, J. C., Touring, R. M., and Brabb, E. E., 1962, Geology of the northern Santa Cruz Mountains, California: California Div. Mines and Geology Bull. 181, p. 179–220.

Dibblee, T. W., Jr., 1972, Rinconada fault in the southern Coast Ranges, California, and its significance: Geol. Soc. America Abs. with Programs, v. 4, no. 3, p. 145–146.

Gribi, E. A., Jr., 1957, Santa Cruz basin holds important promise: Oil and Gas Jour., v. 55, no. 13, p. 113–116.

Leo, G. W., 1967, The plutonic and metamorphic rocks of the Ben Lomond Mountain area, Santa Cruz County, California: California Div. Mines and Geology Spec. Rept. 91, p. 27–43.

Martin, B. D., and Emery, K. O., 1967, Geology of Monterey Canyon, California: Am. Assoc. Petroleum Geologists Bull., v. 51, p. 2281–2304.

Nilsen, T. H., 1971, Sedimentology of the Eocene Butano Sandstone, a continental borderland submarine fan deposit, central Coast Ranges of California [abs.]: Geol. Soc. America Abs. with Program, v. 3, no. 7, p. 659–660.

Rode, Karl, 1930, Geomorphogenie des Ben Lomond, Kalifornien: Zeitschr. P. Geomorph., v. 5, p. 16–78, Trans. by John E. Kesseli, Dept. of Geography, California Univ. (manuscript).

Ross, D. C., 1970, Quartz gabbro and anorthositic gabbro–Markers of offset along the San Andreas fault in the California Coast Ranges: Geol. Soc. America Bull., v. 81, no. 12, p. 3647–3662.

—— 1972a, Petrographic and chemical reconnaissance of some granitic and gneissic rocks near the San Andreas fault from Bodega Head to Cajon Pass, California: U.S. Geol. Survey Prof. Paper 698, 92 p.

—— 1972b, Geologic map of the pre-Cenozoic basement rocks, Gabilan Range, Monterey and San Benito Counties, California: U.S. Geol. Survey Misc. Field Studies Map MF-357, scale 1:125,000.

Starke, G. W., and Howard, A. D., 1968, Polygenetic origin of Monterey Submarine Canyon: Geol. Soc. America Bull., v. 79, no. 7, p. 813–826.

Wiebe, R. A., 1970, Relations of granitic and gabbroic rocks, northern Santa Lucia Range, California: Geol. Soc. America Bull., v. 81, no. 1, p. 105–116.

Jour. Research U.S. Geol. Survey
Vol. 1, No. 3, May-June 1973, p. 283–287

A PHOTOGEOLOGIC METHOD FOR DETERMINING THE DIRECTION OF HORIZONTAL DILATION FROM PATTERNS OF EN ECHELON FRACTURING

By WENDELL A. DUFFIELD and KAZUAKI NAKAMURA[1],
Menlo Park, Calif., Tokyo, Japan

Abstract.—The direction of horizontal dilation in areas characterized by tensional tectonics can be determined from a statistical study of en echelon patterns of fracturing observed on aerial photographs. Relative to a north-south dilation, nearly all directions of zones of dextral (right-lateral) en echelon fractures lie in the northeast quadrant, while those of sinistral (left-lateral) en echelon fractures concentrate in the northwest quadrant. Statistically, directions of the two types of zones define unimodal frequency curves that intersect at about 90 degrees to, and thus define the direction of, applied dilation. The method has been field tested twice and is believed to be suitable for any area characterized by (1) generally unidirectional horizontal strain and (2) an adequate population of geologically contemporaneous fissures, including roughly equal development of sinistral and dextral en echelon arrays. Where exposures and aerial photograph coverage are adequate, the direction can be determined quickly to within about 10 degrees accuracy without fieldwork. The method should be useful for preliminary structural studies, especially in inaccessible areas.

A recently developed photogeologic method for determining the azimuth of horizontal extension for areas characterized by tensional tectonics has been tested in the median zone of southwest Iceland (Nakamura, 1970) and in the Koae fault system of Kilauea Volcano, Hawaii. The method predicts the direction of horizontal extension from the interrelations of the azimuthal frequencies of zones of en echelon fractures and non-en-echelon or neutral fractures.

For both the Icelandic and Hawaiian examples, this predicted direction was initially determined by a quantitative study of the azimuthal frequency of zones of fissures on vertical aerial photographs. Subsequently, a brief field check in Iceland substantiated the predicted results there, and abundant measurements made directly on open cracks and normal faults proved those of the Hawaiian study to be nearly correct within the errors of the field measurements. Thus the photogeologic procedure may have general applicability in all areas that are characterized by (1) generally unidirectional extensional horizontal strain and (2) an adequate population of geologically contemporaneous fissures—neutral and about equally developed sinistral and dextral en echelon arrays. Accordingly, the method should be useful for preliminary structural studies of areas that lie astride loci of spreading in the upper mantle, zones such as the Koae fault system in Hawaii that are being forcibly torn apart by localized volcanic processes, areas where gravity sliding is common, and similar areas where generally unidirectional extensional tectonics prevail.

Acknowledgments.—We thank R. S. Fiske, M. D. Crittenden, and D. A. Swanson for helpful discussions of our study and useful suggestions for improving the manuscript. This paper is an outgrowth of related independent studies by both of us. Nakamura completed the analysis of aerial photographs of the Koae fault system while visiting Kilauea in the fall of 1970, and Duffield later contributed the field measurements. Nakamura thanks R. S. Fiske, D. L. Peck, H. A. Powers, and D. W. Peterson, of the U.S. Geological Survey, for the opportunity to visit the Hawaiian Volcano Observatory at Kilauea.

EXPERIMENTAL BASIS OF METHOD

The primary experimental basis for the new method of study is that a homogeneous brittle material tends to fail by fracturing perpendicular to the direction of pull under an applied tension (for example, see Billings, 1954, p. 94). There are, of course, many combinations of physical-chemical environments and materials under which simple right-angle brittle fractures would not form from such an applied tension, but in general, rocks at and near the surface of the earth will fail in this manner; it is to this environment that the proposed method is applied.

The reasons that tensional fractures often form en echelon patterns are not well understood, but apparently such an arrangement can result from several markedly different states of stress. Nakamura (1970) reported that en echelon arrangement of fractures is common when the trend of the zone of such fractures is oblique to the direction of dilation; Riedel shears are the extreme example in which the zone of fractures parallels dilation. Patterns of en echelon fractures may result from mechanical inhomogenieties in the failing material and

[1] Earthquake Research Institute.

also may result in surface rocks from a nonperpendicular arrangement between tension and a master fracture at some relatively shallow depth. The effectiveness of such master faults in producing en echelon patterns of fractures in overlying material has been demonstrated by Fiske and Cloos (see Fiske and Kinoshita, 1969) and by Fiske and Duffield (unpub. data) in experiments involving the fracturing of clay cakes.

En echelon fracturing resulting from underlying or related strike-slip movement on a master fault is either sinistral or dextral, depending upon the sense of strike-slip offset. However, in general, for areas under active unidirectional horizontal tension, both contemporaneous dextral and sinistral arrays can be expected, and such arrays are evidence of non-strike-slip origin. This criterion together with other types of evidence (for example, the presence of graben-horst topography and the absence of strike-slip offset and structures caused by compression) indicates areas to which the new method may be applied.

CLASSIFICATION OF ZONES OF FRACTURES

Although the arrangement of individual fractures into en echelon arrays may be simple (fig. 1*B*), natural examples are rarely, if ever, so clearly indicated, and their recognition normally requires judgment by the observer. If three or more parallel or semiparallel, generally partly overlapping fractures define a zone that is oblique to the trend of the fractures, we classify them as en echelon. If the zone and the individual fractures parallel one another, we classify the fractures as neutral.

These are simple and standard definitions, but natural sets of fractures may be confusing when studied at different scales. In general, fractures of both en echelon and neutral arrangement form zones of some finite width, and within each type of zone, the length of all fractures is not the same. Thus at one scale a group of fractures may be classified as a single zone of neutral type, but more detailed examination might well indicate the presence of many zones of both neutral and en echelon types.

In practice, the degree of detail of analysis is limited by the scale of available aerial photographs, and we have found that the classification of zones of fractures from photographs agrees very well with classification based on direct field observations, although a greater number of all types of zones is recognized from field study. Presumably, the results should be roughly the same at any scale of examination, but we suggest using a single scale which is most convenient for a given photogeologic study.

IDEAL MODEL AND PROCEDURE

Suppose that an area is characterized by fissures that formed in response to horizontal north-south tension. Experimental studies predict that such breaks will dip steeply and trend east-west. If zones of en echelon fractures are present, those zones which trend between north and east will show a right-lateral or dextral arrangement of fractures, and those between north and west a left-lateral or sinistral arrangement of fractures. Figure 1 is a sketch of a clay cake experiment by R. S. Fiske and Duffield which demonstrates this pattern.

The direction of horizontal extension for such a pattern of fracturing may be determined from the azimuthal frequencies of zones of en echelon fractures (fig. 2). Two smooth unimodal frequency curves, dextral arrays in the northeast quadrant and sinistral arrays in the northwest quadrant, intersect at an azimuth that is approximately perpendicular to the direction of tension. The frequency curve for zones of neutral fractures is centered in this same direction. The relative abundance of any single type of zone is a function of the shape of the underlying template and its relation to the actual direction of pull.

In practice the azimuth and length of the three types of fracture zones are measured and plotted separately, using

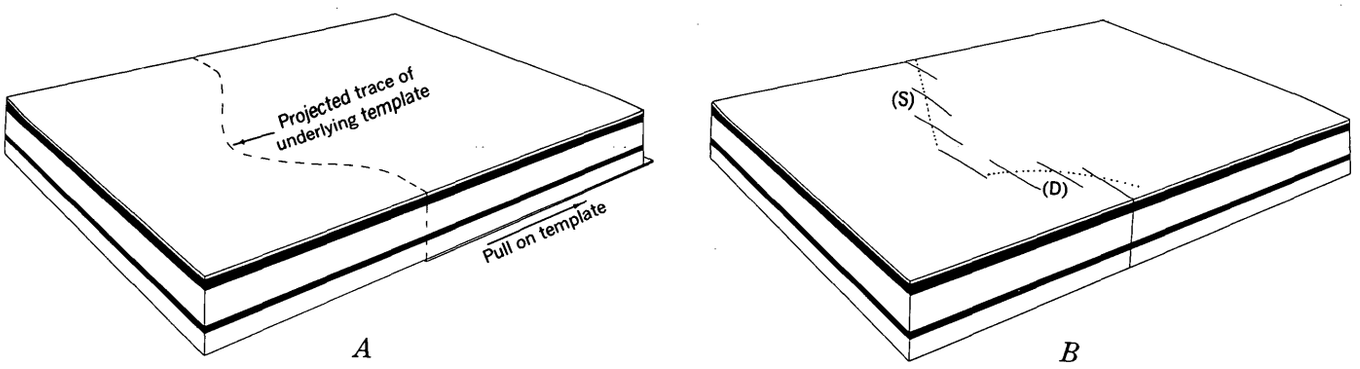

Figure 1.—Simplified sketch showing the pattern of fractures resulting from the unidirectional horizontal dilation of a tabular clay model.

A. The dilation is transmitted to the clay by an underlying template which is pulled in the direction indicated.

B. With continued pull, the clay fractures as indicated. The dotted lines show the average directions of zones of dextral (D) and sinistral (S) en echelon fractures; these directions fall in the northeast and northwest quadrants, respectively, relative to a north-directed pull on the template.

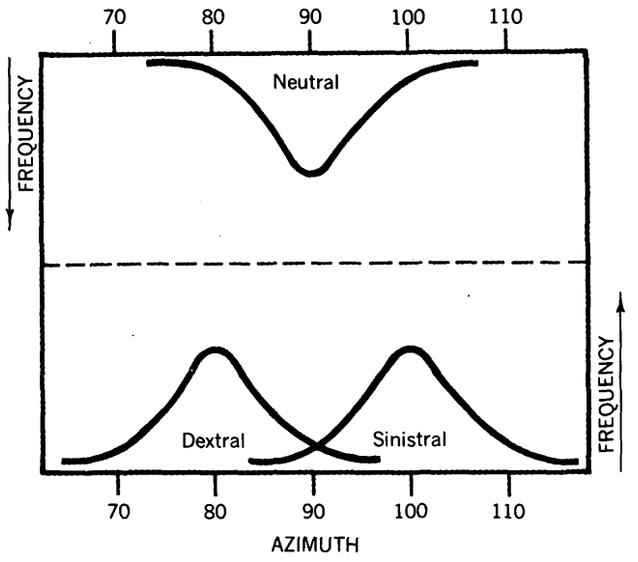

Figure 2.—Summary diagram showing the ideal arrangement of azimuthal frequency of zones of fractures resulting from a unidirectional horizontal tension along a north-south direction. Note that the maximum of the neutral curve and the intersection of curves for the en echelon zones lie on the east-west line.

length as a measure of frequency. Measurement can be made most accurately from constant-scale aerial photographs (orthophotographs) but can also be made adequately by less direct methods.

HAWAIIAN STUDY

The Hawaiian example provided a rigorous test of the new method because a detailed field study was completed subsequent to the preliminary determination of horizontal extension. This procedure permitted a check not only on the validity of the method, but also on the judgment of the photoinvestigator in deciding which fractures are indeed arranged en echelon.

The studied area is the Koae fault system, on the south flank of Kilauea Volcano, Hawaii. This system is about 2 km wide and 12 km long and is characterized by steeply dipping open cracks and normal faults. The fractures occur on a well-exposed part of the volcano and are well preserved since they are relatively young; the fault system itself is still active.

For the preliminary study, both uncorrected and constant-scale vertical aerial photographs were available. Most measurements of azimuth and length were made on zones of normal faulting since they were easiest to interpret; patterns of fracturing for small open cracks were often ambiguous at the scale of available photographs. The measurements were tabulated (table 1) and subsequently compiled as histograms (fig. 3). The histograms compare favorably with the ideal case illustrated in figure 2 and suggest that the direction of horizontal extension across the Koae fault system is about N. 30° W., S. 30° E. Neutral fissures favor a N. 65°–70° E. strike,

Table 1.—*Lengths and azimuths for zones of fissures in the Koae fault system*

Sinistral			Neutral			Dextral		
Photograph length (cm)	True length (km)	Azimuth	Photograph length (cm)	True length (km)	Azimuth	Photograph length (cm)	True length (km)	Azimuth
15....	0.72	112	12.5...	0.60	99	5....	0.24	46
30....	1.44	75	11....	.53	89	14....	.67	54
40....	1.92	94	27.5...	1.32	59	2.5..	.12	59
15....	.72	77	4.5...	.22	70	4....	.19	61
25.5..	1.22	74	8....	.38	58	5....	.24	41
7....	.34	89	10....	.48	69	3....	.14	60
19....	.91	68	16....	.77	64	7....	.34	48
15....	.72	62	12....	.58	79	14....	.67	54
6....	.29	90	9.5...	.46	66	8....	.38	65
7....	.34	63	5....	.24	90	15....	.72	54
26.5..	1.27	69	13....	.62	55	9.5..	.46	36
11.5..	.55	61	11....	.53	60	9.5..	.46	35
7....	.34	79	9.5...	.46	68	7....	.34	77
7....	.34	88	4....	.19	68	7.5..	.36	67
14....	.67	60	7....	.34	53	27....	1.30	48
11....	.53	81	4....	.19	80	5.5..	.26	69
8....	.38	78	11....	.53	68	15....	.72	60
24.5..	1.18	84	7....	.34	70	14....	.67	41
23....	1.10	73	15.5...	.74	78	3....	.14	56
11....	.53	77	8.5...	.41	77	2....	.10	61
9....	.43	69	19.5...	.94	68	14....	.67	58
27....	1.30	90	17....	.82	66	9.5..	.46	69
10....	.48	80	19....	.91	70	6....	.29	73
4.5..	.22	70						
5....	.24	90						

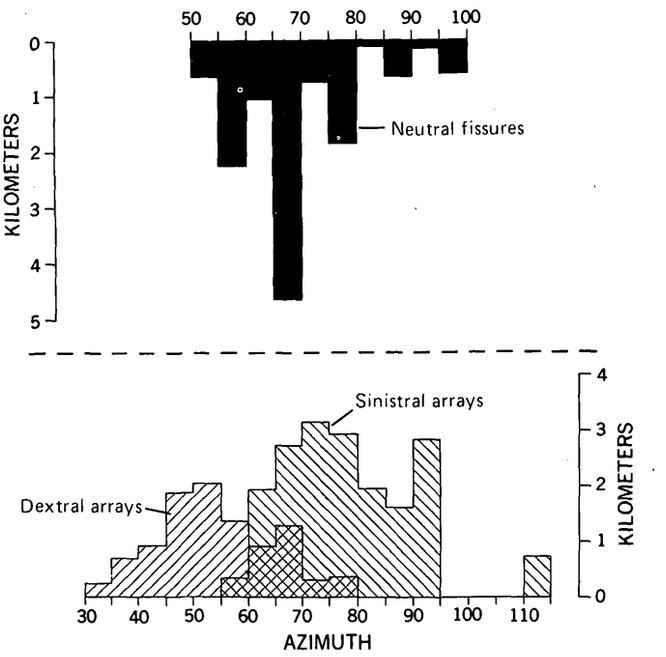

Figure 3.—Histograms showing the azimuthal frequency of zones of fractures for the Koae fault system as determined from aerial photographs. The data from which the histograms were constructed are listed in table 1. Note the similarity between this diagram and figure 2.

approximately at right angles to this indicated opening and parallel to the trend of the entire Koae fault system itself.

Field data used for comparison with these results are part of a detailed (1:4,800 scale) structural mapping project in the Koae fault system. During mapping, individual fissures were routinely measured for trend, and where possible, the azimuth of horizontal opening was also determined. Since most fissures have serrate edges that can mentally be fitted together like pieces of a jigsaw puzzle, nearly all measurements are paired, that is, the trend of fissure and azimuth of opening. Measurements generally are distributed evenly throughout the fault system with regard to approximate total surface length of fracturing per unit area, and fractures of both neutral and en echelon zones are included.

Most measurements were made on open cracks showing little or no vertical offset. Almost invariably, these could be mentally reconstructed easily and unambiguously to yield paired measurements. Normal faults with more than about 1 m of vertical offset were often impossible to reconstruct because of slumping along the plane of the fissure. Thus, the population sampled for the photostudy differed from that of the field study in terms of vertical offset, but the two are believed to be completely comparable in terms of horizontal offset.

All field measurements are subject to some error, mostly caused by slight nonlinearity of individual fissures and by minor difficulties in establishing the precise sense of opening on gaping cracks. The estimated average error for these uncertainties is ±5 degrees. This quantity permits the limits of error to be applied to derived results and also makes it possible to smooth out histograms by redistributing data points within any 10-degree interval. Such smoothing has not been done in this study, but the reader should bear its potential effect in mind.

One hundred and fifty-three paired measurements (trend of fracture and trend of horizontal opening) are summarized in figure 4. Histograms of the trend of individual fissures and the trend of horizontal dilation, which are shown on the same figure, define maxima at azimuths of about 75 degrees (N. 75° E.) and 345 degrees (N. 15° W.), respectively. Thus, within the errors of the method, this azimuth of horizontal dilation as determined from the field measurements differs from that determined from aerial photographs by about 10 degrees. Unrecognized sources of field error may account for this discrepancy. The favored trend of all fractures is essentially the same as that of the neutral fissures of figure 3, indicating that the individual fissures that form en echelon patterns are parallel to each other, to the neutral fissures, and to the entire fault system itself. The slightly elongated pattern of data points in figure 4 reflects a tendency for any individual fissure to open at about right angles to its trend, even though statistically, the two directions favor the above-mentioned orientations.

A comparison of zones of fractures categorized from aerial photographs (table 1) with actual mapped patterns indicates

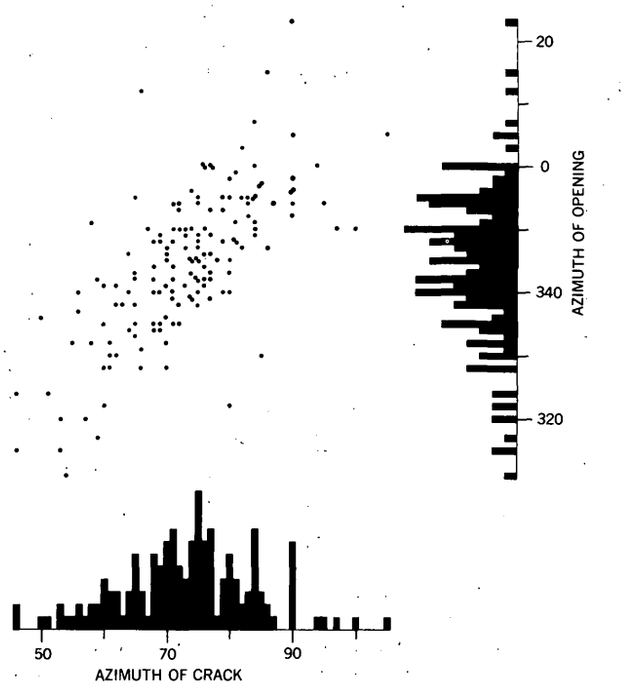

Figure 4.—Graph of paired measurements, trend of crack and trend of horizontal opening, for 153 open cracks of the Koae fault system. Histograms show maxima at about 345-degree azimuth for trend of opening and 75-degree azimuth for trend of crack.

that these predicted classifications are about 90 percent correct. Such "reading error" depends primarily on the degree of preservation and exposure of fissures, the quality of available aerial photographs, and the ability of the photo-investigator to analyze materials correctly. In the Hawaiian study, these sources of error were so small that essentially correct results were obtained; under other similar conditions, sound results can also be expected.

The general validity of the method is confirmed also by the formation of contemporaneous arrays of sinistral and dextral en echelon fractures at Kilauea Volcano in recent years. During the 1955 eruption on the east rift zone of Kilauea, for example, eruptive fissures formed an en echelon array of each sense (Macdonald and Eaton, 1964); direct examination of the fissures and comparison of preeruption and posteruption triangulation surveys indicate that all individual fractures are roughly parallel to one another and that the horizontal opening on them was at right angles to this direction. The azimuth and sense of en echelon arrays relative to this direction were the same as shown in figure 2, the ideal case. Even more recently (September 24–29, 1971), ground cracking associated with an eruption on the southwest rift zone of Kilauea formed similar patterns of fractures with the same interrelations of the various elements (W. A. Duffield, unpub. data).

CONCLUDING REMARKS

Perhaps the most useful aspect of the new method is that sound results can be obtained after only a brief photostudy rather than after lengthy fieldwork. Whenever possible, we recommend that the results of any photostudy be briefly field checked. However, there are circumstances where fieldwork is impractical or impossible, and to these situations the new method has especially valuable applications. Furthermore, for many areas, direct field measurements of horizontal dilation on individual fissures may be impossible; slumping, erosion, and similar destructive processes may quickly destroy the evidence for reconstructing open fissures. Under such conditions, the most detailed of field studies can test only how accurately the arrangement of fissures into en echelon zones was initially determined from aerial photographs.

The type of tectonics (formed by unidirectional tension) to which the method may be applied is restricted, but as more attempts are made to relate structural data to the extensional motions of global plate tectonics, especially on continental regions, this method may become widely applied. The Icelandic study (Nakamura, 1970) provides one example of such an application, and analogous areas, such as the Ethiopian rift system of East Africa, might benefit from a similar analysis. The new method can provide a test for any area which is thought to owe its pattern of fracturing to the transmitted tensional stress of an underlying zone of spreading.

REFERENCES CITED

Billings, M. P., 1954, Structural geology: Englewood Cliffs, N.J., Prentice-Hall, 514 p.

Fiske, R. S., and Kinoshita, W. T., 1969, Rift dilation and seaward displacement of the south flank of Kilauea Volcano, Hawaii [abs.]: Internat. Assoc. Volcanology and Chemistry of the Earth's Interior, Symposium on Volcanoes and their Roots, Oxford, England, p. 53–54.

Macdonald, G. A., and Eaton, J. P., 1964, Hawaiian volcanoes during 1955: U.S. Geol. Survey Bull. 1171, 170 p.

Nakamura, Kazuaki, 1970, En echelon features of Icelandic ground fissures: Acta Naturalia Islandica, v. 2, no. 8, p. 1–15.

Jour. Research U.S. Geol. Survey
Vol. 1, No. 3, May-June 1973, p. 289–292

RADIOELEMENT AND RADIOGENIC HEAT DISTRIBUTION IN DRILL HOLE UCe-1, BELMONT STOCK, CENTRAL NEVADA

By C. M. BUNKER and C. A. BUSH, Denver, Colo.

Abstract.—Uranium, thorium, and potassium concentrations were measured in 60 samples collected from an exploratory hole drilled in the Belmont stock about 40 miles north-northeast of Tonopah, Nev. The results indicate that, at least within 2,000 feet of the surface, the granitic pluton contains radioelement concentrations similar to those in average granodiorites and that local variations in concentrations may reflect the effects of argillic alteration.

An exploratory drill hole, UCe-1, was drilled to provide geologic and geophysical data for evaluating a supplementary nuclear test site. The hole was drilled 2,000 feet into the Belmont stock, a granitic pluton, at approximate Nevada State coordinates N. 1,395,000; E. 429,400 (lat 38°36′ N.; long 116°55′ W.) at an elevation of 7,050±50 feet above mean sea level, about 40 miles north-northeast of Tonopah, Nev. (fig. 1).

In the 340- to 2,000-foot-depth interval the hole penetrated very light gray, medium-grained hypidiomorphic granular granite of Mesozoic age. The granite is well jointed and contains many zones of argillic alteration which are generally joint controlled. The argillized zones are not mineralized and are probably caused by percolating water rather than by hydrothermal solutions (D.C. Hedlund and G.S. Corchary, written commun., 1967). Zones that are moderately or strongly argillized are at the following depths, in feet: 460–468; 1,404–1,407; 1,438–1,444; 1,648–1,650; 1,694–1,694.7; 1,895–1,915; 1,959–1,961; and 1,963–1,966 (D. L. Hoover, written commun., 1967).

Radioelement concentrations were measured in 60 samples selected at intervals of 20 to 50 feet from depths between 365 and 1,997 feet (table 1). These data were obtained initially to determine the radiogenic heat contribution to inhole temperature and heat flow being investigated by A. H. Lachenbruch and John Sass, U.S. Geological Survey. The average values of the data reported here have been compared with averages from other drill holes in a report by Lachenbruch and Bunker (1971). The present report describes the vertical distribution of the radioelements and radiogenic heat in the granite stock.

ANALYTICAL METHOD

The concentrations of the radioelements in the samples were measured by gamma-ray spectrometry. The basic operational procedures and calibration techniques have been described previously (Bunker and Bush, 1966, 1967). The spectra were interpreted with the aid of a linear least-squares computer method which matches the spectrum from a sample to a library of radioelement standards and calculates the concentrations of the radioelements in the sample. The computer method is a modification of a program written by Schonfeld (1966).

Uranium concentrations are determined indirectly by measuring the radium daughters to obtain radium equivalent uranium (RaeU) values. Radium equivalent uranium is the

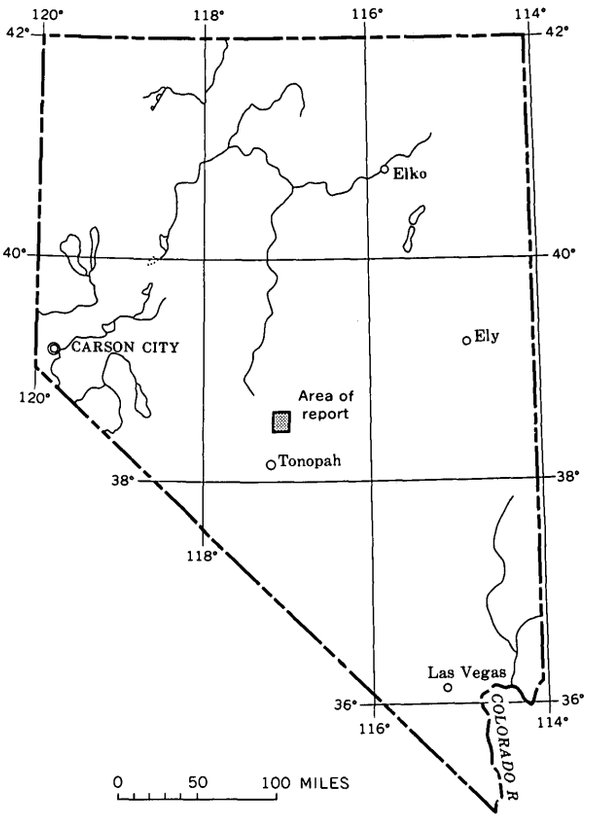

Figure 1.—Index map of Nevada showing area of report.

Table 1.—*Summary of radioelement and radiogenic heat analyses, drill hole UCe-1*
[RaeU, radium equivalent uranium]

Sample depth (feet)	RaeU (ppm)	Th (ppm)	K (percent)	Heat (μcal/g-yr)	Th / RaeU	RaeU / K×10⁻⁴	Th / K×10⁻⁴
365 ...	2.91	12.83	3.83	5.72	4.41	0.76	3.35
391 ...	2.96	15.00	3.67	6.15	5.07	.81	4.09
426 ...	2.70	11.29	3.58	5.20	4.18	.75	3.15
465 ...	10.71	12.23	3.72	11.27	1.14	2.88	3.29
501 ...	2.85	11.01	3.65	5.27	3.86	.78	3.02
550 ...	2.95	11.75	3.76	5.52	3.98	.78	3.12
573 ...	3.15	11.45	3.79	5.61	3.63	.83	3.02
644 ...	2.56	10.93	3.66	5.04	4.27	.70	2.99
672 ...	2.44	11.85	3.67	5.14	4.86	.66	3.23
713 ...	2.86	11.60	3.78	5.43	4.06	.76	3.07
738 ...	3.40	11.63	3.82	5.84	3.42	.89	3.04
763 ...	4.83	10.72	4.68	6.93	2.22	1.03	2.29
795.5 ..	2.50	11.90	3.81	5.23	4.76	.66	3.12
824 ...	2.83	11.41	3.78	5.37	4.03	.75	3.02
851 ...	2.70	11.52	3.65	5.26	4.27	.74	3.16
883 ...	2.96	12.05	3.76	5.59	4.07	.79	3.20
906 ...	2.86	11.82	3.62	5.43	4.13	.79	3.27
933 ...	3.62	11.93	3.63	6.01	3.30	1.00	3.29
956 ...	2.91	11.96	3.64	5.50	4.11	.80	3.29
984 ...	3.63	11.35	3.76	5.94	3.13	.97	3.02
1,013 ...	1.77	10.86	3.79	4.49	6.14	.47	2.87
1,027 ...	2.78	11.52	3.22	5.20	4.14	.86	3.58
1,055 ...	2.87	12.22	3.59	5.51	4.26	.80	3.40
1,080 ...	2.35	10.99	3.76	4.93	4.68	.62	2.92
1,107 ...	6.65	14.47	3.65	8.73	2.18	1.82	3.96
1,129 ...	3.05	11.00	3.64	5.41	3.61	.84	3.02
1,159 ...	2.64	11.81	3.53	5.24	4.47	.75	3.35
1,183 ...	2.33	10.31	3.55	4.72	4.42	.66	2.90
1,206 ...	2.60	11.34	3.55	5.12	4.36	.73	3.19
1,232 ...	2.49	12.74	3.59	5.33	5.12	.69	3.55
1,252 ...	2.33	10.24	3.47	4.69	4.39	.67	2.95
1,280 ...	2.80	9.60	3.47	4.90	3.43	.81	2.77
1,308 ...	1.92	12.79	3.67	4.95	6.66	.52	3.49
1,339 ...	1.81	8.91	3.64	4.09	4.92	.50	2.45
1,374 ...	1.99	9.90	3.50	4.38	4.97	.57	2.83
1,399 ...	1.90	8.78	3.52	4.09	4.62	.54	2.49
1,427 ...	2.18	10.88	3.50	4.71	4.99	.62	3.11
1,454 ...	2.37	11.07	3.69	4.94	4.67	.64	3.00
1,481 ...	2.95	10.47	3.53	5.20	3.55	.84	2.97
1,501 ...	2.22	10.70	3.75	4.77	4.82	.59	2.85
1,526 ...	3.61	10.85	3.46	5.74	3.01	1.04	3.14
1,552 ...	3.31	9.91	4.08	5.50	2.99	.81	2.43
1,587 ...	2.29	10.23	3.62	4.70	4.47	.63	2.83
1,604 ...	2.35	9.86	3.58	4.65	4.20	.66	2.75
1,633 ...	2.54	9.77	3.75	4.82	3.85	.68	2.61
1,657 ...	2.43	11.24	3.39	4.94	4.63	.72	3.32
1,681 ...	2.22	9.76	3.38	4.49	4.40	.66	2.89
1,706 ...	3.42	8.56	3.40	5.13	2.50	1.01	2.52
1,731 ...	2.16	8.46	3.47	4.21	3.92	.62	2.44
1,762 ...	2.46	11.80	3.57	5.12	4.80	.69	3.31
1,778 ...	2.19	14.82	3.52	5.51	6.77	.62	4.21
1,809 ...	2.55	12.65	3.78	5.41	4.96	.67	3.35
1,833 ...	2.94	11.26	3.39	5.31	3.83	.87	3.32
1,859 ...	3.84	11.77	3.58	6.12	3.07	1.07	3.29
1,884 ...	4.50	11.11	3.52	6.46	2.47	1.28	3.16
1,912 ...	3.95	12.31	4.37	6.53	3.12	.90	2.82
1,931 ...	2.87	10.17	3.51	5.08	3.54	.82	2.90
1,950 ...	2.43	9.84	3.57	4.71	4.05	.68	2.76
1,979 ...	3.41	13.66	3.33	6.12	4.01	1.02	4.10
1,997 ...	3.03	9.76	3.26	5.04	3.22	.93	2.99

amount of uranium, under the assumption of radioactive equilibrium, required to support the amount of daughter products that emit the radioactivity measured in a sample. Throughout the report where "U" and "uranium" are used "radium equivalent uranium" is implicit. Although thorium is also measured from daughter products, disequilibrium is improbable because of short half-lives; therefore, the concentrations are considered to be a direct measurement of parent thorium. Potassium is determined from its K^{40} constituent which is proportional to the total potassium. The coefficients of variation for the accuracy of the data included in this report (table 1) are about 5 percent for uranium and thorium and 1 percent for potassium when compared to standards analyzed by isotope dilution methods.

RESULTS

The vertical distributions of the radioelements (fig. 2) indicate a fairly homogeneous rock intersected by zones containing greater concentrations of the radioelements. The character of the distribution is compatible with the available geologic data: variations in concentrations can be expected in well-jointed and altered rock. The data appear to indicate a change in the rock at a depth of about 1,150 feet, below which the radioelement concentrations decrease, although the lower part of the section contains some zones of relatively high concentrations. The apparent differences in the rock above and below 1,150 feet which are observable on the vertical distribution plots are also indicated in histograms of the data (fig. 3). The apparent differences are confirmed by the averages and standard deviations for both potassium and radiogenic heat. However, statistically, uranium and thorium in the upper and lower levels are not significantly different at the 95-percent confidence level. Thus, the apparent differences in uranium and thorium shown on the vertical distribution plots and histograms are really a reflection of the greater variability in concentrations below that depth. The generally higher concentrations in the upper part of the section might be caused by either deep alteration resulting from water moving through the numerous joints or differentiation during intrusion; the available lithologic data do not suggest an explanation. The upper and lower zones are too thin to determine whether systematic changes in concentrations exist that are related to depth (Lachenbruch and Bunker, 1971).

The averages and standard deviations of the radioelements, their ratios, and radiogenic heat are shown in table 2 for the samples above and below 1,150 feet. Values which differed from the mean by more than 3 standard deviations were

Table 2.—*Comparison of radioelement data in drill hole UCe-1 and average concentrations in similar rocks*

	Concentrations in drill hole UCe-1[1] (average ± standard deviation)		Average concentrations (Clark and others, 1966)		
	Above 1,150 ft	Below 1,150 ft	Diorite, quartz diorite	Grano-diorite	Silicic igneous rocks
U (ppm)	2.85±0.41	2.60±0.64	2	2.6	4.7
Th (ppm).....	11.58± .51	11.24±1.5	8.5	9.3	20.0
K (percent)	3.71± .08	3.53± .12	1.10	2.55	3.9
Th/U.....	4.06± .45	4.21± .98	4.3	3.6	4.0
U/K×10⁻⁴	.77± .11	.74± .18	1.8	1	1.3
Th/K×10⁻⁴	3.13± .14	3.06± .42	7.7	3.6	5.0
Heat[2] (μcal/g-yr)...	5.40± .35	5.02± .55	3.5	4.4	8.5

[1] Average concentrations calculated after excluding values which differ from mean by more than 3 standard deviations.
[2] Heat = 0.73 U + 0.20 Th + 0.27 K.

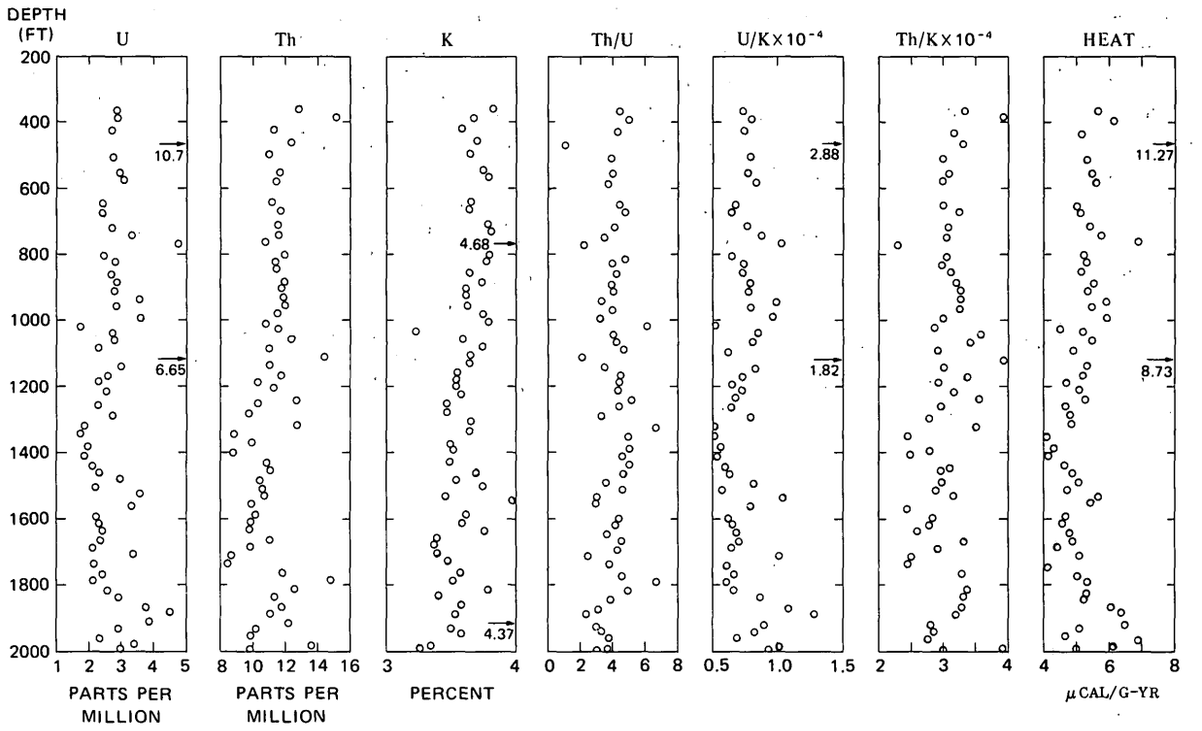

Figure 2.—Radioelement concentrations and ratios, and radiogenic heat in drill hole UCe-1. Arrows indicate points beyond scale limit.

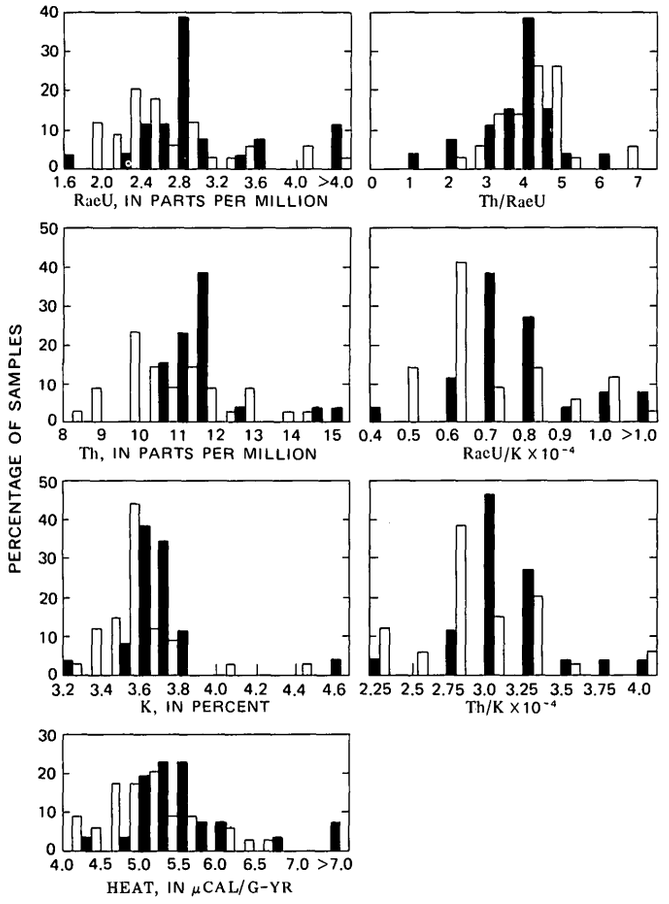

Figure 3.—Frequency distribution of radioelement concentrations and ratios and radiogenic heat. Shaded bars are from interval 365–1,129 feet (26 samples); others are from 1,159–1,997 feet (34 samples).

excluded from the calculations. For comparison, data are included for average abundances in similar rocks as summarized by Clark, Peterman, and Heier (1966).

Uranium concentration ranges from 1.8 to 10.7 ppm, but in most samples it ranges from 1.9 to 3.4 ppm, which is similar to the average concentrations in diorite, quartz diorite, and granodiorite. Thorium concentration ranges from 8.4 to 15 ppm, but in most samples it ranges from 9.6 to 12.2 ppm, slightly more than the average for granodiorite. The potassium concentration is remarkably constant throughout the depth of the hole, and with few exceptions it ranges from 3.4 to 3.8 percent; this range lies between the averages for granodiorite and monzonite. The constancy of the potassium concentrations supports the conclusion of D. C. Hedlund and G. S. Corchary (written commun., 1967) that the argillized alteration is caused by percolating water; hydrothermal alteration often causes changes in potassium concentrations. Most of the Th/U ratios range from 3 to 5, which is normal for granitic rocks. The $U/K \times 10^{-4}$ ratios in most of the samples range from 0.5 to 0.9, which is lower than normal for silicic rocks containing the concentrations measured here, and indicates that the rock either contains excess potassium or is deficient in uranium. $Th/K \times 10^{-4}$ ratios, which range from 2.8 to 3.3, are slightly lower than the average for granodiorite. The radiogenic heat, calculated from the radioelement concentrations, ranges mostly from 4.4 to 5.8 μcal/g-yr, which is slightly higher than that calculated for the average granodiorite.

The radioelement data indicate that the Belmont stock is not a typical granite in the upper 2,000 feet penetrated by drill hole UCe-1. The uranium and thorium concentrations indicate a rock in the intermediate class, similar to a granodiorite. The potassium concentrations are greater than the average for granodiorite and slightly less than the average for more silicic igneous rocks. Local variations from average concentrations may be caused by the effects of the numerous zones of argillic alteration.

REFERENCES CITED

Bunker, C. M., and Bush, C. A., 1966, Uranium, thorium, and radium analyses by gamma-ray spectrometry (0.184–0.352 million electron volts), *in* Geological Survey Research 1966: U.S. Geol. Survey Prof. Paper 550-B, p. B176–B181.

—— 1967, A comparison of potassium analyses by gamma-ray spectrometry and other techniques, *in* Geological Survey Research 1967: U.S. Geol. Survey Prof. Paper 575-B, p. B164–B169.

Clark, S. P., Jr., Peterman, Z. E., and Heier, K. S., 1966, Abundances of uranium, thorium, and potassium, Sec. 24 *in* Handbook of physical constants (revised ed.): Geol. Soc. America Mem. 97, p. 521–541.

Lachenbruch, A. H., and Bunker, C. M., 1971, Vertical gradients of heat production in the continental crust, 2. Some estimates from borehole data: Jour. Geophys. Research, v. 76, no. 17, p. 3852–3860.

Schonfeld, Ernest, 1966, Alpha M—An improved computer program for determining radioisotopes by least-squares resolution of the gamma-ray spectra: U.S. Natl. Lab., Oak Ridge, Tenn. [Pub.] ORNL-3975, 42 p.

Jour. Research U.S. Geol. Survey
Vol. 1, No. 3, May-June 1973, p. 293–299

GEOLOGY OF A SYSTEM OF SUBMARINE CANYONS SOUTH OF PUERTO RICO

By JAMES V. A. TRUMBULL and LOUIS E. GARRISON,
Corpus Christi, Tex.

Work done in cooperation with the Puerto Rico Economic Development Administration

Abstract.—A strongly dendritic submarine canyon system with four major canyons occupies a 30-km indentation in the insular shelf off the south coast of Puerto Rico between Guánica and Ponce. Each canyon has several headward branches at depths of 100 to 1,100 m. Each of the five major rivers that reach the coast between Guánica and Ponce is opposite a canyon head, and off each of the rivers a channel 20 to 30 m deep is incised into the insular shelf. The entire canyon system is 40 km long and terminates at a depth of about 3.3 km; no fan or other constructional feature appears to have been formed. A 410-km continuous seismic profiling survey shows that three unconformable stratigraphic units underlie the canyon area. One sample of indurated clay of probable Miocene age was dredged from a canyon-wall outcrop of the middle stratigraphic unit. The three stratigraphic units may be roughly correlative with (in ascending order) the Juana Díaz Formation, the Ponce Limestone, and an unnamed upper section found in a nearby drill hole ashore. Canyon-axis sediment at depths of 700 to 2,200 m is entirely of pelagic origin, indicating that sediment is not now being transported down the canyons.

During the conduct of marine geophysical work by the U.S. Geological Survey off the south coast of Puerto Rico in January 1968, bathymetric records indicated the presence of a small submarine canyon trending south-southwest off Punta Cuchara. Through the cooperation of the National Ocean Survey (then the U.S. Coast and Geodetic Survey), detailed soundings were made in the area of the suspected canyon in 1969, and the preliminary data were released to the Geological Survey. From those uncorrected soundings, a bathymetric map (fig. 1) was made that revealed the presence of a major submarine canyon system on the insular slope between Guánica and Ponce. This canyon system is here referred to as the Guayanilla Canyon system; its four feeder canyons are here called, from west to east, Guánica Canyon, Guayanilla Canyon, Cuchara Canyon, and Muertos Canyon. The existence of all four canyons was pointed out by Athearn (1971), but his bathymetric map did not extend far enough seaward to show that the four canyons form one dendritic system.

During a cruise to the area in 1970, the bathymetric map was field checked, more than 410 km of continuous seismic reflection profiles were made, and samples were gathered from the wallrock and from the unconsolidated sediment along the canyon axes. Preliminary results of that work are presented here.

The continuous seismic reflection profiler used in this study discharged 9,000 joules of stored electrical energy at intervals of 4 seconds. For simplicity, reflection traveltimes have been converted to depth, with an assumed sound velocity in sediment of 2 km/sec. Selection of this figure is based on the presumed carbonate lithology inferred from onshore mapping (Briggs and Akers, 1965) and on results of seismic refraction work on the south coastal plain of Puerto Rico (Denning, 1955).

Acknowledgments.—We thank our U.S. Geological Survey colleagues Jacky W. Lee and Stephen C. Wolf for their skilled operation of seismic equipment and other assistance at sea; Ruth Todd for identification of Foraminifera; Ray Martin for contouring the canyon bathymetry; and John Aaron for information added during review. We also thank the National Ocean Survey for the sounding data from which the bathymetric chart was derived. Arnie Junger gave valuable advice in the technique of determining the effect of rough topography on seismic records.

TOPOGRAPHY

The bathymetry of the Guayanilla Canyon system and adjacent insular shelf is shown in figure 1, and the salient characteristics of the canyons are listed and compared with the characteristics of other known submarine canyons of the world in table 1.

The four canyons form a well-developed tributary system. Each of them has at least three headward branches. Muertos Canyon joins Cuchara Canyon at a depth of about 1,550 m, and Cuchara Canyon joins Guayanilla Canyon at about 1,900 m. Guánica Canyon loses its V-shaped cross section at a closed topographic depression at a depth of about 1,700 m, and it loses its identification as a canyon a few kilometers further downslope. It too is clearly confluent with Guayanilla Canyon

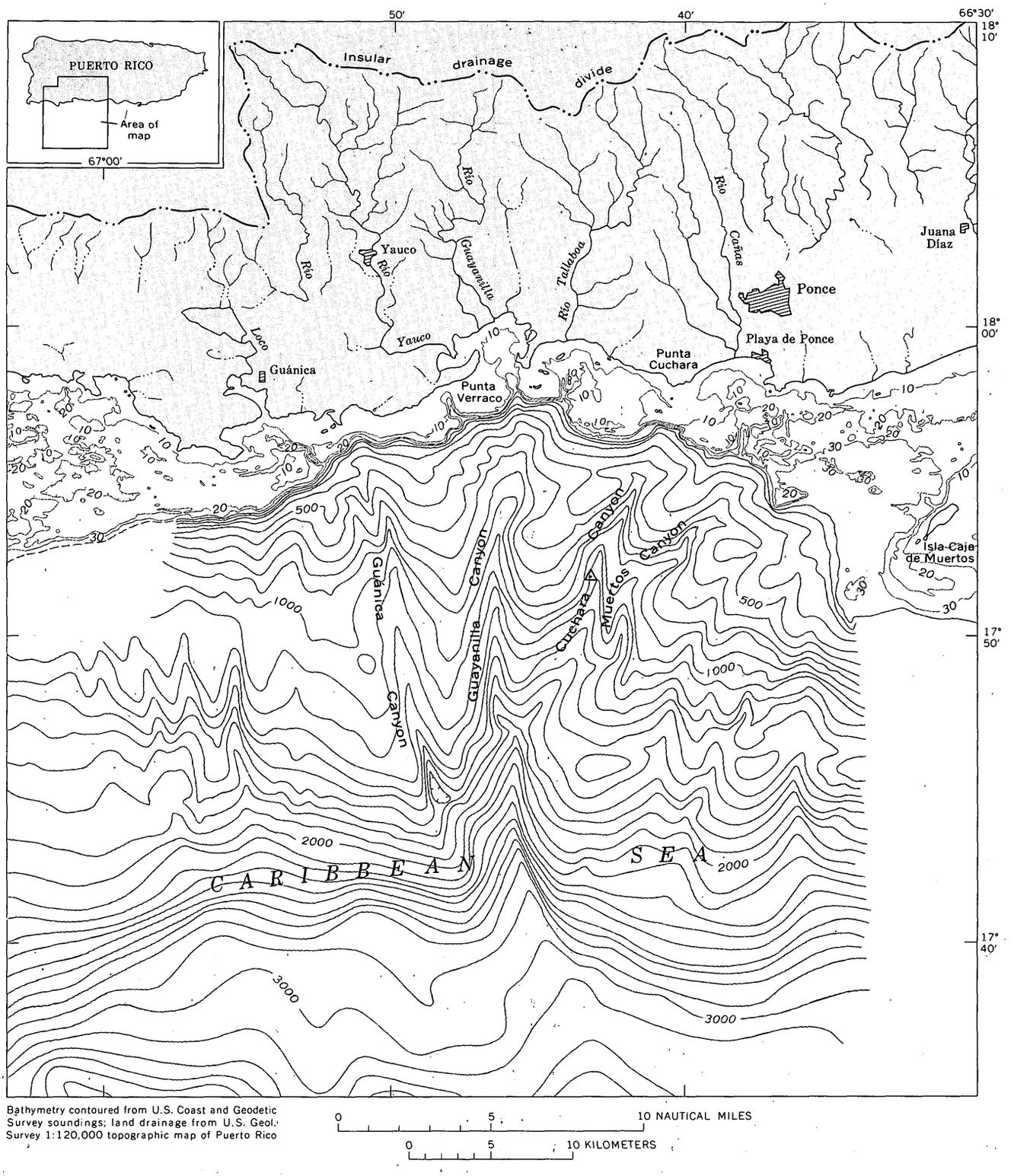

Figure 1.–Topography of the Guayanilla Canyon system and adjacent insular shelf. Contour interval 100 m with supplementary 10-, 20-, and 30-m contours. Triangle near center of map shows location of dredged sample. The discontinuous nature of the land drainage in this area is discussed by Bogart, Arnow, and Crooks (1964, p. 72): "Rivers which cross coastal lowlands * * * show diminishing flows in the seaward direction, most of them becoming dry during the dry season of the year, except flow occurs in some of them in the last half mile or so to the sea * * *. Ground water is recharged from the streams."

Table 1.—*Comparison of four Puerto Rico submarine canyons with other known submarine canyons of the world*

[Data on averages for other canyons are from Shepard and Dill (1966)]

Canyon characteristic		Four Puerto Rico canyons	Average of all other canyons
Length	km	40	55
Depth at head	m	100–400	107
Depth at outer termination.	km	3	2.1
Coast embayed or straight.		Embayed.	Equal numbers of each type.
Distance of head from land.	km	2–5	Majority are close.
Relation to land valleys.		Strongly related.	80 percent related.
Shelf channels		Small, well developed.	Rare.
Land sediment now entering.		No	57 percent no.
Gradient	m/km	63	58
Profile		Relatively even below steeper head.	Most concave upward.
Maximum wall height	m	500–1,000	915
Axial trend		Gently curving.	Sinuous to gently curving.
Tributaries below heads.		All have tributaries.	87 percent have tributaries.
Transverse profile		Mostly V-shaped.	80 percent V-shaped.
Wall material		Sedimentary rock.	Virtually all rock, 55 percent sedimentary.

as a hanging valley. Thus Guayanilla Canyon is the master canyon of the system.

On the evidence of available soundings, Guayanilla Canyon loses its valley characteristics at about lat 17°35′ N., the lower border of figure 1. Farther south is Muertos Trough, whose east-trending axis, with greatest depths near 5,050 m, is at about lat 17°20′ N. Small inflections in bathymetric contours as deep as 4,300 m indicate that Guayanilla Canyon may continue in some form to that depth. No depositional fan or other constructional feature formed of material excavated from or carried through the canyon appears to be present.

Five samples of unconsolidated sediment from the axes of Guayanilla and Cuchara Canyons at depths ranging from 700 to 2,200 m are composed entirely of the remains of pelagic organisms, indicating that little or no land-derived sediment is now being transported down those canyons.

The most striking characteristic of the four submarine canyons is their close relationship to the width of the insular shelf, to the nearby river systems, and to channels in the insular shelf.

The upper reaches of the four canyons occupy an indentation in the insular shelf that extends about 35 km from Guánica to Playa de Ponce (fig. 1). The shelf is only 1 to 5 km wide in the area occupied by the canyons, but it is 9 to 10 km wide west of the canyon system, and 15 to 18 km wide to the east. Figure 1 also shows that in this part of Puerto Rico, the larger rivers are opposite the canyon area and that the rivers east and west of the canyon area are discontinuous.

The geology of the land area opposite the canyon system and the narrow part of the shelf is also distinctive. As pointed out by our colleague John Aaron, that area is the only part of the south coastal plain where middle Tertiary rocks are extensive. East of Juana Díaz and west of Guánica they occur only as very isolated and very small patches. All else is alluvium or volcanic complex. This might mean that canyon formation could have been promoted by, among other factors, the relatively incompetent nature of these rocks.

The heads of the submarine canyons are directly opposite the mouths of major rivers, excepting only the head of Cuchara Canyon, discussed in the next paragraph. As figure 1 shows, the head of Guánica Canyon is opposite the Bahia de Guánica, into which the Río Loco flows. The three major headward branches of Guayanilla Canyon are directly in line with Ríos Guayanilla and Tallaboa and the previous trend of the Río Yauco (see below). The head of Muertos Canyon is opposite the Bahia de Ponce, into which the Río Cañas flows. Furthermore, each of the canyons except Cuchara is linked to its river by a channel cut into the shelf. The shelf channels are well developed, although not of impressive dimensions: the 20- and 30-m depth contours extend 2 to 3½ km across the insular shelf (fig. 1).

Cuchara Canyon alone is not associated with a shelf channel. Clearly Muertos Canyon connects with the Río Cañas system through the shelf channel southwest of Playa de Ponce. Because Cuchara Canyon and Muertos Canyon both are east of the divide separating the Río Tallaboa system from the Río Cañas system, and because this divide continues seaward to the confluence of those two canyons with the main Guayanilla Canyon, it seems likely that both canyons are related to the Río Cañas. Cuchara Canyon may therefore be an older extension of the Río Cañas system that was closed off, perhaps by uplift or upbuilding of the present shelf, Muertos Canyon being formed later.

The relation between the Río Yauco and the shelf channel south of Punta Verraco is not immediately clear from the map (fig. 1), for the Río Yauco does not now discharge near the shelf channel. It previously did, however, as is shown in a report on the Guánica-Guayanilla Bay area by Grossman (1963, p. B116), who stated:

> That the Río Yauco formerly followed a more direct course to the Caribbean is indicated by the broad valley that extends from the present valley of the river southeastward * * * to the Caribbean Sea * * * [west of Punta Verraco] * * *. This "abandoned" valley is drained by an undersized ephemeral stream that flows southeastward to the blocked exit to the sea and then doubles back [northeastward] and empties into Guayanilla Bay.

STRATIGRAPHY

Interpretation of the seismic profiler records (fig. 2) shows that three bedded rock units are present throughout most of the upper canyon area.

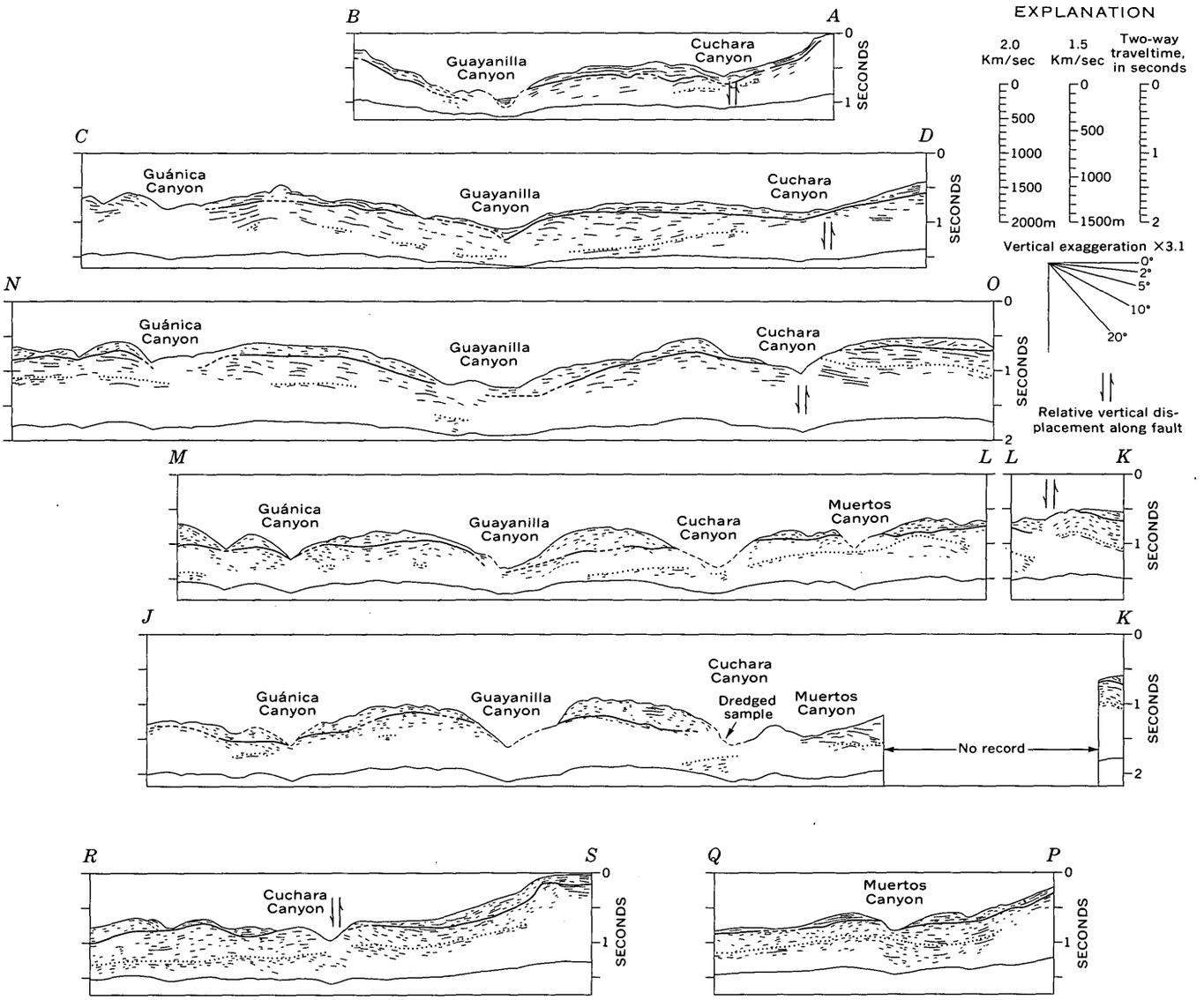

Figure 2.—Simplified tracings of selected seismic profiles. See figure 3 for locations. Heavy line designates contact between upper and middle stratigraphic units; dotted line designates contact between middle and lower units. Continuous line profile below each seismic profile shows the calculated distorting effect of topography on a theoretical horizontal reflecting bed at depth. Horizontal scale is not the same in all profiles because strong current in survey area caused variation in ship speed over the ground.

The upper unit averages about 150 m in thickness on the topographically high areas between canyons, becomes progressively thinner down the canyon flanks, and is absent below depths ranging from 700 m in the upper reaches of Cuchara and Muertos Canyons to 1,000 m in the middle reaches of Guayanilla Canyon (fig. 3). The upper unit is characterized by strong, closely spaced internal reflectors, especially on the profiles near land. These internal reflecting horizons are generally parallel both to the present topographic surface and to the eroded surface of the underlying middle unit. The progressive thinning and pinchout of the upper unit on the canyon flanks is therefore predominantly a result of nondeposition rather than of erosion, though some erosion on the canyon flanks is evident. The surface on which the upper unit was deposited had the general topographic form of the present surface, so that sediment deposited on the intercanyon areas and not in the canyons acted to preserve and accentuate the preexisting topography. Age of the upper unit is not directly known, but it lies unconformably on beds of probable Miocene age.

The middle stratigraphic unit lacks prominent continuous reflecting horizons. Bedding is generally even, though slight internal unconformities are not uncommon. The middle unit was deposited throughout the area covered by seismic profiles. In general, it is 400 to 500 m thick in the area of upper Guayanilla Canyon in the north-central part of the area, and

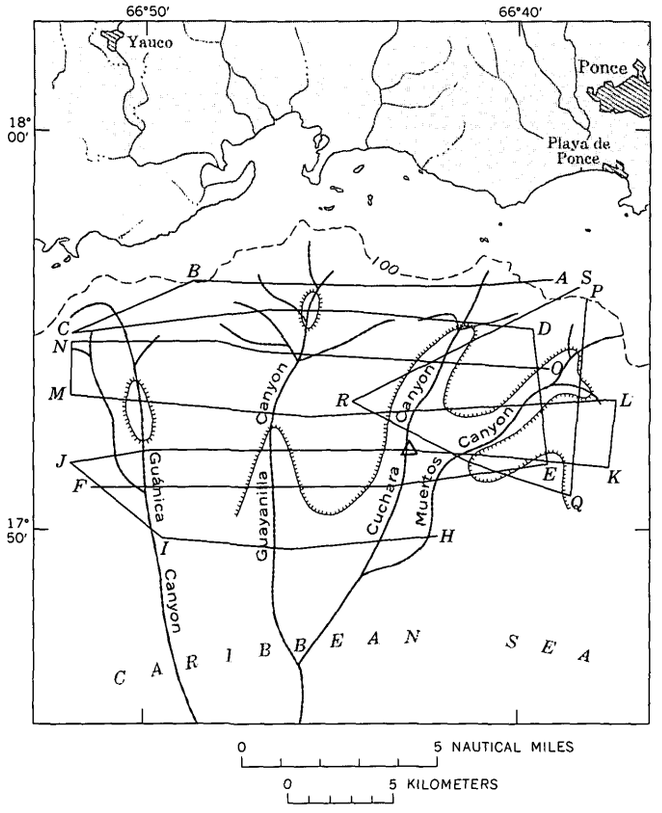

Figure 3.—Location of seismic profiles (fig. 2) and extent of upper stratigraphic unit. Ticks indicate the side of the boundary line on which the upper stratigraphic unit is present. Dashed 100-m bathymetric contour indicates approximate edge of insular shelf. Heavy gray lines are canyon axes.

250 to 300 m thick in the upper reaches of Cuchara and Muertos Canyons. Thickness variations of the middle unit are not correlative with the location of canyon axes or the intercanyon topographic highs.

It appears that at least the tributary canyons Cuchara and Muertos were cut into the middle unit, as shown by the truncation of middle unit reflectors in profiles *R–S* and *Q–P* (fig. 2). In Guayanilla Canyon, downcutting into the middle unit is indicated by an apparent truncation of reflectors in profiles *B–A* and *C–D*; thinning of this unit beneath the canyon is apparent in many of the profiles.

In most places the middle unit lies conformably on the lower unit, but unconformity exists, indicating at least a slight erosional cycle between deposition of the lower and middle units.

The top of the lower unit is characterized by a prominent reflector, but the reflector and hence the unit could be identified on less than half the total length of profiles. The character of seismic returns from within the lower unit shows that, like the middle unit, it is rather even bedded and contains minor internal unconformities. Maximum seismic penetration into the lower unit was 450 m. No base could be defined, and no change in character with depth was noted. Erosion of the top of the lower unit is evident in only a few places. Within the area surveyed, the lower unit crops out only in the east bank of Cuchara Canyon on line *N–O*, in the upthrown block of a fault.

On most profiles where it could be identified, the top of the lower unit is subparallel to the topography of the sea floor. Much of this is caused by the effect of topography on the attitude of subbottom reflectors as shown in the profiles. As illustrated by the continuous line profiles below each seismic profile in figure 2, the effect of topography in other than level areas is to rotate all reflectors toward parallelism with the bottom. Thus a truly horizontal reflector would appear to dip toward a canyon axis.

Only one sample of what appears to be canyon wallrock has been obtained to date. Dredging at a depth of 1,030–1,170 m on the west side of Cuchara Canyon (fig. 1) produced pieces of moderately well indurated, light-olive-gray clay from what is thought to be the middle unit (fig. 2, profile *J–K*). Four species of Foraminifera from this sample indicate a probable Miocene age (Ruth Todd, written commun., 1970). Rounded limestone fragments found in the same dredge haul are tentatively dated as no younger than Oligocene on the basis of one species of Foraminifera. Presumably they were eroded from farther up the canyon, where they may have been derived from the lower unit.

According to Ruth Todd (written commun., 1970), the units sampled and the Holocene ooze with which the samples are mixed were probably deposited at generally similar depths.

The stratigraphic relations and terminology of the Tertiary rocks of the land bordering the canyon area are complex (Zapp and others, 1948; Seiglie and Bermúdez, 1969; Moussa and Seiglie, 1970), but as a simplification we can say that the Juana Díaz Formation is of Oligocene and early Miocene age and is composed of shale, sandy limestone, and conglomerate. It is as much as 655 m thick. The Ponce Limestone is of Miocene age and is principally limestone with lenses of clay. It is as much as 1,300 m thick.

In an exploratory well drilled near the coast southeast of Ponce, about 9 km from the nearest seismic profile of this study, the Juana Díaz Formation was found to be about 335 m thick, and the Ponce Limestone to be about 366 m thick (Glover, 1971, fig. 30). Overlying the Ponce Limestone is an unnamed sequence of sand, gravel, and limestone beds about 150 m thick.

On the basis of geologic age and thickness, the lower stratigraphic unit in the seismic profiles may correlate with the Juana Díaz Formation, the middle stratigraphic unit with the Ponce Limestone, and the upper stratigraphic unit with the unnamed upper section of the exploratory well.

STRUCTURE

The well-developed dendritic pattern of the Guayanilla Canyon system would seem to preclude any extensive struc-

tural control of canyon location. Furthermore the primarily north-south orientation of the canyons is not in accord with the main nearby structural trends. In the exposed coastal plain to the north, the principal alinement of faulting and folding is east and northwest, in accordance with the older structural trends of that part of the island (Zapp and others, 1948; Briggs and Akers, 1965). To the east on the submerged Muertos shelf, faulting of the rocks along northeasterly trends has been described (Garrison, 1969).

Some faulting in the eastern part of the canyon system is seen in the seismic profiles, however, and the upper part of Cuchara Canyon may be fault controlled. The fault shown near the east end of profile *N–O* (fig. 2) has an estimated vertical displacement of slightly less than 500 m on the basis of the offset of the middle stratigraphic unit. The upthrown block of the fault forms the east wall of Cuchara Canyon. This fault can also be tentatively identified beneath Cuchara Canyon in profiles *R–S*, *C–D*, and *B–A*, but it is not evident on profiles crossing Cuchara Canyon south of profile *N–O*.

A second fault is seen on profile *L–K*, where the estimated vertical displacement is 250–400 m. This fault is not discernible on any of the adjacent profiles; whether this is because it dies out or because of poor records is not known.

DISCUSSION

The close correspondence between river-cut land valleys and the heads of submarine canyons surely shows a genetic relationship. The canyons have cut into the middle stratigraphic unit, which is of probable Miocene age, and the youngest rocks eroded by the rivers are in the Ponce Limestone, also of Miocene age (Briggs and Akers, 1965). Thus the land and the submarine valleys may have started forming at the same time.

The excellent correspondence of land and sea valleys across the insular shelf could be taken as an indication of subaerial canyon origin, as could the dendritic tributary pattern of the canyons on the insular slope. These characteristics are shared by most of the submarine canyons throughout the world, however (table 1), and the hypothesis of worldwide subaerial canyon erosion requires an episode of worldwide sea-level lowering on the order of several kilometers. The absence of evidence for this makes it difficult to invoke a subaerial origin for other than perhaps the shallow part of the Guayanilla Canyon system.

The insular shelf forms a prominent nickpoint in the overall longitudinal profile of the Guayanilla river-canyon system shown in figure 4. In a detailed study of a land valley–sea valley system of similar longitudinal profile, Woodford (1951) concluded that a prominent nickpoint eliminated submergence of a river valley as a possible mode of canyon origin. In observing that Woodford's conclusion was justified, Shepard and Dill (1966, p. 319) went on to say that:

> It seems apparent that the typical concave profile of submarine canyons, with its steepest element in shallow water near the canyon head, is an indication that the profile is adjusted to the present sea level, or at least a sea level close to that of the present day. This does not disprove an original subaerial cutting of the submarine canyons, but it does show that some form of submarine erosion must have greatly reshaped these valleys.

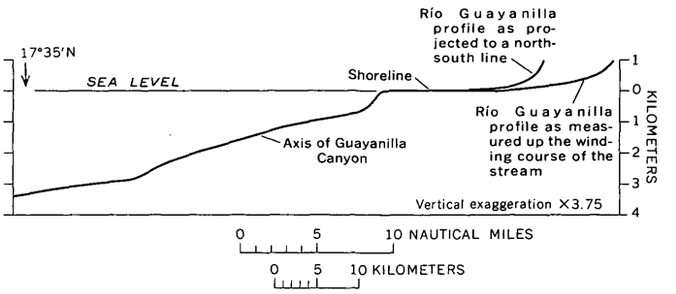

Figure 4.—Longitudinal profile of Río Guayanilla and Guayanilla Canyon.

The prism of sediments beneath the insular shelf forms the nickpoint in figure 4. If that prism was cut through early in the erosion cycle and later filled, or if it was formed after the main erosion cycle, the river-canyon system could well have had a continuous gradient. This would accord with the hypothesis of subaerial canyon erosion. We have as yet no information whether such extensive cutting and filling took place in the heads of the Guayanilla Canyon system. As to the possibility of upbuilding of the insular shelf as a whole since canyon formation, profiles *B–A* and *R–S* of figure 2 show that the middle stratigraphic unit forms a significant part of the prism of shelf sediments. The canyon has eroded the middle unit and therefore postdates it. Presumably then the insular shelf was present in some form when the canyon was eroded.

The extensive headward branching of all four canyons shown in figure 3 appears to be a response to the steep gradient of the outer edge of the prism of sediment that forms the insular shelf. Thus at least some canyon erosion at depths generally between 100 and 1,100 m has occurred since formation of the shelf.

The small channels cut into the surface of the outer shelf between river mouths and canyon heads are at the most only slightly more than 30 m deep. They were probably formed subaerially during Pleistocene glacial-stage withdrawals of sea level.

REFERENCES CITED

Athearn, W. D., 1971, Upper slope bathymetry off Guayanilla and Ponce, Puerto Rico, *in* Caribbean Geol. Conf., 5th, St. Thomas, Virgin Islands, 1968, Trans.: Flushing, N.Y., Queens College Press (New York City Univ. Queens Coll., Dept. Geology Geol. Bull. 5), p. 41–43.

Bogart, D. B., Arnow, Ted, and Crooks, J. W., 1964, Water resources of Puerto Rico–A progress report: Puerto Rico Water Resources Authority Water-Resources Bull. 4, [120 p].

Briggs, R. P., and Akers, J. P., 1965, Hydrogeologic map of Puerto Rico and adjacent islands: U.S. Geol. Survey Hydrol. Inv. Atlas HA-197.

Denning, W. H., 1955, Preliminary results of geophysical exploration for gas and oil on the south coast of Puerto Rico: Puerto Rico, Dept. Indus. Research, Div. Mineralogy and Geology Bull. 2, 17 p. (mimeo).

Garrison, L. E., 1969, Structural geology of the Muertos insular shelf, Puerto Rico: U.S. Geol. Survey open-file report, 9 p.

Glover, Lynn, III, 1971, Geology of the Coamo area, Puerto Rico, and its relation to the volcanic arc-trench phenomena: U.S. Geol. Survey Prof. Paper 636, 102 p.

Grossman, I. G., 1963, Geology of the Guánica-Guayanilla Bay area, southwestern Puerto Rico: Art. 29 *in* U.S. Geol. Survey Prof. Paper 475-B, p. B114–B116.

Moussa, M. T., and Seiglie, G. A., 1970, Revision of mid-Tertiary stratigraphy of southwestern Puerto Rico: Am. Assoc. Petroleum Geologists Bull., v. 54, no. 10, p. 1887–1898.

Seiglie, G. A., and Bermúdez, P. J., 1969, Informe preliminar sobre los foraminíferos del terciario del sur de Puerto Rico, Pt. 1: Caribbean Jour. Sci., v. 9, nos. 1–2, p. 67–80.

Shepard, F. P., and Dill, R. F., 1966, Submarine canyons and other sea valleys: Chicago, Rand McNally and Co., 381 p.

Woodford, A. O., 1951, Stream gradients and Monterey sea valley: Geol. Soc. America Bull., v. 62, no. 7, p. 799–852.

Zapp, A. D., Bergquist, H. R., and Thomas, C. R., 1948, Tertiary geology of the coastal plains of Puerto Rico: U.S. Geol. Survey Oil and Gas Inv. Prelim. Map OM-85, 2 sheets.

Jour. Research U.S. Geol. Survey
Vol. 1, No. 3, May-June 1973, p. 301–307

A SPECTROCHEMICAL METHOD FOR DETERMINING THE COMPOSITION OF NATIVE GOLD

By A. L. SUTTON, R. G. HAVENS, and
C. L. SAINSBURY, Denver, Colo.

Abstract.—The spectrochemical method described herein for determining trace, minor, and major element distribution in native gold is applicable over a wide range of particle sizes and over a very large concentration range. The matrices of samples and standards are very closely matched. The method was tested on 100 nuggets from a gold sample collected in Alaska. The data show that the method is adequate for 30 of the 31 elements checked; only the mercury values are not acceptable. The data also show that more than one sample is necessary for a complete evaluation of all elements in one geologic location.

The following spectrochemical method was developed to satisfy requests by U.S. Geological Survey geologists for the determination of trace and minor elemental composition of native gold. A d-c arc technique was used because low detection limits were of interest. Warren and Thompson (1944) used a d-c arc excitation to determine minor element composition of gold. They reported the elements as either faint (<0.1 percent), medium (0.1–0.5 percent), or strong (>0.5 percent). For this study we believed that a six-step semiquantitative method was adequate. The procedure had to apply to samples with large variations in both weight and particle size.

Later, requests for more quantitative results for copper and silver were received. The small size of most of the samples eliminated the possibility of an additional method for these two elements. The heterogeneity of the samples also made the use of two separate methods for each element undesirable if relationships between elements were to be determined. The basic method was changed slightly at this time in an attempt to improve the copper and silver results. Owing to the limited number of analytical lines available for both elements, only silver showed any improvement.

Also included in this report is the analysis of 100 randomly selected nuggets from a small locality in Alaska to illustrate the variation in their composition. Additional information on variation is included in a paper by Antweiler and Sutton (1970). Desborough (1970), Desborough, Raymond, and Iagmin (1970), and Desborough, Raymond, and Soule (1970) have investigated major and minor element distributions within grains using the electron microprobe. The spectrochemical method described in this paper cannot show distribution within a single grain, but it does furnish data on many trace elements as well as major and minor elements for a whole grain.

Prior to the analysis of the 100 nuggets, the question of sample preparation arose. Most samples have a coating of oxides that contain trace elements. This was also noted by Crook (1939). Samples were analyzed both with and without cleaning, and the results are given in the present paper.

REAGENTS AND EQUIPMENT

Hydrofluoric acid: Reagent grade.

Hydrochloric acid: Triple distilled, constant boiling.

Nitric acid: Triple distilled.

$HAuCl_4 \cdot 3H_2O$: B&A purified grade.

Gold solution: Dissolve 10 g $HAuCl_4 \cdot 3H_2O$ in 20 ml of constant-boiling hydrochloric acid and dilute to 25 ml.

Gold control sample 1: To approximate the composition of the samples, melt quantities of Johnson and Matthey gold, silver, and copper in a graphite electrode using an acetylene flame.

Gold control sample 2: Weigh 10 mg of any good silicate reference sample (such as W-1, G-1, Glass reference standards) into a plastic test tube. (See below.) Add 50 µl of gold solution, 1 ml of concentrated hydrofluoric acid, and evaporate to dryness on a steam bath.

Sealing solution: Dissolve 100 ml of Fletch-lac glue in 100 ml of acetone. Fletch-lac is available from R. A. Bohning Adhesives Co.

Standard stock solutions: Three stock solutions for silver are made to contain 10, 4.64, and 2.15 mg in 100 µl of .2 *N* nitric acid. Each solution is diluted by factors of 10 to give a complete range of 10 to 0.00001 mg of silver per 100 µl of solution.

Silicate standards: Silicate standards are prepared as described by Myers, Havens, and Dunton (1961).

Test tubes: 12 by 75 mm polypropylene.

Pipets: 5¾ inches by 7.0 mm OD disposable capillary pipet (heavy wall glass).

Ultrasonic cleaner: Any small ultrasonic cleaner with an output of at least 25 watts.

Hotplate: A block of aluminum with holes to accommodate 12 electrodes is placed on a hotplate and the temperature controlled with a Variac. The holes are 1 inch deep. In one corner of the block a thermometer is suspended in a well filled with mineral oil.

Spectrograph: A Wadsworth-mounted grating spectrograph, equipped with a 600-grooves-per-mm grating and having a reciprocal linear dispersion of 5.24 A per mm in the first order.

Electrodes: Lower electrode, 0.242-inch diameter, with a thin wall cavity. Ultra Carbon Corp. type, performed electrode No. 3170. Upper electrode, 0.125-inch diameter by 1.5 inches long, cut from graphite rods obtained from Union Carbide Corp.

Graphite powder: Ultra Carbon Corp., type UCP-2 nonpelletizing graphite powder.

Photographic plates: Eastman Kodak type III-O X-thin plates, developed at 20°C in D-19 developer for 4 minutes with intermittent nitrogen agitation.

Microdensitometer: Direct reading projection microdensitometer fitted with a line-width measuring device described by Barnett (1967).

SAMPLE PREPARATION PROCEDURE

[Note.—This sample preparation procedure is not used when a submitter requests that the sample be analyzed "as received."]

1. Weigh half of the sample (not to exceed 500 mg) into a plastic tube. Add 1 ml of concentrated hydrofluoric acid and leach for 16 hours on a steam bath.
2. Transfer the test tube to the ultrasonic cleaner for 10 minutes.
3. Decant off the hydrofluoric acid solution and reserve it for analysis.
4. Add 1 ml of distilled water to the test tube and place it in the ultrasonic cleaner for 10 minutes. Discard this wash.
5. Examine each sample under a binocular microscope for any remaining coatings, foreign material, and inclusions.
6. Flatten the larger nuggets, using the base of an agate mortar as an anvil and the pestle as a hammer. Place a foam pad under the mortar to absorb part of the shock. Light taps are sufficient to flatten the gold.
7. With a pair of small scissors, cut the sample into small squares weighing 5–10 mg and containing no visible inclusions.

ANALYTICAL PROCEDURE

A. *Preparation of standard plates (quantitative method).*— Add 100 μl of each stock silver solution and 100 μl of distilled water as a blank to plastic tubes. Treat each solution as follows:

1. Add 50 μl of gold solution.
2. Heat on a steam bath until about two drops of solution remain in each test tube.
3. While the samples are on the steam bath, seal a quantity of electrodes by adding six drops of sealing solution to each electrode. Allow the solvent to evaporate at room temperature and repeat this step.
4. Transfer the contents with a disposable pipet to a sealed electrode, preheated to 75°–85°C.
5. Add 15 mg of graphite powder.
6. Add two drops of acetone to settle graphite powder, and dry at room temperature.

Each standard plate should contain 16 concentrations of the silver standard, one blank solution, three pegmatite bases containing 1 percent Fe_2O_3 for emulsion calibration, and three No. 1 gold control samples.

B. *Preparation of standard plates (semiquantitative method).*— Weigh 10 mg of each silicate standard into plastic test tubes. The elements in each standard are grouped according to table 1. Treat each standard as follows:

1. Add 50 μl of gold solution.
2. Add 0.5 ml of hydrofluoric acid to remove silica.
3. Heat to dryness on a steam bath.
4. Add three drops of nitric acid and six drops of hydrochloric acid and evaporate to about two drops.
5. Transfer the contents to a sealed, preheated electrode and evaporate to dryness.
6. Add 15 mg of graphite powder.
7. Add two drops of acetone and dry at room temperature.

Table 1.—*Standards for part B of procedure*

Standard	Elements	Concentration range (percent)
1	Ag	0.0001–100
	Cu	.0001–1
2	Fe	.001–1
3	Ti, Mn, Co, Ni, Zr	.0001–1
4	Ba, La, Ga	.0001–1
5	Be, V, Cr, Mo, Sn	.0001–1
6	Zn, Cd, Bi, Te	.001–1
7	Pb, Sc, B	.0001–1
8	Nb	.0001–1
9	Pd, Pt, Rh	.0001–.1
10	Ir, Os, Ru	.0001–.1

C. *Preparation of sample plates.*—

1. Weigh a sample of as much as 10 mg into a plastic test tube.
2. Add six drops of hydrochloric acid and two drops of nitric acid to each test tube.
3. Heat on a steam bath until the reaction of aqua regia on the gold stops. Samples with a silver content between about 20 and 70 percent will not completely go into solution. Place the test tubes in the ultrasonic cleaner to assist digestion.
4. When about two drops of sample remain in the test tubes, transfer both solid and liquid to a sealed, preheated electrode. Wash the test tubes twice with two-drop portions of concentrated hydrochloric acid. Repeat steps 6 and 7 of the previous section.

Each plate of samples should also contain wash solutions from the sample preparation procedure, three No. 2 gold control samples, and three pegmatite bases containing approximately 1 percent Fe_2O_3 for emulsion calibration.

D. *Spectrographic procedure.*—

1. Arc the samples and standards in a 5-amp d-c arc for 20 seconds and then 13 amps for an additional 80 seconds.
2. Measure the silver lines on a microdensitometer. Line width measurements are used when the transmission falls below 10 percent.

Table 2.—*Analytical lines and their analytical ranges*

Element	Wavelength (angstroms)	Analytical range (micrograms)	Element	Wavelength (angstroms)	Analytical range (micrograms)	Element	Wavelength (angstroms)	Analytical range (micrograms)
Ag	3280.68	100–0.01	Ga	2943.64	100–0.1	Ru	3436.74	10–0.5
	3382.89	100–.01	Ir	3220.78	10–.5	Sc	4246.83	100–.1
	2721.77	10,000–100	La	4333.73	100–.5	Sn	2839.99	100–.3
B	2496.78	100–.7	Mn	2933.06	100–.5		3175.05	100–.3
	2497.73	100–.5		2939.30	100–.5	Te	2385.76	100–20
Ba	4554.03	100–.1		2801.06	.5–.1		2383.25	100–20
Be	2348.61	100–.05	Mo	3170.35	100–.05	Ti	3088.02	10–.1
Bi	3067.72	100–.5		3193.97	100–.05		3152.25	100–10
Cd	3261.06	100–1	Nb	3163.40	100–.2	V	4379.24	10–.1
Co	3453.50	100–.1	Ni	3414.76	100–.1		3183.98	100–.1
Cr	4254.35	100–.1	Os	3301.56	10–.5	Y	3242.28	100–.1
Cu	3273.96	[1]10–.05	Pb	2833.07	20–.5	Yb	3289.37	100–.1
	3247.54	[1]10–.05		2663.17	100–20	Zn	3345.02	100–5
	2824.37	100–.5	Pd	3404.58	10–.05		3345.57	100–5
Fe	3020.64	10–.5	Pt	2659.45	10–.2		3302.59	100–2
	3021.07	10–.5	Rh	3396.85	10–.05	Zr	3273.05	100–2
	3222.07	100–.5					3279.26	100–.1
	3225.79	100–.5						
	3217.38	100–10						

[1] Lower limit due to a reagent blank.

3. Prepare analytical curves and report silver as a quantitative value.
4. All other elements are compared visually and reported as six-step semiquantitative values.
5. Wash solutions from the sample preparation procedure are compared visually and reported qualitatively.

The lines and analytical ranges for the elements are reported in table 2. The methods of emulsion calibration and determination of exposure conditions are described by Bastron, Barnett, and Murata (1960).

VARIABILITY STUDIES

The analyses of 100 nuggets split from a sample collected at a single placer on the Seward Peninsula, Alaska, are reported in this paper. The sample came from a placer being mined by Mr. Bon Davis and Mr. W. Dickman on the south headwater of Gold Run (lat 65°4′25″ N.; long 166°25′30″ W.). Because of the limited area, it was assumed that this sample was derived from a single mineralized source, and that the 100 nuggets would provide a statistically reliable answer on the variation in trace elements in placer gold from a single source.

Many of the nuggets in this sample were coated with iron oxides; others had distinct inclusions of silicates and (or) sulfides. Two grams of this sample was split into four parts and cleaned in hydrofluoric acid for 16 hours. Two splits were recombined and 100 random nuggets from these splits were selected for emission spectrographic analysis, and 10 random nuggets from a third split were submitted for atomic absorption analysis. The fourth split was heated to its melting point and homogenized for 5 minutes. The melted bead was flattened and cut into pieces weighing 5–10 mg. Of these pieces, 10 were submitted for emission spectrographic analysis and 10 for atomic absorption analysis. The difference between the distribution of copper and silver in the melted and unmelted samples was used to estimate the precision and accuracy for the analytical methods used. For comparison with the analyzed nuggets, an additional 188 nuggets from the original sample were mounted in cold-setting plastic, polished, and examined with the reflecting microscope for inclusions and zoning.

RESULTS AND DISCUSSION

Sample preparation

Table 3 shows the analytical data for four nuggets of gold, selected at random from the original 100 nuggets, of which two were cleaned and two were not cleaned. This is just one of several such sets of data—all showing a similar pattern.

The concentration of the various elements in the wash solution was calculated on the basis of parts per million from the original 2-g sample. These values plus the values determined from the cleaned nuggets should equal the values from the uncleaned nuggets. The checks are well within the error of the procedure for Al, Co, Cr, Mg, Mn, Ni, Ti, and V. The iron values are disappointing because iron determinations are usually better than this. No explanation other than a random sampling error is available. The poor checks on the results of the elements calcium, boron, and sodium are due to contamination by the hydrofluoric acid. Because of a lack of interest in these three elements, no attempt was made to purify the hydrofluoric acid.

We believe that these results explain why some reports show a larger number of trace elements in gold than we are finding. Nevertheless, we realize that this cleaning process will not remove all of the sulfides nor all of the heavy minerals.

On the basis of the very small amount of silver, gold, and copper detected in the wash solution—less than 1 percent of the total if they all came from the gold—we believe that we are

Table 3.—*Comparison of values (in parts per million) in two cleaned nuggets and two uncleaned nuggets of gold*

Element	Cleaned nuggets			Uncleaned nuggets
	Values in cleaned nuggets	Values in wash solution[1]	Total	
Ag	>100,000	0.2	>100,000	>100,000
Au	>100,000	10	>100,000	>100,000
B	<50; <50	.3	<50	10; 200
Ba	10; 10	20	30	50; 300
Be	<5; <5	.02	<5	<5; <5
Bi	<50; <50	<.1	<50	<50; <50
Cd	<100; <100	<.5	<100	<100; <100
Co	<10; <10	2	2	<10; <10
Cr	3; 3	3	6	5; 5
Cu	700; 1,000	7	700; 1,000	1,000; 1,000
Fe	10; 10	150	160	2,000; 2,000
Ga	<10; <10	.3	<10	<10; <10
Mn	<5; <5	5	5	5; 7
Mo	<5; <5	<.03	<5	<5; <5
Nb	<20; <20	.5	<20	<20; <20
Ni	<10; <20	10	<20	10; 10
Pb	<50; <50	10	<60	<50; <50
Pd	<2; <2	<.02	<2	<2; <2
Pt	<20; <20	<.5	<20	<20; <20
Sc	<10; <10	.7	<10	<10; <10
Sn	<30; <50	<.1	<30	<30; <30
Ti	10; 10	100	110	500; 500
V	<10; <10	7	7	7; 7
Y	<10; <10	.3	<10	<10; <10
Yb	<10; <10	.....	<10	<10; <10
Zn	<200; <200	<2	<200	<200; <200
Zr	<10 <10	2	2	10; 10
Al	<10; <10	200	200	100; 100
Ca	<50 <50	100	100	<50; 1,500
Na	<500; <500	300	<800	<500; 1,500
Hg[2]	1,500; 10,000	.....	.....	2,000; 2,000

[1] Calculated for a 10-mg sample. Detection limits are lower because the starting sample weight was 2 g.
[2] Not normally looked for.

Table 4.—*Control sample data*

Element	Best known value	Geometric mean	Geometric deviation[1]	Results
Gold alloys (values in percent)				
Ag	9.41	8.17	1.14	6.43–9.43
	33.10	30.3	1.19	24.8–34
	36.00	34.9	1.13	32.0–38
Cu	.056	.0644	1.30	.05–.1
	[2].20±.03	.1931	1.44	.15–.3
	[2].53±.10	.5107	1.44	.3–.7
	[3]<.001	.....	....	.0002
Gold control samples prepared from silicate reference samples (values in ppm in the rock)				
Fe	48,000	.....	....	>10,000
Ag	36	50	1.55	20–70
B	55	45	3.12	20–100
Ba[4]	85	116	1.23	100–147
Be	50	17	1.62	7–20
Bi	40	55	1.22	50–70
Cd	30	.....	....	<30
Co	30	74	1.29	50–100
Cr	50	44	1.35	30–50
Cu	55	88	1.21	70–100
Ga	5	[5]4.1	[5]2.00	<5–7
Ir	30	.....	....	<50
La	55	68	1.59	30–100
Mn	250	171	1.51	100–300
Mo	45	26	1.52	15–50
Nb	42	20	1.00	20–20
Ni	55	88	1.21	70–100
Os	.....	.....	....	<50
Pb	70	31	1.25	20–50
Pd	45	39	1.22	30–50
Pt	<50	.....	....	<50
Rh	18	16	1.35	10–20
Ru	<10	.....	....	<50
Sc	<5	.....	....	<10
Sn	45	.....	....	<30–70
Ti	45	82	1.23	30–100
V	45	51	1.51	30–100
Y	50	62	1.38	50–100
Yb	<1	.....	....	<1
Zn	50	.....	....	<200
Zr	40	44	1.34	30–70

[1] Geometric deviation or antilog of the log standard deviation.
[2] Electron microprobe analysis by George Desborough.
[3] Sigmund Cohn Corp. 5-9/s gold wire (10 determinations).
[4] Several obvious contaminations not included in this calculation.
[5] A value one order of magnitude below the "less-than value" is used for the calculation of the geometric mean and deviation.

not significantly changing the original composition of the gold by our washing technique. Extremely small particles of gold and the presence of mercury could present a problem, however. One sample containing gold tellurides did show significant amounts of tellurium in the wash solution and only minor concentrations of tellurium in the washed gold.

The washing time of 16 hours seems long, but several shorter washes did not completely remove the coatings. After the original washing and splitting of the 2-g sample there was an insufficient number of nuggets for the emission spectrographic analysis, so a few additional nuggets were taken and washed for only 8 hours. The effects of this shorter washing time are demonstrated by the fact that most of the samples (table 5) that contained titanium (18 of 22 samples) and most of those that contained iron (seven of 12 samples) were washed only 8 hours.

Analytical procedure

Table 4 gives the trace element content of the control samples used to evaluate this method. Over a period of 3 years 93 control samples were analyzed; the results should give a realistic measure of accuracy and precision for one operator and one laboratory.

Quantitative silver values are biased low, but the precision is good. Copper values are well within the six-step semiquantitative precision and accuracy limits. Low-level copper values, although more precise than the higher level copper values, tend to be biased about one step high. Niobium is very precise, but is low compared to the known values. Molybdenum and lead are low, probably owing to the presence of volatile chlorides and fluorides. Beryllium is also low, but the reason for the low value is not known.

The extremely volatile $SnCl_4$ is lost completely in some samples in which tin is near the detection limit; in samples of high tin concentrations some tin remains but results are low.

Table 5.—*Atomic absorption (AA) and emission spectrographic (ES) data for the 100-nugget study*

Element	Method	Geometric mean (ppm, except as noted)	Geometric deviation	Range of values (ppm except as noted)	Number of samples in which detected
Ag	AA[1]	[2]8.02	1.26	[2]6.10–12.8	[3]10
Ag	ES	[2]7.04	1.30	[2]3.7–18	100
Cu	ES	660	2.52	70–5,000	100
Pb[4]	ES	2.92	4.10	<15–150	20
Co[4]	ES	1.11	1.75	<7–70	4
Cr	ES	.....	....	<3–5	2
Ni	ES	.....	....	<2–7	2
Ti	ES	.....	....	<10–200	22
Fe	ES	.....	....	<7–70	12

[1] Atomic absorption analyses by Claude Huffman, Jr.
[2] Values in percent.
[3] Only 10 samples were run by atomic absorption.
[4] A value one order of magnitude below the lowest value reported is substituted for N (not detected).

(Somewhere in the procedure there is an erratic source of barium contamination which we have tried several times to locate but without success.) The remaining elements exhibit reasonable accuracy and precision for a semiquantitative method. Platinum, palladium, and rhodium give good analytical curves and could be done quantitatively.

The principal advantage of the procedure described in this paper is the ability to make standards that very closely approximate the samples. It is extremely difficult and impractical to make alloys that contain 1–100 ppm of many elements, but in solution these elements can be added easily. Failure to use standards closely approximating the sample can cause errors of orders of magnitude for some elements.

Contamination from solutions and the necessity of handling the samples several times are the primary disadvantages of this procedure. Fortunately the elements that contaminate most often (Ba, Cu, Mg) either are high enough that a small blank does not cause an appreciable error or they are of little interest. Owing to the gold matrix, detection limits are two to three steps higher on some elements than they are in a silicate matrix.

Additional information on the accuracy and precision of copper and silver determinations follows.

Variability studies

For the 100 nuggets used in the present study the element concentrations were determined by the emission spectrographic method, and for 10 additional nuggets the concentrations were also determined by the atomic absorption method (table 5). The two methods show good agreement for silver, as shown by the geometric mean values of 8.02 and 7.04, respectively. The geometric deviation of both methods is about the same—1.26 and 1.30. Geometric means and deviations were not calculated for iron and titanium because these elements are present primarily in the coatings.

Table 6.—*Data on homogenized nugget for variability studies*

Element	Method	Geometric mean (percent)	Geometric deviation	Range of results (percent)	Number of determinations
Ag	AA[1]	7.89	1.07	7.22–8.87	10
Ag	ES[2]	7.70	1.09	7.14–8.93	10
Cu	ES[2]	.0584	1.22	.0500–.0700	10

[1] Atomic absorption analyses, by J. A. Thomas, Claude Huffman, Jr., and A. L. Sutton, Jr.
[2] Emission spectrographic analyses, by A. L. Sutton, Jr.

Table 6 gives the results of the sample split after it was melted into one nugget, flattened, and cut into individual samples. The geometric deviations of the original sample and the homogenized sample show that the portion of the total deviation due to the analytical procedures is small by comparison. This is especially true of the copper results.

Figures 1, 2, and 3 are histograms of the silver, copper, and lead in one split of the sample and in the homogenized split. Lead values in the homogenized split are all below the detection limit, thus no "after" histogram was drawn for this element. For the purpose of these diagrams, quantitative silver values were converted to 12-step brackets.

Silver shows a fairly normal distribution curve, but copper is far from normal. The distributions for the homogenized samples show that the copper distribution cannot be attributed to analytical error. There is some hint of a bimodal distribution of copper, and thus the possibility of separate small veins as sources for the gold cannot be ruled out.

Only gold, silver, and copper were detected in all 100 nuggets from the sample used for this study. Lead was detected in 20 percent of the samples, cobalt in 4 percent, and nickel and chromium in 2 percent. Only two nuggets out of 188 mounted nuggets examined with the microscope were found to have visible sulfide inclusions, so it is doubtful that all the lead was in this form. In addition, figure 3 indicates the possibility of a distribution of lead with a mean below the detection limit. Titanium and iron have not been discussed here because the major contribution to these elements appears to be from the coatings. This points out the need for more than a single sample to obtain an overall estimate of the trace elements to be found in one area. Additional unpublished work on trace and minor elements in gold has shown that this sample was relatively pure in comparison with samples representing geologic sources larger than the one picked for this study.

In addition to the elements reported here, mercury was detected in most of the samples. Because of the volatility of mercury, we were not able to determine its concentrations to our satisfaction, and thus it was not reported. We believe, however, that future studies must take mercury into consideration.

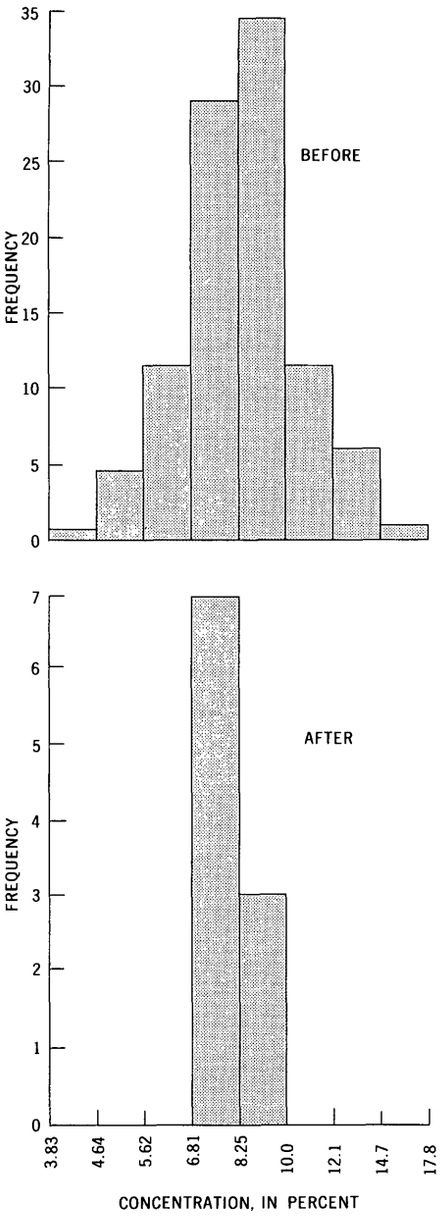

Figure 1.—Histograms of the silver content in gold nuggets before and after the nuggets were homogenized at 1,300°C.

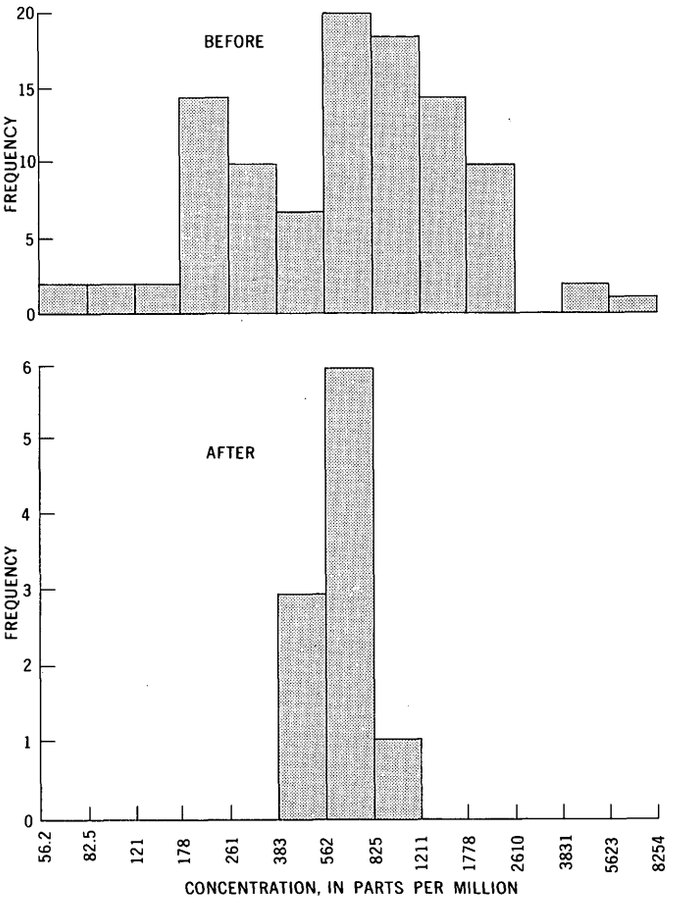

Figure 2.—Histograms of the copper content in gold nuggets before and after the nuggets were homogenized at 1,300°C.

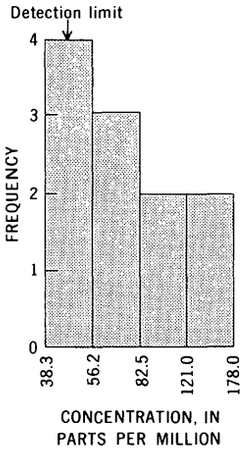

Figure 3.—Histogram of the lead content in gold nuggets before the nuggets were heated to 1,300°C.

REFERENCES CITED

Antweiler, J. C., and Sutton, A. L., Jr., 1970, Spectrochemical analyses of native gold samples: U.S. Geol. Survey Rept. USGS GD-70-003, 28 p.; available only from U.S. Dept. Commerce, Natl. Tech. Inf. Service, Springfield, Va. 22151, as Rept. PB1-94809.

Barnett, P. R., 1967, Device for measuring spectral linewidths: Appl. Spectroscopy, v. 21, no. 2, p. 128–130.

Bastron, Harry, Barnett, P. R., and Murata, K. J., 1960, Method for the quantitative spectrochemical analysis of rocks, minerals, ores, and other materials by a powder d-c arc technique: U.S. Geol. Survey Bull. 1084-G, p. 165–182.

Crook, W. J., 1939, Preliminary spectrographic and metallographic study of native gold: Metals Technology, v. 6, no. 2, Tech. Pub. 998, p. 1–14.

Desborough, G. A., 1970, Silver depletion indicated by microanalysis of gold from placer occurrences, Western United States: Econ. Geology, v. 65, no. 3, p. 304–311.

Desborough, G. A., Raymond, W. H., and Iagmin, P. J., 1970, Distribution of silver and copper in placer gold derived from the northeastern part of the Colorado mineral belt: Econ. Geology, v. 65, no. 8, p. 937–944.

Desborough, G. A., Raymond, W. H., and Soule, Courtney, 1970, Placer gold of unique fineness in Douglas and Elbert Counties, Colorado, *in* Geological Survey Research 1970: U.S. Geol. Survey Prof. Paper 700-D, p. D134–D139.

Myers, A. T., Havens, R. G., and Dunton, P. J., 1961, A spectrochemical method for the semiquantitative analysis of rocks, minerals, and ores: U.S. Geol. Survey Bull. 1084-I, p. 207–229.

Warren, H. V., and Thompson, R. M., 1944, Minor elements in gold: Econ. Geology, v. 39, no. 7, p. 457–471.

Jour. Research U.S. Geol. Survey
Vol. 1, No. 3, May-June 1973, p. 309–314

TWO DIAMICTONS IN A LANDSLIDE SCARP ON ADMIRALTY ISLAND, ALASKA, AND THE TECTONIC INSIGNIFICANCE OF AN INTERVENING PEAT BED

By ROBERT D. MILLER, Denver, Colo.

Abstract.—Two till-like diamictons, 700 feet above present sea level on Admiralty Island, Alaska, are separated by peat near the top of a landslide scarp. The lower diamicton is glaciomarine; the upper diamicton is probably a mudflow. The lower diamicton contains the foraminifer *Elphidium clavatum* Cushman, a species typical of fiords. Similar diamicton crops out along Gastineau Channel near Juneau, 15 miles eastward. Diamicton in both areas reflects deposition in glacier-free fiords during land depression and sea transgression. Consequently, till-like deposits less than 700 feet above sea level elsewhere in southeastern Alaska should be considered as possibly glaciomarine. Sliding occurred after late 1962, but before July 1964; the March 27, 1964, Alaska earthquake might have caused sliding of diamicton saturated by melting snow and spring rains. The peat in the landslide scarp has a published radiocarbon date of 3,400±250 years B.P. (W-1955). The peat was expected to be older, and to relate to Holocene tectonic movement of Admiralty Island. The unexpectedly young date led to additional field study that showed the material over the peat to be a probable mudflow derived from glaciomarine diamicton upvalley; the date has no tectonic significance.

Two till-like diamictons, which are separated by a woody peaty layer, are exposed in the scarp of a large landslide about 15 miles westward from Juneau, Alaska, on Mansfield Peninsula, Admiralty Island, Alaska (fig. 1). A radiocarbon date places the age of the peaty layer, which lies about 5 feet below the top of the scarp, at 3,400±250 years B.P. (Marsters and others, 1969, p. 224). The lower diamicton is glaciomarine in origin and is composed of heterogeneous till-like mixtures of clay-sized particles, silt, sand, and pebbles, and scattered cobbles and boulders; broken barnacle and mollusk shells and unbroken Foraminifera are scattered throughout the deposit. The diamicton overlying the peaty layer has similar textural characteristics, but it is believed to be a mudflow derived from glaciomarine diamicton exposed upvalley.

This report describes the glaciomarine deposit on Admiralty Island, relates this deposit to the glaciomarine deposits on Douglas Island and the mainland near Juneau, emphasizes that these shell-rich diamictons are glaciomarine in orgin—not "marine till"—and presents data to prevent misinterpretation of the tectonic meaning of the woody peaty layer. In addition, the landslide is deemed worthy of description because of its location, type of material involved, the multiple types of movement related to the landslide, and the relationship of the landslide to the geologic environment.

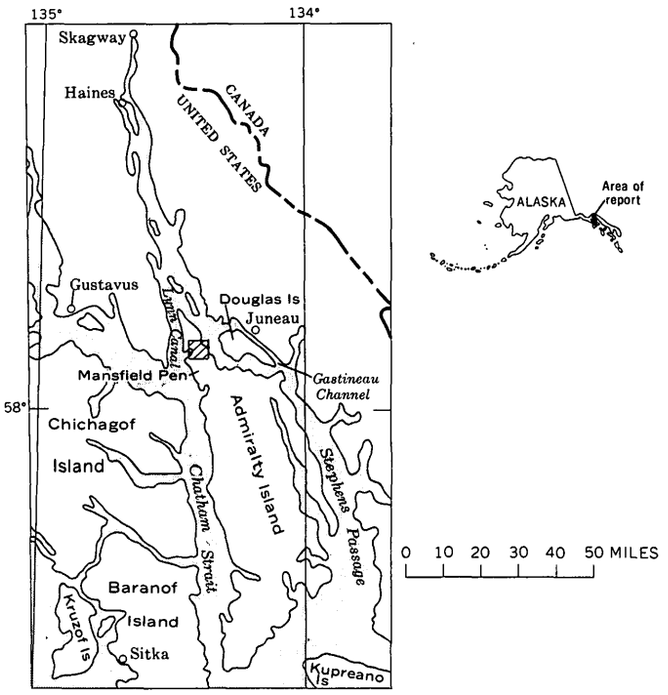

Figure 1.—Sketch map showing the portion of Mansfield Peninsula, Admiralty Island, that is enlarged in figure 2.

DESCRIPTION OF THE LANDSLIDE

The landslide that provided the exposure of diamicton occurred sometime before the last week of July 1964, but to my knowledge was not visited by anyone until the fall of 1965. This massive landslide is in an area of Admiralty Island that is somewhat off the path of most hikers and of most aircraft flying westward from Juneau. Keith Hart, Auke Bay, Alaska, kindly provided me with a resumé of the events that led to his visit to the landslide (written commun., 1967).

The possibility of a landslide on Admiralty Island apparently was inferred first by Keith Hart and A. J. Carr while they were hiking along Bear Creek (fig. 2) in the last week of July 1964. They noticed an intense coloration of the water in the lower part of Bear Creek and high-water marks conspicuously indicated by layers of silt covering the vegetation high on the stream bank. The turbidity was as pronounced during subsequent visits to the Bear Creek area in 1964, and later in July 1965, as it was during the first visit. In September 1965, Hart and Alfred Gordon, Juneau, followed the turbid water upstream along the southern branch of Bear Creek that flows from the northeastern slope of Robert Barron Peak. About 1½ miles from the junction with Bear Creek, they stood at the base of the main scarp of the landslide (fig. 3).

Keith Hart collected a sample of the diamicton from the northernmost part of the main scarp at an altitude of about 695 feet above sea level. In the summer of 1966, Hart gave the sample to me for analysis (fig. 4, sample 2). The sample contained numerous individuals of the foraminifer *Elphidium clavatum* Cushman (Ruth Todd and Doris Low, written commun., 1967), one of the most widely distributed species in the glaciomarine deposits on the mainland near Juneau (Miller, 1972, tables 5 and 7).

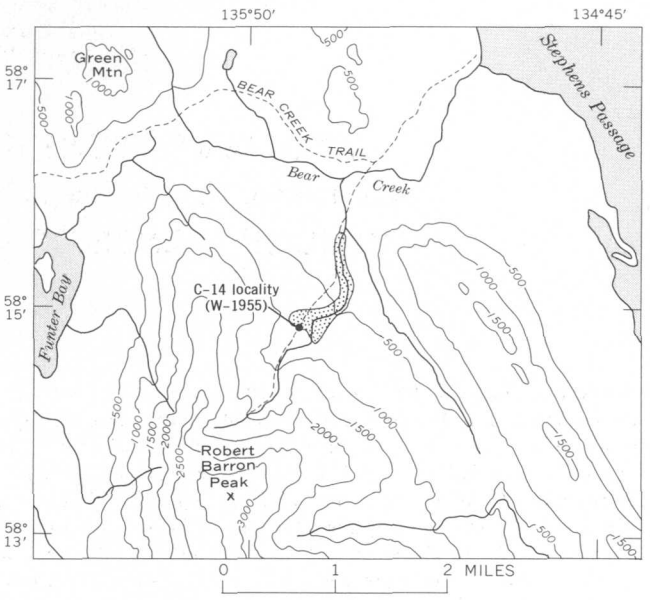

Figure 2.—Sketch map showing the areal extent of the landslide, emphasized by stipple pattern, on the northeastern slope of Robert Barron Peak, Mansfield Peninsula, Admiralty Island, Alaska. Base from U.S. Geological Survey topographic quadrangles: Juneau A-3, 1950, and Juneau B-3, 1962. Contour interval 500 feet.

Figure 3.—Aerial oblique view of the landslide, September 1966. Locations of C^{14} sample W-1955 and materials samples 1, 2, and 3 are indicated. H is the position of the helicopter in figure 5*A*; S marks the area of slump blocks with slight reverse dips shown by the trees; cb marks the area of coherent blocks of slump and slide material.

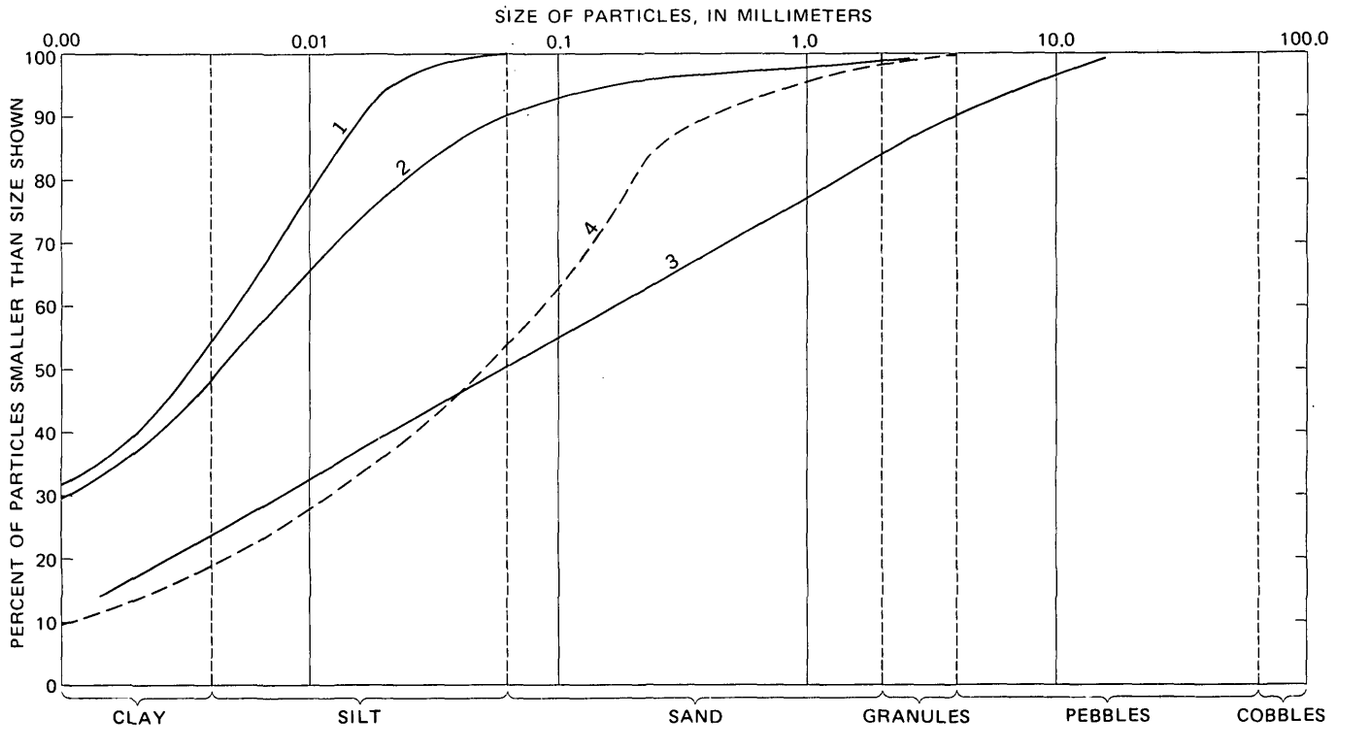

Figure 4.—Particle-size distribution curves comparing samples 1 and 2, collected below the peat zone in glaciomarine deposit in the main scarp of the landslide, and sample 3, collected above the peat zone, with a composite curve (4) of the average of 12 samples of glaciomarine material collected on the mainland near Juneau and on Douglas Island.

I subsequently made two visits to the landslide area by helicopter: one in 1966, with V. K. Berwick, and one in 1968, with J. A. McConaghy, both with the U.S. Geological Survey in Juneau. The landslide was clearly visible from the air in 1966 (fig. 3) as a mass of jumbled tree-covered blocks on a bluish scar in the dark-green forest. In 1968, the landslide was less conspicuous when viewed from the air although still visible; grass and brush mottled the bluish scar and obscured landforms previously identifiable from the air and from the ground (fig. 5*A* and *B*).

The main scarp of the landslide is slightly more than one-quarter mile long. The northern end of the scarp is 95 feet high and has an altitude at the top of 735 feet above sea level, as determined from the altimeter in the helicopter. The woody peaty zone 1½ feet thick crops out 5 feet below the surface and is found only near the northern end of the scarp. A low sag separates the northern end from the southern end of the scarp, which is only 50 to 60 feet high.

The landslide apparently moved from a slope that had failed in the past. Preslide aerial photographs (taken July 1962) of this part of Mansfield Peninsula reveal a steep tree-covered slope where the landslide scarp now exists. This steep slope is interpreted to be an old landslide scarp. Similar tree-covered slopes are found in nearly identical topographic situations along the streams south of this particular branch of Bear Creek. The terrain above the steep slope on the southern branch of Bear Creek is covered by trees and muskeg. The stream valley at this point of the steep slope is incised into the general surface that bounds the stream on either side.

The volume involved in the landslide is not known. From the appearance of the landslide scarp, and by locating the area on the prelandslide photography, I estimate that a relatively small thickness of the prelandslide slope was involved in the landslide.

Water necessary to cause the slide by lubrication and possible saturation of the slope material probably came from several sources: the southern branch of Bear Creek, which flows over the landslide scarp at the southern edge of the main scarp; several smaller streams whose boulder-laden channels hang at the edge of the scarp; and melting snow and spring rains.

Surface expression of the landslide material reflects at least three types of movement: flowage, horizontal translation, and rotation. Natural levees are well developed along the northern edge of the slide and range in height from 1 to 10 feet. The presence of these levees suggests at least local flowage. Excessive lubrication elsewhere along the landslide scarp permitted some of the tree-covered terrain to glide relatively short distances downvalley as discrete units. The more saturated material flowed downvalley to form a narrow lobe that now marks the maximum extent of this particular landslide. Older landslides may have extended farther downstream, but the area near the confluence of the southern branch with Bear Creek was not examined on the ground.

Landslide blocks of all sizes cover the path of the landslide. Large blocks of material that slid on a gently inclined surface

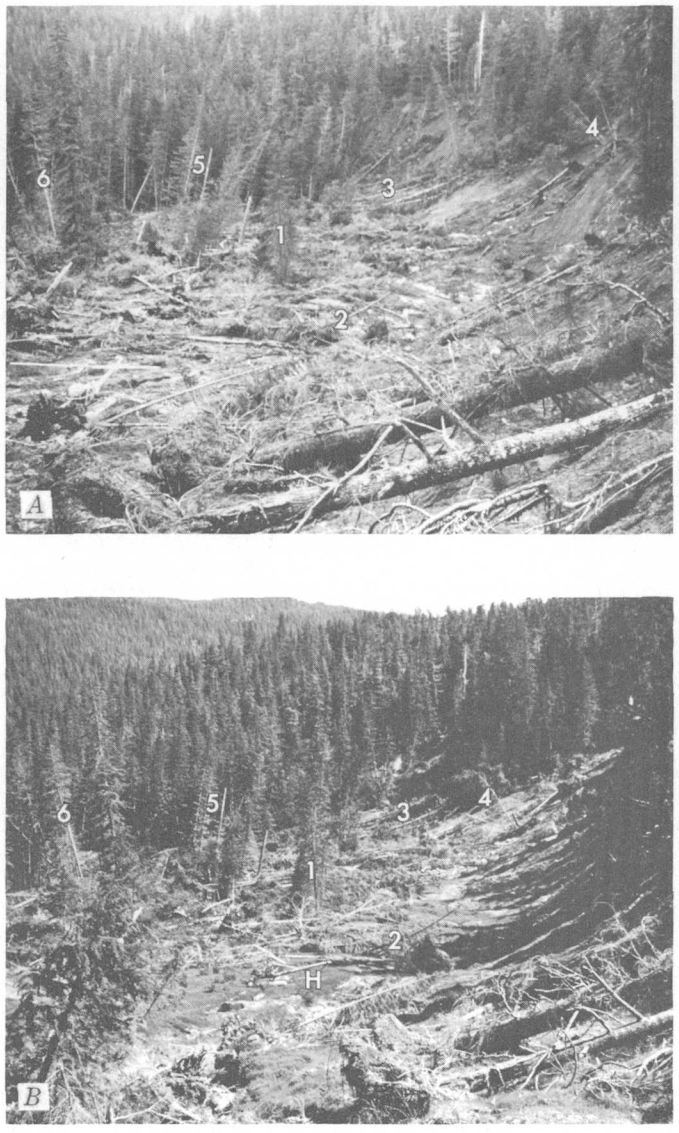

Figure 5.—Landslide scarp, Admiralty Island, Alaska. *A*, photograph taken September 1966; *B*, photograph taken July 1968. Selected identical features in the two photographs are marked by matching numbers. H in photograph *B* is the position occupied by the helicopter in photograph *A*. The trees at 4 moved downslope during the 2-year interval between photographs.

have almost upright trees and are generally confined to the wide upper part of the valley below the main scarp. Smaller blocks that have nearly vertically standing trees form islands separated by the glaciomarine diamicton floor, which retains striations that extend beneath the transported blocks. Small rotated blocks almost line the base of the landslide scarp (fig. 5, points 5 and 3) and contain trees with more than 10° of backward tilt. One of the largest rotated blocks is several hundred feet long; it moved from the southern margin of the landslide toward the center of the valley (fig. 3, point S). A small scarp separates this block from the undisturbed hillside. Trees on this block have backward tilts of about 10°.

Erosion subsequent to the 1964 sliding provided the silt that discolored Bear Creek for several years. Erosion channels, which are floored with boulders 1–3 feet in diameter, separate mounds of tree-covered glaciomarine diamicton 30–40 feet high. Whether these eroded mounds represent glide blocks or material that did not slide is not known. Such erosion apparently continued intermittently for at least several years. Figure 5*A* shows one group of trees (point 4) standing high on the main landslide scarp in 1966; figure 5*B* shows the same trees at the base of the scarp in 1968. Thus, it is also probable that the scarp as exposed in 1966 was modified from the original configuration of the scarp that existed immediately after the original slide took place.

The isolation of the landslide area resulted in an apparent delay between the occurrence and recognition of the landslide. Consequently, absolute determination of the triggering action is not possible. Photographs taken July 1962 show that the terrain had no fresh landslide scars. One event that occurred regionally during the interval between late 1962 and mid-1964 was the March 27, 1964, Alaska earthquake. The Juneau area, only 15 miles away, was affected to differing degrees. The heaviest rolling shocks apparently were concentrated in the valley of the Mendenhall River, about 8 miles northwest of Juneau, and the control tower at the airport located at the lower end of the valley was temporarily abandoned (von Hake and Cloud, 1966, p. 54). It seems plausible to assume that parts of Admiralty Island were equally affected by the shocks; if so, one might speculate and tentatively attribute the triggering action of the Admiralty Island landslide to the shock waves and shaking caused by the earthquake.

DEPOSITS IN THE LANDSLIDE SCARP

The material in the landslide scarp is considered here to correlate with the diamicton of the glaciomarine deposits exposed along the mountain slopes bounding the fiords in the Juneau area, and in the bluffs along Gastineau Channel. All these deposits—whether accumulated on Admiralty or Douglas Islands, or on the mainland—contain numerous scattered boulders 3 feet or more in diameter dispersed throughout a relatively fine grained matrix. Fragments larger than cobbles were not collected in samples of the diamicton, and all remaining pieces larger than 64 mm were removed before the samples were subjected to mechanical analysis. The fine-grained matrix in the landslide scarp is predominantly silt and clay. Two samples collected from the diamicton below the peat layer (fig. 4, curves 1 and 2) reflect the same general textural distribution as the samples of the more sandy matrix reflected in curve 4, which is the average of 12 samples of glaciomarine deposits collected on the mainland and Douglas Island. In addition, the species of Foraminifera from the diamicton in the landslide scarp is part of the fauna that is typical of accumulation in fiords where the water was probably less than 50 fathoms deep (Ruth Todd and Doris Low, written commun., 1967). The finer grained character of

the Admiralty Island samples probably is due to the more quiet water associated with the former fiord that extended as an elongate valley into which this part of the glaciomarine sequence was deposited. The fiords nearer Juneau are closer to the mainland source areas that provided much of the materials that were deposited as glaciomarine diamicton.

Judged from available field and laboratory data, the glaciomarine diamicton accumulated on Admiralty Island in the same manner as the diamicton accumulated on the mainland. Much of the diamicton on the mainland near Juneau has been called "marine till" in the past, but as determined from geologic field evidence in the Juneau area, a glacier-free environment existed along the fiords during deposition of the diamicton. Radiocarbon dates determined for shells within the older delta deposits that lie about 200–250 feet above sea level along the mountain slopes bounding the fiords and the dates determined for shells in diamicton beneath the delta deposits and elsewhere along the fiord walls are similar. The presence of deltas rather than kames along the fiords requires that the glaciers retreated from the area before the deltas formed in open water. The similar ages for the diamicton and the delta deposits indicate a similar glacier-free environment for the diamicton as well. According to the interpretation of the depositional story in the Juneau area (Miller, 1972), the first phase of deposition was the accumulation of the stony fossiliferous diamicton during a maximum submergence of the land in latest Pleistocene time and earliest Holocene time and during the first part of land emergence in early Holocene time. Marine waters occupied the formerly ice-filled but still depressed fiords around Juneau, and by inference, Admiralty Island. As the land rebounded and the galciomarine diamicton emerged above water, waves reworked the upper few feet of the material and helped stratify the deposits in an environment of nearshore shallow water. The numerous coarse fragments typical of the diamicton are believed to represent transport by bergs and sea ice. Nearly midway through the emergence cycle, a slowing or halting of unknown duration apparently occurred, as shown by the older deltas perched along the mountain slopes. These deposits probably were graded to sea level at the time of deposition. During this interval, the rise in sea level apparently exceeded land uplift and relatively quiet water existed along the shores. A fossiliferous stony clayey silty sandy layer of glaciomarine diamicton then buried the delta deposits. Land emergence subsequently accelerated and exceeded the rise in sea level. Glaciomarine deposits accumulated in the water until the total emergence was completed, thereby exposing fossiliferous deposits high on the slopes of the mountains and far up fiords and tributary valleys.

Apparently most of the fossiliferous diamicton, in at least this part of southeastern alaska, that lies below a minimum altitude of about 700 feet above sea level is a glaciomarine deposit rather than marine till. The main landslide scarp is one of two high exposures of Foraminifera-bearing diamicton currently known to me in this region. The second exposure is slightly higher, cropping out at 750 feet above sea level, and is on the mainland northwest of Juneau, along Montana Creek (Miller, 1972, p. 94). The closeness in altitude of these two deposits lends support to the interpretation that the Juneau-Admiralty Island area was more or less uniformly depressed as a result of the weight from glacial ice of Pleistocene age. The ice-free fiords in this area filled with marine waters and slowly emerged above water level at about the same time in response to the absence of the load from the glaciers.

INTERPRETATION OF THE WOODY PEATY LAYER AND THE RADIOCARBON DATE

The woody peaty layer in the main scarp of the landslide (fig. 6) was interpreted in 1966 as lying in normal depositional and stratigraphic position and as reflecting an interruption of glaciomarine deposition. It was anticipated that similar ages would be found for materials from the peat layer and from shell materials collected from older delta deposits near Juneau. Accordingly, the potential importance of a date from the peaty horizon is emphasized in my transmittal comment regarding the anticipated radiocarbon date, as reported in Marsters, Spiker, and Rubin (1969, p. 224) "*** peat in

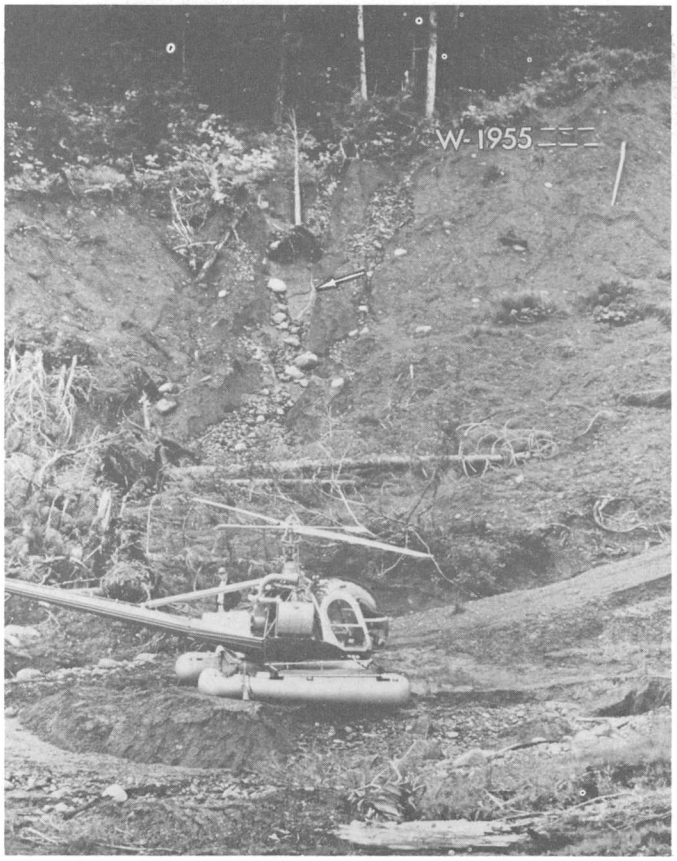

Figure 6.—Part of the main scarp of the landslide; September 1966. Locality of radiocarbon sample W-1955 is indicated. Bedding in the washed area of the scarp is shown by the arrow. Note numerous cobbles and boulders in diamicton away from drainage channels; these fragments are in place.

highest known marine deposit in area; age critical for determination of rate of uplift and detection of possible tectonic movement between Admiralty Island and Douglas and the mainland."

The radiocarbon age of 3,400±250 years B.P. (W-1955, Marsters and others, 1969, p. 224) determined for the Admiralty Island sample, however, is younger than the 10,000–12,000-year ages obtained from shells in the older delta deposits on the mainland (Miller, 1972, p. 70). Glaciomarine deposits above the sand and gravel deposits in the older deltas are slightly younger; one such deposit on Douglas Island contains molluscan shells dated at 9,150±800 years B.P. (W-2395, Meyer Rubin, written commun., Jan. 15, 1970). Glaciomarine deposits beneath the older delta at this locality are dated at 10,760±500 years B.P. (W-2394, Meyer Rubin, written commun., Jan. 15, 1970). Earlier determinations of dates from diamicton led me to expect a date within the 10,000-year range for the peat sample from Admiralty Island. The resulting younger date could be misinterpreted from the comment in Marsters, Spiker, and Rubin (1969, p. 224) to mean that Admiralty Island had an enormous amount of rebound after an abnormally prolonged period of submergence.

In 1968, I reexamined the peat bed in the light of the 3,400-year-old radiocarbon date and found that the depositional relationship between the peat bed and the fossiliferous diamicton was not as clearly exposed in 1966 as I had believed; consequently, the importance of the peat bed is overstated in Marsters, Spiker, and Rubin (1969). By 1968, erosion of the main scarp had created gullies 4–6 feet deep which exposed the relationship of the peat bed to the overlying materials.

The deposit on top of the peaty layer apparently is composed of material that moved down the valley and buried a land surface composed of peat and wood fragments. The particle-size curves in figure 4 provide contrasts that seem to indicate different depositional conditions. The nearly straight line curve (3) derived for the material above the peat layer indicates a deposit that has a wide distribution of grain sizes; this curve is in contrast with those curves of the better sorted materials that show a dominance of one particular grain size. Such curves are 1 and 2 from the diamicton in the main scarp below the peat layer, and curve 4 from the deposits of diamicton on the mainland. Curves similar to 4 were obtained for glaciomarine deposits on the mainland of British Columbia and Vancouver Island, British Columbia, Canada (Armstrong, 1957, p. 4; Fyles, 1963, p. 21). I interpret the straight-line curve to be indicative of depositional conditions that are completely different from those of a glaciomarine environment.

Straight-line curves are typical of deposits related to mass movement and glacial deposition. Straight-line curves have been obtained from lahars and mudflows on Mount St. Helens, Oreg. (Mullineaux and Crandell, 1962, p. 860, 863), and on Mount Rainier, Wash. (Crandell, 1971, p. 28, 41, 55, 66), and from glacial till in the Puget Sound area (Mullineaux, 1970, p. 35).

The brief examination of the exposures in and near the landslide scarp did not resolve the mode of origin of the material above the peat bed. However, the young age of the peat requires that any overlying till be Neoglacial in age; the Neoglaciation apparently started in the Juneau area about 3,500 years ago (Heusser, 1960, p. 186). Deposits of this glaciation characteristically retain recognizable topographic forms where seen in the Juneau area (Miller, 1972, p. 53). There are no such recognizable glacial features in the valley directly above the landslide on Admiralty Island.

Mass movement, probably a mudflow, is a likely origin for the material above the peat. The texture, color, and consistency of this material and of the material beneath the peat are similar. In addition, laboratory tests of mainland diamicton, to which I relate the Admiralty Island deposits, show that many of the deposits of diamicton have a high affinity for water, but a correspondingly critical range between stability and flowage as the percentage of moisture increases (Miller, 1972, p. 99). It seems reasonable to me to consider the deposit that buried the ground surface about 3,400 years ago as a mudflow that was derived from saturated glaciomarine diamicton exposed upvalley from the present landslide scarp. Such an interpretation does not require recent tectonic activity to account for the young age of the peat.

REFERENCES CITED

Armstrong, J. E, 1957, Surficial geology of New Westminster map-area, British Columbia: Canada Geol. Survey Paper 57-5, rept. and map 16-1957, 25 p.

Crandell, D. R., 1971, Postglacial lahars from Mount Rainier volcano, Washington: U.S. Geol. Survey Prof. Paper 677, 75 p.

Fyles, J. G., 1963, Surficial geology of Horne Lake and Parksville map-areas, Vancouver Island, British Columbia: Canada Geol. Survey Mem. 318, 142 p.

Heusser, C. J., 1960, Late-Pleistocene environments of North Pacific North America; an elaboration of late-glacial and postglacial climatic, physiographic, and biotic changes: Am. Geog. Soc. Spec. Pub. 35, 308 p.

Marsters, Beverly, Spiker, Elliott, and Rubin, Meyer, 1969, U.S. Geological Survey radiocarbon dates X: Radiocarbon, v. 11, no. 1, p. 210–227.

Miller, R. D., 1972, Surficial geology of the Juneau urban area and vicinity, Alaska, with emphasis on earthquake and other geologic hazards: U.S. Geol. Survey open-file report, 107 p.

Mullineaux, D. R., 1970, Geology of the Renton, Auburn, and Black Diamond quadrangles, King County, Washington: U.S. Geol. Survey Prof. Paper 672, 92 p.

Mullineaux, D. R., and Crandell, D. R., 1962, Recent lahars from Mount St. Helens, Washington: Geol. Soc. America Bull., v. 73, no. 7, p. 855–870.

von Hake, C. A., and Cloud, W. K., 1966, United States earthquakes, 1964: U.S. Coast and Geod. Survey [Pub.], 91 p.

Jour. Research U.S. Geol. Survey
Vol. 1, No. 3, May-June 1973, p. 315–325

CAN SATELLITE PHOTOGRAPHY CONTRIBUTE TO TOPOGRAPHIC MAPPING?

By FREDERICK J. DOYLE, McLean, Va.

Abstract.—Photographs taken on early space missions, in the Gemini-Apollo series, demonstrated the usefulness of the long view for cartography despite acknowledged shortcomings. Later developments, such as ERTS and Skylab, will provide far more data about Earth, but mostly in planimetric form. The third dimension, height, which makes the map representation topographic, is not easy to measure at orbital altitudes. The capability of current and near-future systems is not likely to do much for topographic mapping at scales larger than 1:250,000, but the benefits in planimetric mapping may be better than even the optimists hoped for.

As one reviews the accomplishments of the last decade, there can be little doubt that the routine achievement of successful missions in space is the most technologically significant. Photogrammetrists and cartographers naturally look upon orbiting spacecraft as a logical step in the progression from planetable to aircraft to satellite. They can foresee the same kind of quantum jump in production, geometric accuracy, and content of topographic maps which occurred when aerial photogrammetry replaced ground surveys. At the same time they are frustrated because as of this date there has been only one space camera system in which photogrammetric principles were considered in the design and operation of the camera.

HASSELBLAD PHOTOGRAPHY

Throughout the manned space program, Hasselblad and Maurer cameras were used for still photography. These are both 70-mm film cameras with interchangeable lenses of various focal lengths. In the Mercury and Gemini programs, over 2,400 color photographs were obtained. Many of them are exceptionally beautiful and certainly historical. Scientifically they demonstrated the utility of the synoptic view for geologic, hydrologic, and geographic interpretation of the Earth's surface. They also demonstrated that, apart from cloud cover, photographing through the Earth's atmosphere did not impose as great a problem as had been anticipated.

Though cartography was not an objective for the Gemini missions, and photographs were not acquired in typical mapping sequences, some attempts were made to demonstrate the potential usefulness of space photographs for map compilation. A single frame exposed from Gemini 7 over the Cape Kennedy, Fla., area was compared with the existing 1:250,000-scale map, and new cultural features were located. Mosaics of Peru and the Southwestern United States were assembled from rectified prints of the Gemini photographs. Geologic and land-use maps were compiled to demonstrate the utility for small-scale thematic mapping.

In April 1968, the unmanned Apollo 6 Earth-orbiting mission carried an intervalometer-controlled Maurer 70-mm film camera with 76-mm focal length. A sequence of near-vertical stereophotographs over the Southwestern United States was obtained. One photograph at original scale 1:2,730,000 of the Dallas-Fort Worth, Tex., area was compared with the existing 1:250,000 topographic map. By measuring the coordinates of identified points on an enlarged and rectified print and comparing them with coordinates scaled from large-scale (1:24,000) maps, it was found that the space photograph could be used to check the planimetric accuracy of the small-scale map. Furthermore it was clearly demonstrated that linear cultural features such as roads and railroads, whose actual dimensions were far less than the ground resolution of the photograph, could be detected and indeed recognized on the photograph. In addition the limits of urbanized areas were easily visible on the photograph. The report on the study concluded that the space photograph was useful for map revision in terms of both planimetric position and content.

The Apollo 9 manned Earth-orbiting mission in March 1969 carried an experiment known as SO-65. The principal objective of the experiment was to simulate the multispectral photographs of the Earth Resources Technology Satellite (ERTS). Four 70-mm Hasselblad cameras with 80-mm lenses were mounted in a fixture which held their optical axes parallel and provided simultaneous exposures by all four shutters. The camera array was mounted in the hatch window of the Apollo Command Module. The spacecraft was oriented so that the camera axes were vertical, and five strips of pictures across the Southern United States were obtained under exceptionally favorable weather conditions. Three black-and-white films were exposed through appropriate filters to give the red, green,

and near-infrared spectral bands proposed for the ERTS television cameras. The fourth camera obtained color infrared photographs which simulate the effects of superimposing the three black-and-white pictures. These pictures have been used extensively to determine the procedures for automatic thematic mapping of Earth resources.

Two frames of the red band covered approximately the area of the 1:250,000 Phoenix, Ariz., map sheet. These were rectified and enlarged nearly 10 times by fitting to detail points identified on the map and the photographs. The mosaic was then printed as an image base for the standard line map. A number of different color schemes were tried, and versions were produced both with and without contours (fig. 1). The maps have been widely circulated in the cartographic community, and the reaction has been overwhelmingly, though not unanimously, favorable. The black and white reproductions in this paper do not show the added advantages of color enhancement of the image base.

On the standard line map, wherever white paper appears there is no information. The terrain morphology, the field patterns, and other characteristics of the area are more clearly shown by the photographic image. At the same time, all the information from the conventional line map is also available.

Though the Phoenix line map had been recently checked for accuracy and revised for content, the photoimage base disclosed corrections to both accuracy and content. In several areas there was an obvious mismatch between the photographic and the line data. Checking against large-scale maps disclosed that the error was in the line map and not in the image. In other areas, the photoimage showed new cultural features constructed since the line map was revised.

Though the Phoenix 1:250,000 space photomap may be considered a qualified success, it should be evaluated more as a forerunner of things to come rather than as an example of the limits of utility of space photographs for cartography.

LUNAR CAMERA SYSTEMS

Photogrammetrists will readily recognize that the Hasselblad cameras are not to be compared with the sophisticated mapping cameras used in aircraft. When focal lengths of 150 and 600 mm and formats of 230 mm are used at altitudes up to 10,000 m in aircraft, it is patently absurd to expect comparable information with focal lengths of 80 mm and formats of 70 mm from spacecraft at nearly 20 times the altitude.

For reasons difficult to rationalize, the lunar exploration program has been able to obtain better cameras than have been used in the Earth program. Through lunar Apollo mission 12, the Hasselblad camera was again used with interchangeable lenses of focal lengths 60, 80, 250, and 500 mm. The 60-mm lens was used primarily for documentary photographs within the spacecraft and for operations on the lunar surface. The 80-mm lens was used with the camera mounted on a bracket in the Command Module hatch window to obtain near-vertical stereo strips from lunar orbit much like the Apollo Earth photography. The 250-mm lens was used handheld to take oblique photographs of sites of particular geologic interest. On Apollo 12 an attempt was made to photograph potential landing sites for future missions by using the 500-mm lens. To provide both forward-motion compensation and adequate stereo base, the camera was bracket mounted in the hatch window. The entire spacecraft was pitched in synchronism with its forward motion to keep the same scene in the field of view. This complicated operation restricted the number of targets that could be photographed, because of the necessity of completely reorienting the spacecraft as a unit between scenes, and it was only marginally successful in providing the hoped-for high resolution.

In October 1969 the Apollo Orbital Science Photographic Team was formed to recommend the photographic equipment and operations which would get the maximum scientific return from the remaining missions. However, the team was not completely free in selecting the camera systems to be employed. It was necessary to choose cameras that were either available or developed to the extent that they could meet the rigid timetable of qualification for the Apollo missions, which were at that time scheduled at approximately 4-month intervals. Furthermore, severe space and operating requirements had to be met. Consequently the cameras selected were compromises adapted from existing equipment.

Lunar Topographic Camera

The first new photographic system was a modified Hycon (now Actron Industries, Inc.) KA-74 reconnaissance camera of 460-mm focal length, exposing 430 frames in each magazine of 130-mm roll film. The camera was mounted on a special fixture in the Command Module hatch window. Forward-motion compensation was provided by rocking the entire camera in its mount during the exposure. Adequate stereo base was obtained by taking pictures with the camera axis vertical on one revolution and directed 20° aft on the succeeding revolution.

The camera was carried aboard Apollo 13 and was actually mounted in position ready for lunar approach photography when the oxygen tanks exploded and the mission was aborted. It was carried again on Apollo 14, but a transistor failure resulted in only about 80 good frames being obtained. A further modified version of the KA-74 will be carried on Skylab as the S-190B Earth Terrain Camera.

Lunar Panoramic Camera

With Apollo 15, 16, and 17, lunar photography took on new dimensions. In a section of the Service Module known as the SIM (Scientific Instrumentation Module) various orbital science experiments were mounted. A major component of the SIM was a panoramic camera to provide high-resolution photographs of large areas of the lunar surface. The camera

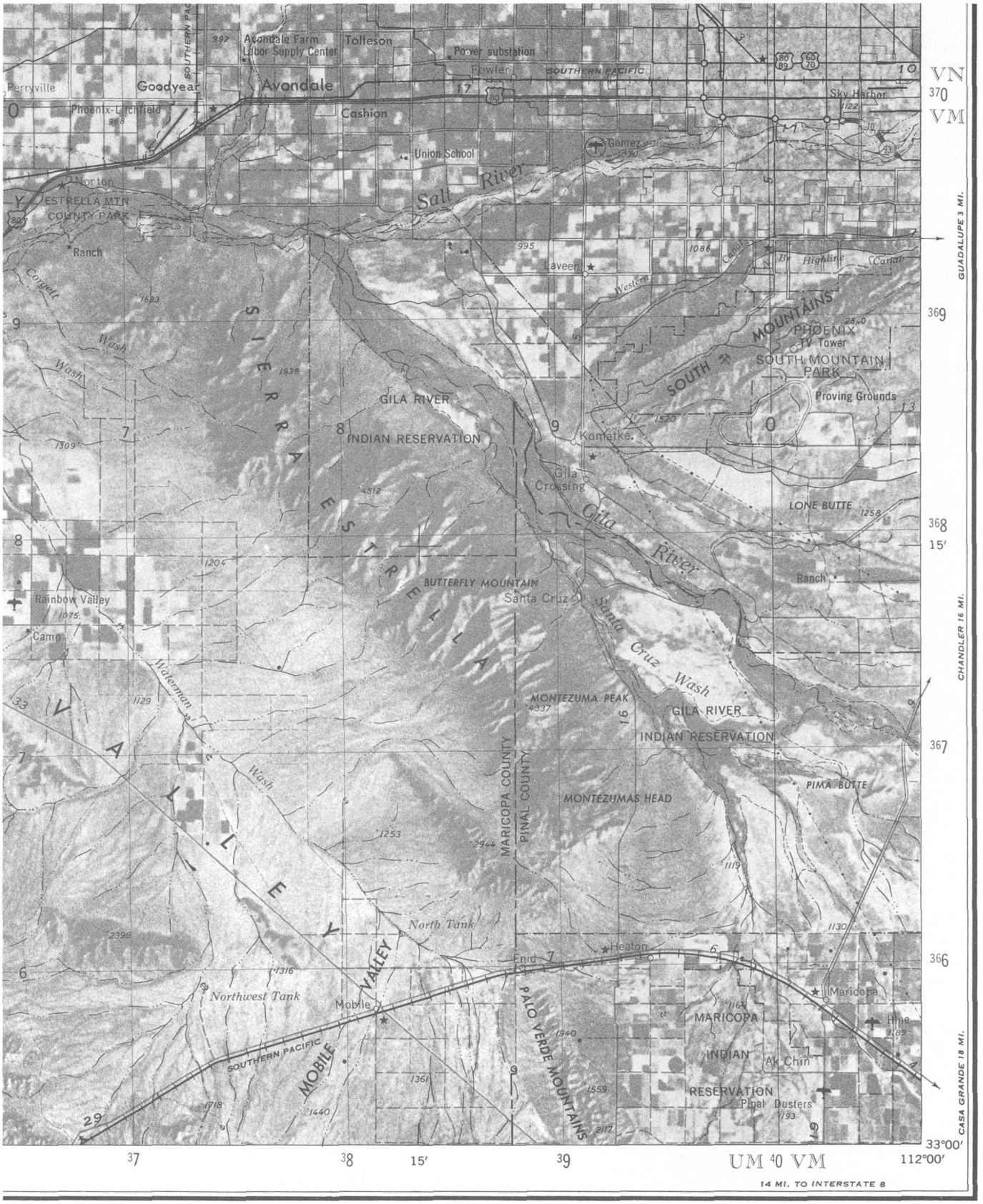

Figure 1.—Apollo space photograph provides image base for standard 1:250,000-scale topographic map. Original map has photoimage base printed in brown, and line detail in conventional colors of black, red, blue, and green.

had a 610-mm focal length and an aperture of f/3.5. The 108° sweep angle exposed a frame 115 by 1,270 mm on 130-mm roll film. A total of 1,900 m of thin-base film provided 1,650 exposures.

The camera, constructed by Itek Corp., is a modification of an existing rotating-optical-bar camera. Its principal elements (fig. 2) are the main frame, which mounts rigidly to the spacecraft and carries the supply and takeup film rolls; the stereo gimbal assembly, which can rotate about a transverse axis to provide stereo convergence and forward-motion compensation; and the roll-frame assembly, which carries the rotating lens and moving-film rollers.

Stereo coverage can be obtained by rocking the camera 12.5° forward or aft between succeeding exposures. A V/H (velocity/height) sensor provides the signal for controlling the forward-motion compensation, which is also obtained by rocking the camera. A light sensor mounted on the stereo gimbal adjusts the exposure time by modifying the width of the slit. From the nominal operating altitude of 111 km, the camera provides about 2-m surface resolution at the spacecraft nadir. In the monoscopic mode each frame covers 300 km across track by 20 km along track, and each vertical photograph overlaps the preceding one by 10 percent at the nadir. In the stereo mode, the camera rocks through the 25° convergence angle between each pair of exposures. The forward exposure from station 1 and the aft exposure from station 6 overlap by 100 percent to form a stereomodel, and each succeeding stereomodel overlaps the preceding one by 10 percent.

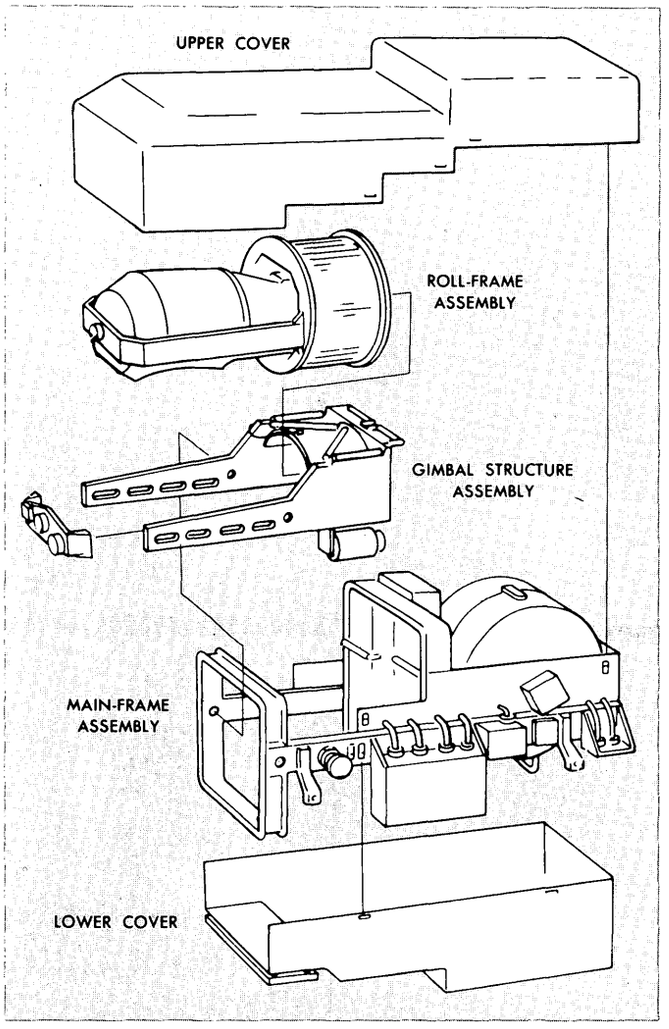

Figure 2.—Principal elements of Lunar Panoramic Camera.

For many applications it is desirable to transform the panoramic photographs into equivalent vertical photographs, and a special transforming printer was constructed to do so. The rectifier (fig. 3) is an analog of the camera system. The film is carried on a cylindrical platen whose radius is equal to the 610-m equivalent focal length of the camera. Longitudinal displacement of the film with respect to the center of the arc compensates for roll of the spacecraft. A moving light source traverses the length of the film to make the exposure. The projection lens rotates at a variable rate to assure sharp focus at all positions. The projected image is then reflected to the easel. The tilt of the easel can be adjusted to compensate for the 12.5° stereo convergence as well as for spacecraft pitch. The longitudinal curvature of the easel can be adjusted to simulate the curvature of the lunar surface for orbital altitudes up to 150 km.

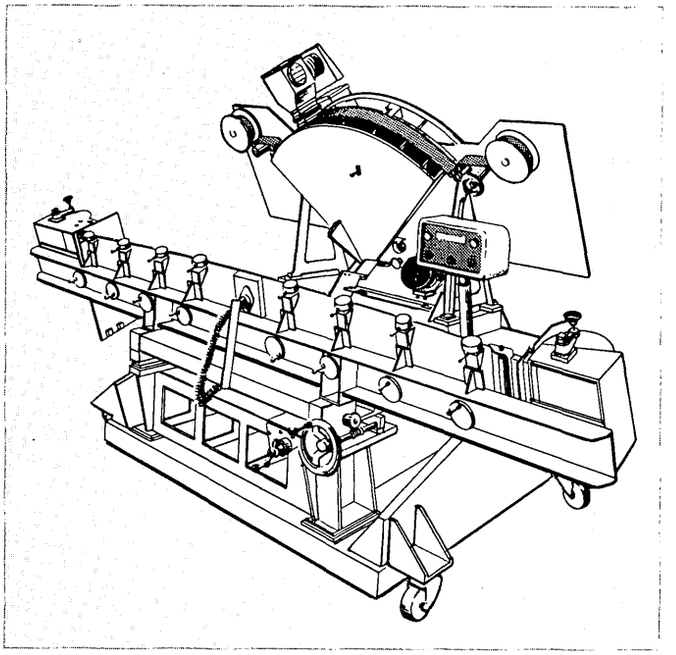

Figure 3.—Rectifier for lunar panoramic photographs.

The rectified pictures have a nadir enlargement of approximately 1.8 times but are restricted to a scan angle of 35° on either side of the nadir. The resolution, measured at the input scale, varies from 90 line pairs per millimeter on axis to 50 line

pairs per millimeter at 35° maximum scan. The displacement of images from all causes is specified as 1 mm circular probable error. Thus the rectified pictures are not designed for photogrammetric use but have adequate geometry for photointerpretation.

Mapping Camera System

Mounted on the front shelf of the SIM on Apollo missions 15 through 17 was a Mapping Camera System (fig. 4) composed of a terrain camera, a stellar camera, a laser altimeter, and a precise timing mechanism.

The terrain camera had a 75-mm focal length, f/4.5 lens and exposed a 115- by 115-mm format on 130-mm roll film. The glass-plate focal plane was engraved with a 10-mm reseau. Two sets of artificially illuminated fiducials and one set of naturally illuminated fiducials were provided. A data block on each frame of the terrain camera recorded the midpoint of each exposure to ±1 msec. The flight height measured by the laser altimeter and the shutter open time to ±0.1 msec were also recorded. A manually adjusted V/H mechanism provided forward-motion compensation with an accuracy of 3 percent by moving the focal plane during the camera exposure. Automatic exposure control set the between-the-lens shutter in five steps between 1/15 and 1/240 second.

The resolution on the lunar surface depends upon solar altitude and the accuracy of forward-motion compensation. For the nominal altitude of 111 km and exposure on Kodak 3400 film, the high-contrast resolution at low solar altitude was about 20 m per line pair, decreasing to about 50 m for low-contrast resolution at high solar altitude.

The forward overlap of successive frames was adjusted preflight. The available 3,600 exposures permitted the total overflown area to be photographed with 78 percent forward overlap and 55 percent side overlap, meaning that every point on the ground was seen on four consecutive photographs with a maximum base-height ratio of 1.0. In addition to providing geometric strength for triangulation, the four views permit study of the Moon's peculiar photometric characteristics.

The stellar camera was directed to the side of the orbital plane and 4° above the horizon so that no part of the lunar surface was included in the field of view. The lens is 75-mm focal length, f/2.8, and exposes a 25- by 32-mm format on 35-mm film. Four fiducials and a 5-mm reseau on the glass focal plane were edge illuminated to record on the film. Prefogging has the additional advantage of hypersensitizing the film for stellar exposure. A fixed exposure time of 1.5 seconds provided an average of 25 star images per frame, depending on the location of the field of view in the celestial sphere. The laser altimeter was mounted with its transmission and receiving optical axes parallel to those of the terrain camera, and its accuracy was about ±2 m.

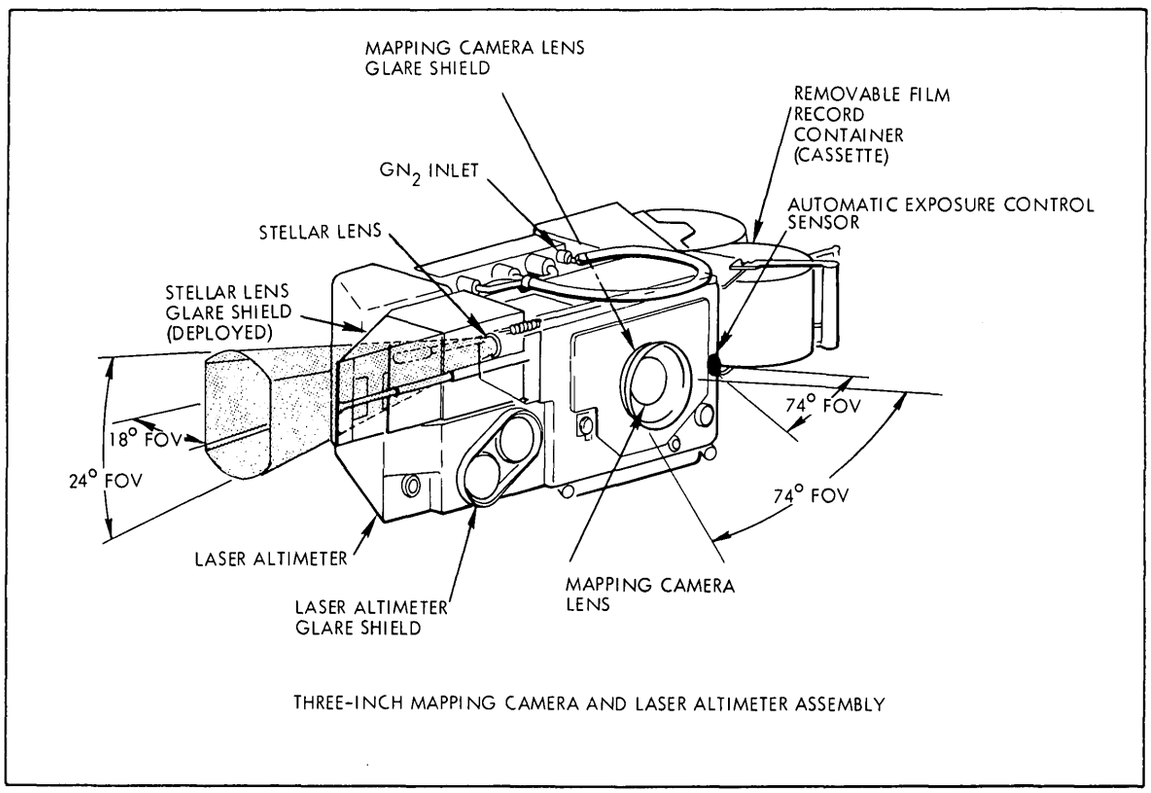

Figure 4.—Mapping Camera System for Apollo 15–17.

The terrain and stellar cameras were built by Fairchild Space and Defense Systems. The laser altimeter was built by RCA Aerospace Systems, but Fairchild was responsible for integrating it into the mapping camera package. The installation of all systems in the SIM was the responsibility of North American Rockwell.

Film recovery

The photographic films from both the panoramic and the mapping camera systems were accumulated in special quick-release magazines. The astronaut left the Command Module, activated a single handle which cut the film, closed the light-tight compartment, and released the film-return magazine. The magazines were stowed in the Command Module for the journey back to Earth.

The design and construction of these complicated camera systems, their qualification for operation in a manned spacecraft, and extensive planning for the data analysis of the lunar photographs inspire confidence that an adequate system could be devised for topographic mapping of the Earth at scales compatible with existing cartographic standards.

RATIONALE FOR AN EARTH MAPPING SYSTEM

Before attempting to define a useful system of topographic mapping from space data, we must examine some of the factors involved. A topographic map contains three kinds of information:

Content—the details represented on the map.

Position—the reference graticule.

Elevation—spot heights and contour lines.

Any mapping system must be able to provide all of these.

Map content is obtained from photographic resolution and scale, or more directly from ground resolution. It is difficult to establish a linear relation between map scale and required ground resolution because some features, like roads and railroads, must be shown on a map regardless of its scale. However, by considering the photograph as an image base (photomosaic or orthophotograph) for the map, a useful criterion can be produced.

Under normal conditions the unaided human eye resolves about 5 line pairs per millimeter. To retain that resolution in the final map, the photograph should have better resolution, say at least 10 line pairs per millimeter, to allow for inevitable losses in processing. Therefore the ground resolution of the image base map would be 1/10 mm times the map scale number:

$$R_g = 10^{-4} S_m \ , \tag{1}$$

where

R_g = ground resolution, in meters, and

S_m = map scale number.

Obviously not all map content is obtainable directly from photographs, regardless of scale or ground resolution, whether taken from aircraft or space. Data such as political boundaries, place names, and detail obscured by vegetation must be compiled on the ground or from other sources. The fact that linear features whose lateral dimension is well below the resolution limit can nevertheless be identified works in favor of small-scale photographs.

In aircraft photography, external factors such as attitude rates, vibration, and atmospheric anomalies generally restrict photographic resolution to 25 to 30 line pairs per millimeter regardless of the laboratory-determined lens-film performance. In the space environment all the degrading factors are considerably reduced so that the actual photographs may have nearly the same resolution as measured in the laboratory.

Large-scale maps (S_m<25,000) are usually compiled with up to 5 times enlargement between airphotograph and map scale. Medium-scale maps (25,000<S_m<100,000) are compiled at 1 to 2 times enlargement between photograph and map. Small-scale maps (S_m>100,000) are usually assembled from existing larger scale source materials rather than compiled directly from photographs. The restrictions, however, generally result from the operational limits of aircraft, cameras, and photogrammetric instruments, rather than from the information inherent in the photographs. According to the criterion established, high-resolution space photographs can be enlarged until their equivalent resolution is 10 line pairs per millimeter.

$$M_a = r_p/10, \tag{2}$$

where

M_a = allowable enlargement from photo to map scale, and

r_p = original photo resolution, in line pairs per millimeter.

The second kind of map information is planimetric position. Absolute position is generally provided by reference to ground control points. For a space system, however, orbital tracking data can provide spacecraft position to a high order of accuracy. When the tracking data are coupled with precise camera attitude data and time of exposure, an independent means of determining absolute position is available.

Within a stereomodel or a photogrammetric triangulation, the internal positional accuracy is equal to the product of the photograph scale and the error in measuring or identifying a point on the picture:

$$\sigma_p = S_p \sigma_r \ , \tag{3}$$

where

σ_p = standard error in position of a ground point,

σ_r = residual measuring error, and

S_p = photograph scale number.

U.S. National Map Accuracy Standards (NMAS) require that the standard error of point positions should not exceed 0.3

mm at the published map scale:

$$\sigma_p = 3 \times 10^{-4} S_m . \quad (4)$$

The third kind of information on a topographic map is terrain relief depicted by contour lines, spot elevations, and sometimes shaded relief. In conventional aerial mapping, vertical control points are established with an accuracy of 0.1 to 0.2 of the contour interval. A statistical interpretation of NMAS requires that

$$\sigma_h = 0.3 \text{ c.i.} , \quad (5)$$

where

σ_h = standard error of elevation, and
c.i. = contour interval.

It may be noted in passing, however, that recent tests by the U.S. Geological Survey have demonstrated that if a stereomodel is properly adjusted to redundant vertical control points, contours at an interval equal to the standard error can be compiled and still meet NMAS.

Elevation data are obtained from aerial photographs by means of image parallax, which depends on the camera configuration, the image scale, and the measuring accuracy:

$$\sigma_h = S_p (H/B) \sigma_r , \quad (6)$$

where H/B is the reciprocal of the base-height ratio.

The critical requirements for maps at various scales can be derived by applying formulas 1, 4, and 5, with the results given in table 1. A fixed contour interval does not necessarily go with a given map scale. An interval fine enough to depict the character of the terrain will be chosen. The values listed in table 1 represent the performance objectives against which a space cartographic system should be evaluated.

Table 1.—*Map accuracy requirements, in meters*

Map scale number S_m	Ground resolution R_g	Std. error position σ_p	Contour interval c.i.	Std. error elevation σ_h
1,000,000	100	300	100	30
250,000	25	75	50	15
100,000	10	30	25	8
50,000	5	15	10	3
25,000	2.5	7.5	5	1.5

SPACE CAMERA SYSTEM FOR EARTH MAPPING

In the summer of 1967, NASA (National Aeronautics and Space Administration) asked the National Academy of Sciences to study "Useful Applications of Earth Oriented Satellites." Thirteen panel reports were presented, discussing a variety of interests. Although differing in details, the Forestry, Agriculture, Geography, Geology, and Hydrology Panels confirmed their requirements for a television system providing repetitive cover at relatively coarse resolution.

The Geodesy-Cartography Panel attacked the problems of providing data for geodetic control and topographic mapping on a worldwide basis. The Geodetic Satellite Program is now producing a worldwide network of some 40 stations in a unified geocentric coordinate system. Continental intensification networks, if carried to completion as recommended by the panel, will locate points with better than 3-m accuracy at about 800-km spacing. These points, together with existing geodetic control, can form the foundation for map compilation at scales as large as 1:25,000.

The panel recommended two camera systems: a metric camera system for complete small-scale mapping and establishing control for large-scale mapping, and a long-focal-length convergent camera system for providing the detail necessary for large-scale map compilation. The recommended metric camera system would comprise:

- A vertical frame camera with 305-mm focal length, 230- by 365-mm format, and 70-percent forward overlap between frames.
- A stellar-altitude camera with 150-mm focal length and 70-mm format, synchronized with the terrain camera.
- A laser altimeter measuring the distance from camera to terrain in synchronism with each camera exposure.
- A timing device to record the midpoint of each exposure.

Though the panel did not define the large-scale camera in detail, the panoramic camera from the lunar program would be an obvious candidate. The major parameters of the camera systems are summarized in table 2.

To retain the geometric integrity of the photographs, the panel recommended physical recovery of the film rather than transmission of the images by some form of television system. The general procedure would be to mount the cameras in the spacecraft and feed the exposed film to the attached reentry capsule (fig. 5). When the photographic mission has been

Table 2.—*Parameters of space camera systems*

	Control camera (frame)	Stellar camera (frame)	Compilation camera (panoramic)
Focal length . . . . . mm . .	305	150	610
Film width . . . . . mm . .	240	70	125
Sweep angle . . . . . degrees . .	. . . .	. . . .	70
Format . . . . . mm . .	230 by 365	60 by 60	115 by 1270
Convergent angle . . . . . degrees . .	. . . .	. . . .	30
Overlap between frames . . . . . percent . .	70	. . . .	100
Base-height ratio	.72	. . . .	.54
Resolution (AWAR[1], in line pairs per mm)	50	. . . .	135

[1] AWAR, area weighted average resolutions.

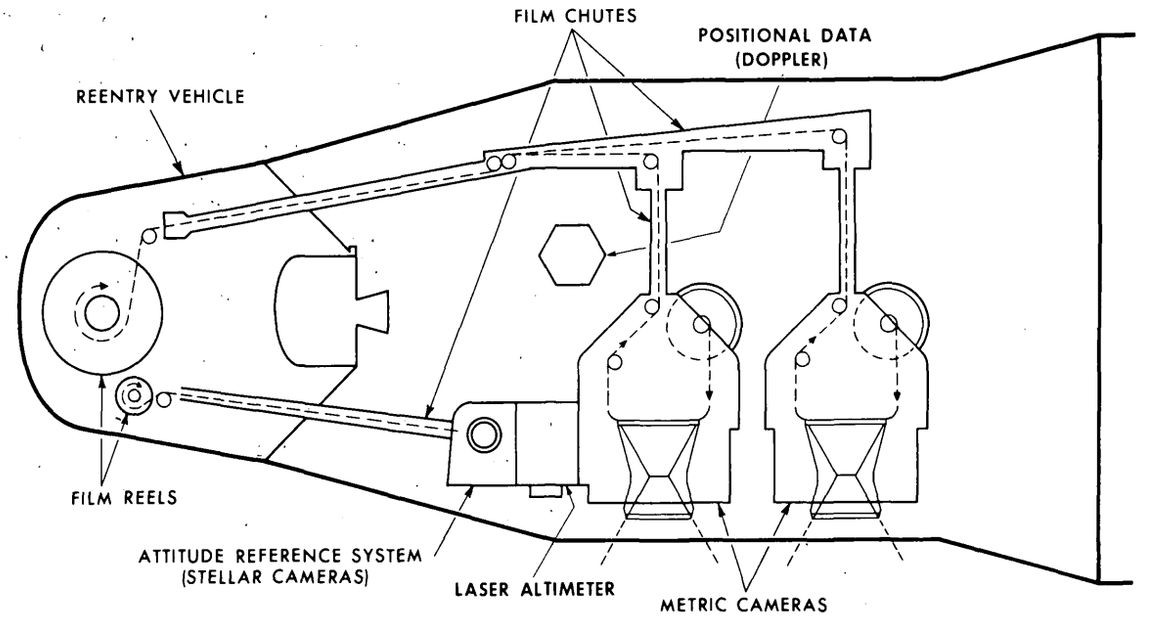

Figure 5.—Design of film-return system.

completed, the recovery vehicle would be separated from the spacecraft and reenter the atmosphere. A parachute would be deployed, and the film package would be picked up by aircraft. An operating altitude of about 200 km was recommended in order to obtain an adequate lifetime for the satellite.

In evaluating the expected performance of the system, a critical factor is the residual image coordinate error, σ_r. In analytical triangulation with conventional aerial photographs, σ_r = 7 μm is regularly obtained in a single stereomodel, and σ_r = 15 μm in a strip of 6 to 10 photographs between control points. With space photography there is good reason to believe that these values can be appreciably reduced. Contributing factors include:

Better photograph resolution.

Reseau to indicate film deformations.

Attitude constraints for each stereopair, obtained from the stellar photographs.

Exposure-station positions, obtained from orbital tracking data.

Scale restraint in each stereopair, obtained from the laser altimetry.

It is expected that σ_r = 5 μm can be obtained in a single stereomodel and σ_r = 10 μm in a triangulated block.

When the appropriate values are substituted in formulas 2, 3, and 6, the expected performance of the two camera systems is as listed in table 3. It should be noted that no absolute values are listed for the panoramic photographs because the panoramic camera has very poor inherent geometry. The concept, therefore, is to establish the control for large-scale mapping with photographs taken by the frame camera, and then use the high-resolution panoramic photographs to compile the planimetry and contours.

Table 3.—*Expected performance of space cameras*

	Control camera	Compilation camera
Photograph scale S_p	655,000	328,000
Ground resolution R_g ..... m	13	2.4
Allowable enlargement M_a	5	13.5
Maximum map scale S_m	130,000	24,000
Coverage per frame ..... km	150 by 240	38 by 280
Relative accuracy (σ_r=5μm):		
Position σ_p ..... m	3.3	1.6
Elevation σ_h ..... m	4.6	3.0
Contour interval ..... m	13.7	9.0
Absolute accuracy (σ_r=10μm):		
Position σ_p ..... m	6.5	....
Elevation σ_h ..... m	9.2	....
Contour interval ..... m	27.5	....

By comparing the performance values in table 3 with the map requirement values in table 1, it is apparent that the systems can satisfy mapping needs as shown in table 4.

If the photographs from the control camera were enlarged 2.6 times to form a photoimage base for a map at 1:250,000 scale, a single frame would more than cover a standard map sheet. Within the limits of a stereomodel—the central third of each frame—terrain relief of nearly 400 m could be accommodated without exceeding the allowable planimetric displacement. One can imagine the improvement in the Phoenix 1:250,000 space photomap if the resolution of the photoimagery were increased fourfold.

Table 4.—*Maximum mapping capacity of recommended camera systems*

	Control camera	Compilation camera
Relative mapping		
Content for map scale	130,000	25,000
Position accuracy for map scale	25,000	25,000
Elevation accuracy for contour interval (meters)	15	10
Absolute mapping		
Content for map scale	130,000	25,000
Position accuracy for map scale	25,000	25,000
Elevation accuracy for contour interval (meters)	25	....

Similarly if a 1:25,000-scale map sheet is located near the center of a panoramic photograph, nearly 300 m of relief can be accommodated without exceeding planimetric accuracy requirements.

Contours at the indicated intervals of 10 to 25 m will not be easily obtained. Conventional photogrammetric instruments operate at a C-factor (C = altitude/c.i.) of 1,000 to 2,500. It would require C = 8,000 to 20,000 to reach the values inherent in the photography. Analytical plotting instruments or computer derivation of contours from digitized elevations are possible solutions to the problem. One should not be surprised that new data handling techniques may be needed to exploit the capability of space photography. After all, the optical-mechanical plotting instrument required for aerial photogrammetry represented quite a development beyond the planetable and alidade used in ground surveys.

Obviously, one could argue that any of the assumed values should be a factor of 2 larger or smaller. What is needed is an experiment to determine how well actual performance will conform to that predicted. The U.S. Geological Survey has proposed to NASA that a system with the characteristics of the control camera be flown. It is not yet a funded project, but topographic mappers look forward to it as the best approach to the application of space photography to their requirements.

WHAT ABOUT ECONOMICS?

Several contractors have submitted proposals to NASA to build a photogrammetric satellite as described at a cost between $15 and $20 million per mission. The exact capability cannot be determined until the system is designed, but the National Academy of Sciences estimated that 90 kg of film could be carried—enough to photograph 20 million km^2, or enough to cover the entire United States twice. The cost per square kilometer is directly competitive with the most economical aircraft photography. The obvious problem, however, is that 1,000 km^2 would cost the same amount as 20 million km^2. Thus space photography is economical only for extremely large areas.

The economic analysis must include the photogrammetric and cartographic reduction as well as the cost of photography. To cover the United States with the proposed space frame photographs would require less than 1,000 stereomodels as opposed to over 100,000 with high-altitude aircraft photographs. A large part of the advantage might be lost if conventional line drafting methods are employed for map production. But as has been pointed out, the central part of each frame is orthographic within the limits of the National Map Accuracy Standards. Therefore, one can conclude that annotated orthophotomaps might be the most practical way of producing useful maps of extensive areas on a timely basis.

The formats and focal lengths of space photographs are, to a large extent, incompatible with current photogrammetric instrumentation. Clearly, if satellite photography is to be useful for production, detailed consideration and planning is required throughout the whole course of the mapping cycle, extending as far as a reeducation of map users who may find it necessary to revise their notions of what an acceptable map is.

WHAT ABOUT CLOUDS?

Extensive studies of weather-satellite pictures to predict the probability of obtaining cloud-free photographs from space indicate that a space system with a lifetime adequate for four passes over each area will achieve about 97 percent successful photography. The system will require ground control of the satellite cameras in accordance with weather predictions.

WHAT ARE THE IMMEDIATE PROSPECTS?

Apart from weather satellites, only two NASA projects for photographing the Earth from space are currently funded. The first of these is the Earth Resources Technology Satellite (ERTS), which carries three television cameras and a four-channel multispectral scanner. It is designed fundamentally to provide repetitive coverage for monitoring time-variant phenomena. Thematic mapping is an important part of the utilization of the records, and the resolution of the pictures is adequate as an image base for maps at scale 1:1,000,000 and possibly larger. But the system does not provide stereoscopic coverage, and topographic mapping is not an objective.

The other project is Skylab, designed primarily to investigate the problems of man operating for extended periods in space. An empty S-IVB rocket will be converted into a laboratory capable of supporting three men for periods of up to 56 days. The Apollo Command and Service Module will be used as a ferry to change crews in Skylab, which will be occupied three different times during its lifetime of one year. It is planned to launch Skylab in the spring of 1973. Its operating altitude will be 435 km, and the orbit inclination will be 50°. It will carry two photographic systems.

The first is a multispectral photographic experiment designated S-190A. Itek Corporation developed an array of six cameras (fig. 6), of 150-mm focal length and f/2.8 aperture, recording on 70-mm film. The optical axes of all cameras are accurately alined, and the focal length and lens distortions are matched so that all pictures can be accurately registered. Forward-motion compensation will be provided by rocking the frame that carries the six cameras. Four black-and-white spectral bands of 0.1-μm bandwidth between 0.5 and 0.9 μm are planned. The other two cameras will carry color and color-infrared film.

The second photographic experiment carried on Skylab A will be the 460-mm Actron camera from the lunar program. It has been modified for operation in Earth orbit and is designated S-190B, the Earth Terrain Camera (ETC)(fig. 7). A fixed mount is contemplated, with convergent stereo provided by pitching the entire spacecraft as it passes over an experimental area.

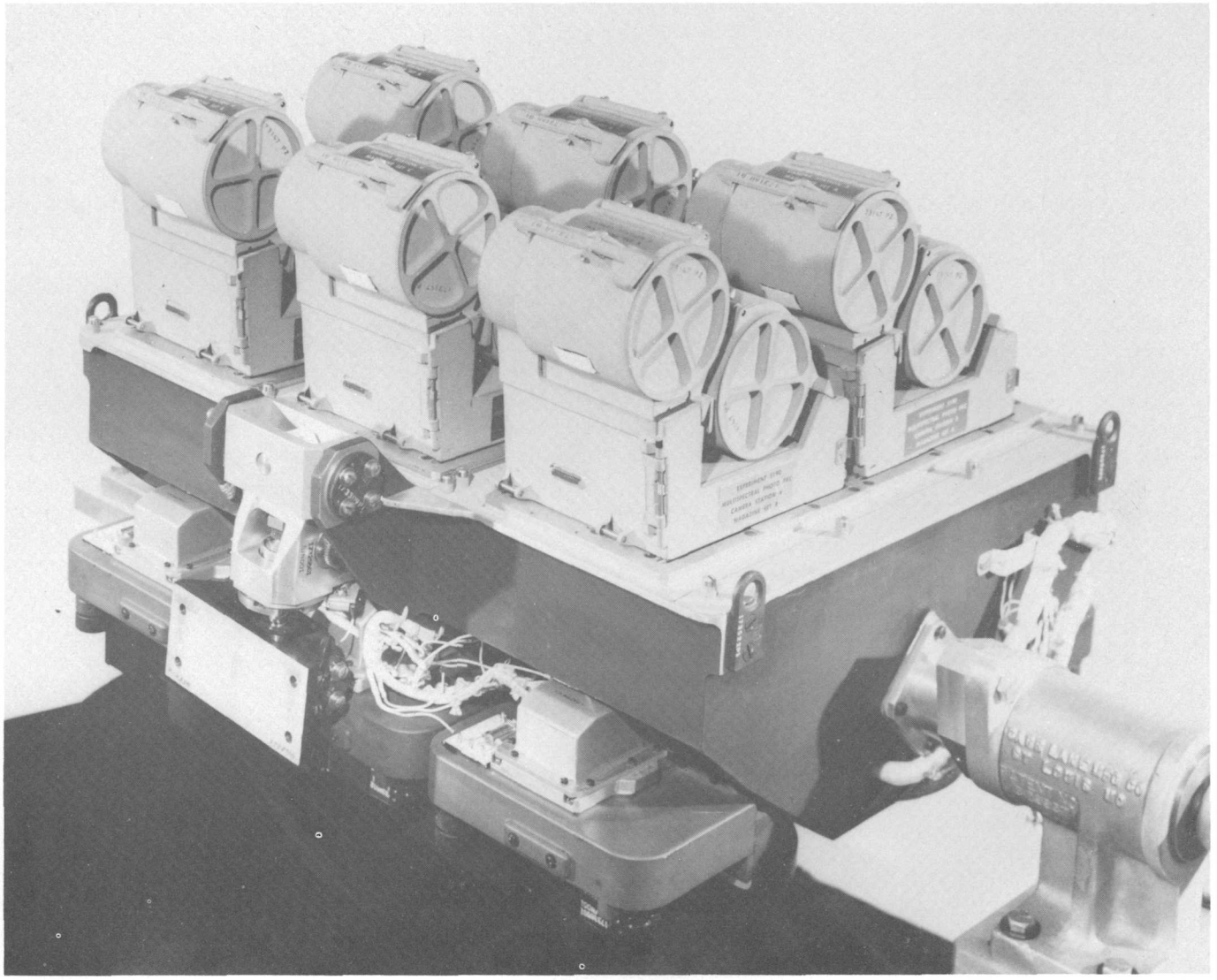

Figure 6.—Skylab S-190A Multispectral Camera.

Both systems will resolve about 80 line pairs per millimeter for usual ground-object contrasts. Neither system will have precise timing, attitude, or altimetry support data. Primary application will be for interpretation of Earth resources information. Mapping potential, evaluated by formulas 2, 3, 5, and 6, is given in table 5.

The tabulated values obviously do not approach those expected from the proposed 305-mm frame camera system, supplemented by the 610-mm panoramic camera. Nevertheless the photographs will be an appreciable improvement over those obtained from Gemini and Apollo.

CONCLUSION

The space program to date has produced some astonishing photographs. Many of them have been of compelling interest from the historical, pictorial, and interpretative points of view. So far as photogrammetrists are concerned, however, the pictures have presented far more problems than they have solved. It is easy to question why things have been done and are being done in the ways described. Most of the reasons have nothing to do with science, but with finances and politics. However, there can be no doubt that, as the difficulties of operation for men and machines in space are overcome, the advantages of space will be applied to the routine production of both thematic and topographic maps for the benefit of all mankind.

Table 5.—*Cartographic potential of S-190A and S-190B cameras in Skylab*

	S-190A	S-190B
Photo scale S_p	2,900,000	945,000
Ground resolution R_g m	36	12
Allowable enlargement M_a	8	8
Maximum map scale S_m	360,000	118,000
Coverage per frame km	174 by 174	109 by 109
Base-height ratio	.16	0.45 (25° conv.)
Accuracy (σ_r=10μm):		
Position σ_p m	30	10
Elevation σ_h m	180	20
Contour interval m	550	60

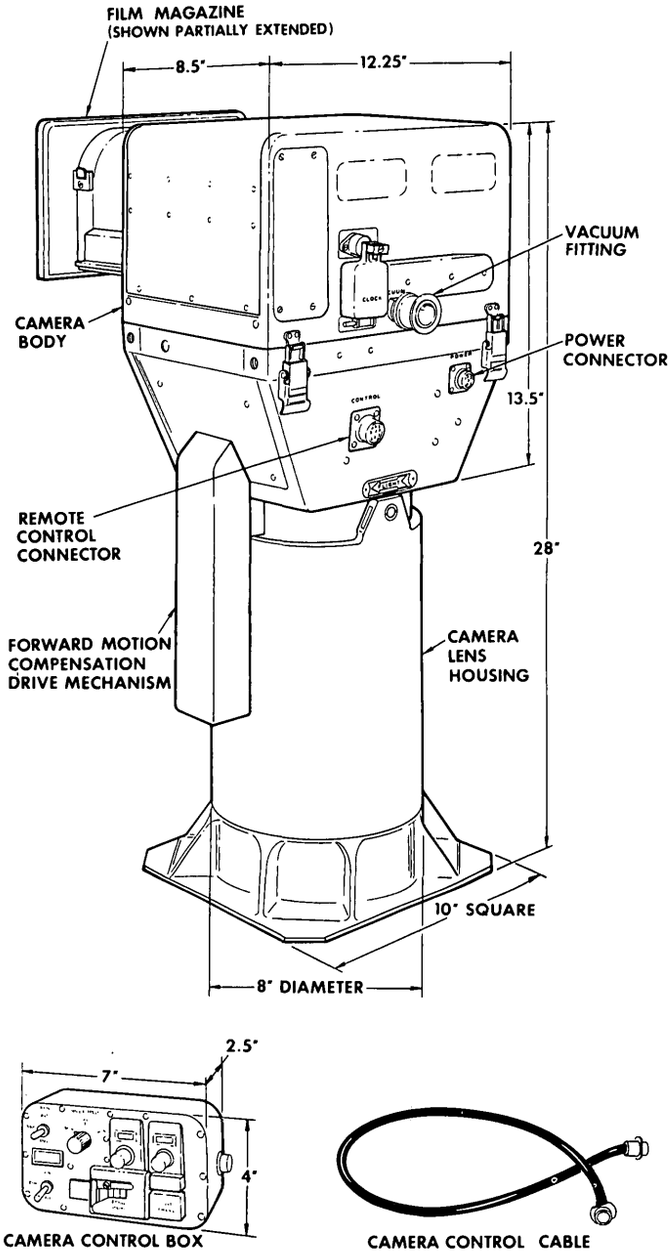

Figure 7.—Diagram of S-190B Earth Terrain Camera.

Jour. Research U.S. Geol. Survey
Vol. 1, No. 3, May-June 1973, p. 327—339

PHOTOIMAGES FOR MAP BASES

By MORRIS L. McKENZIE, McLean, Va.

Abstract.—Maps with aerial photograph image bases have gained wide popularity. The orthophotomap presents an abundance of ground detail and information that cannot be shown on a line map with standard cartographic symbols. In preparing a map base covering areas of little relief, the imagery is fitted to map control with a conventional rectifier, but for areas of significant relief, the photographs are reproduced in an orthophotoscope to remove the effects of both camera tilt and terrain relief.

The photoimage map has attained high status with both the map user and mapmaker. Geologists, geographers, hydrologists, engineers, surveyors, and city planners are finding photomaps useful as working bases. Photoimage map bases can be produced quickly and thus provide current map information either as a separate product or in combination with line symbols. The production of a photoimage base lends itself to automation with the use of equipment already developed. The automatic production of a true line map has not yet been attained.

TYPES OF PHOTOIMAGE MAPS

Terminology and definitions for various photoimage products and processes have not been universally established. Consequently, some agencies, including the U.S. Geological Survey, have their own terminology. The descriptions below are based on Geological Survey usage.

A photomap is a map on a base containing photoimagery which is retained as a part of the representation. It may incorporate special cartographic treatment, image enhancement, color separation, or a combination of these.

An orthophotomap (fig. 1) is a photomap prepared from an orthophotograph or a precisely controlled assembly of orthophotographs. It is generally published in standard map format with a geographic graticule and plane coordinate grid ticks. Color-enhanced imagery and cartographic symbols—including contours and (or) elevations, boundaries, and labels—are added as required to suit the area and intended use of the map. The prefix "ortho" implies that the horizontal position of the image base is within limits specified by the National Map Accuracy Standards.

An orthophotoquad (fig. 2) is a map of standard accuracy prepared from an orthophotograph or a mosaic of orthophotographs in quadrangle format, with little or no cartographic enhancement. It contains a geographic graticule, a reference grid or grid ticks, and appropriate map collar information, but no cartographic symbols or contours. Orthophotoquads are reproduced in final form either photographically, lithographically, or by the diazo process.

PHOTOMAPPING INSTRUMENTS

The relative positions of images in an aerial photograph are seriously influenced by camera tilt and terrain relief. If the terrain is relatively flat, then image displacements due to camera tilt are removed with a conventional rectifier. The photograph to be rectified is tilted and positioned relative to the film plane so that image points projected from the photographs are fitted to the plotted positions of these points on the film plane.

If the amount of distortion in the photograph due to relief is too great for correction by simple rectification, then the photograph is scanned in an orthophotoscope (fig. 3). In this instrument, images are projected onto a platen having a slot about 5 mm in length, which exposes the film beneath. The platen is automatically driven in the y direction (perpendicular to the flight line) with automatic stepover in the x direction (along the flight line) at the end of each y scan. The operator controls the z motion (up and down) of the platen so as to keep the exposing slot in contact with the apparent surface of the three-dimensional terrain model. Thus the photoimagery is reproduced at a common scale in a series of narrow contiguous strips (Scher, 1964).

PROCESSING

Positive photographic prints are made, all at a common scale, of the various orthophotonegatives covering the area to be mapped. They are then mosaicked to form a single photoimage base. Some orthophotos are made from a single high-altitude photograph that covers the entire area to be mapped, and mosaicking is not needed.

If the map is to be produced lithographically, the continuous-tone imagery of the mosaic is converted to minute, random-dot patterns for making pressplates (Clark, 1971).

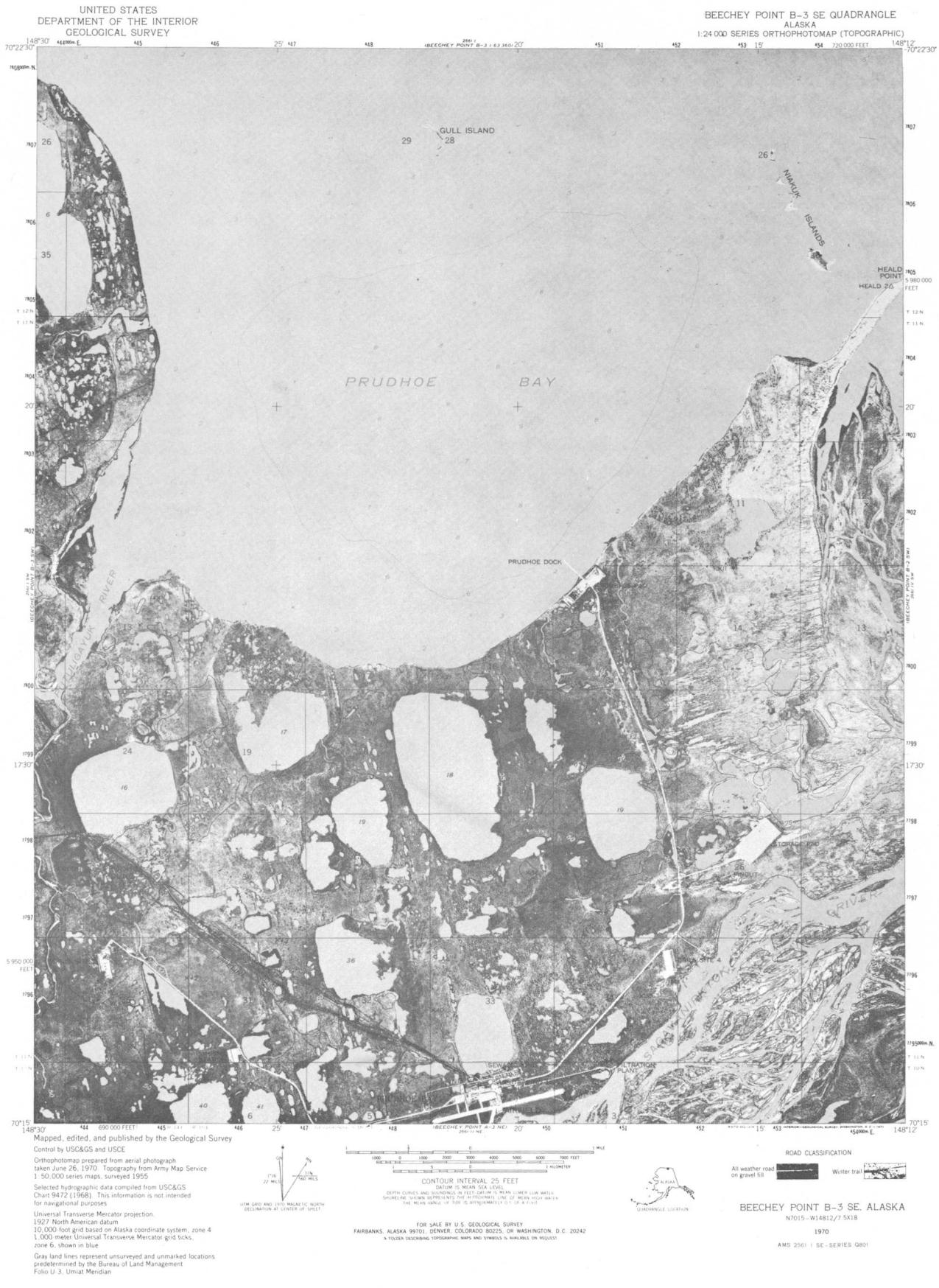

Figure 1.—Orthophotomap of Beechey Point B-3 SE quadrangle, Alaska (reduced from 1:24,000-scale multicolor edition).

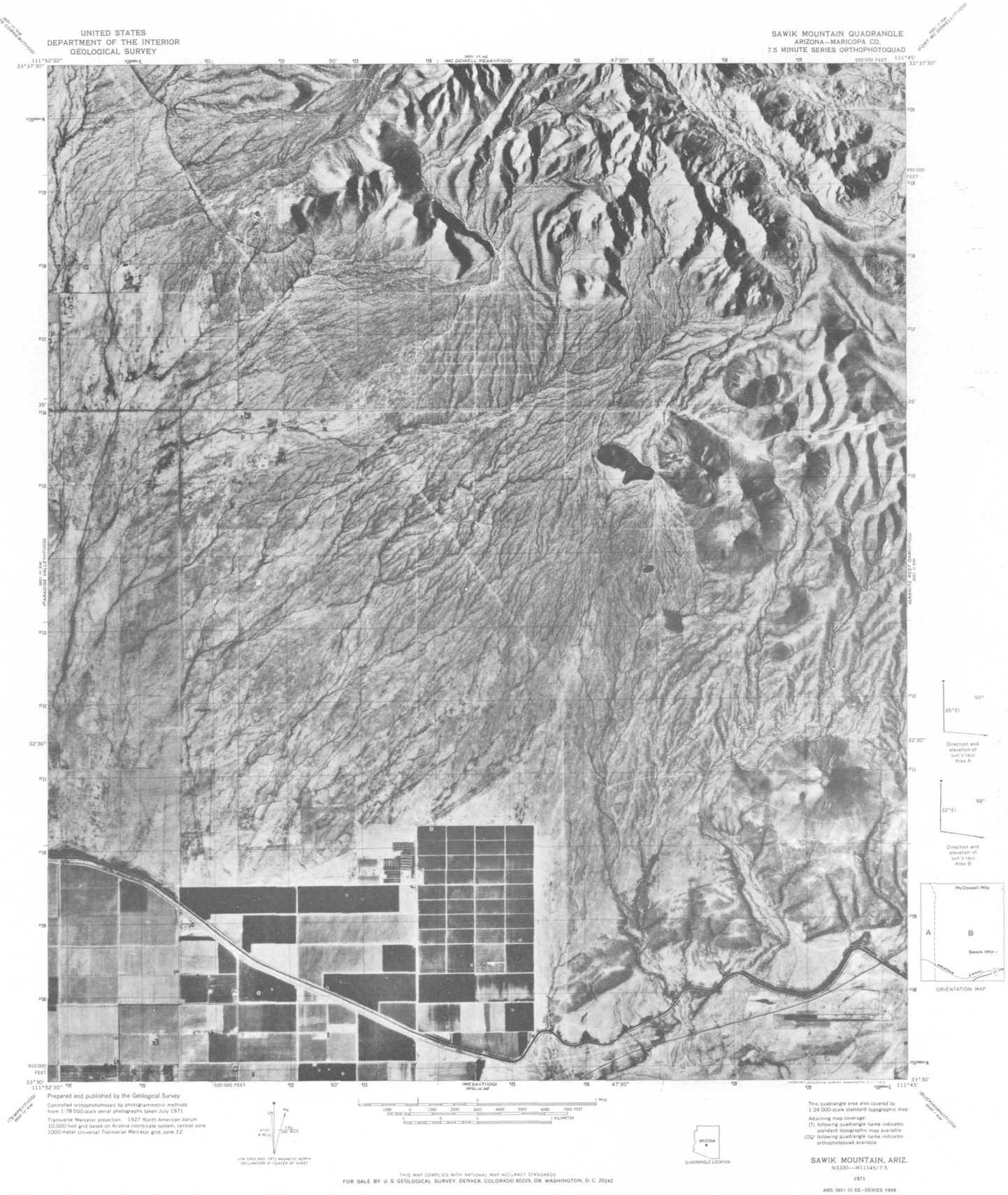

Figure 2.—Orthophotoquad of Sawik Mountain, Ariz., 7½-minute quadrangle (reduced from 1:24,000-scale monocolor edition).

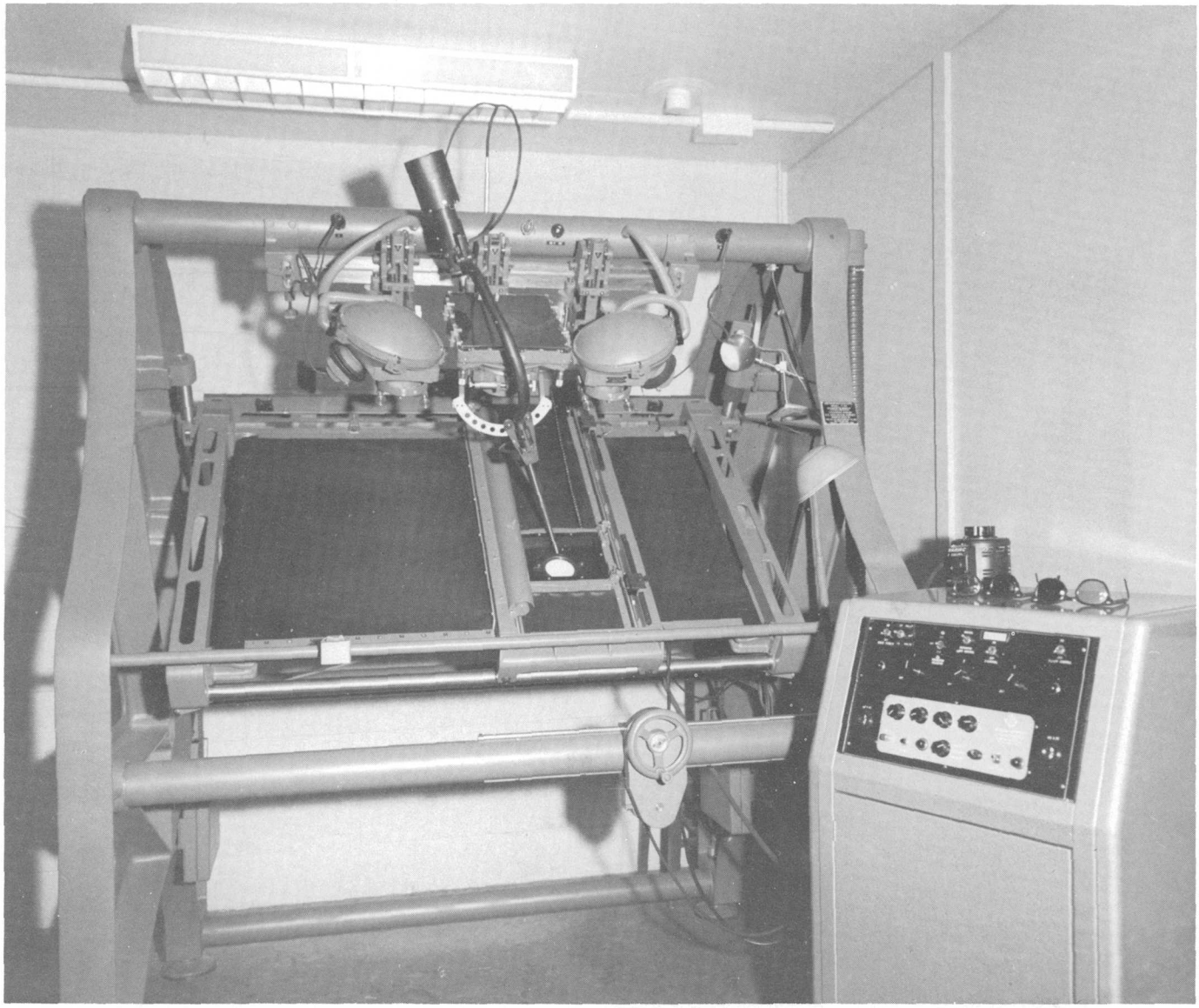

Figure 3.—Orthophotoscope, used to print orthophotographs corrected for distortion due to high relief.

Best results have been obtained with a method known as photolysis, in which a continuous-tone negative is contact printed to a matte-surface film by prolonged exposure to high-intensity ultraviolet light. The matte-surface film thus produces an extremely low contrast positive. Contact printing from the positive produces a random-dot negative on high-contrast lithographic film. Imagery from the random-dot negative can be transferred to the pressplate without the use of a halftone screen.

Orthophotomaps are usually made from black-and-white photographs, and therefore color imagery on the printed map must be artificially produced by appropriate ink colors. By masking techniques, pressplates are made for printing selected parts of the photoimagery in basic colors or a combination of colors. Thus a variety of tones and colors are available for depicting ground imagery in more recognizable colors than nature provides; that is, woodland can be accentuated with green, water features with blue, barren lands with tan or brown, and so on.

UTILITY OF PHOTOIMAGERY

Geology.—Geologists deserve much credit for fostering the development of the first Geological Survey orthophotoscope in the early 1950's. They recognized the usefulness of a true-scale photograph for geologic studies. Figure 4, top, is a part of a topographic line map of North Emblem Reservoir, Wyo., containing prominent geologic features. Figure 4, bottom, is an orthophotomap of the same area. One needs

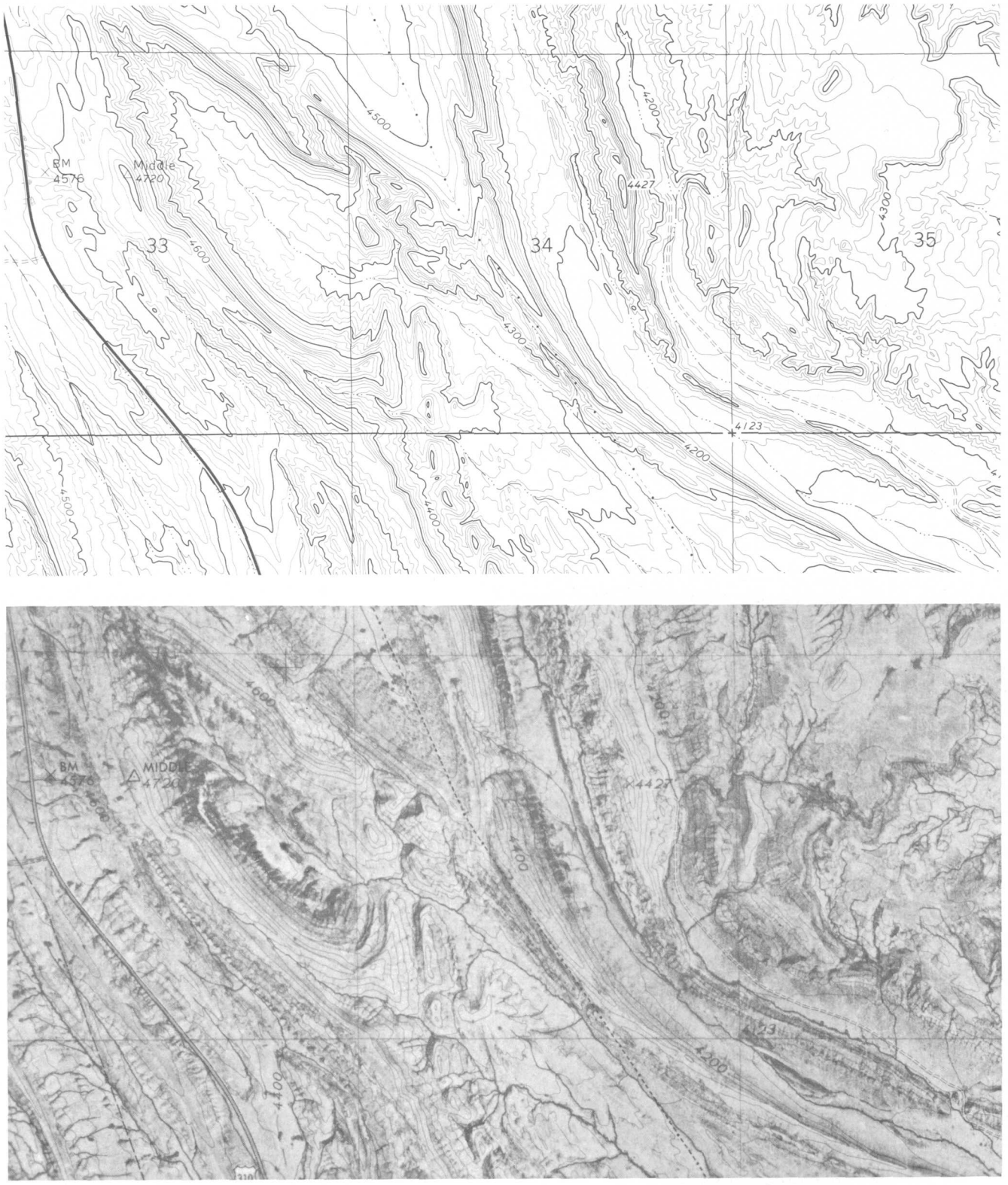

Figure 4.—Part of the North Emblem Reservoir, Wyo., 7½-minute quadrangle. *Top, topographic map; bottom, orthophotomap.* (Reproduced from multicolor editions.)

only to compare these two products to appreciate the value of the photoimage base to the geologist.[1]

Hydrology.—On the orthophotomap of Antelope Island, Utah (fig. 5), the extent of water recession of the Great Salt Lake is clearly discernible, and bottom features can be seen in shallow-water areas. This type of detail is not depicted on the line map covering the same area.

Urban planning.—Figure 6 is a part of an orthophotomap of the Dallas, Tex., area. The amount of urban detail vital to city planners that is shown automatically on an orthophotomap is not practical or even possible to show on a conventional line map.

Natural resources survey.—Figure 7, bottom, is a part of an orthophotomap of Royal Palm Ranger Station, Fla., and figure 7, top, is a part of the line map of the same area. The line map appears grossly inadequate when compared with the wealth of information and detail imaged in the orthophotomap. Even such detail as salt-water encroachment and marshland limits can be discerned on the photographs and portrayed in distinctive colors in the printed map. The orthophotomap provides many images for orienting the map to ground features, a valuable aid to the explorer.

Line map complement.—Figure 8, top, is a part of a line map of the Asbury Park, N.J., area which has undergone extensive development. Figure 8, bottom, a part of an orthophotoquad of the same area, shows the extent of development since the line map was published. The monocolor orthophotoquad provides a convenient method of providing the map user with up-to-date map information. The time required to produce an orthophotoquad is a fraction of that required to publish a standard orthophotomap or line map.

ORTHOPHOTOMAPPING RESEARCH

The two prime goals of orthophotomapping research are improved image quality and automation of the process. Instruments are being designed with the intent of reaching both of these objectives. The newly designed Orthophotomat (fig. 9) is equipped with a single projector rather than two or three projectors that require anaglyphic filtering (Hughes and others, 1971). The single plate is leveled and positioned to predetermined locations of pass points on a base sheet. The x, y, and z motions of the film platen and exposing slot of the Orthophotomat are automatically driven by the Autoline (fig. 10), which locks onto and follows the profiles previously extracted from a stereomodel.

The only link in this approach that has not been fully developed is the process of automatically extracting profiles from stereomodels. Profiles are now being extracted manually with a modified projection-type stereoplotter. The tracing table of the plotter is equipped with a special coordinatograph, which records vertical profiles in a horizontal plane as the operator scans the stereomodel in strips. The operator must keep the floating mark in contact with the ground surface in the stereomodel by manually manipulating the floating mark.

An automatic approach for extracting profiles is under development (Lewis and Hughes, 1970). The trace of intersecting, corresponding rays at ground level is recorded on film (fig. 11) by moving the stereoplotter projectors upwards as film is pulled across a slot extending the full length of the stereomodel. A profile is formed along a line of intersecting ray traces. For the next profile, the slot is moved over one increment and the process cycle repeated (fig. 12); or multiple slots are used to extract multiple profiles in one cycle. The research effort is now aimed at automatically isolating the profiles from the extraneous images formed in the process.

FUTURE PROSPECTS

During the first few years of development, the orthophotomap was not widely accepted, but the demand for this type of map is increasing rapidly. At present, most orthophotomaps supplement or complement the corresponding line map. However, the orthophotomap, in some terrain types, is coming into demand as a product preferred over the line map. It is conceivable that in the not-too-distant future the Geological Survey will provide a photoimage base as a standard product, either as content of an orthophotomap or as a separate orthophotoquad to complement the standard line map.

REFERENCES CITED

Clark, Clyde, 1971, Reproduction of orthophotographics: Am. Soc. Photogrammetry Orthophoto Workshop, Washington, D.C., Jan. 18–21, 1971, Proc.

Hughes, T. A., Shope, A. R., and Baxter, F. S., 1971, USGS Automatic Orthophoto System: Photogramm. Eng., v. 37, no. 10, p. 1055–1062.

Lewis, J. G., and Hughes, T. A., 1970, Stereoscopic profiling by intersection of ray traces: Am. Soc. Photogrammetry and Am. Cong. on Surveying and Mapping Fall Tech. Conf., Denver, Colo., Oct. 7–11, 1970, Proc.

Scher, M. B., 1964, Research in orthophotography: Photogramm. Eng., v. 30, no. 5, p. 756–762.

[1] The black-and-white reproductions in this paper do not show the added advantages of color enhancement of the imagery on orthophotomaps.

[Figures 5–12 follow this page]

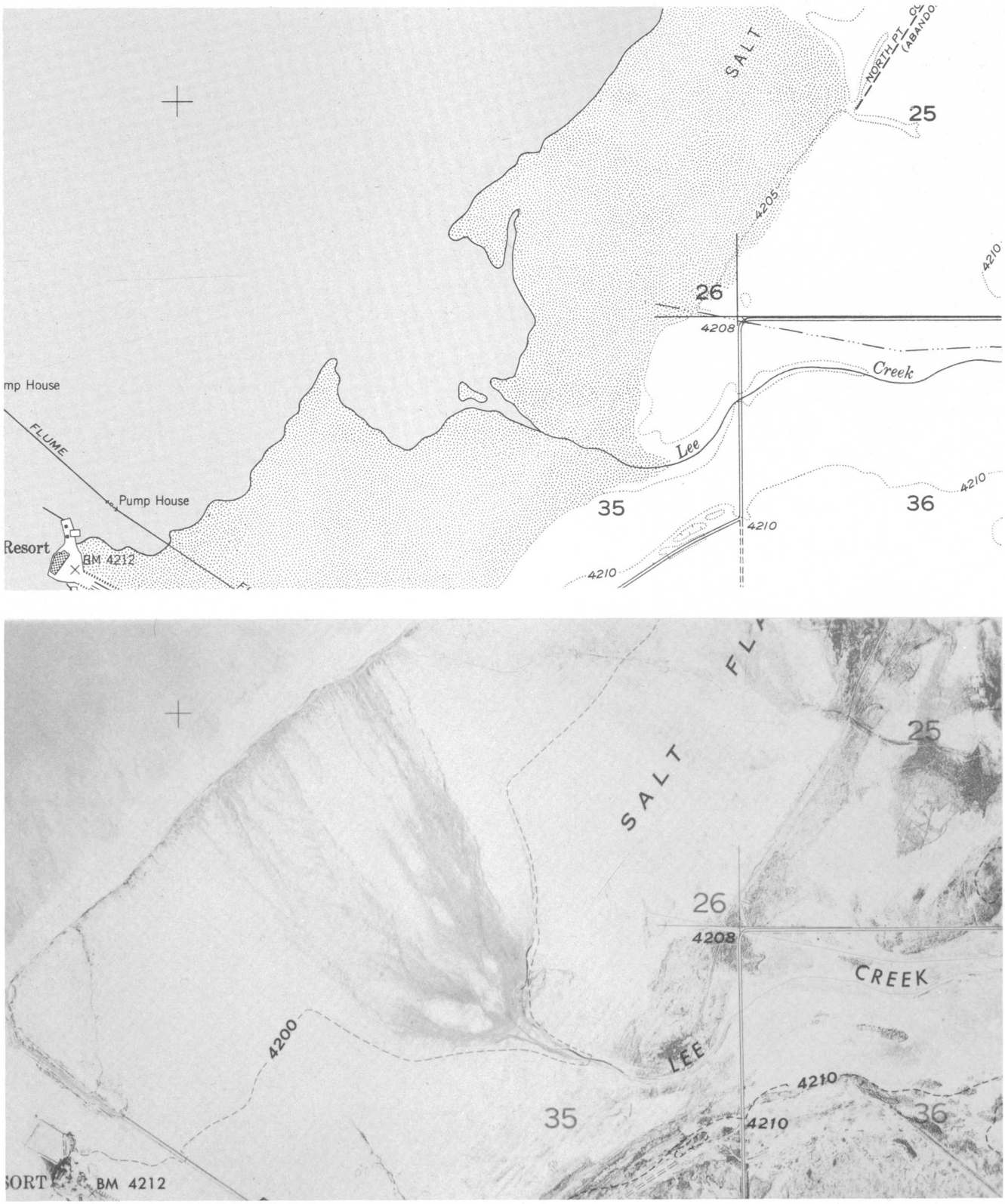

Figure 5.—Part of the Antelope Island, Utah, 7½-minute quadrangle. Top, topographic map; bottom, orthophotomap. (Reproduced from multicolor editions.)

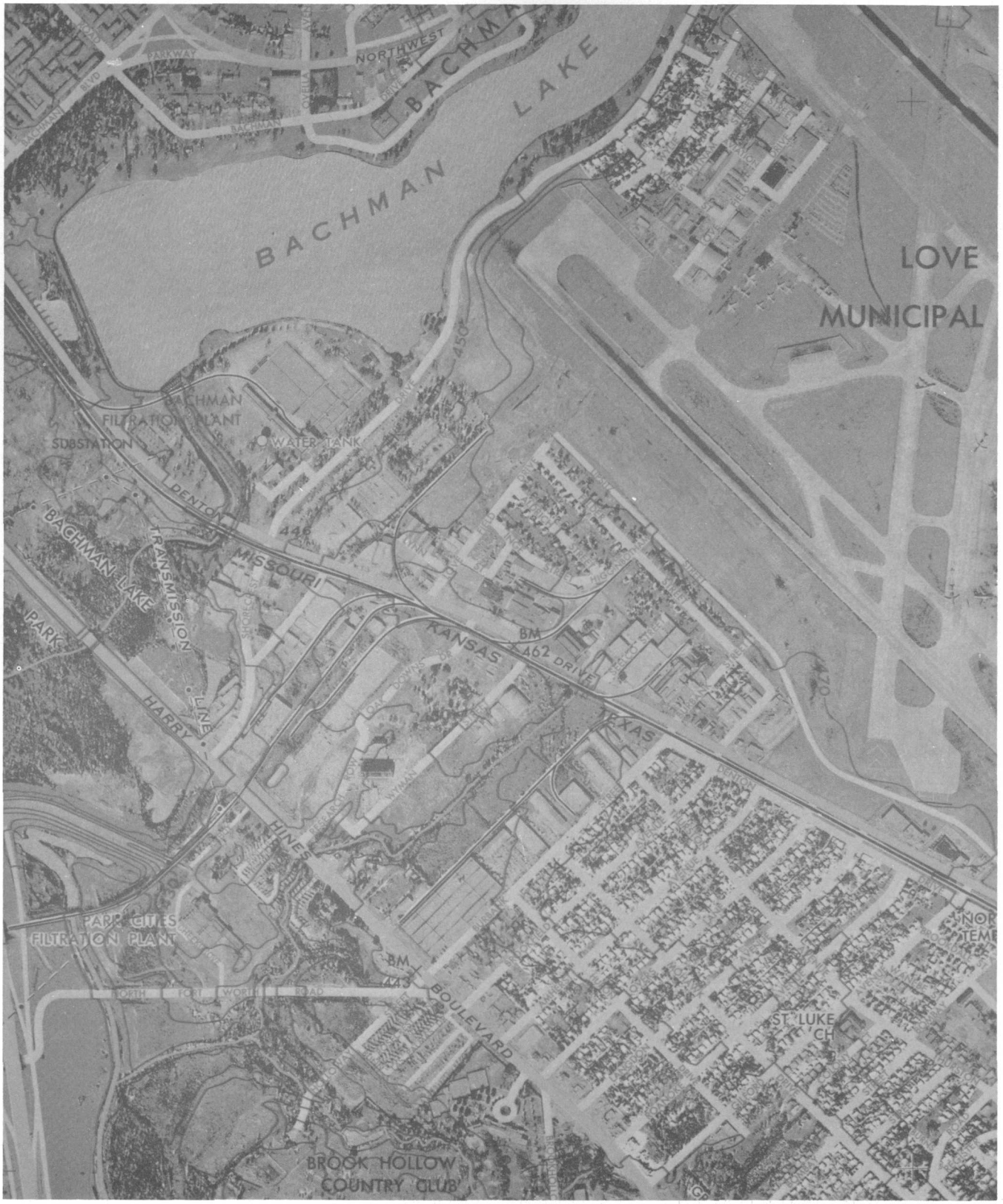

Figure 6.—Part of Dallas, Tex., experimental orthophotomap. (Reproduced from multicolor edition.)

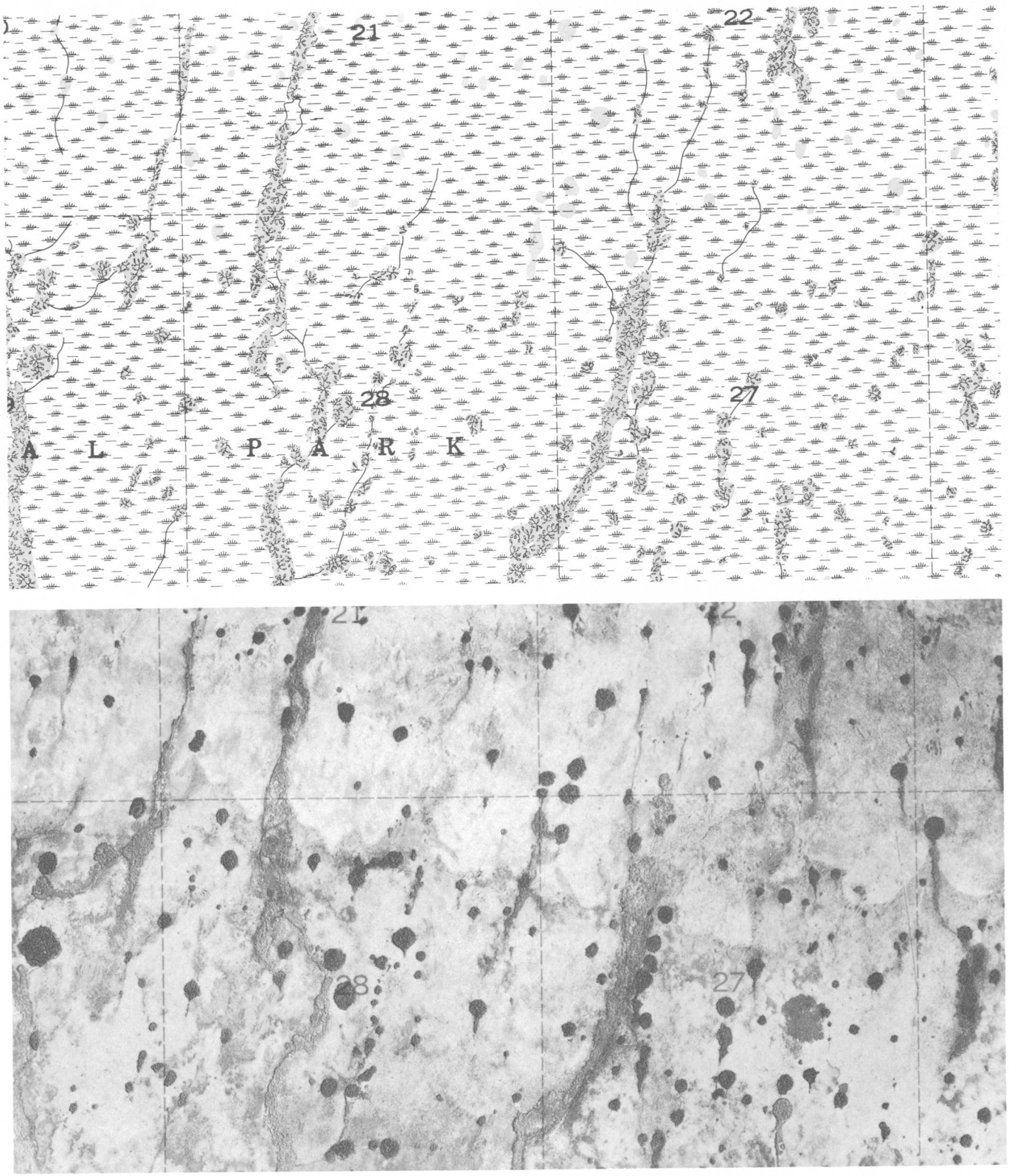

Figure 7.—Part of the Royal Palm Ranger Station, Fla., 7½-minute quadrangle. Top, topographic map; bottom, orthophotomap. (Reproduced from multicolor editions.)

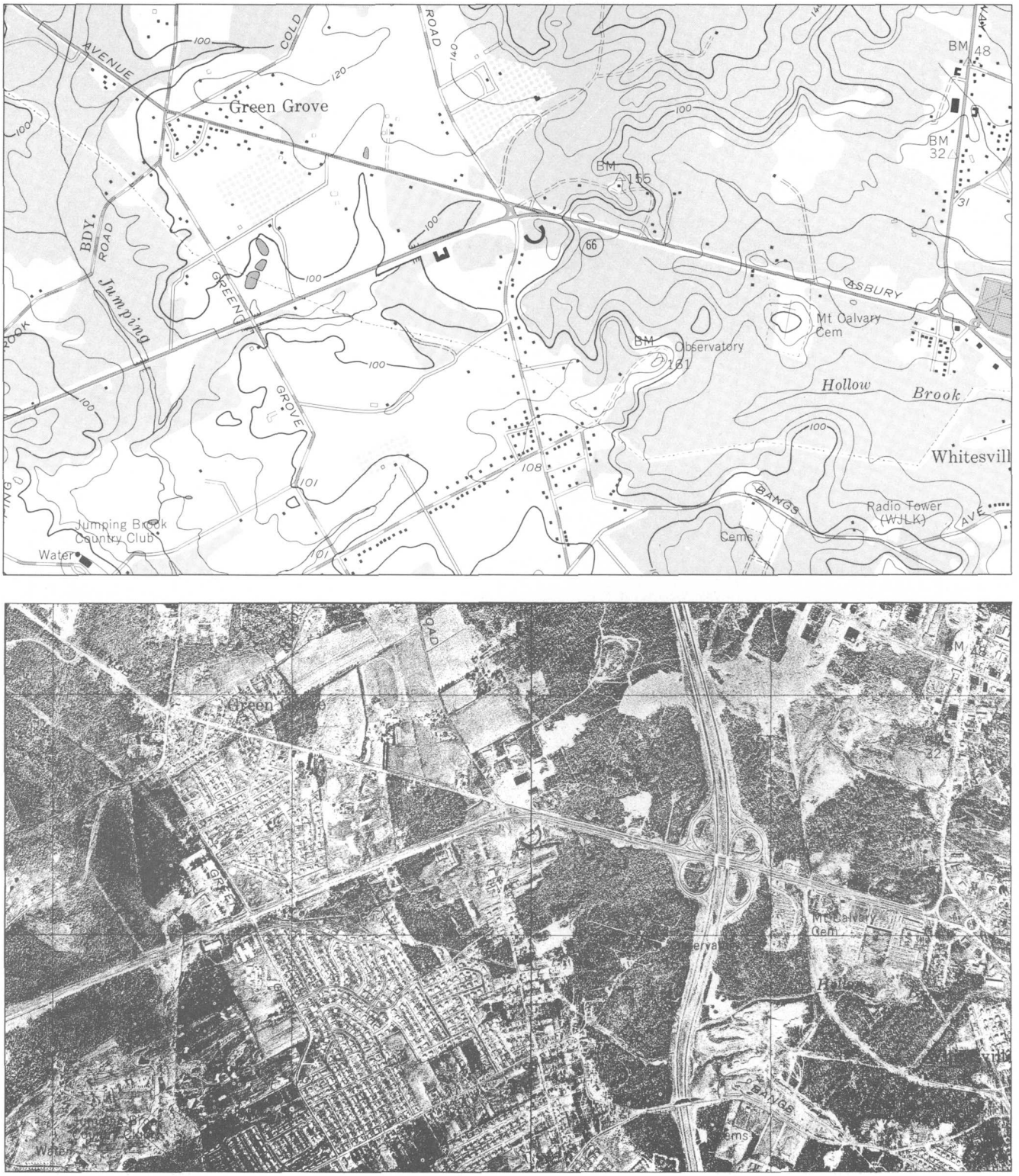

Figure 8.—Part of the Asbury Park, N.J., 7½-minute quadrangle. Top, topographic map; bottom, orthophotoquad. (Reproduced from multicolor and monocolor editions.)

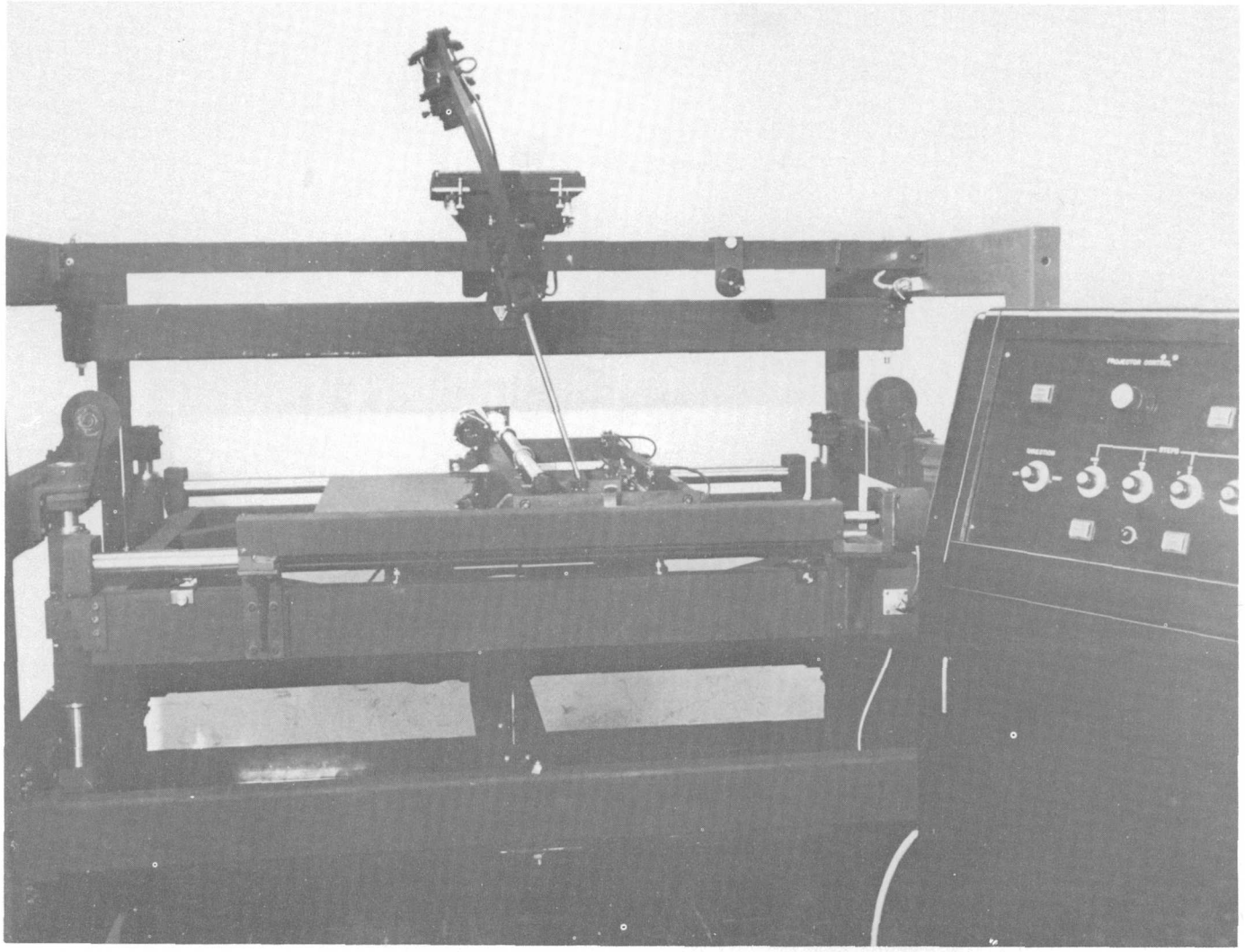

Figure 9.—Orthophotomat, used with Autoline (fig. 10) to print orthophotographs.

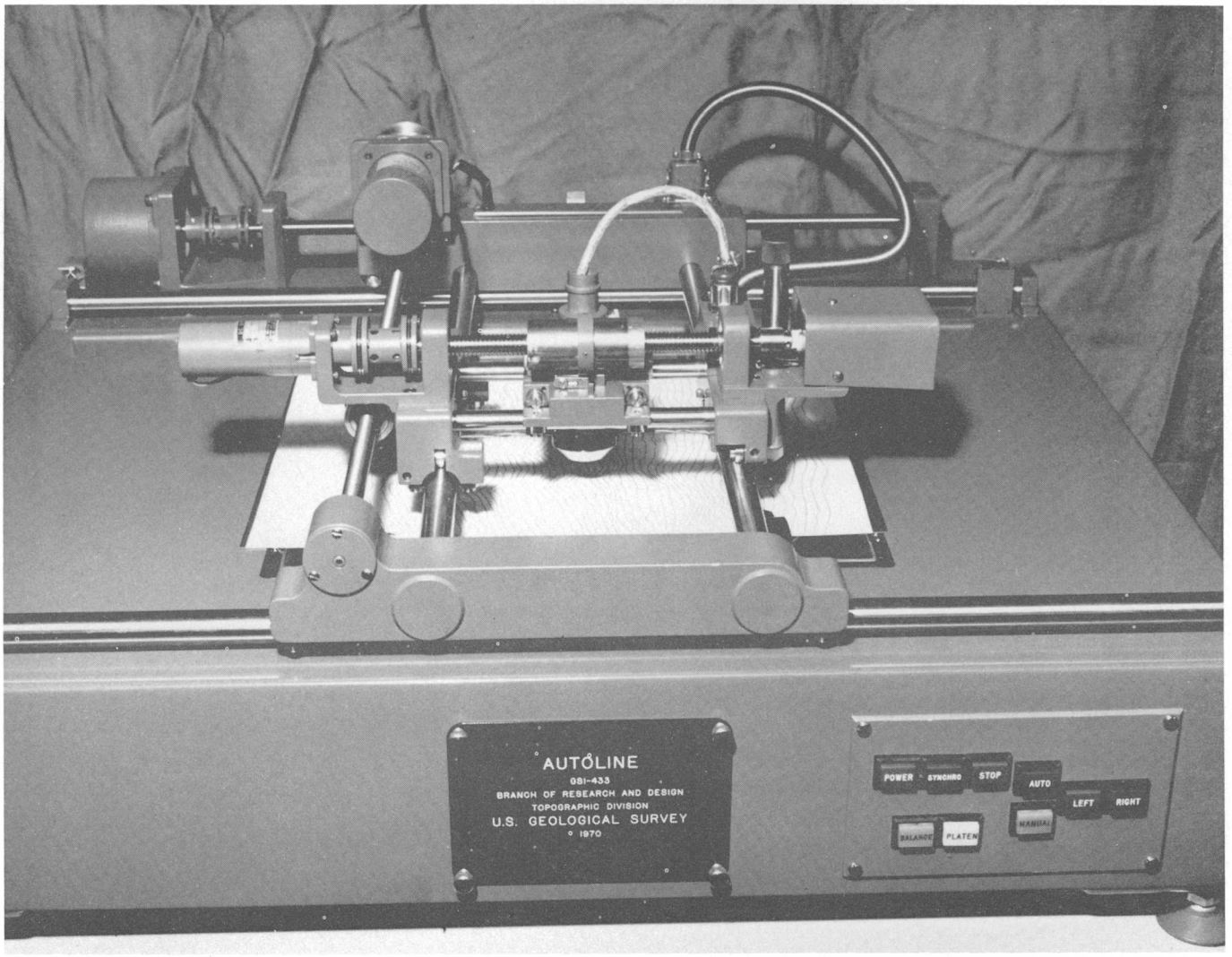

Figure 10.—Autoline, used with terrain profiles to drive the scanning motions of the Orthophotomat (fig. 9).

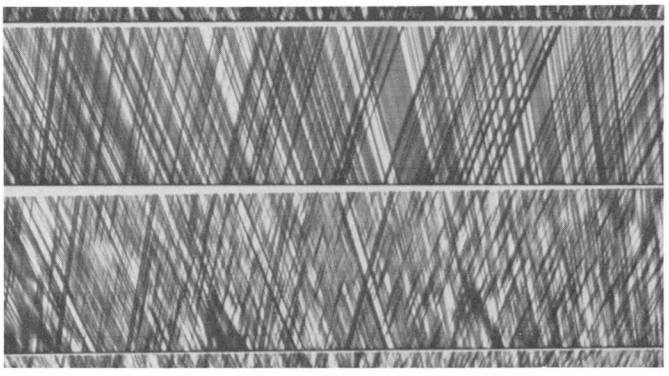

Figure 11.—Profiles formed by the intersection of corresponding image rays.

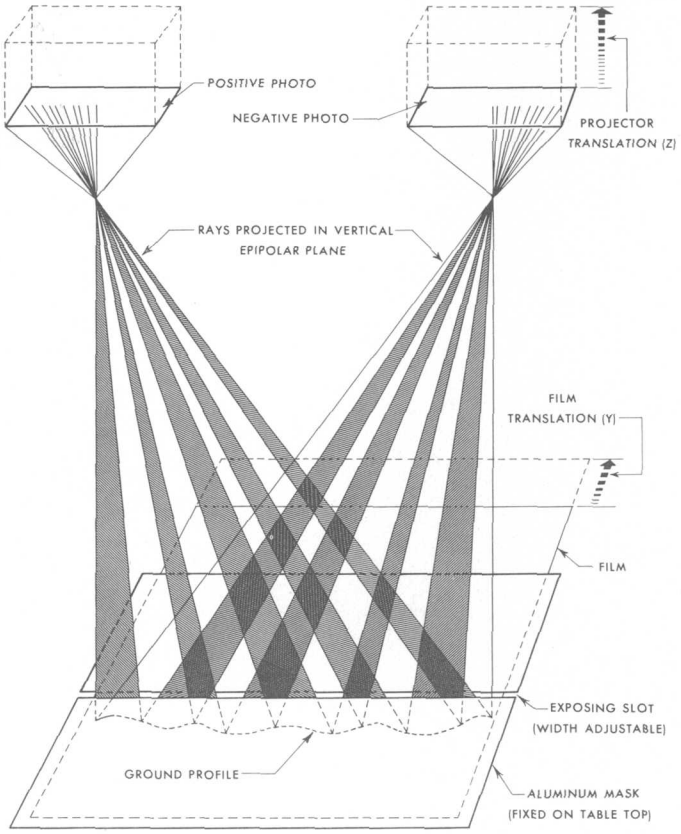

Figure 12.–Schematic of profile scanning operation.

Jour. Research U.S. Geol. Survey
Vol. 1, No. 3, May-June 1973, p. 341–344

MICROBIOLOGICAL ASPECTS OF GROUND-WATER RECHARGE—INJECTION OF PURIFIED UNCHLORINATED SEWAGE EFFLUENT AT BAY PARK, LONG ISLAND, NEW YORK

By GARRY G. EHRLICH, THEODORE A. EHLKE, and JOHN VECCHIOLI,
Menlo Park, Calif., Albany, N.Y., Mineola, N.Y.

Prepared in cooperation with the Nassau County Department of Public Works

Abstract.—Unchlorinated, tertiary-treated sewage effluent was injected through a well at Bay Park, Long Island, N.Y., into a sand aquifer at a rate of 340 gpm for 10 days. Massive, biologically produced slime deposits formed in the filter pack immediately adjacent to the well screen. Observed head buildup in the recharge well was correlated with the formation of these deposits. Comparison of results from this test with results of earlier tests suggests that formation of these deposits may be avoided by addition of chlorine to the injectant.

The performance of a recharge well is adversely affected by factors that decrease the permeability of the receiving formation in the vicinity of the well. Clogging caused by the accumulation of organic and inorganic particulate matter in a mat at the aquifer face is one such factor. Evidence for particulate clogging of injection wells was presented by the California State Water Pollution Control Board (1954) and Rebhun and Schwarz (1968). The California group (1954, p. 165) found that the rate of clogging was directly proportional to the amount of solids injected in any period of time. They further concluded that biological activity in the particulate mat decreased the rate of accumulation of organic solids and thereby reduced the rate of clogging. Rebhun and Schwarz suggested that bacterial growth and its associated decomposition products enhanced the rate of solids buildup and therefore increased the rate of well clogging. These apparently contradictory conclusions may have resulted from different circumstances in the two studies, and each might be correct for the conditions that prevailed during the tests.

Using reclaimed water (tertiary-treated sewage effluent) as the injectant, Ehrlich, Ehlke, and Vecchioli (1972) found that microbial growth near a recharge well at Bay Park, Long Island, N.Y., was effectively suppressed if the residual chlorine level of the injectant was maintained at about 2 mg/l. In a further evaluation of the specific effect of microbial growth on clogging of the Bay Park well, the authors injected unchlorinated reclaimed water into the well. They found that in the absence of the high residual chlorine level vigorous microbial growth occurred in the vicinity of the well.

METHODS

The experimental recharge facility and the water-treatment process at Bay Park have been described previously (Cohen and Durfor, 1967; Peters and Rose, 1968). Reclaimed water from the tertiary treatment process was injected into the Bay Park well under positive head at a rate of 340 gpm for 10 days. The total quantity of reclaimed water injected was about 5 million gallons. Chemical quality of the water used in this test (table 1) was virtually the same as that used in earlier tests (Vecchioli, 1970; Ehrlich and others, 1972) except that the water was not chlorinated before injection.

Total-coliform, fecal-coliform, and fecal-streptococci counts were made by membrane-filter methods described by the American Public Health Association and others (1971, p. 678–688; p. 690–691). Total bacteria counts were made by filtering measured volumes of water through membrane filters (mean pore size, 0.45 μm). The exposed filters were placed on plates of plate-count agar, bacterial-laden side up, and incubated at 30°C (Celsius). Plates were counted after 24 hours of incubation. Bacterial quality of the injectant is listed in table 2.

The bacterial population of the aquifer near the well screen was determined by evaluating the contents of a special probe. This probe was built from a piece of stainless-steel well screen 2 inches in diameter and 19 inches in length. After the probe had been filled with sand from the aquifer, it was autoclaved until the contents were sterile. Before the start of injection, the sterile sand-filled probe was lowered into an observation well in the filter pack surrounding the recharge well and was suspended at about the midlength of the filter pack (at a depth of about 450 feet). The precise distance between the observation well and the main screen of the injection well is unknown, but it is probably less than 9 inches. The probe was removed

Table 1.—*Chemical and physical quality of the recharge water in the test of November 30 to December 10, 1970*

[Observed values are based on 10 daily composite samples. Each composite sample consists of four samples collected throughout the day. Values for aluminum, iron, and manganese are in micrograms per liter; all other parameters except pH, specific conductance, and water temperature are in milligrams per liter]

Parameter	Observed values		Median
	Maximum	Minimum	
Silica (SiO_2)	14	13	14
Aluminum (Al), total	400	0	100
Iron (Fe), total	580	200	310
Manganese (Mn), dissolved	100	6	70
Calcium (Ca)	18	14	16
Magnesium (Mg)	7.2	6.2	6.3
Sodium (Na)	84	79	81
Potassium (K)	12	11	11
Bicarbonate (HCO_3)	64	0	6
Sulfate (SO_4)	161	119	136
Chloride (Cl)	92	83	86
Fluoride (F)	.1	0	.1
Organic nitrogen (N)	5.0	.82	1.4
Nitrite nitrogen (N)	.01	.00	.00
Ammonia nitrogen (N)	28	25	26
Nitrate nitrogen (N)	.0	.0	.0
Phosphate as PO_4, total	.49	.20	.34
Dissolved solids, residue at 180°C	396	365	376
Dissolved solids, calculated from determined constituents.	464	333	373
Total solids, residue, volatile	51	17	34
Hardness as $CaCO_3$ (Ca, Mg)	74	61	67
Noncarbonate hardness	67	22	59
Specific conductance (μmhos/cm at 25°C).	840	778	815
pH	6.3	6.0	6.1
Water temperature (°C)	19	18	18
Dissolved oxygen (DO)	5.2	3.8	4.3
Chemical oxygen demand (COD), 0.025*N* $K_2Cr_2O_7$.	17	7	14
Detergents (MBAS)	.18	.04	.14

Table 2.—*Bacterial quality of the recharge water in the test of November 30 to December 10, 1970*

[All results in colonies per 100 ml]

Elapsed time (days)	Total bacteria	Total coliforms	Fecal coliforms	Fecal streptococci
1	2.2×10^5	1.0×10^4	200	[1]1
2	29×10^5	2.7×10^4	1,200	80
3	1.4×10^5	1.0×10^4	.....	[1]11
4	3.7×10^5	4.7×10^4	2,000	39
5	3.3×10^5	6.0×10^4	1,500	31
6	2.9×10^5	6.1×10^4	[1]750	30
7	1.2×10^5	6.0×10^4	1,100	[1]10
8	1.2×10^5	5.4×10^4	2,200	[1]15
9	1.9×10^5	5.5×10^4	960	22

[1] Estimated count based on nonideal colony count.

Table 3.—*Bacterial counts made by membrane-filter methods of material recovered from sand probe*

[All counts given as colonies per 100 ml of pore volume. Pore volume, calculated on the basis of weight of sand sampled, was assumed to be 30 percent of the total volume; bulk density was assumed to be 2 g/cm^3]

Type of bacteria	Bacterial count
Total	1.0×10^8
Coliform	1.0×10^6
Fecal coliform	3.5×10^3
Fecal streptococci	Not detected.

Table 4.—*Bacterial counts made by membrane-filter methods of water recovered from injection well at Bay Park, Long Island, N.Y., after injection test of November 30 to December 10, 1970*

[All counts given as colonies per 100 ml of pore volume]

Type of bacteria	Bacterial count
Total	2.0×10^5
Coliform	8.3×10^4
Fecal coliform	2.8×10^3
Fecal streptococci	57

immediately after injection ended. A known weight of material from the center of the probe was suspended in sterile, buffered dilution water. Samples of the suspension and dilutions were planted in plate-count agar as described by the American Public Health Association and others (1971, p. 660–662). Bacterial counts of probe material were calculated on the basis of estimated pore volume of the sample based on sample weight, bulk density, and an assumed void volume of 30 percent (table 3).

Redevelopment of the injection well was started immediately after the end of the injection test. Samples for microbiological study were taken immediately after the water in the well casing had been removed. (table 4).

RESULTS AND DISCUSSION

Specific capacity of the injection well decreased from 26.5 gpm per foot of head buildup at the start of the test to 11 gpm per foot of head buildup after 10 days. Curves showing rate of head buildup in the present test (test 8) and three other tests in which the injectant was chlorinated are given in figure 1. Earlier testing at comparable injection rates showed that the rate of clogging depended mainly on the turbidity of the injectant (Vecchioli and Ku, 1970; Ehrlich and others, 1972). Turbidity of the injectant in this test was consistently low, and averaged less than the turbidities in the other tests (table 5). Turbidity is a measure of the suspended-solids content of the

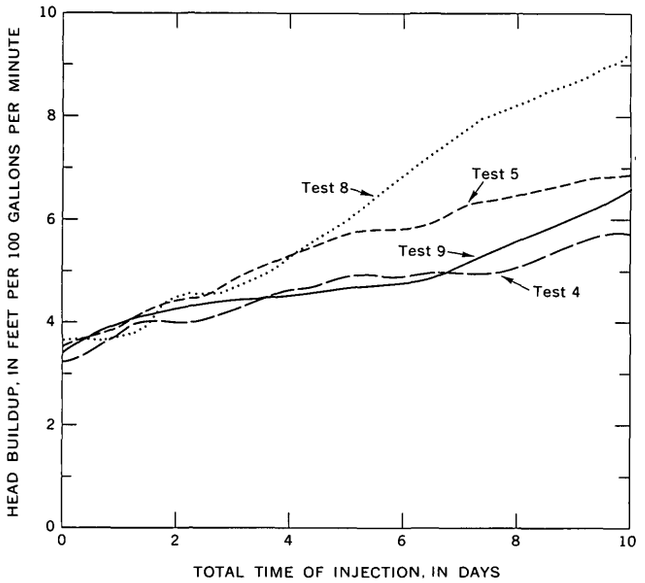

Figure 1.—Head buildup at the injection well as a function of time for present test (test 8) and three other tests. Chlorinated effluent was used in tests 4, 5, and 9.

Table 5.—*Turbidity of injectant*

Injection test	Turbidity (mg/l as SiO_2)	
	Range	Average
4	0.2–1.8	0.9
5	.1–1.6	.6
8	0–.3	.1
9	0–1.5	.3

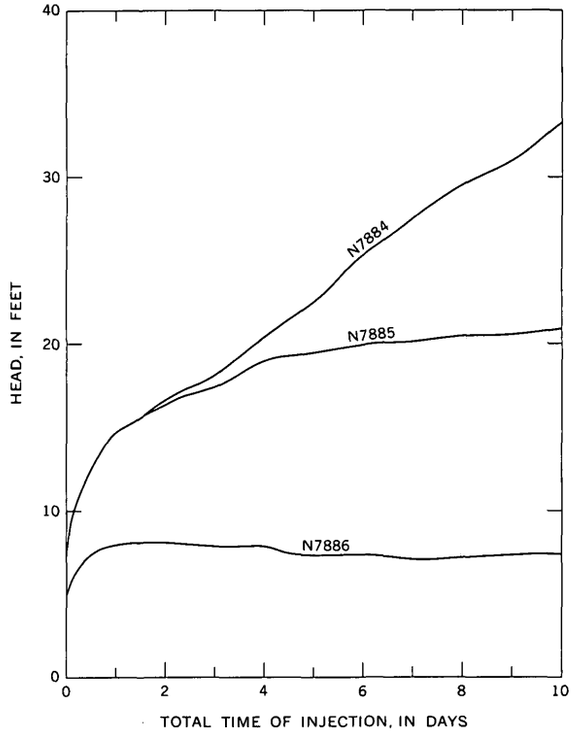

Figure 2.—Head as a function of time for the recharge well (N7884), the observation well in the filter pack (N7885), and an observation well 20 feet from the recharge well (N7886), for recharge test 8.

injectant. Thus, the increased rate of head buildup observed in test 8 (fig. 1) could not be ascribed to physical clogging by inert particulate matter.

In all injection tests but test 8, the head buildup in an observation well within the filter pack of the recharge well was virtually the same as that in the injection well. In this test, however, after the second day of injection, the head in the injection well rose at a more rapid rate than that in the filter pack (fig. 2). Near the end of the test the head in the injection well (well N7884) was about 12 feet higher than that in the observation well (well 7885). The observed head difference suggests that much of the clogging in this test occurred in the filter pack immediately adjacent to the recharge-well screen or on the recharge-well screen. A lesser amount of clogging probably occurred beyond the filter pack at the aquifer face where most of the clogging had occurred in other tests.

The filter pack of the injection well consists almost entirely of subrounded, moderately spherical particles of quartz, chert, and quartzite (Cohen and Durfor, 1966, p. D257). At least 95 percent of this material is in the size range from 1 to 3 mm. Hence, because of the large size of the filter-pack pores, it is unlikely that the observed clogging of the filter pack resulted directly from filtration of particulate matter or bacterial cells in the injectant.

The first water recovered from the formation after the end of test 8 was moderately turbid and showed little tendency for settlement of suspended material on standing. Approximately 75 percent of the suspended material was volatile at 550°C. This property suggests that the material was composed largely of organic matter. In an earlier test in which chlorinated reclaimed water was used as the injectant the volatility of the suspended matter was only about 25 percent (Ehrlich and others, 1972, p. B242). Because the injectant had received virtually the same treatment before injection in both tests (except for chlorination) the threefold increase in volatile matter noticed in the particulate material recovered after test 8 cannot be ascribed solely to differences in preinjection treatment.

Bacterial counts of the first water to be recovered from the filter pack were much higher after test 8 than in comparable samples recovered after injection of chlorinated reclaimed water (2.0×10^5 colonies per milliliter in this sample versus 5×10^3 colonies per milliliter; Ehrlich and others, 1972, p. B243). Total-bacteria, total-coliform, and fecal-coliform counts of the repumped water were approximately the same as in the injectant.

The sand-filled probe, suspended in the filter-pack observation well during the test, was observed to be coated with a

slimy gelatinous material when recovered after test 8. Sand grains inside the probe were cemented into larger aggregates by this slimy material. Such slime formation had not been observed when chlorinated injectant was recharged. Bacterial densities of 1.0×10^8 colonies per 100 cm^3 of pore volume were recorded for material from the center of the probe (table 3). The bacterial density of the interstices of the sand probe was about 500 times the bacterial densities of the injectant or the repumped water. The coliform-bacteria count of the probe was about 10 times that of the injectant and the first repumped water. Fecal-coliform and fecal-streptococcal counts were about the same in the probe, the injectant, and the first repumped water.

Coliform bacteria, which accounted for about half the total bacterial count of the injectant during much of the test, constituted only about 1 percent of the probe bacterial population. If one assumes that the ratio of coliform bacteria to total bacteria captured in the probe by filtration was the same as the ratio in the injectant, then the observed reduced ratio results either from more rapid die-off of coliform organisms relative to other bacterial species or slower multiplication of coliform bacteria relative to other species. In any event, these results indicate that coliform bacteria are less significant in the injection regime than other species of bacteria. This suggests that increased attention to other bacterial types would be desirable in future studies rather than the restricted attention to coliform and other pollution-indicating organisms that has characterized earlier work on the microbiology of artificial recharge.

The results of test 8 suggest that microbial growths and associated slimes generated by new growth caused much of the observed loss in specific capacity of the recharge well. There was no evidence for the establishment of a biological equilibrium as suggested by the California workers (1954, p. 165). Growth of bacteria in the filter pack and at the formation face and attendant clogging may be avoided by addition of chlorine to the injectant as shown in previous tests (Ehrlich and others, 1972).

REFERENCES CITED

American Public Health Association, American Waterworks Association, and Water Pollution Control Federation, 1971 (13th ed.), Standard methods for the examination of water and wastewater: New York, Am. Public Health Assoc., 874 p.

California State Water Pollution Control Board, 1954, Report on the investigation of travel of pollution: Sacramento, Calif., California State Water Pollution Control Board Pub. 11, 218 p.

Cohen, Philip, and Durfor, C. N., 1966, Design and construction of a unique injection well on Long Island, N.Y., *in* Geological Survey Research 1966: U.S. Geol. Survey Prof. Paper 550-D, p. D253–D257.

——1967, Artificial recharge experiments utilizing renovated sewage-plant effluent–A feasibility study at Bay Park, New York, U.S.A., *in* Artificial recharge and management of aquifers–Symposium of Haifa, 1967: Internat. Assoc. Sci. Hydrology Pub. 72, p. 193–199.

Ehrlich, G. G., Ehlke, T. A., and Vecchioli, John, 1972, Microbiological aspects of ground-water recharge–Injection of purified chlorinated sewage effluent, *in* Geological Survey Research 1972: U.S. Geol. Survey Prof. Paper 800-B, p. B241–B245.

Peters, J. H., and Rose, J. L., 1968, Water conservation by reclamation and recharge: Am. Soc. Civil Engineers Proc., Jour. Sanitary Eng. Div., v. 94, no. SA4, p. 625–639.

Rebhun, M., and Schwarz, J., 1968, Clogging and contamination processes in recharge wells: Water Resources Research, v. 4, no. 6, p. 1207–1217.

Vecchioli, John, 1970, A note on bacterial growth around a recharge well at Bay Park, Long Island, N.Y.: Water Resources Research, v. 6, no. 5, p. 1415–1419.

Vecchioli, John, and Ku, H. F. H., 1970, Preliminary results of injecting highly treated sewage-plant effluent into a deep sand aquifer at Bay Park, New York: U.S. Geol. Survey open-file rept., 53 p., 6 figs.

Jour. Research U.S. Geol. Survey
Vol. 1, No. 3, May-June 1973, p. 345–350

CHANGE IN POTENTIOMETRIC HEAD IN THE LLOYD AQUIFER, LONG ISLAND, NEW YORK

By G. E. KIMMEL, Mineola, N.Y.

Work done in cooperation with the Nassau County Department of Public Works, the New York State Department of Environmental Conservation, Division of Water Resources, the Suffolk County Department of Health, and the Suffolk County Water Authority

Abstract.—The potentiometric surface of the Lloyd aquifer in 1970 locally was as much as 40 feet lower than in 1900. During this period, withdrawal of water from wells was estimated to exceed 300 billion gallons, and the amount of water released from aquifer storage by compressive forces was estimated to be 1.6 billion gallons (about 0.5 percent of the withdrawal). The remainder of the withdrawal was derived from downward leakage through overlying aquifers and confining layers and by the displacement of fresh water in the aquifer by landward movement of salty ground water.

The ground-water reservoir of Long Island is the source of water supply for about 4 million people. The Lloyd aquifer, the lowest unit of this reservoir, is a major source of water for public supply and industrial use in places where overlying units contain salty water or where such units are heavily pumped.

Much of the historical information for this report was collected by the U.S. Geological Survey as part of various State and county cooperative programs from 1930 to 1970. The data collected by N. J. Lusczynski were especially helpful. The cooperation of water companies, water districts, and industries on Long Island in the water-level-measurement program is greatly appreciated.

This report documents the regional changes in potentiometric head in the Lloyd aquifer from 1900 to 1970 and considers the sources of the water withdrawn from the aquifer.

GEOHYDROLOGY

Long Island is underlain by a wedge of unconsolidated deposits, which overlies a southeastward-dipping bedrock floor (fig. 1). The bedrock is overlain by three major units of Cretaceous age—the Lloyd and Magothy aquifers and the intervening Raritan clay. The Cretaceous units are overlain by deposits of Pleistocene age whose thickness varies widely. In the northern part of the island, deep channels cut in the deposits of Cretaceous age have been filled with as much as several hundred feet of undifferentiated deposits of clay and gravel of Pleistocene age. Along the south shore, the Gardiners Clay of Pleistocene age overlies the Magothy aquifer.

Moraine and outwash deposits overlie the Magothy aquifer, the undifferentiated deposits of Pleistocene age, and the Gardiners Clay. The saturated parts of the moraine and the outwash deposits are termed "the upper glacial aquifer" (Cohen and others, 1968, p. 18), and that aquifer ranges in thickness from 0 to 100 feet. Generally, in the central part of the island, the flow of water from the upper glacial aquifer to the Magothy aquifer is unrestricted by intervening clay layers. However, along the south shore, and also in other places along the margins of the island, the Gardiners Clay or other clay layers of Pleistocene age confine water in the underlying deposits.

The ground-water reservoir extends vertically from the bedrock floor to the water table, which is at an altitude of 60 to 80 feet in the central part of the island, and laterally to the interfaces between fresh and salty water. The interfaces lie mainly at the shore or seaward from it. Locally, however, salty water underlies parts of the ground-water reservoir in the western part of the island (Lusczynski, 1952; Lusczynski and Swarzenski, 1966; Perlmutter and others, 1959; and Soren, 1971). Salty water also underlies fresh-water lenses on the north and south forks at the east end of the island (Crandell, 1963; Perlmutter and Crandell, 1959; and Perlmutter and DeLuca, 1963). Data considered later in this report suggest that, with the exception of the north and south forks and part of northern Queens County, the Lloyd aquifer contains fresh water everywhere beneath Long Island. In other words, except as noted, the interfaces between fresh and salty water in the Lloyd aquifer are seaward of the shores of Long Island.

LLOYD AQUIFER

The Lloyd aquifer overlies bedrock and is the basal unit of the ground-water reservoir on Long Island. In a study of the regional aspects of the ground-water reservoir on Long Island,

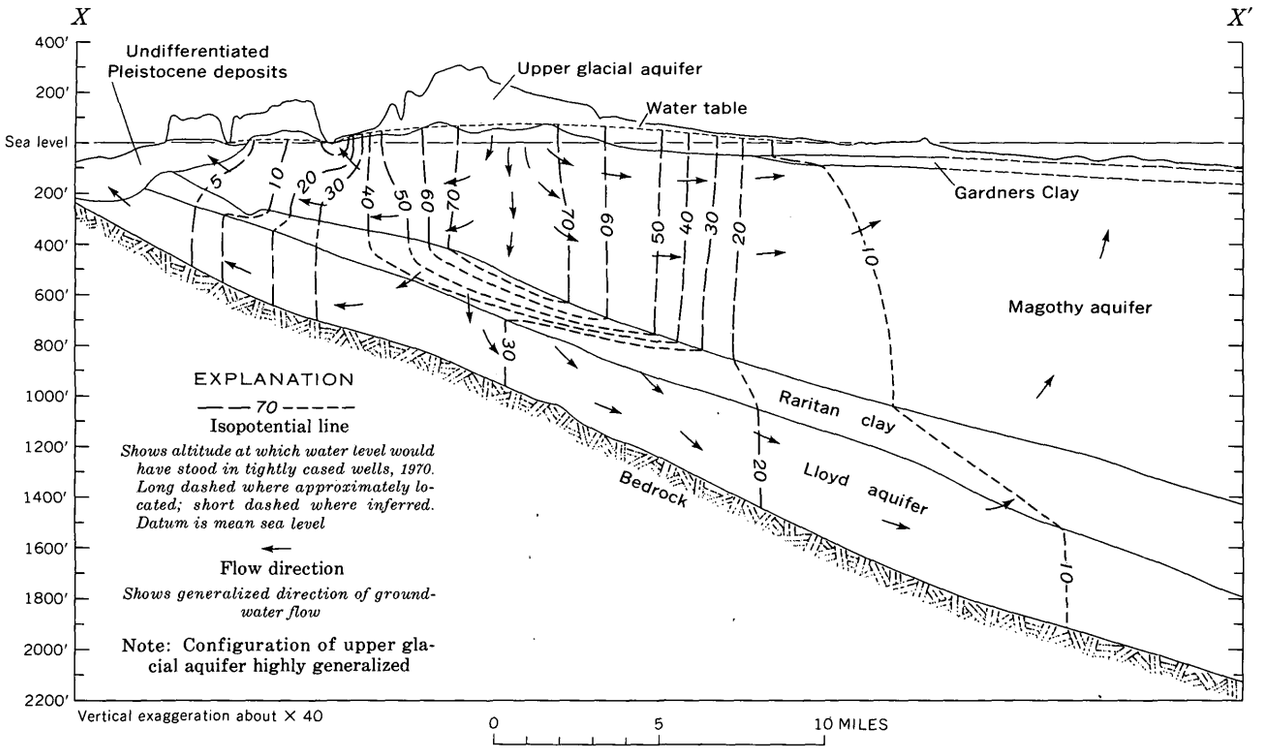

Figure 1.—Generalized hydrogeologic section showing isopotential lines in 1970 in the ground-water reservoir near the Nassau-Suffolk County line on Long Island, N.Y. Location of section is shown in figure 4. Hydrogeologic units from Cohen, Franke, and Foxworthy (1968).

McClymonds and Franke (1972) found that the thickness of the Lloyd increases irregularly in a southeasterly direction in western Long Island and in a southerly direction in central and eastern Long Island. The Lloyd pinches out between the bedrock and the overlying Raritan clay in the northwestern part of the island (fig. 4) and increases in thickness to a maximum of 450 feet in the southern part of the island. McClymonds and Franke estimated that the transmissivity of the Lloyd ranges from less than 20,000 gal day^{-1} ft^{-1} (2,700 $ft^2 day^{-1}$) along the north shore to 140,000 gal $day^{-1} ft^{-1}$ (19,000 $ft^2 day^{-1}$) in southern Nassau County. The transmissivity ranges from 60,000 to 100,000 gal $day^{-1} ft^{-1}$ (8,000–13,000 $ft^2 day^{-1}$) in Suffolk County, mainly owing to the lower hydraulic conductivity there. The top of the Lloyd aquifer slopes southeastward about 60 ft/mi (Suter and others, 1949).

Near the north shore of Long Island, east of central Queens County, the Lloyd aquifer is truncated and abuts undifferentiated deposits of Pleistocene age. (See figure 4.) The geologic and the hydrologic relations between the Lloyd aquifer and the abutting undifferentiated deposits of Pleistocene age suggest that these deposits are in close lateral hydraulic continuity. (For example, see Swarzenski, 1963, pl. 4.) Thus, some wells tapping the contiguous deposits of Pleistocene age north of the Lloyd aquifer were used to construct the potentiometric maps and the net-change map in this report.

The Lloyd is recharged from precipitation along a narrow band in the middle of the island. From there, ground water moves downward through the overlying aquifers and confining layers into the Lloyd (fig. 1). In several places near the northern part of the island, channels have been cut into the Lloyd and have been backfilled with highly permeable sand and gravel of Pleistocene age (Soren, 1971, pl. 1). These channels facilitate movement of water into and out of the Lloyd aquifer.

As of 1971, most of the discharge from the Lloyd in western Long Island was through wells; but, under the more nearly natural conditions that prevail in eastern Long Island, most of the discharge from the aquifer occurs by movement of the water laterally outward toward the shore and then upward into the bays and the ocean.

Withdrawals

From 1910 to 1970, cumulative withdrawal from wells from the Lloyd aquifer was estimated to be 300 billion gallons (fig. 2). Although major development of the aquifer began in Kings and western Queens Counties, centers of major withdrawals have shifted eastward to central Queens and Nassau Counties. By 1970 the cumulative withdrawal from wells from the Lloyd in Nassau County was 160 billion gallons and in Queens County was 120 billion gallons. By 1950, cumulative with-

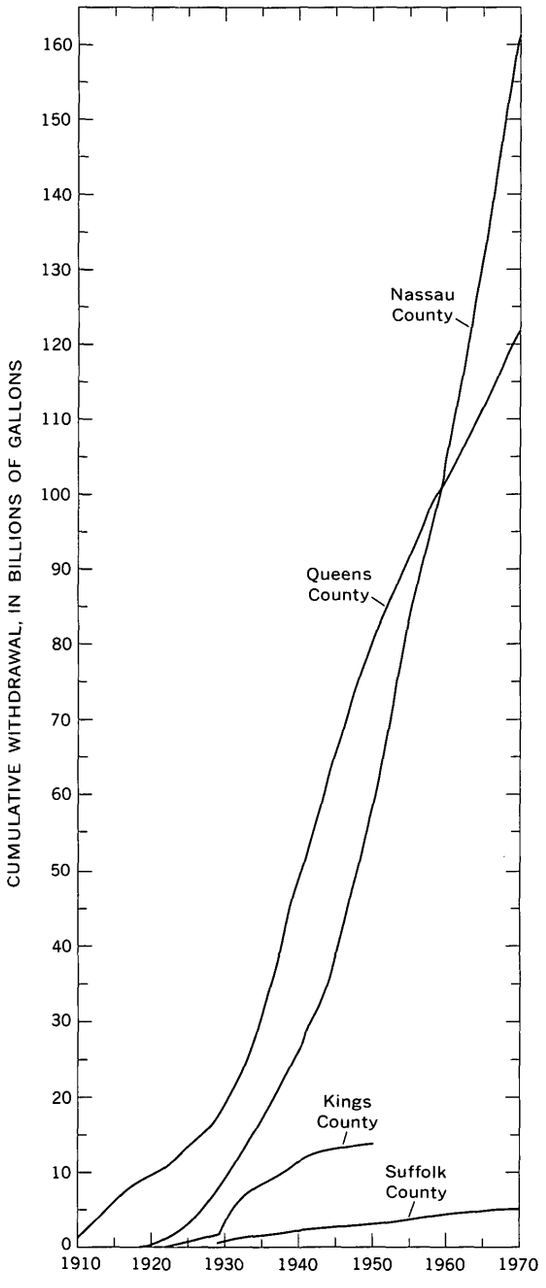

Figure 2.—Cumulative withdrawals of water from wells from the Lloyd aquifer on Long Island, N.Y., 1910 to 1970. Data for 1910 to 1950 are from Lusczynski and Roberts (1952), and data for 1950 to 1970 are from New York State Department of Environmental Conservation (written commun., 1971).

drawal in Kings County was 14 billion gallons. Withdrawals in Kings County have been insignificant since then. The cumulative withdrawal in Suffolk County was 6 billion gallons by 1970.

Major centers of withdrawal from the Lloyd in 1970 (fig. 3) were the peninsula areas along the north shore of Nassau County, central Queens County, and Long Beach. In this part

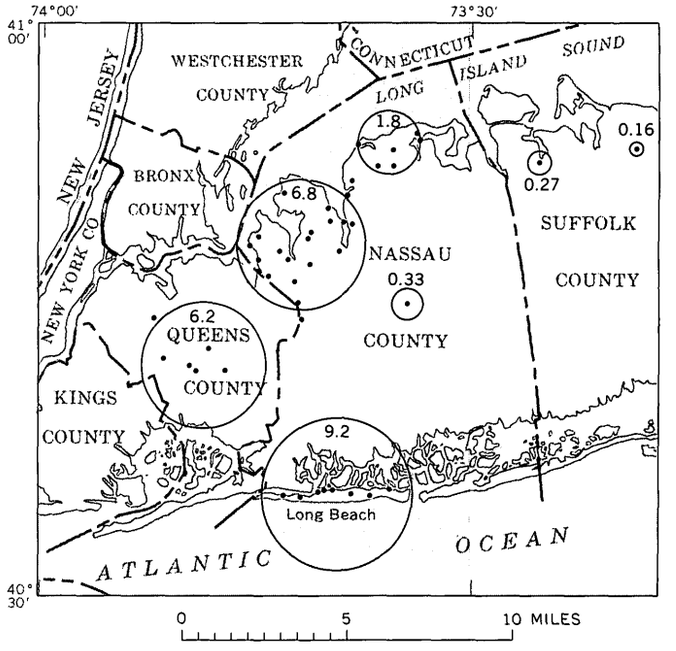

Figure 3.—Withdrawal from the Lloyd aquifer in western Long Island, N.Y., 1970. Dot indicates location of pumping well; figure is withdrawal in millions of gallons per day from wells in and near circle; diameter of circle is proportional to withdrawal.

of western Long Island, withdrawal from the Lloyd aquifer averaged 24 million gal day^{-1} in 1970. In central Nassau County and in northwestern Suffolk County, respectively, withdrawal averaged 0.3 and 0.4 million gal day^{-1} in 1970.

Potentiometric surfaces

Potentiometric maps of the Lloyd aquifer are shown for various times and parts of Long Island in reports by Isbister (1966, fig. 12), Lusczynski and Swarzenski (1966, fig. 9), Swarzenski (1963, pl. 11), Soren (1971, pl. 2), and Warren, de Laguna, and Lusczynski (1968, fig. 34). A report of the U.S. Geological Survey (1952) contains a potentiometric map of the Lloyd for western Long Island.

The most recent potentiometric map (fig. 4) was constructed from measurements in observation and public-supply wells in December 1970 and in January 1971. In areas where water levels are known to be significantly affected by nearby pumping, most of the pumping wells were shut off before measurements were made in either the pumping well or in nearby observation wells; however, one well in Long Beach and two wells in central Queens County could not be shut off. Because most of the measured wells are in heavily pumped areas, potentiometric heads at the time of measurements (December 1970–January 1971) were higher than during most of the year. Wells affected by tidal fluctuations were measured at high tide, or the water-level measurements were converted to equivalent high-tide readings.

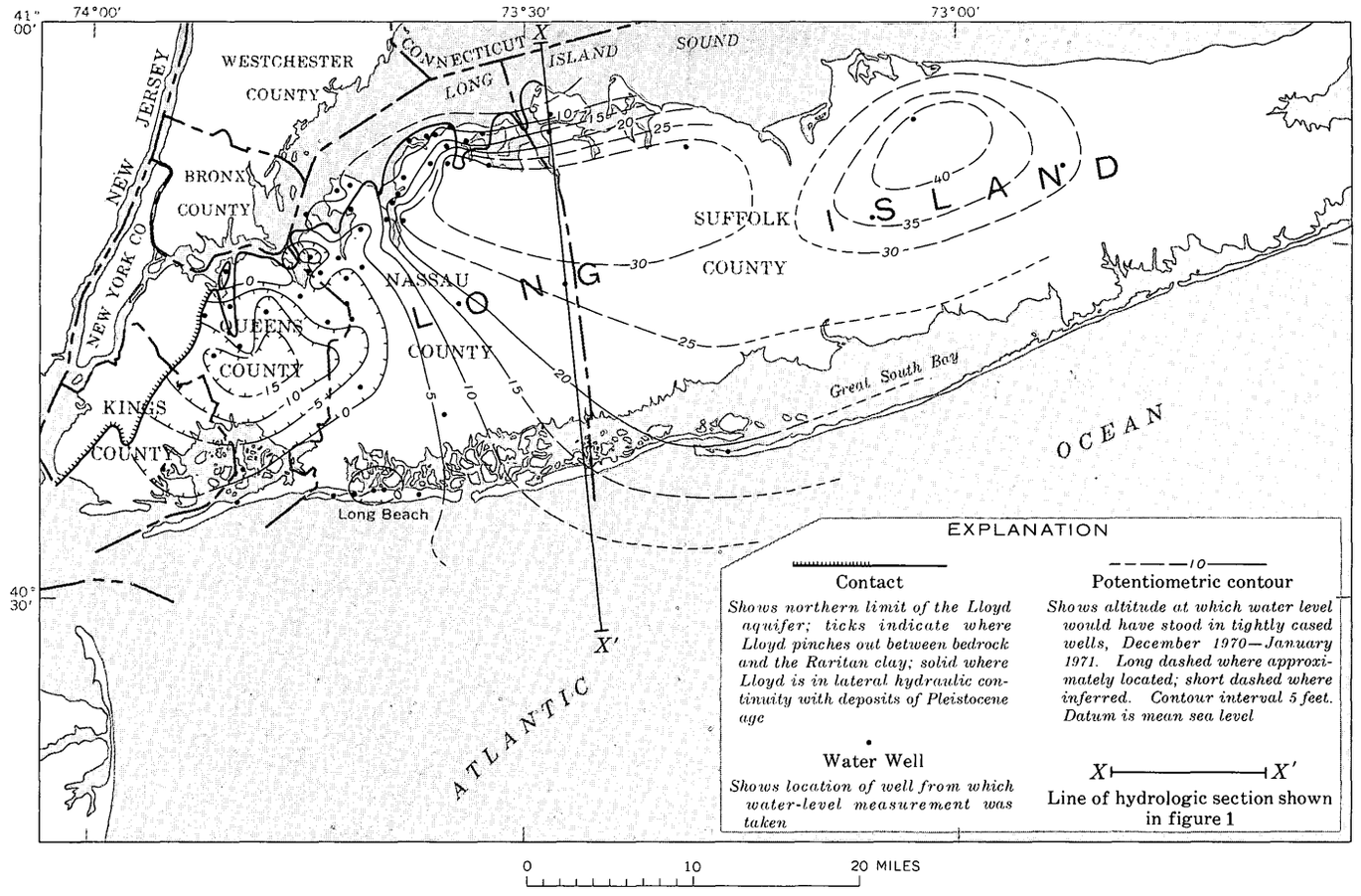

Figure 4.—Potentiometric surface of water in the Lloyd aquifer and contiguous hydraulically equivalent aquifers on Long Island, N.Y., December 1970–January 1971.

In central Queens County the potentiometric surface in 1970 (fig. 4) showed a major depression, which, locally, was more than 15 feet below sea level. Although the maximum depth of this depression could not be determined accurately, it may have been as much as 30 feet below sea level under nonpumping conditions. The effect of pumping is also evident from the contorted contours in northwestern Nassau and the depression on southern Nassau County.

Under natural predevelopment conditions and over a long period of time, average annual recharge to and discharge from the Lloyd aquifer were equal, and the potentiometric head remained virtually unchanged except for minor short-term fluctuations. Withdrawals of water from wells since the early 1900's have upset the balance between recharge and discharge and have caused significant widespread declines in potentiometric head. To assess the declines, the inferred potentiometric surface in about 1900, before significant withdrawals affected heads in the Lloyd (fig. 5), was reconstructed. This potentiometric surface is based on the earliest available data and in places is adjusted empirically to compensate for the effects of local pumpage at the time or before the time that the earliest water levels were measured.

Net change in head

The inferred net change in head in the Lloyd aquifer in western Long Island from 1900 to 1970 is shown on figure 6. Some features on the map deserve special note. First, the lines of equal change terminate in the west, where the aquifer overlaps bedrock and thins to a featheredge. Second, the areas of greatest declines in head do not coincide with the areas of greatest withdrawal in 1970 (fig. 3) because of numerous factors, including the history of withdrawal, areal differences in the hydraulic properties of the aquifer (transmissivity and storage coefficient), and marked differences in the geometry and the boundaries of the aquifer.

Source of water withdrawn

The estimated decrease in the amount of water in storage in the Lloyd aquifer from 1900 to 1970 can be computed by mutiplying the volume of net decline (based on the net-change map shown in fig. 6) by the estimated average storage coefficeint of the deposits in which the head declined. The storage coefficient is defined as the volume of water an aquifer

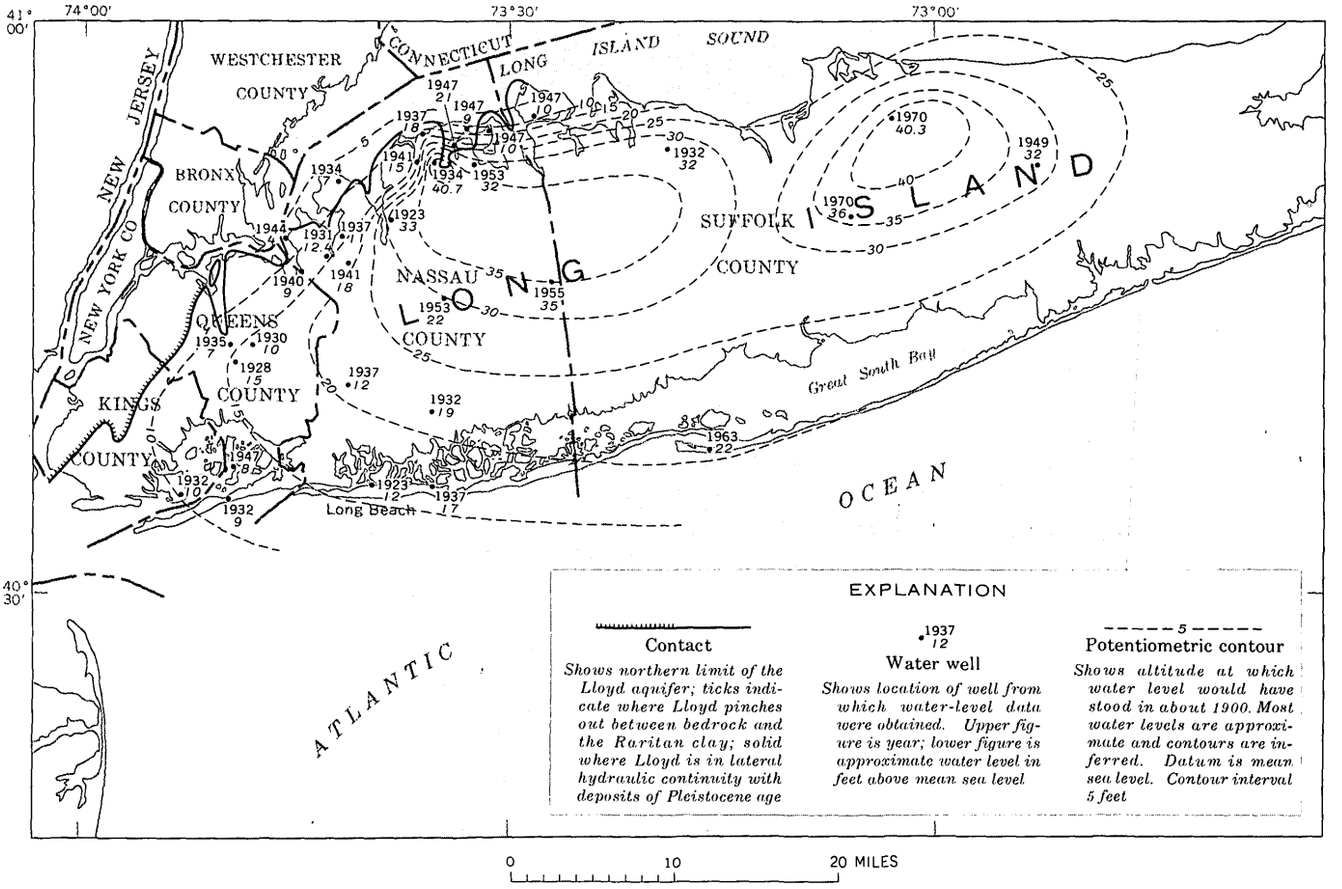

Figure 5.—Inferred potentiometric surface of water in the Lloyd aquifer and contiguous hydraulically equivalent aquifers on Long Island, N.Y., in about 1900.

releases from or takes into storage per unit of surface area of the aquifer per unit change in head. The storage coefficient S for confined aquifers, such as the Lloyd, reportedly ranges from 10^{-3} to 10^{-5} (Ferris and others, 1962). Jacob (1941) found that the storage coefficient in the Lloyd in southern Queens County was about 3×10^{-4}. When one uses the largest probable value for the storage coefficient of the Lloyd, 10^{-3}, the computed maximum decrease in the amount of water in storage in the Lloyd aquifer from 1900 to 1970 is 1.6 billion gallons. This figure represents only about 0.5 percent of the gross withdrawals from the aquifer during that period (estimated to exceed 300 billion gallons). The source of most of the withdrawal from the Lloyd aquifer was probably a combination of downward leakage from and through the confining layers and downward leakage through highly permeable channel-fill deposits.

A significant but unknown quantity of fresh water also was displaced in the Lloyd aquifer by the landward movement of salty ground water. The chloride content of water from some wells tapping the Lloyd aquifer and the Pleistocene deposits hydraulically connected to the Lloyd along the north shore of Long Island has increased from time to time because of local salt-water intrusion (Soren, 1971, p. A32–A34; Swarzenski, 1963, p. 52–53). In 1971, the chloride content of two public-supply wells screened in Pleistocene deposits adjacent to the Lloyd in northeastern Nassau County was more than 100 mg/l (Nassau County Department of Health, written commun., 1972).

The interface between fresh and salty water in the Lloyd is still (1971) seaward of Long Beach and the other barrier beaches along the south shore of Long Island (Lusczynski and Swarzenski, 1966; Cohen and Kimmel, 1970). However, withdrawal from the Lloyd and the net declines in head shown in figure 6 almost certainly have caused and (or) have accelerated the landward movement of salty water in the Lloyd aquifer along the south shore. The rate and the extent of that movement are unknown.

REFERENCES CITED

Cohen, Philip, Franke, O. L., and Foxworthy, B. L., 1968, An atlas of Long Island's water resources: New York State Water Resources Comm. Bull. 62, 117 p.

Cohen, Philip, and Kimmel, G. E., 1970, Status of salt-water encroachment in 1969 in southern Nassau and southeastern Queens Counties,

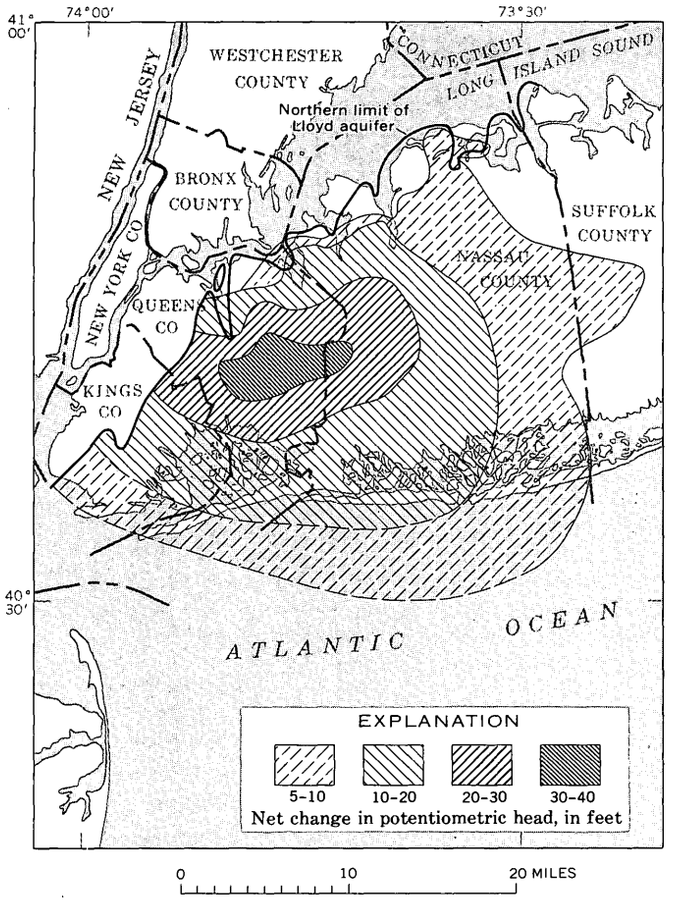

Figure 6.–Inferred net change in potentiometric head in the Lloyd aquifer and contiguous hydraulically equivalent aquifers from about 1900 to 1970 in western Long Island, N.Y. Lines of equal net change are dashed where uncertain.

Long Island, New York, *in* Geological Survey Research 1970: U.S. Geol. Survey Prof. Paper 700–D, p. D281–D286.

Crandell, H. C., 1963, Geology and ground-water resources of the town of Southold, Suffolk County, New York: U.S. Geol. Survey Water-Supply Paper 1619–GG, 36 p.

Ferris, J. G., Knowles, D. B., Brown, R. H., and Stallman, R. W., 1962, Theory of aquifer tests: U.S. Geol. Survey Water-Supply Paper 1536–E, p. 69–174.

Isbister, John, 1966, Geology and hydrology of northeastern Nassau County, Long Island, New York: U.S. Geol. Survey Water-Supply Paper 1825, 89 p. [1967]

Jacob, C. E., 1941, Notes on the elasticity of the Lloyd sand on Long Island, New York: Am. Geophys. Union Trans., v. 22, pt. 3, p. 783–787.

Lusczynski, N. J., 1952, The recovery of ground-water levels in Brooklyn, New York, from 1947 to 1950: U.S. Geol. Survey Circ. 167, 29 p.

Lusczynski, N. J., and Roberts, C. M., 1952, Withdrawal of ground water from the Lloyd sand member on Long Island, N.Y., from 1904 to 1950: U.S. Geol. Survey open-file rept., 7 figs, 6 tables, 4 pls.

Lusczynski, N. J., and Swarzenski, W. V., 1966, Salt-water encroachment in southern Nassau and southeastern Queens Counties, Long Island, New York: U.S. Geol. Survey Water-Supply Paper 1613–F, 76 p.

McClymonds, N. E., and Franke, O. L., 1972, Water-transmitting properties of aquifers on Long Island, New York: U.S. Geol. Survey Prof. Paper 627–E, 24 p.

Perlmutter, N. M., and Crandell, H. C., 1959, Geology and ground-water supplies of the south-shore beaches of Long Island, New York *in* Lowe, K. E., ed., Modern aspects of the geology of New York City and environs: New York Acad. Sci. Annals, v. 80, art. 4, p. 1060–1076.

Perlmutter, N. M., Geraghty, J. J., and Upson, J. E., 1959, The relation between fresh and salty ground water in southern Nassau and southeastern Queens Counties, Long Island, New York: Econ. Geology, v. 54, p. 416–435.

Perlmutter, N. M., and DeLuca, F. A., 1963, Availability of fresh ground water, Montauk Point area, Suffolk County, Long Island, New York: U.S. Geol. Survey Water-Supply Paper 1613–B, 39 p.

Soren, Julian, 1971, Ground-water and geohydrologic conditions in Queens County, Long Island, New York: U.S. Geol. Survey Water-Supply Paper 2001–A, 39 p.

Suter, Russell, de Laguna, Wallace, and Perlmutter, N. M., 1949, Mapping of geologic formations and aquifers of Long Island, New York: New York State Water Power and Control Comm. Bull. GW–18, 212 p.

Swarzenski, W. V., 1963, Hydrogeology of northwestern Nassau and northeastern Queens Counties, Long Island, New York: U.S. Geol. Survey Water-Supply Paper 1657, 90 p.

U.S. Geological Survey, 1952, The piezometric surface of the Lloyd sand, Long Island, New York in 1947: U.S. Geol. Survey open-file rept. 1 table, 1 map, 3 pls.

Warren, M. A., de Laguna, Wallace, and Lusczynski, N. J., 1968, Hydrology of Brookhaven National Laboratory and vicinity, Suffolk County, New York: U.S. Geol. Survey Bulletin 1156-C, 127 p.

Jour. Research U.S. Geol. Survey
Vol. 1, No. 3, May-June 1973, p. 351–360

CONCEPTS OF KARST DEVELOPMENT IN RELATION TO INTERPRETATION OF SURFACE RUNOFF

By H. E. LeGRAND and V. T. STRINGFIELD,
Raleigh, N.C., Washington, D.C.

Abstract.—Some unusual characteristics of streamflow occur in regions underlain by carbonate rocks. The streamflow characteristics are related to processes of karstification, these processes being dependent on circulation of subsurface water and solution of the rock to form characteristic topography and underground cavern systems. Very highly cavernous and permeable unsaturated zones tend to keep the water table depressed below land surface in many karst regions, a condition that leads to a low density of perennial streams. The uneven distribution of permeability beneath surface karst streams causes them to lose or gain water, depending on the position of the water table with reference to stream level. The conventional techniques of interpolation and extrapolation that have been reasonably successful in approximating streamflow of ungaged sites in nonkarstic regions have only limited use in karst regions. An understanding of principles of karstification and an understanding of the hydrogeologic framework of a carbonate terrane provide a useful basis for evaluating the streamflow characteristics.

The science of surface-water hydrology has developed greatly during the past two decades, and sophisticated techniques have been devised to predict critical high-flow and low-flow characteristics of streams. Although recognition has been made of the importance of geology to streamflow, distinctive relationships between rock terranes and streamflow have not been fully explored. Streams in some carbonate-rock terranes have unusual characteristics, and even the spectacular phenomena of disappearing and reappearing streams are fairly common; the disappearing stream flows into a sinkhole or swallow hole, where the stream has an underground flow for some distance before emerging as a large spring, from where its surface course continues. The unusual streamflow characteristics are related to the general processes of karstification, these processes being dependent on circulation of subsurface water and solution of the carbonate rock to form characteristic topography, as well as cavern systems. The purpose of this paper is to give concepts on the development of stream networks and on stream characteristics in regions underlain by carbonate rocks that have undergone karstification. Through a better understanding of the processes involved in karstification, more accurate interpretation of runoff from such regions will result.

KARST FEATURES AND THEIR DEVELOPMENT

Where carbonate rocks are widespread there are generally surface and subsurface features that differ from those of less soluble rocks. Depressions sometimes develop that reflect areas where the underlying rock has been carried away in solution. These depressions, called sinkholes, usually form where the surface collapses into a large cavity beneath. The depressions are commonly somewhat round, and where they coalesce there is a tendency for elongated solution valleys to form. Surface water drains into the sinks, dissolving the rock as it moves into the ground-water system. A wide range of topographic conditions occurs on carbonate terranes. The term "karst topography" has been applied to carbonate-rock areas where sinkholes abound and streamless valleys are common. Even karst forms differ from place to place, some of these differences having led to the concept of a karst cycle (Grund, 1914, p. 621–640) in which a distinct sequence of topographic forms has been recognized. As will be indicated later, certain discernible karst features that are related in a sense to stages of karst development are also related to surface water and to other hydrologic conditions.

In the early youthful stage, surface streams cut valleys into the carbonate rocks and drain off the circulating ground water that has percolated downward through fractures in the rock to the water table and then moved somewhat laterally toward the surface streams. The fractures become enlarged by solutional erosion while water readily infiltrates the terrane and readily discharges from it. The enlarged fractures represent an increase in permeability. As a result of the increasing permeability, the water table becomes progressively lower in the terrane, and some local subsidence of the surface occurs as sinks. Some of the fractures continue to be enlarged into caverns and other large openings as interstream drainage is diverted underground. During the late youthful stage almost all of the original surface streams have been diverted to underground courses. Topographic relief may be appreciable; deep sinks, and in some places cone-shaped hills, are common on the landscape.

The youthful stage passes into maturity as sinks enlarge and coalesce into dry valleys. Very little of the original plateau

surface remains. Sinkholes and undulating topography are common, and almost all precipitation goes underground immediately; this diffused infiltrating water tends to move to a low level and tends to become concentrated in a large opening, emerging as a large spring. During the mature stage the air-filled cavern systems are at their ultimate size, especially beneath the higher topographic features. Also during the mature stage the underlying aquifer is fully developed from the viewpoint of having its arterial solution openings fully enlarged.

In the old-age stage the valleys have become wide and somewhat flat, and most of the ridges between the valleys have been reduced except for isolated hills and knobs. Caverns that were once air-filled have been destroyed by collapse of the land surface. The land surface in general has been lowered to the extent that the water table is near land surface, and surface streams no longer go underground.

The concept of the karst cycle would have little merit if it were regarded as a cycle involving only time. The karst cycle considered here represents a sequence of topographic features to which a sequence of time should be applied only when referring to a restricted part of the carbonate-rock terrane. Youthful, mature, and old-age topographic features are considered as migratory in space with geologic time. Mature karst topography is generally widespread and is the setting for much of the discussion in this paper. An understanding of the evolution of karst topography leads to advanced understanding of the development and distribution of permeability in carbonate-rock aquifers and to the character of surface water.

The chief karst regions of the United States are shown in general on figure 1; some of them are briefly described by Stringfield and LeGrand (1969, p. 361–371). There are many informative publications on karst as indicated in an annotated bibliography (LaMoreaux and others, 1970); a recent book (Herak and Stringfield, eds., 1971) summarizes the karst of the Northern Hemisphere. Yet some aspects of karst, such as the relation of surface-water hydrology to ground-water hydrology, have not been fully studied.

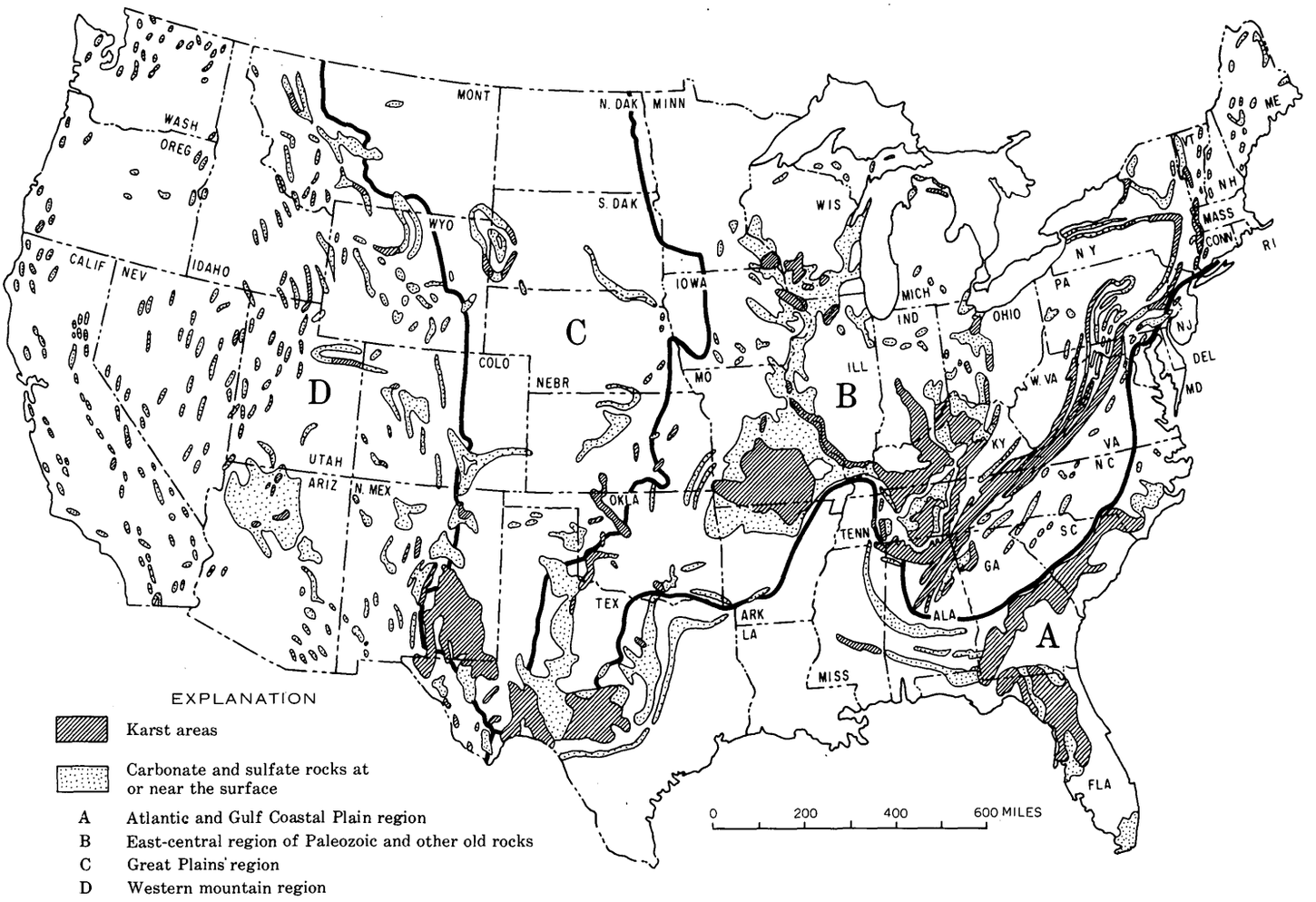

Figure 1.—Map of the United States, showing generalized ground-water regions (A–D) and major karst areas. (Regions adapted from Meinzer, 1939, and karst areas from Davies, 1970).

SURFACE DRAINAGE NETWORK IN KARST REGIONS

Fully developed karst regions are characterized by the scarcity of surface streams, even under humid conditions. In fact, the combination of thin soils and absence of surface streams causes some humid karst regions to appear more arid than they are. Many coastal karst regions, such as parts of the Mediterranean coast, the Yucatan Peninsula, and some islands of the Caribbean, have no streams; in these places water from precipitation moves downward into the limestone quickly, and then it travels laterally to coastal discharge points at or below sea level. The discharge points are less obscure in interior karst regions because at least one spring or surface stream must drain water to a low place at the land surface. If not within the karst region, the discharge may be along the contact with surrounding less soluble rocks.

Major trunk streams are the general rule, these streams representing the base level toward which much of the ground water moves laterally. The trunk streams do not necessarily have a dendritic or treelike pattern, so common in nearby structureless terranes of clastic rocks. Trellis drainage is not common except where structural control is strong; an example of trellis karst drainage is the folded Appalachian region where long parallel karst valleys alternate with sandstone ridges. A characteristic feature of the trunk stream is the scarcity of tributary surface streams. Suggestions of former tributary streams are elongated dry valleys with hummocky topography leading from the trunk stream outward into coves and reentrants in upland areas. An example can be seen on the Sparta, Tenn., 7½-minute quadrangle, where Bear Cove extends eastward from Calfkiller River through the town of Sparta into the higher Cumberland Plateau.

Most trunk streams are cut into karst plateaus. Strongly meandering courses in deep channels are common, Calfkiller River in Tennessee and the White and Gasconade Rivers on the Salem Plateau in Missouri being examples. Among the most spectacular entrenched meanders in a karst region is the Ardeche River in southern France, which flows in a canyon 31 km long (Avias, 1972, p. 141). Flood plains along karst streams are not especially common, although broad solution plains in which trunk streams flow represent lowland plateaus that may be bordered by an escarpment and a higher plateau (fig. 2).

The scarcity of streams in karst regions is related to the distribution of permeability; the caverns and enlarged solution openings are a result of the permeability that has developed by the karstification processes. Although not specifically considering karst terranes, both Jacob (1944, p. 566) and Carlston (1963, p. 5) demonstrated that as permeability, or transmissivity, increases, drainage density should decrease, and as transmissivity decreases, drainage density should increase. A relation of low stream density and high permeability in karst regions is readily observable, but LeGrand (1970, p. 1247) showed that high density of streams does not necessarily prevail in poorly karstified impermeable carbonate rocks.

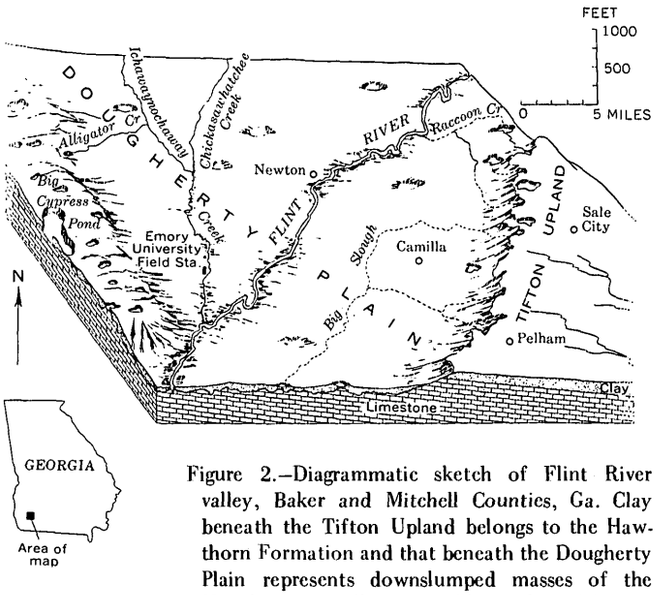

Figure 2.—Diagrammatic sketch of Flint River valley, Baker and Mitchell Counties, Ga. Clay beneath the Tifton Upland belongs to the Hawthorn Formation and that beneath the Dougherty Plain represents downslumped masses of the Hawthorn as well as insoluble residue of former limestone beds (after Hendricks and Goodwin, 1952; Herrick and LeGrand, 1964).

CHARACTER OF DRAINAGE BASINS IN KARST REGIONS

Hydrologists in the United States have conventionally used "flow per square mile" as the comparative unit of surface flow measurement. The size of the contributing drainage basin in nonkarstic regions has generally been easy to derive because topographic and ground-water divides almost coincide. In karst regions, however, there is little or no relation between topographic and ground-water divides in many places.

A study by White and Schmidt (1966) in a maturely karsted limestone system in Pocahontas County, W. Va., by use of dye tracing and underground mapping techniques, shows that the Swago Creek underground drainage is unrelated to surface drainage. They indicate that underground drainage lines cross major surface divides, and that the water table is almost flat but has a gentle slope toward Swago Creek.

In artesian systems of both carbonate and noncarbonate aquifers far from major recharge and discharge areas, the surface and subsurface flows of water are not closely related. However, where carbonate aquifers extend from a water-table recharge area to an artesian system a variety of surface and subsurface flow relations exists (Stringfield, 1964, p. C168). Surface stream characteristics generally should change considerably where a stream cuts through the noncarbonate and less soluble cover into underlying soluble carbonate rocks. Solution by circulating water then initiates karstification and increases the permeability of the rocks in the stream valley. This phenomenon may be noted in some regions, such as in north-central Florida. Here the Santa Fe River rises east of the Suwannee River and flows westward on an upland region

where the noncarbonate beds of the Hawthorn Formation overlie the principal artesian carbonate aquifer (Stringfield, 1966, p. 14). In its lower course, the Santa Fe River flows on and in the cavernous limestone aquifer. As described by Clark and others (1962, p. 39–48) the flow characteristics of the upper part and the lower part of the Santa Fe basin differ considerably. The flow characteristics change abruptly in the vicinity of O'leno State Park, about 6 miles north of High Springs, where the river disappears underground, then reappears about 3 miles away. Below that point, streamflow increases rapidly as the river flows through the channel cut in the limestone. Almost all of the increase in flow in the lower basin is from the artesian aquifer. Few tributary streams feed the lower river except those that flow from springs such as Ichatucknee Springs near Hildreth. In the lower part of the basin the section of the river between High Springs and Fort White has an average annual runoff of 84.7 inches, more than 1½ times the annual rainfall on the 130-sq-mi area. This runoff is the highest of any area of like size in Florida.

The polje type of karst, typically displayed in the Dalmatian area of Yugoslavia and shown in figure 3, offers a good example of underground drainage beneath topographic divides. The Ljubljanica River, in the polje area, has several alternate surface and subsurface stretches as it burrows through at least three carbonate-rock ridges (Lewicki, 1967, p. 261). A similar situation of water traversing an area beneath carbonate ridges in Nevada has been described (Winograd, 1962; Maxey, 1968).

The complexities of subsurface drainage divides are greatest in broad karst regions having several perennial streams. The problem is less complex where the karst is confined between nonkarstic rocks and where one major karst stream is present. Such a stream is the Sequatchie River in east Tennessee, which is entrenched in a karst valley a few miles wide and about 75 miles long.

The indefinite boundaries of the subsurface karst drainage areas as discussed above are spatial because there are many examples to show that the topographic divides are not the same as the ground-water divides. In addition to this lack of concordance of topographic and ground-water divides in karst regions, there can be a change in the size of a ground-water drainage area with time, especially with changes of precipitation during seasons of the year. The drying up of some streams is common in karst areas, a fact that may be evidence of the gaining ability of an adjacent karst stream. The migration of subsurface drainage divides between wet and dry seasons is a significant aspect of karst hydrology that has not been fully recognized. A study of the cyclic regime of karst streams between wet and dry seasons, coupled with subsurface water tracing experiments, gives evidence that creeping of divides does occur (fig. 3).

FLOODS AND HIGH FLOW

An understanding of karstification leads to the suggestion that floods in carbonate-rock terranes may be less severe than those in other terranes. It may be reasoned that precipitation in karst regions does not run off rapidly on the surface but is largely diverted to temporary storage in caverns. This water in temporary storage is soon depleted because water moves readily from the large openings through circuitous channels to springs and surface streams, but the rate of subsurface movement is slower than that of surface water which might otherwise move overland to a stream. There is evidence that temporary storage of precipitation in karst regions results in subdued high-water stages of streams during floods.

The behavior of annual floods in limestone basins in Pennsylvania has been described by White and Reich (1970). They show the mean annual floods per square mile of basin area for parts of several physiographic provinces which include noncarbonate rocks and limestones. The flood data in figure 4 were compiled by White and Reich from data taken from U.S. Geological Survey Water-Supply Papers containing records of streamflow. The limestone basins which are located in the thick carbonate part of the geologic section are shown as solid triangles in figure 4. The mean annual floods per unit area for these basins are low and are independent of drainage area. Those basins lying mainly on noncarbonate rocks have mean annual floods three to nine times greater than those underlain by carbonate rock. According to White and Reich (1970, p.

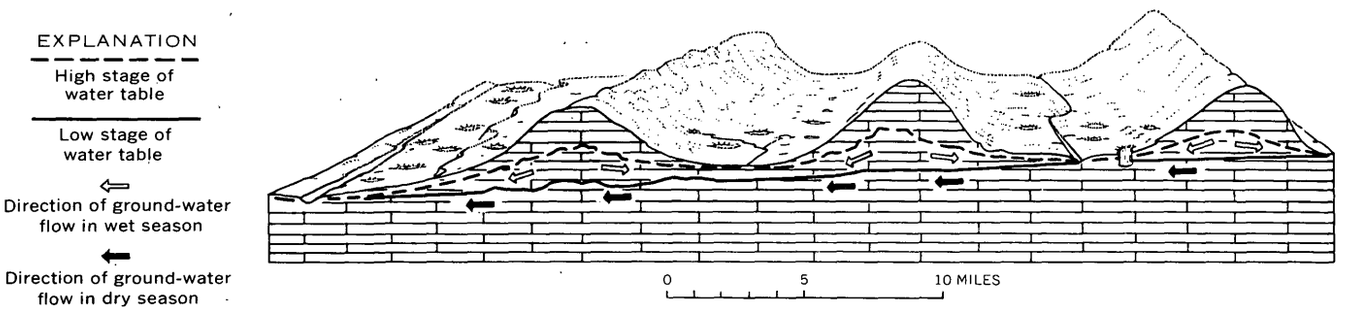

Figure 3.—Profile of a polje-type karstified carbonate terrane, showing seasonal fluctuation of the water table, the uneven profile of the water table resulting from differences in permeability, and the diversion of ground water beneath ridges during dry seasons (LeGrand and Stringfield, 1971).

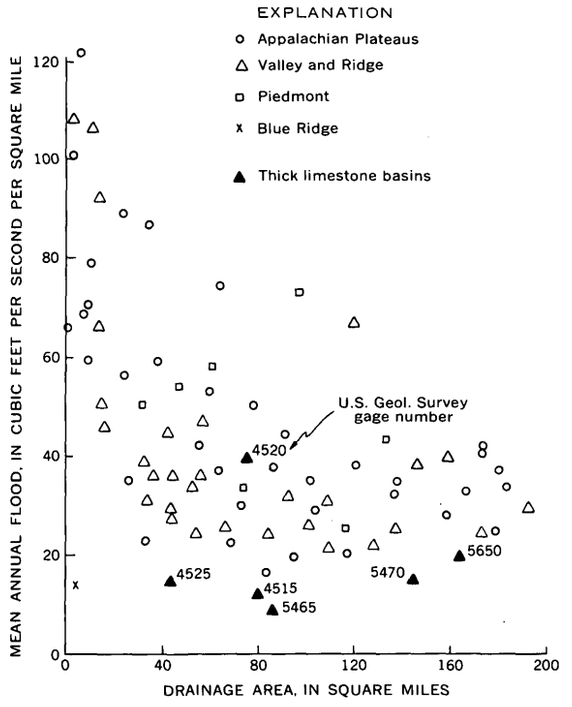

Figure 4.—Mean annual floods for carbonate and noncarbonate drainage basins, Pennsylvania. Comparatively low mean annual floods occur in the valleys underlain by thick carbonate rocks in the Valley and Ridge province (after White and Reich, 1970).

193), the mean annual floods were calculated for 114 basins which ranged from 2 to 200 sq mi in area. The average period of record used was 25 years. High values were obtained from watersheds on shales and sandstones. Extremely low mean annual floods occurred where there was extensive thick and cavernous limestone above the water table within the basin.

Another hydrologic parameter that can be used to show the effect of lithology is the shape of the flood hydrograph as indicated by the peak discharge and the high-flow duration. White and Reich (1970, p. 194) concluded:

> An important effect of the presence of limestone is the smoothing action on the flood peak. The open sinkholes can accept storm excess and thus add temporarily to the ground water storage. Water is then released, via the springs, over the next few days. The temporary storage lasts a short duration with respect to ground-water discharge but a long duration with respect to passage of a flood crest.

Hydrographs of a carbonate basin, Spring Creek, and a typical Pennsylvania noncarbonate basin, Little Fishing Creek, are shown in figure 5 to illustrate this smoothing action. The reduced peaks illustrated are the result of spreading the volume of water over long periods in the limestone basin.

The influence of karst on the hydrological characteristics of rivers in Russia has been studied by Gavrilov (1967, p. 544). He reports that the influence of karst on maximum discharge is indicated by the smoothing of the flood hydrograph and by the lower peak discharge.

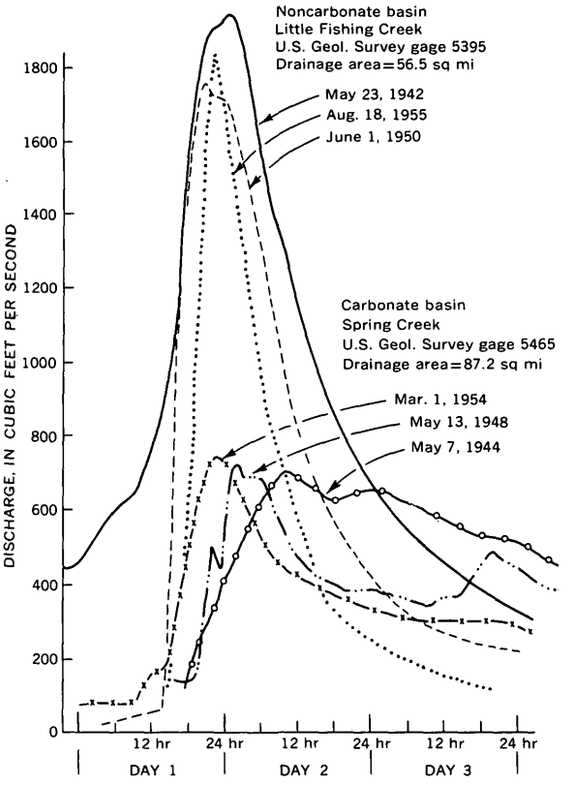

Figure 5.—Distinction between a limestone and noncarbonate basin in Pennsylvania, on the basis of the variation of peak discharge and high-flow duration during floods (after White and Reich, 1970).

LOW-FLOW CHARACTERISTICS OF KARST STREAMS

The tendency toward a smooth effect or moderation of flood flow in karst regions might be expected to lead to a smoothing effect of low flow also to the extent that a karst stream might have an annual lowest 7-day flow somewhat higher than that of a stream on noncarbonate rocks. Major trunk streams do have higher than normal base flows, but erratic patterns of base flow characterize many tributary or smaller karst streams.

The erratic pattern of base flow is demonstrated in Swatara Creek basin, Pennsylvania, where streams in the limestone area have a greater range in low-flow yields than those in adjacent noncarbonate rocks; the low flows in the limestone range from 0.60 to 0 mgd per sq mi (Stuart and others, 1967, p. 3). Almost all karst regions have streams that go dry during dry seasons, but less obvious are the many streams that lose part of their flow in certain places. Skelton (1966, p. 17) made a series of discharge measurements (fig. 6) during base flow periods in 1953 which indicated that large water losses occurred in a reach of the Gasconade River in Missouri that is underlain by solution channels. Burchett and Moore (1971, p. 37) pointed out that during dry weather periods a stretch of East Fork Stones River in central Tennessee loses considerable

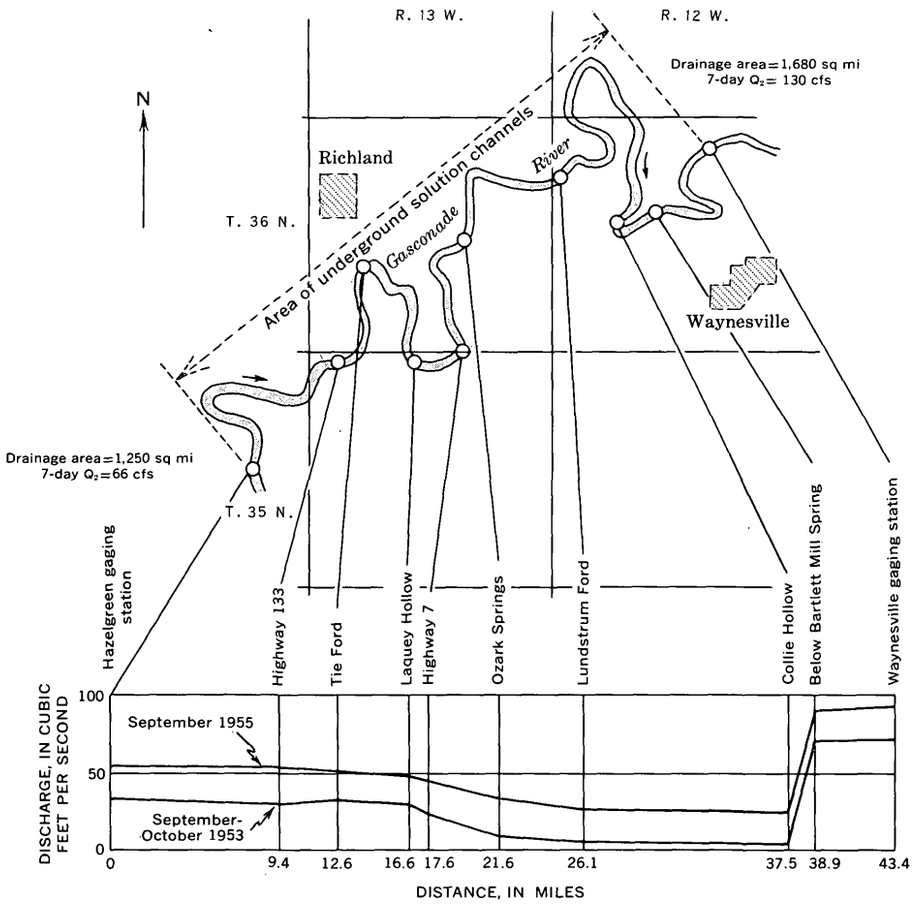

Figure 6.–How streamflow is decreased by infiltration to underground solution channels as evidenced by decreasing base flow in a reach of Gasconade River, Mo. (Skelton, 1966).

water by underflow to subsurface solution cavities, although no points of large water losses are visible.

DISCONTINUITIES OF SURFACE STREAMS DRAINING KARST

Almost all humid karst regions have surface streams that are discontinuous in certain stretches. Most such streams lose water in a specific place, commonly referred to as a swallow hole, from which place the water flows in subsurface conduits to a place of emergence, called a resurgence. For instance, Malott (1952) noted the Lost River in southern Indiana as an excellent example of a disappearing and reappearing stream (fig. 7). Thornbury (1965, p. 194) described this river:

> The Lost River drainage basin encompasses some 350 square miles and can be divided into three rather distinct parts: a lower part in which the stream is a deeply entrenched surface stream, a middle abandoned dry-bed stretch that is used only after heavy rains, and an upper part in which Lost River is an unentrenched surface stream. The middle part of its route crosses the portion of the karst plain upon the St. Louis and Ste. Genevieve limestones. This limestone plain is dotted with thousands of sinkholes and is practically devoid of surface streams. The meandering abandoned dry-bed route of Lost River across this plain *** is 22 miles long, whereas its underground route is only 8 miles long and is directly down the regional dip. Lost River sinks in a series of swallow holes ranging in altitude from 620 to 560 feet. After extremely heavy rains all its water may not be accommodated by these swallow holes, and the excess goes around the dry-bed channel. Lost River reappears at the end of its underground route as a karst spring at an altitude of 490 feet.

The northern part of Puerto Rico is another karst area having numerous discontinuous surface streams. These streams head in the volcanic region to the south before cutting rather narrow but deep gorges in rugged karst, after which they have underground courses for a distance of a mile or more. The underground courses of such streams as the Río Camuy and Río Tanama are suggested at the land surface beneath long irregular dry valleys. Both streams reappear as large springs emerging from coves.

In the central United States where noncarbonate rocks lie above low-lying karst regions small surface streams emerge from coves in noncarbonate rocks and have perennial flows until they go underground in the bordering karst areas; their underground courses can be approximated by the long dry

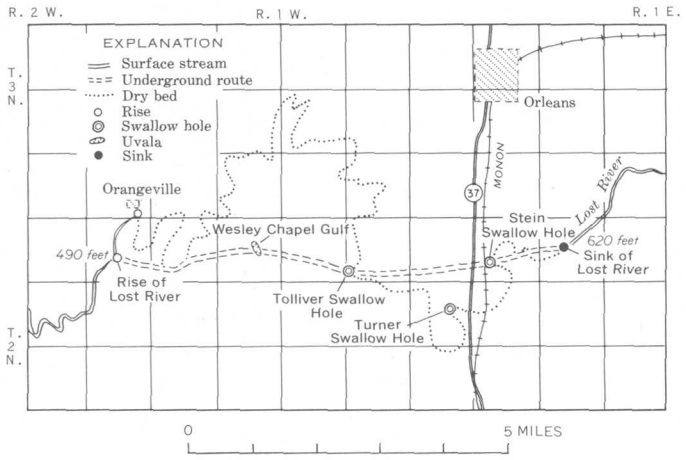

Figure 7.—Map of middle part of Lost River, Orange County, Ind., showing discontinuous flow (after Malott, 1952).

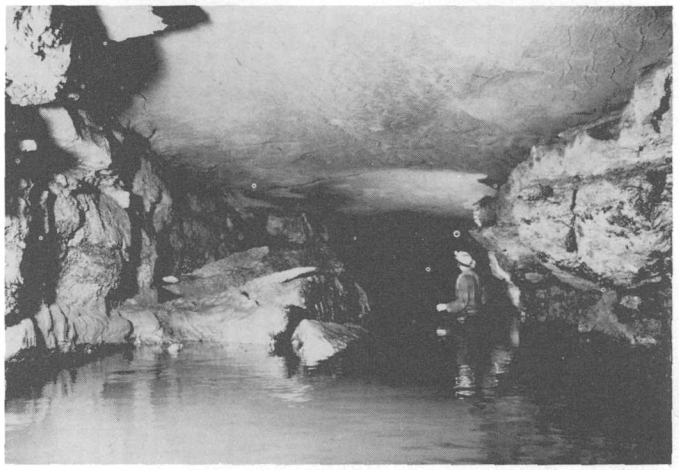

Figure 8.—Typical master trunk conduit. A view of the 3-mile-long stream passage in Overholt Blowing Cave, W. Va. (photograph by W. B. White).

valleys leading to trunk streams. Several examples of these short disappearing streams can be seen on the Sparta, Tenn., 7½-minute quadrangle.

It is reasonable to assume that beneath the discontinuous stretches of karst streams the waters are not diffused but flow as subsurface cave streams. This is evidenced by speleologists, who have noted cave streams in many karst lands (see fig. 8). Cave streams are very abundant and form a sort of arterial flow pattern in the upper part of the saturated zone in many karst areas.

White and Schmidt (1966) gave an elaborate discussion of cave streams in east-central West Virginia and showed (p. 553) that

> some of the drainage more or less follows the surface drainage lines, and thus merely has the effect of underdraining the valleys. These drainage lines are termed "well behaved". In other parts of the area, subsurface drainage conduits do not parallel surface drainage lines but cross surface divides and carry water out of the small drainage basins by unobvious routes. These drainage lines are termed "misbehaved".

Some carbonate-rock streams lose water gradually instead of suddenly through a swallow hole. Excellent examples are the Nueces, Frio, and Sabinal Rivers which flow on the Edwards limestone aquifer in the Balcones Fault Zone of south-central Texas. These streams head in and drain the Edwards Plateau upstream from the fault zone. In the Balcones Fault Zone, the Edwards is downfaulted along numerous faults and as a consequence the streams lose water by seepage into solution openings along fractures where the streams flow on the limestone (Sayre and Bennett, 1942). Infiltration of river water into the underlying limestone contributes most of the recharge to the aquifer that supplies water for the city of San Antonio. The capability of water in the streams to infiltrate the limestone is exemplified by the Nueces River within the recharge area to the Edwards aquifer as shown by the following data at Laguna weather gage. On October 20, 1962, the average daily flow at the Laguna gage was 901 cfs, the peak discharge for that day being 3,210 cfs; the difference between the average flow and the peak flow for that day represents some of the water lost by seepage into the underlying Edwards aquifer (U.S. Army Corps Engineers, 1970). The Martha Brae River, of northern Jamaica, West Indies, is another example of a stream that loses part, but not all, of its water in a stretch through a karst region.

Streams flowing eastward from the structural dome of the Black Hills in South Dakota cross a belt of cavernous limestone several miles wide. Here many small streams lose their entire flow to sinkholes, and even the larger streams show perceptibly decreased flow at the eastern border of the outcrop belt (Gries and others, 1968, p. 57–58). The streams tend to regain their lost water from large springs located slightly east of and downgradient from the limestone belt (Rahn and Gries, 1971).

In many karst regions the loss of water from a stream is local, and the water is generally regained at some resurgence less than several miles from the point of loss; however, in the Edwards aquifer in Texas and others in broad karst plateaus, the regain of water may be tens of miles away, even in different drainage basins. Where streams in coastal karst areas lose water by seepage into streambeds and sinkholes, there may be no regain of water as it moves in subsurface channels to the sea.

The uneven distribution of permeability and of topographic conditions is responsible for the intriguing karst phenomena of disappearing and reappearing surface streams. These seemingly mysterious phenomena can best be understood by considering the underground and missing segment of the stream as being in a relatively permeable zone and a segment upgradient from the swallow hole as being in a relatively impermeable zone.

There are current and potential problems relating to streams that have discontinuous surface courses. Harvey and Skelton

(1968) have described the movement of effluent from a sewage treatment plant at Springfield, Mo., into Wilson Creek; near the outfall of the treatment plant both water and effluent are lost underground before reappearing at a resurgence 1.4 miles away, where the surface course of the creek continues. The effluent at Springfield received secondary treatment—a condition that might not be objectionable along surface stretches of some streams where aeration is effective—but the limited aeration in the subsurface stretch made the effluent objectionable. In addition to the problem of poor aeration in the ground, any polluted water in the subsurface stretch of a karst river might be easily drawn toward pumping wells. Also there is no assurance that it will be contained in a single subsurface channel of flow; instead it might spread in two or more branching directions of flow.

Stretches of some surface streams in karst areas may have channels in relatively impermeable carbonate rocks or in an intervening shale bed, the level of the stream being higher than the underlying karst water table. If a natural or manmade opening develops between the streambed and underlying karst water a partial or complete loss of surface water could result. The lower course of the Río Cobre, draining the karstland of south-central Jamaica, is such a stream as it flows on clays of an alluvial plain. Near the border of the karst and alluvial plain the underlying karst water level is lower than river level, a condition that represents a potential loss of river water in this zone. The streamflow records show no water loss during low flows, and the stream level is above the water level in the limestone (Richard Davis, Hydrogeologist, United Nations Food and Agricultural Organization, Kingston, Jamaica, West Indies, oral commun., May 1971). Probably there is loss of water to the limestone during flood stages when the water level in the river rises above the silted part of the channel. The water level of stretches of stream channels with respect to a karst water table is an important hydrological consideration, and on karst hydrological maps a distinction between the terms "karst water-table stretches" and "nonkarstic stretches" would be helpful.

SURFACE RESERVOIRS IN KARST REGIONS

The problem of leaky reservoirs in karst areas centers on the distribution of permeability in karstified rocks. The permeability is unevenly distributed, and, unlike in insoluble rocks, the permeability is developed as water high in dissolved carbon dioxide content moves through joints and other openings to places of discharge. The following well-established generalizations indicate that the permeability of carbonate aquifers is commonly different from that of other aquifers:

1. Circulation of water and solution activity tend to be greatest in the upper part of the zone of saturation and tend to lessen with increased depth.
2. The moderately large openings in the path of bulk flow of ground water tend to enlarge by solution action, in contrast to small openings not in the path of bulk flow which enlarge only slightly.

Almost all surface reservoirs are hydrologically connected with the saturated zone of the ground-water system. A dam designed to raise the water level of the reservoir must also raise the adjacent and subjacent water table. A rise in the water table around a reservoir in nonkarstic rocks, especially of poor to moderate permeability, is nearly always certain; in karst rocks, on the other hand, a rise in the water table is less certain. Karst topography is characteristically underlain by carbonate rocks in which large solution channels are separated by large volumes of poorly permeable carbonates. The large solution channels in the zone of saturation resemble in some ways the surface drainage network on some noncarbonate rocks of humid regions. The volume of solution channels, representing the gross permeability, tends to decline almost exponentially with increasing distance below the water table. The zone of saturation of the aquifer is commonly thin, lenticular, and elongate, and its base is indefinite or arbitrary. The unsaturated zone tends to be very permeable and cavernous. The reservoir problems must focus on the very permeable material around the reservoirs that allows water to flow away freely and that thwarts a rise in the water table. The general nature of solution openings can be approximated by hydrogeological observations and inferences, but techniques of outlining specific solution openings before drilling are not available.

CONCLUSIONS

The great ranges of natural conditions that influence streamflow in carbonate-rock terranes and the scarcity of a synthesis of data prevent a useful statistical analysis of the characteristics of streamflow in these terranes. The conventional techniques of interpolation and extrapolation that have been reasonably successful in approximating streamflow of ungaged sites in nonkarstic regions have only limited use in karst regions. An understanding of principles of karstification and an understanding of the hydrogeologic framework of a carbonate terrane provide a useful basis for evaluating the streamflow characteristics.

A karst terrane has its own characteristic distribution of permeability, both in the unsaturated and saturated zones, which is a major factor in controlling the streamflow. The very highly cavernous and permeable unsaturated zone tends to keep the water table depressed below land surface in much of karst regions and in turn leads to a low density of perennial streams. The major trunk stream tends to have a high base flow because ground water continues to drain toward it after the water table falls below the level of some tributary streams, at which time the tributary streams go dry. A shifting of ground-water divides away from the major trunk stream during dry seasons causes a temporary enlargement of some drainage basins and the movement of ground water as underflow

beneath some upland areas. The high permeability in the unsaturated zone tends to cause flood stages to be smoothed out to the extent that the floods are lower in height and longer in time than those in noncarbonate regions. The smoothing out of flood stages occurs because (1) precipitation is quickly drained underground where it has a somewhat slower movement through solution channels to a surface stream than would overland flow, and (2) water in a rising stream tends to spread laterally during a flood into adjacent air-filled cavities and thereby to subdue a potential flood.

Big springs, rather than small springs and diffuse seepage, are the general rule in mature karst regions. The big springs emerge from underground streams or cave rivers. Some of the underground streams are the subsurface links in discontinuous surface streams that disappear underground and reappear as springs elsewhere. Most of the underground streams, however, are large solution openings at the top of the saturated zone which carry much of the ground water to springs. The underground streams tend to branch upgradient in arterial fashion and represent the more permeable parts of the saturated zone; the water table is depressed along the arterial system so that the underground stream meets the surface stream almost at grade.

The uneven distribution of permeability beneath surface karst streams causes them to lose or gain water, depending on the position of the water table with reference to stream level. A surface stream may disappear or lose water where the losing stretch is very permeable, and it may gain water where the rock is less permeable to the extent that the water table is above stream level.

The uneven distribution of both permeability and topography between karst and adjacent nonkarst terranes causes many surface streams to gain or lose much water near the rock boundaries. Many surface streams flowing from clastic rocks onto lower lying karst rocks disappear into swallow holes before reappearing elsewhere as karst springs. Many underground karst streams emerge as springs at the boundary of nonkarst rocks where they then follow a surface course.

REFERENCES CITED

Avias, J., 1972, Karst of France, *in* Important karst regions of the Northern Hemisphere, chap. 5: Amsterdam, Elsevier Publishing Co., p. 124–184.

Burchett, C. R., and Moore, G. K., 1971, Water resources in the upper Stones River basin, central Tennessee: Tennessee Div. Water Resources, Water Resources Ser. No. 8, 62 p.

Carlston, C. W., 1963, Drainage density and streamflow: U.S. Geol. Survey Prof. Paper 422-C, 8 p.

Clark, W. E., Musgrove, R. H., Menke, C. G., and Cagle, J. W., Jr., 1962, Interim report on the water resources of Alachua, Bradford, Clay, and Union Counties, Florida: Florida Geol. Survey Inf. Circ. 36, 92 p.

Davies, W. E., 1970, Map of karst areas, *in* National atlas of the United States of America: U.S. Geol. Survey, p. 77.

Gavrilov, A. M., 1967, On the problem of the influence of karst on the hydrological regime of rivers, *in* Hydrology of fractured rocks: Dubrovnik Symposium, October 1965, Proc. Internat. Assoc. Sci. Hydrology Pub. 74, v. 2, p. 544–562.

Gries, J. P., Niven, D. W., and Crooks, T. J., 1968, Recharge of the Pahasapa Limestone aquifer from stream losses, Black Hills, South Dakota: South Dakota Acad. Sci. Proc., v. 47, p. 56–61.

Grund, Alfred, 1914, Der Geographische Zyklus im karst: Zeitschr. der Gesellschaft fur Erdkunde zu Berlin, p. 621–640.

Harvey, E. J., and Skelton, John, 1968, Hydrologic study of a waste-disposal problem in a karst area at Springfield, Missouri, *in* Geological Survey Research 1968: U.S. Geol. Survey Prof. Paper 600-C, p. C217–C220.

Hendricks, E. L., and Goodwin, M. H., Jr., 1952, Water-level fluctuations in limestone sinks in southwestern Georgia: U.S. Geol. Survey Water-Supply Paper 1110-E, p. 157–246.

Herak, Milan, and Stringfield, V. T., eds., 1971, Important karst regions of the Northern Hemisphere: Amsterdam, Elsevier Publishing Co., 488 p.

Herrick, S. M., and LeGrand, H. E., 1964, Solution subsidence of a limestone terrane in southwest Georgia: Internat. Assoc. Sci. Hydrology Bull., v. 9, no. 2, p. 25–36.

Jacob, C. E., 1944, Correlation of ground-water levels and precipitation on Long Island, New York, Pt. 1, Theory: Am. Geophys. Union Trans., 24th Ann. Mtg., p. 564–573.

LaMoreaux, P. E., Raymond, Dorothy, and Joiner, T. J., 1970, Hydrology of limestone terranes, annotated bibliography of carbonate rocks: Alabama Geol. Survey Bull. 94, pt. A, 242 p.

LeGrand, H. E., 1970, Comparative hydrogeology: An example of its use: Geol. Soc. America Bull., v. 81, p. 1243–1248.

LeGrand, H. E., and Stringfield, V. T., 1971, Water levels in carbonate rock terranes: Ground Water, v. 9, no. 3, p. 4–10.

Lewicki, Friderik, 1967, The basic hydrologic characteristics of the karst river Ljubljanica, *in* Hydrology of fractured rocks: Dubrovnik Symposium, October 1965, Proc., Internat. Assoc. Sci. Hydrology Pub. 73, v. 1, p. 255–262.

Malott, C. A., 1952, The swallow-holes of Lost River, Orange County, Indiana: Indiana Acad. Sci. Proc., v. 61, p. 187–231.

Maxey, G. B., 1968, Hydrogeology of desert basins: Ground Water, v. 6, no. 5, p. 10–22.

Meinzer, O. E., 1939, Ground water in the United States, a summary of ground-water conditions and resources, utilization of water from wells and springs, methods of scientific investigation, and literature relating to the subject: U.S. Geol. Survey Water-Supply Paper 836-D, p. 157–232.

Rahn, P. H., and Gries, J. P., 1971, Estimating recharge to limestone aquifers based on spring discharge: Geol. Soc. America, Abs. with Programs, v. 3, no. 7, p. 677.

Sayre, A. N., and Bennett, R. R., 1942, Recharge, movement, and discharge in the Edwards limestone reservoir, Texas: Am. Geophys. Union Trans., v. 23, p. 19–27.

Skelton, John, 1966, Low flow characteristics of Missouri streams: Missouri Geol. Survey and Water Resources, Water Resources Rept. 20, 95 p.

Stringfield, V. T., 1964, Relation of surface-water hydrology to the principal artesian aquifer in Florida and southeastern Georgia, *in* Geological Survey Research 1964: U.S. Geol. Survey Prof. Paper 501-C, p. C164–C169.

—— 1966, Artesian water in Tertiary limestone in the southeastern States: U.S. Geol. Survey Prof. Paper 517, 226 p. [1967]

Stringfield, V. T., and LeGrand, H. E., 1969, Hydrology of carbonate-rock terranes—A review, with special reference to the United States: Jour. Hydrology, v. 8, nos. 3 and 4, p. 349–417.

Stuart, W. T., Schneider, W. J., and Crooks, J. W., 1967, Swatara Creek basin of southeastern Pennsylvania—An evaluation of its hydrologic system: U.S. Geol. Survey Water-Supply Paper 1829, 79 p.

Thornbury, W. D., 1965, Regional geomorphology of the United States: New York, John Wiley & Sons, 609 p.

U.S. Army Corps Engineers, 1970, Survey report on Edwards underground reservoir, Guadalupe, San Antonio, and Nueces River and tributaries: U.S. Army Corps Engineers, Fort Worth District, v. 2, app. 2, p. II–67.

White, E. L., and Reich, B. M., 1970, Behavior of annual floods in limestone basins in Pennsylvania: Jour. Hydrology, v. 10, p. 193–198.

White, W. B., and Schmidt, V. A., 1966, Hydrology of a karst area in east-central West Virginia: Water Resources Research, v. 2, no. 3, p. 549–560.

Winograd, I. J., 1962, Interbasin movement of ground water at the Nevada Test Site, Nevada: Art. 104 *in* U.S. Geol. Survey Prof. Paper 450-C, p. C108–C111.

Jour. Research U.S. Geol. Survey
Vol. 1, No. 3, May-June 1973, p. 361–366

THE FRACTIONATION OF HUMIC ACIDS FROM NATURAL WATER SYSTEMS

By R. L. WERSHAW and D. J. PINCKNEY, Lakewood, Colo.

Abstract.—Humic acids, the most abundant organic components of natural water systems, are complex mixtures of molecular aggregates of different chemical and physical properties. The first step in the study of such a mixture is the fractionation of the mixture. The most common approach with humic acids is to attempt to obtain a molecular weight fractionation by gel-permeation chromatography. However, since the preponderance of evidence indicates that the components of humic acid do not fulfill the basic criteria of uniform shape and chemical structure necessary for obtaining a molecular fractionation on gel-permeation media, molecular weight distributions in humic acids cannot be evaluated by this method. A fractionation dependent upon chemical structure can be obtained by the manipulation of elution conditions on a gel-permeation column. This procedure provides a beginning in the isolation and identification of discrete components of humic acids.

Progress in the elucidation of molecular structure of humic acid and also of fulvic acid has been extremely slow. As a consequence, a detailed understanding of their interactions in soil and water systems is lacking. It has been realized for a long time that the humic and fulvic acid extracts from soils, sediments, and waters are complex mixtures of chemically different molecular species. Any study of the chemistry of humic or fulvic acids must therefore begin with the isolation of these various molecular species.

Sephadex[1] gel-permeation chromatography, which has been particularly valuable in the molecular weight fractionation of mixtures of closely related molecules such as globular proteins or polysaccharides, has been used extensively in attempts to fractionate humic and fulvic acids according to molecular weight (see review by Swift and Posner, 1971). Most of the workers have tacitly assumed in interpreting their data that all the particles in a given humic or fulvic acid sample were of the same shape and chemical structure, for if these two conditions did not obtain then one could not evaluate relative molecular weights from elution volumes (Determann, 1969).

The effect of differences in shape on apparent molecular weights calculated from Sephadex elution volumes has been graphically demonstrated by the work of Chao and Einstein (1969) on globular and flexible, disordered proteins. They have shown that the molecular weights of flexible, disordered proteins calculated by comparing the elution volumes of the proteins with those of globular proteins are considerably higher than the molecular weights obtained by equilibrium ultracentrifugation. Schnitzer and Skinner (1968), working with fulvic acids, which are apparently similar to humic acids, found that the molecular weights of the fulvic acid fractions calculated from gel-permeation chromatography data were 3 to 10 times higher than those determined for the same fractions by vapor pressure osmometry, freezing point depression, and ultracentrifugation. Therefore, since it has not been established that humic acid molecules are uniform in shape or in chemical structure, molecular weight distributions determined by gel-permeation chromatography are, at best, of doubtful value.

In the absence of evidence to the contrary, one can only assume that a given humic acid sample is a heterogeneous mixture of particles of different shapes and different chemical structures. In a heterogeneous mixture of different chemical species, it is more fruitful to attempt to increase the chemical homogeneity of the fractions than to try to obtain a molecular weight fractionation. This is especially true for humic and fulvic acids which form molecular aggregates in solution (Wershaw and Pinckney, 1971, 1973).

The work of Wershaw and Burcar (1967), Wildenhain and Henseke (1967), and Bailly and Margulis (1968) suggests that it should be possible to increase the chemical homogeneity of humic acid fractions by adsorption chromatography on Sephadex gels. In order to obtain chemical fractionation the functional groups of various humic acid fractions must interact with the functional groups of the gel-permeation medium. The amount of interaction between a given humic acid molecule and the gel will be dependent on the functional-group composition of the molecule; therefore, different types of molecules will move through the gel column at different speeds. In order to obtain maximum fractionation, we have attempted to enhance this differential interaction. This is exactly the opposite of the practice in normal gel-permeation chromatography, where it is desired that the interactions between gel molecules and the sample molecules be minimized.

[1] Sephadex is a registered trademark of Pharmacia Fine Chemicals, Inc. Use of the term in this paper is for descriptive purposes only and does not constitute an endorsement of the product by the U.S. Geological Survey.

There is very little detailed information on the chemical structure of humic acids. However, that information which is available suggests that humic acids are principally aromatic in nature, containing phenol, quinone, and acid groups. In addition to the aromatic functional groups, amine and alcohol groups and ether linkages are apparently also present in most humic acids (see Flaig, 1970, and Kononova, 1966).

Phenols, quinones, and aromatic acids in general strongly interact with Sephadex dextran gels. Gelotte (1960) was the first to make a detailed study of sorption of compounds by Sephadex. He found that compounds containing aromatic and heterocyclic groups, and basic compounds were adsorbed to Sephadex. The adsorptions were most pronounced when the Sephadex column was equilibrated with distilled water, and when distilled water was used an an eluant. Demetriou and others (1968) have demonstrated that by manipulation of the ion strength of eluant, it is possible to obtain fractionation of substituted phenolic and heterocyclic compounds. Adsorptive effects were found to be operative in both distilled water and electrolyte solutions. Janson (1967) has shown in his review of the literature on adsorption on Sephadex that there are two types of departure from ideal molecular sieving behavior on Sephadex gels. Some solutes may be retarded in their movement through the gel by adsorption or attractive electrostatic interactions, whereas others will be excluded from the gel by repressive forces and will move through the column more rapidly than normal. Janson has pointed out that dextran gels, such as Sephadex, have a particular affinity for aromatic compounds and other compounds with large numbers of π electrons. Brook and Munday (1970) have shown that the hydroxyl, amino, or carboxyl groups of monosubstituted derivatives of phenols, anilines, and benzoic acids interact with the ether linkage and the hydroxyl groups on the dextran chains. Their work also indicates that the degree of interaction between these monosubstituted derivatives and dextran gels can be correlated by the Hammett equation.

Sephadex adsorption chromatography has been used for separation of closely related aromatic and heterocyclic compounds (Miranda and others, 1962, Demetriou and others, 1968, and Woof and Pierce, 1967). Reeves, Kaiser, and Finley (1970) have devised a method for the separation of azo and azomethine dyes by gel-permeation chromatography on Sephadex G-25 and G-50. Using 0.01 *N* KOH as an eluant they were able to separate dye isomers.

The fact that sodium humates form aggregates will also affect their fractionation on Sephadex. As Andrews (1970) has pointed out, compounds which form molecular aggregates in solution will behave in at least three different ways on gel-permeation columns. Those compounds which form stable aggregates that do not dissociate under the physical and chemical conditions of the procedure will move through the column as though the aggregates were simply large molecules. If, however, the aggregates are in equilibrium with their dissociated constituent units, then the elution volume of the aggregated system will be concentration dependent. In addition, there will be some spreading of the solute on the column. If the aggregates are complexes of different molecular species, then in some instances gel-permeation chromatography will bring about dissociation of the otherwise stable aggregates.

EXPERIMENTAL PROCEDURE

The humic acids used in this study were extracted from both soils and natural waters. The soil extraction procedure with 0.1 *N* NaOH was the same as that outlined in Wershaw and others (1967) except that the extractions were carried out in closed Teflon bottles that were completely filled with soil and extraction solution. The water samples were concentrated to about 20 percent of the original volume by freeze concentration (Shapiro, 1961). The humic acid in both the soil and water samples was precipitated by lowering the pH of the solution to 1 with hydrochloric acid. The humic acid was separated from the solution by centrifugation and washed three times with water. After washing, the sodium salt of the humic acid was prepared by dissolving the humic acid in excess sodium hydroxide. In our early work, we dialyzed the solutions to remove excess sodium hydroxide; however, we found that we were losing some material. Therefore, we now add only enough sodium hydroxide to dissolve the humic acid; the pH of the solutions after the addition of sodium hydroxide is between 7 and 9. This product is then lyophilized.

Column chromatography of the sodium humate samples from various environments was carried out on Sephadex G-50, G-25, and G-100 columns prepared in the usual manner prescribed by the manufacturer. All of the Sephadex was allowed to swell in distilled water, and the columns were packed with Sephadex suspended in distilled water.

A variety of column sizes was used; however, most of the work was done on columns 4.2 cm in diameter and 30.5 cm in length. One-percent solutions of the various sodium humate samples to be fractionated were prepared, and the pH of each solution was adjusted to values between 11.2 and 11.6 with sodium hydroxide. A 10-ml aliquot of the solution was applied to the Sephadex column, and the column was eluted with distilled water. The first fractionation of each sample was carried out on a Sephadex Superfine G-50 column, and the fractions were collected and lyophilized. The first fraction to come off the G-50 column was refractionated on Sephadex Superfine G-100 columns, and the rest of the fractions were refractionated on Sephadex Superfine G-25 columns. From 10 to 12 subfractions were obtained. In the refractionation procedure, the lyophilized fractions were dissolved in water and eluted from the columns with water; these subfractions were then lyophilized.

Results similar to those of Sephadex column chromatography may be obtained by Sephadex thin-layer chromatography. The thin-layer technique permits the comparison of a

number of small samples on the same thin-layer plate under the same elution conditions.

The procedure for the low-angle X-ray scattering studies to determine particle size distribution of fractions in solution is described in Wershaw and Pinckney (1973).

Description of soils extracted for humic acids

North Carolina sandy soil.—This soil was taken from the Bh horizon of the Leon-Lakewood soil association, of the coastal plain, Brunswick County, N.C. It is a dark medium sand with a very low clay content and about 2 percent organic carbon. (For a complete description, see Malcolm, 1964).

Florida sandy soil.—This sample of Rutledge mucky fine sand was collected from the poorly drained area along Cypress Creek, Vineland, Orange County, Fla. This soil is a sandy surface soil which is normally 4 to 12 inches thick. It has been classified as a humic clay soil by Leighty and others (1960).

Lagunita soil.—This soil was taken from an alpine bog in the Sangre de Cristo Mountains, Mora County, N. Mex. (sec. 25, T. 23 N., R. 14 E., New Mexico Principal Meridian) at an elevation of about 11,040 feet. The upper 3 to 4 inches of vegetation was removed, and the next 12 inches of soil was sampled. It is high in decaying organic matter consisting mainly of dead roots. Before extraction, as much of the root material as possible was removed. (For a more complete description of the soils in the area, see Carleton, 1971.)

Washington organic soil.—A composite sample made up of Spalding peat, Rifle peat, and undifferentiated alluvial soil was taken from eight sampling sites along Grovers Creek, Kitsap County, Wash. The peats consist mainly of organic material with little or no mineral material. The undifferentiated alluvial soil occurs in strips 100 to 200 feet wide along the stream. In addition to peat, it contains decaying organic matter, sand, and clay (Wildermuth and others, 1939).

Description of water sample extracted for humic acid

Alamosa water.—The water comes from a zone 200 to 400 feet beneath the land surface; it normally has a color of about 520 APHA (American Public Health Association) units, and the pH is about 8. This water is in contact with peat beds of the Alamosa Formation, and apparently the humic acids in the water come from these beds. The well from which this water was taken is in sec. 13, T. 39 N., R. 10 E., Alamosa County, Colo.

Discussion of the results

The characterization of the elution behavior of a particular fraction from a gel-permeation chromatography column requires the use of a parameter which is independent of the column dimensions. The parameter most frequently used for this is K_d, which is defined by the equation

$$K_d = \frac{V_e - V_o}{V_t - V_o},$$

where V_e is the elution volume of the fraction, V_o is the void volume of the column, and V_t is the total volume of the column. It is generally assumed that K_d values less than one indicate that normal molecular sieving is taking place and that values greater than one indicate that the fraction is being sorbed by the column medium. However, the work of Baetz and Diehl (1968) suggests that adsorption may even play a role in the fractionation of compounds with K_d values less than one. They were able to separate mixtures of 0,0'-dihydroxyazobenzene dyes on Sephadex G-10 using 0.001 *N* NaOH as an eluant. All of the dyes had K_d values less than one; however, they found that the normal elution order of higher molecular weight compounds coming off the column before lower molecular weight compounds was not followed. A compound of molecular weight 504 was eluted from the column after a dye with a molecular weight of 359. Baetz and Diehl (1968) have attributed this reversal in elution order to differential adsorption of the two species.

Elution curves for several different sodium humates from Sephadex G-50 columns are given in figure 1. In general it will be noted that the chromatograms are very similar for the fractionation of the various sodium humate samples on G-50. The first fraction is eluted at the void volume of the column in every instance ($K_d = 0$). Another fraction is eluted at approximately the total column volume ($K_d = 1$); this fraction is in general the most abundant fraction. Between this fraction, which is designated fraction 4, and the first fraction, normally two other fractions are eluted. The relative positions and abundances of these fractions are different in different humic acids. In addition to these fractions, in several of the humic acids that were studied, two other fractions have been detected. One of these comes off the column much later than fraction 4 and has been designated fraction 5; between this fraction and fraction 4 a green band is sometimes seen on the column. This band is generally so weak that it does not show up as an absorption peak on the spectrophotometer trace.

The North Carolina humic acid green band has been tentatively identified as being the same as the so-called green humic acid isolated by Kumada and Hurst (1967). Sato and Kumada (1967) have identified this substance as a derivative of 4,9-dihydroxyperylene-3,10-quinone. Kumada and Hurst (1967) isolated the green humic acid fraction by chromatography of a humic acid sample on a Sephadex G-25 column. Lowe and Tsang (1970), using the same procedure, have been able to isolate green humic acids from different forest soils in British Columbia. The isolation of what appears to be a single chemical compound or at least a group of closely related compounds lends support to the proposition that the separation of chemically distinct species can be accomplished by Sephadex chromatography.

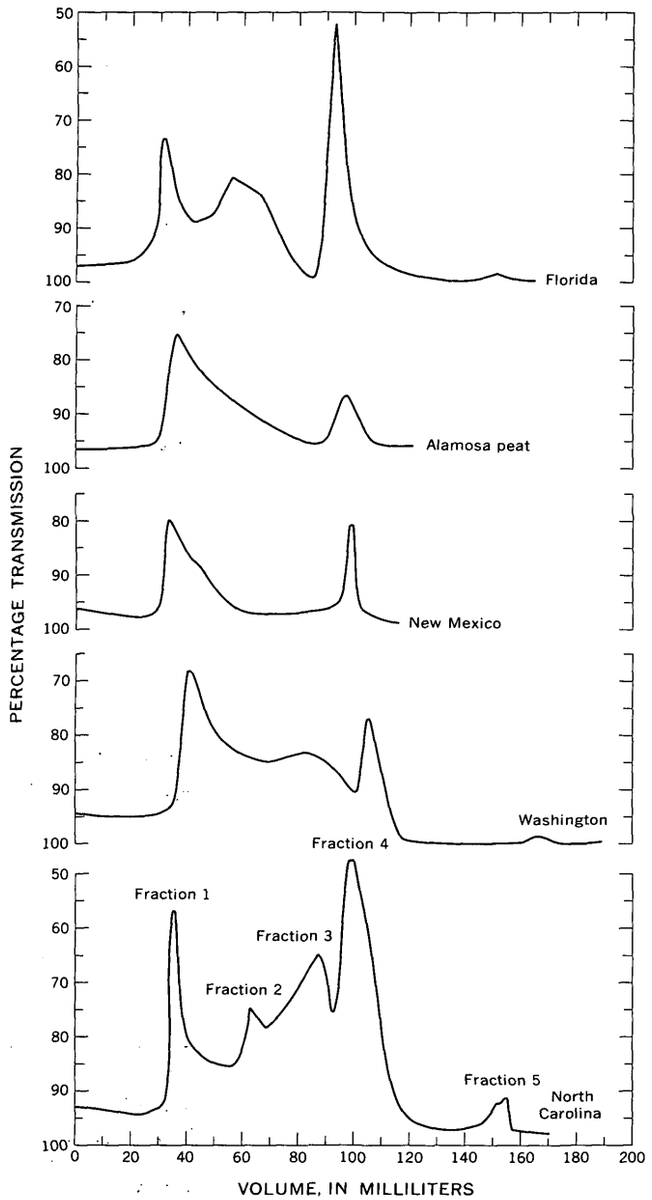

Figure 1.—Elution curves for different humic acids on G-50 columns. The transmission at 600 nm of the eluant was continuously monitored in a 0.125-ml, 5-mm-path-length flow cell.

Simple molecular sieving may only be used to explain the separation of fraction 1 on the Sephadex G-50 columns; a more complex mechanism must be used to explain the other separations. The fractions that are eluted after fraction 4 (that is, at volumes greater than the total column) are obviously being separated by a mechanism other than molecular sieving. Generally this type of behavior has been attributed to adsorption of the fraction by gel. The separation of fractions 2, 3, and 4 cannot be explained by molecular sieving alone, for low-angle X-ray scattering showed that each of these fractions is polydisperse under conditions found in the column (Wershaw and Pinckney, 1971). The smallest particles in most of these polydisperse systems are small enough to enter the Sephadex G-50 gel. Therefore, the fractionation that is taking place is most likely due to both adsorption of the sodium humate molecules by the gel and molecular sieving. The sorption of the fractions probably takes place both on the outer surfaces of gel spheres and in their interiors. However, the adsorption properties of the interiors of the Sephadex beads are apparently different from those of the outside surfaces of the beads (Dr. Monty Lee, oral commun., 1971).

Generalized diagrams of the appearance of the G-25 and G-100 columns on which the G-50 fractions were refractionated are shown in figure 2. The diagrams depict the column appearance at the time that the first fraction reached the bottom of the column. These diagrams show that the G-50 fractions will refractionate into discrete bands on G-25 and G-100 columns.

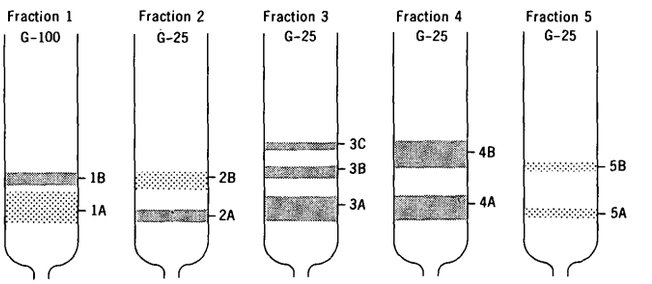

Figure 2.—The refractionation of G-50 fractions on G-100 and G-25 columns.

The additional fractionation that is obtained on one grade of Sephadex after initial fractionation on another grade probably results from differences in both pore size and functional-group distribution between the various grades. Sephadex is a cross-linked dextran polysaccharide in which the dextran strands are cross-linked by hydroxyether groups. The degree of cross-linking is greater the lower the Sephadex number, thus Sephadex G-50 has fewer cross-links and larger voids than G-25. The differences in cross-link distribution between the various grades of Sephadex affect not only the molecular sieving properties of the Sephadex but also its adsorption properties. The cross-linked dextran chains contain a few terminal carboxylic acid groups which will act as ion exchange sites. In Sephadex grades with more cross-links, more ion exchange sites are present; therefore, in distilled water these grades will act as weak ion exchangers.

A detailed study by Wershaw and Pinckney (1973) of the particle size distributions in solutions of these subfractions at different pH values provides us with an insight into the complexity of the separation mechanism on the Sephadex columns. The subfractions that we have isolated form molecular aggregates in solution; the degree of aggregation is a function of pH. All of the subfractions are highly aggregated at

pH 3.5; however at higher pH values three different types of behavior have been detected:

1. Little change in degree of aggregation above pH 3.5;
2. Continual decrease in amount of aggregation with increasing pH; and
3. Decrease in aggregation with increasing pH up to about pH 7 at which point the particles are completely disaggregated, and then reaggregation above pH 7 (Wershaw and Pinckney, 1971).

The subfractions 1A from most of the samples exhibit type 1 behavior. However, the subfractions 1A from some of the sodium humates after collection and freeze drying could not be completely redissolved in some or all of the buffers that were used. Examination of these samples by X-ray diffraction revealed that they contained appreciable amounts of montmorillonite which was probably bound to the sodium humate.

The third category of behavior is sometimes detected in some of the subfractions of fraction 2. However, since fraction 2 is indistinct in many samples, it is not always possible to compare its subfractions from one sample to another.

Most of the subfractions exhibit behavior of the second category. Even in highly alkaline solutions the molecules of these fractions are aggregated to some extent in a continuous distribution of particle sizes from those that are larger than pores of G-50 or even G-100 to those that are smaller than the pores.

As Janson (1967) has pointed out, since much more surface is exposed on the inside of the gel beads than on the outside, the molecules that are being fractionated must enter the gel medium before an appreciable amount of material can interact with the gel. Therefore, in attempting to understand the mechanism of interaction of sodium humate particles with Sephadex gels it is necessary to know the sizes of pores in the gel beads. These sizes may be evaluated from data on the exclusion limits for globular proteins. Since the Sephadex gels have been widely used for fractionation of globular proteins, the minimum molecular weights of globular proteins that are excluded from the gels have been well established.[2] Therefore by plotting radii of gyration versus molecular weights of globular proteins, one can determine the minimum sizes of the molecules that are excluded from the gels. These data indicate that molecules having a radii of gyration greater than about 12 A will be excluded from G-25, greater than 21 A from G-50, and greater than 35 A from G-100. Thus the larger sodium humate aggregates will be completely excluded from the gel along with the associated clay–humic acid particles.

The elution behavior of the aggregate will be altered if the component particles of the aggregate enter and interact with the particles of the gel. Since, in general, sodium humates are more disaggregated at high pH values, the introduction of the samples onto the G-50 columns at pH values of about 11 will enhance the penetration of the sodium humate into gel pores. The molecules of the various fractions will migrate through the column at different rates that are dependent on both the chemical and physical properties of the fractions. This process will tend to disaggregate a mixed aggregate into its component fractions. This mechanism for the fractionation of mixed aggregates probably accounts for the initial fractionation of sodium humate on Sephadex G-50 columns.

Werhsaw and others (1967) have detected particles with radii of gyration in excess of 100 A in an unfractionated sodium humate sample. Further work has revealed, however, that particles small enough to penetrate the pores of Sephadex G-50 are also present. The distribution of particle sizes changes with pH, and therefore there is apparently a dynamic equilibrium between the mixed aggregates and their component particles. The entrance of smaller particles into the pores of the Sephadex will create osmotic pressure differences between the inside and outside of gel beads and further complicate the fractionation mechanism (Well, 1972).

Monahan, DeLuca, and Wershaw (1972) have demonstrated by ultraviolet-visible absorption spectrophotometry and fluorescence spectrophotometry that the degree of aggregation of the sodium humate molecules is also a function of concentration. Their results also show that the different subfractions of the North Carolina sodium humate are chemically different. At very low concentrations, each of the fractions has a distinctive spectrum which is due to an unassociated monomer. At higher concentrations aggregation of the monomers markedly alters the spectra and obscures the spectral differences.

CONCLUSIONS

The fractionation of humic acid salts on Sephadex is probably due to the interaction of at least three different processes; molecular sieving, adsorption, and ion exchange. Since the different grades of Sephadex have different molecular sieving, adsorption, and ion exchange properties, it is not surprising that one grade of Sephadex will fractionate a material that was not fractionated on another grade. Chromatography on Sephadex gels, therefore, provides a convenient means for chemically fractionating and comparing sodium humates from different environments.

The fractionation procedures described here provide a first step in the continuing effort to unravel the complex chemical and physical structure of humic acids. In order to obtain detailed structural information about the components of a complex mixture such as natural humic acid, one must first isolate the components and then subject each one of them to analysis. It is hopeless to attempt to work with the unfractionated mixture.

Additional fractionation procedures must now be devised for the refinement of the separations that have already been obtained. In this way an eventual capability to isolate homogeneous, identifiable components will be reached. Assay

[2] See "Sephadex gel filtration in theory and practice," 1970, available from Pharmacia Fine Chemicals, Inc., Piscataway, N.J.

procedures will then be necessary to identify and assess the purity of these components.

REFERENCES CITED

Andrews, P., 1970, Estimation of molecular size and molecular weights of biological compounds by gel filtration, *in* David Glick, ed., Methods of biological analysis, v. 18: New York, Interscience, p. 1–53.

Baetz, A. L., and Diehl, Harvey, 1968, Separation on a Sephadex column of a complex mixture of azo dyes used as fluorometric chelating agents: Jour. Chromatography, v. 34, p. 534–536.

Bailly, Jean-Rene, and Margulis, Henri, 1968, Etude de quelques acides humiques sur gel de dextrane: Plant and Soil, v. 29, p. 343–361.

Brook, A. J. W., and Munday, K. C., 1970, The interaction of phenols, anilines and benzoic acids with Sephadex gels: Jour. Chromatography, v. 47, p. 1–8.

Carleton, J. O., 1971, Soil resource inventory for the east half Carson National Forest: U.S. Forest Service in-service report, 220 p. (Available in Santa Fe, N. Mex., office.)

Chao, Li-Pen, and Einstein, E. R., 1969, Estimation of the molecular weight of flexible disordered proteins by exclusion chromatography: Jour. Chromatography, v. 42, p. 485–492.

Demetriou, J. A., Macias R., F. M., McArthur, M. J., and Beattie, J. M., 1968, Gel filtration chromatography of fluorescent phenolic and heterocyclic compounds: Jour. Chromatography, v. 34, p. 342–350.

Determann, Helmut, 1969, Principles of gel chromatography, *in* Giddings, J. C., and Keller, R. A., Advances in chromatography, v. 8: New York, Marcel Dekker, p. 3–45.

Flaig, Wolfgang, 1970, Contribution à la connaissance de la constitution et de la synthèse des acides humiques: Extrait de Science du Sol, no. 2, Supplément au Bulletin de L'Association Francaise pour l'Etude du Sol, p. 39–72.

Gelotte, Bertil, 1960, Studies on gel filtration sorption properties of the bed material Sephadex: Jour. Chromatography, v. 3, p. 330–342.

Janson, Jan-Christer, 1967, Adsorption phenomena on Sephadex: Jour. Chromatography, v. 28, p. 12–20.

Kononova, M. M., 1966, Soil organic matter, its nature, its role in soil formation and in soil fertility: London, Pergamon Press, 544 p.

Kumada, Kyoichi, and Hurst, H. M., 1967, Green humic acid and its possible origin as a fungal metabolite: Nature, v. 214, p. 631–633.

Leighty, R. G., Brewer, D. T., Smith, W. R., Cruz, O. E., Evenson, E. H., Matanzo, F., Taylor, D. S., Craig, R. M., Diamond, W. G., Mathews, E. D., Morgan, M. S., White, H. O., and Hasty, A. H., 1960, Soil survey, Orange County, Florida: U.S. Dept. Agriculture Soil Conservation Service Series 1957, no. 5, 63 p.

Lowe, L. E., and Tsang, W-C., 1970, Distribution of a green humic acid component in forest humus layers of British Columbia: Canadian Jour. Soil Sci., v. 50, p. 456–457.

Malcolm, R. L., 1964, Mobile soil organic matter and its interactions with clay minerals and sesquioxides: North Carolina State Univ. Ph. D. thesis, 148 p.; available on microfilm, Univ. Micro Films, Ann Arbor, Mich.

Miranda, Francois, Rochat, Hervé, and Lissitzky, Serge, 1962, Propriétés échangeuses d'ions du gel de dextrane (Sephadex) application á la mise au point d'une technique de rétention réversible des protéines basiques de faible poids moléculaire: Jour. Chromatography, v. 7, p. 142–154.

Monahan, A. R., DeLuca, A. F., and Wershaw, R. L., 1972, Spectroscopic characterization of humic acid fractions in aqueous media: Am. Chem. Soc. mtg., New York, Aug. 27–Sept. 1, 1972, Proc. (In press)

Reeves, R. L., Kaiser, R. S., and Finley, K. T., 1970, The separation and purification of ionic azo and azomethine dyes by gel permeation chromatography: Jour. Chromatography, v. 47, p. 217–223.

Sato, Osamu, and Kumada, Kyoichi, 1967, The chemical nature of the green fraction of p type humic acid: Soil Sci. and Plant Nutrition, v. 13, p. 121–122.

Schnitzer, M., and Skinner, S. I. M., 1968, Gel filtration of fulvic acid, a soil humic compound, *in* Isotopes and radiation in soil organic-matter studies: Vienna, Internat. Atomic Energy Agency, p. 41–55.

Shapiro, Joseph, 1961, Freezing-out, a safe technique for concentration of dilute solutions: Science, v. 133, p. 2063–2064.

Swift, R. S., and Posner, A. M., 1971, Gel chromatography of humic acid: Jour. Soil Sci., v. 22, p. 237–249.

Well, J. D., 1972, Possible source of error in osmometry with salt-free polyelectrolyte solutions: Nature Physical Science, v. 237, p. 59–60.

Wershaw, R. L., and Burcar, P. J., 1967, Physical-chemical properties of naturally occurring polyelectrolytes–I. Sodium humate: Am. Water Resources Conf., 3d, San Francisco, Calif., Nov. 8–10, 1967, Proc., p. 351–364.

Wershaw, R. L., Burcar, P. J., Sutula, C. L., and Wiginton, B. J., 1967, Sodium humate solution studied with small-angle X-ray scattering: Science, v. 157, no. 3795, p. 1429–1431.

Wershaw, R. L., and Pinckney, D. J., 1971, Association and dissociation of a humic acid fraction as a function of pH, *in* Geological Survey Research 1971: U.S. Geol. Survey Prof. Paper 750-D, p. D216–D218.

—— 1973, Determination of the association and dissociation of humic acid fractions by small angle X-ray scattering: U.S. Geol. Survey Jour. Research (In press).

Wildenhain, Wolfgang, and Henseke, Günter, 1967, Fraktionierung von fulvosäuren an Sephadex und charakterisierung durch farbreaktionen: Zeitschr. Anal. Chemie, v. 229, p. 271–281.

Wildermuth, Robert, Perkins, S. O., Pasco, R. E., and Hubbard, E. H., 1939, Soil survey, Kitsap County, Washington: U.S. Dept. Agriculture, Bureau of Chemistry and Soils Series 1934, no. 12, 41 p.

Woof, J. B., and Pierce, J. S., 1967, Separation of complex mixtures of polyhydroxy phenols on columns of Sephadex: Jour. Chromatography, v. 28, p. 94–103.

Jour. Research U.S. Geol. Survey
Vol. 1, No. 3, May-June 1973, p. 367–370

FLUORITE EQUILIBRIA IN THERMAL SPRINGS OF THE SNAKE RIVER BASIN, IDAHO

By C. E. ROBERSON and ROBERT SCHOEN, Menlo Park, Calif.

Abstract.—Some thermal water sources of the Snake River basin, Idaho, are near saturation with respect to fluorite. That mineral was identified by X-ray diffraction in precipitates induced in three water samples by adding sodium fluoride. The derived solubility product (K_{SO}) for zero ionic strength was close to that calculated from Latimer's thermodynamic data ($10^{-9.77}$). The relative ease of precipitation of fluorite from these water samples indicates that equilibrium with respect to fluorite may occur in some ground-water systems.

A recent study by one of us (Schoen, 1972) of the hydrochemistry at the National Reactor Testing Station (NRTS) included some discussion of thermal waters which have relatively high fluoride-ion (F^-) concentrations (up to 15 mg F^-/l). Calculation of activity products suggested that some of the sources were near equilibrium with respect to fluorite ($CaF_{2\ c}$). Implications relating to geochemistry as well as to possible sampling difficulties led us to examine more closely fluoride equilibria in the water sources in question. To demonstrate experimentally that the solutions were near equilibrium with respect to fluorite, small amounts of sodium fluoride were added to each. This caused calcium fluoride (CaF_2) to precipitate from filtered portions of the source samples. Activity products, before and after precipitation, were compared with data in the literature for the solubility product for fluorite.

Acknowledgments.—We thank our colleagues of the U.S. Geological Survey—J. D. Hem for his very helpful comments and D. W. Brown for doing computer calculations in connection with his review.

EXPERIMENTAL METHODS

Samples 2095–2101 were first analyzed for major and other constituents (table 1) by methods described by Brown,

Table 1.—*Chemical analyses of water samples from thermal sources, Idaho*

[Values are in milligrams per liter, except for values in parentheses]

Sample No.	2095	2096	2097	2098	2099	2100	2101
SiO_2	34	24	33	44	80	97	27
Al	<0.2	<0.2	<0.2	<0.2	<0.2	<0.2	<0.2
Fe	.08	.04	.10	.05	.00	.00	.27
Mn	.05	.01	.22	.02	.02	.00	.00
Ca	90	133	430	150	51	1.0	55
Mg	16	31	81	30	.2	.01	11
Na	28	3.9	1,530	311	541	106	63
K	15	4.4	192	71	20	1.5	22
Li	.05	.02	2.3	.47	1.4	.04	.08
NH_4	.26	.32	5.2	.00	.24	.13	.80
Alkalinity (as HCO_3^-)	171	165	1,080	736	48	159	367
SO_4	184	314	756	144	56	28	25
Cl	7.7	1.0	2,360	361	869	25	13
F	5.6	1.6	4.8	1.1	7.7	15	1.6
NO_3	.0	.4	2.6	1.4	1.5	.0	.2
PO_4	.02	.03	.06	.06	.01	.07	.02
B	.09	.00	4.6	.95	.20	.20	.26
Specific conductance (mhos$\times 10^{-6}$, 25°C)	(687)	(839)	(9,190)	(2,410)	(3,020)	(479)	(652)
pH	(7.84)	(7.52)	(6.67)	(7.56)	(7.94)	(9.14)	(7.68)
Dissolved solids (calculated)	470	595	5,950	1,480	1,650	358	401
Temperature (°C)	(48.2)	(42.2)	(47.8)	(48.9)	(95.6)	(59.4)	(50.0)

Sample localities in Idaho

2095, Lidy Hot Springs, Clark County.
2096, Green Canyon Hot Springs, Madison County.
2097, Heise Hot Springs, Jefferson County.
2098, Lava Hot Springs, Bannock County.
2099, Frazier boiling well, Cassia County.
2100, Banbury Hot Springs, Twin Falls County.
2101, Condie Hot Springs, Blaine County.

Skougstad, and Fishman (1970). Fluoride concentrations in table 1 were determined by both a colorimetric method and a specific-ion electrode method. The latter method employed a pH 8 buffer rather than that described by Brown, Skougstad, and Fishman (1970). Results by both methods were in close agreement. Then portions of samples 2095, 2097, 2099, and 2100 were filtered through membranes having 0.1-μm porosity. To 100.0-ml portions of the filtrate, 1.00 ml 0.100 *M* NaF was added, increasing the total fluoride content in each by 1.9 mg F^- (or by 19 mg/l).

The solutions were stored at room temperature. Fluoride activities were measured at 10 days and again at 30 days; at the latter time visible precipitates were noted. Also at 30 days analytical concentrations for Ca^{2+} and F^- were determined. Calcium activities were measured by an Orion 92-20 electrode, and fluoride activities by an Orion 94-09 electrode.[1] Measurements were made at 25°±0.1°C.

The precipitates were identified as fluorite by X-ray diffraction.

RESULTS AND DISCUSSION

To test the sample sources for saturation with respect to fluorite, the data of table 1 were used to calculate activity products (table 2) for the reaction $CaF_{2\ c} = Ca^{2+} + 2F^-$. The values for ionic strength, log $[Ca^{2+}]$, log $[F^-]$, and log $[Ca^{2+}][F^-]^2$ expressed in table 2 were calculated from total analytical (complexed and uncomplexed) concentrations, using a computer program (Kharaka and others, written commun., 1973) which calculates thermodynamic activities of individual aqueous ions and their complexes. These calculations are performed by first calculating approximate ionic strength from total analytical concentrations. Then approximate activities for all aqueous species are obtained from the resultant temperature-corrected Debye-Hückel activity coefficients, complex-ion dissociation constants, and total analytical concentrations. The ionic strength is then recalculated and the calculations are repeated until no significant changes (±0.5 percent) in ion activities occur with successive iteration cycles.

[1] The use of brand names in this report does not imply endorsement by the U.S. Geological Survey. Equivalent equipment can be used for the processes.

The principal ligands which involved from 10 to 27 percent of the calcium in the different samples were SO_4^{2-} and HCO_3^-, whereas the predominant fluoride complex involving only 0.1 to 6 percent of the fluoride was MgF^+.

Equilibrium constants representing in-place temperatures were estimated from the relation,

$$\int_{T_1}^{T_2} d\ln K = \int_{T_1}^{T_2} \frac{\Delta H^\circ_R dT}{RT_2} \text{ (Klotz, 1964, p. 159).}$$

Integration and rearrangement provides

$$\log K_{T_2} = \frac{\Delta H^\circ_R/RT_1 - \Delta H^\circ_R/RT_2}{2.303} + \log K_{T_1}$$

where T_1 is taken as 25°C (298°K). The equilibrium constant K_{T_1} (later called K_{S0}) is taken as $10^{-9.77}$ (discussed in next section). The heat of reaction ΔH°_R is calculated from heats of formation values (Latimer, 1952) for the species in the fluorite solubility reaction.

The effect of pressure on the equilibrium constant or the activity product was not considered.

Comparison of activity products $[Ca^{2+}][F^-]^2$ with K_{S0} (table 2) suggests that three water samples (2095, 2097, and 2099) are only slightly undersaturated with respect to fluorite at temperatures measured when the samples were collected. Upon cooling, the samples would be even closer to saturation ($-\log K_{S0}$ at 25°C = 9.77).

To four of the samples (2095, 2097, 2099 and 2100), sodium fluoride was added (1.9 mg F^-/100-ml sample) to supersaturate the solutions with respect to fluorite and to observe whether precipitation would be readily induced in this way. Actually, for sample 2100, the amount of fluoride added was not sufficient to cause precipitation that could be observed visually or analytically ($-\log [Ca^{2+}][F^-]^2 = 10.3$). The other samples, after adding sodium fluoride, were supersaturated with respect to fluorite by nearly an order of magnitude. Precipitates were visible in these samples (2095, 2097, and 2099) within 30 days. Activities of fluoride $[F^-]$ were measured before, 10 days after, and 30 days after adding sodium fluoride (table 3).

Table 2.—*Calculations to test equilibrium with respect to fluorite*

Sample No.	Temperature (°C)	Ionic strength	Calcium		Fluoride		Log K_{S0} at sample temperature	Log $[Ca^{2+}][F^-]^2$
			mg/l	Log $[Ca^{2+}]$	mg/l	Log $[F^-]$		
2095	48.2	0.0100	90	−2.921	5.6	−3.593	−9.60	−10.11
2096	42.2	.0135	133	−2.783	1.6	−4.153	−9.64	−11.09
2097	47.8	.1090	430	−2.521	4.8	−3.772	−9.60	−10.07
2098	48.9	.0283	150	−2.824	1.1	−4.335	−9.59	−11.49
2099	95.6	.0279	51	−3.230	7.7	−3.472	−9.32	−10.18
2100	59.4	.0053	1.0	−4.892	15	−3.139	−9.53	−11.17
2101	50.0	.0083	55	−3.114	1.6	−4.130	−9.59	−11.37

Table 3.—*Data from measurements made on solutions to which 1.9 mg F^- (as sodium fluoride) was added to 100-ml sample (25°C, 1 atm)*

Sample No.	$-\log [F^-]$[a]		$-\log [Ca^{2+}]$[b]	$-\log [Ca^{2+}][F^-]^2$ [c] ($-\log K_{S0}$=9.77)
	10 days	30 days	30 days	
2095	3.23	3.26	3.24	9.76
2097	3.25	3.30	3.01	9.61
2099	3.25	3.28	3.33	9.89
2100	2.80	2.78	4.89[d]	10.21

[a]Measured by Orion 94-09 electrode.
[b]Measured by Orion 92-20 electrode.
[c]Calculated from $-\log [Ca^{2+}]$ and $-\log [F^-]$, both after 30-day aging.
[d]Electrode measurement, not shown, was in error. This value (same as in table 2) is used because analytical measurement showed that the calcium concentration had not changed.

The fact that $[F^-]$ measured at 10 days after adding sodium fluoride was nearly the same as that observed after 30 days suggests that a precipitate may have been present at 10 days, but it could not be detected visually; therefore, no attempt was made to examine it. After 30 days the precipitates were removed by filtration through 1-inch-diameter filter membranes having a porosity of 0.1 μm. The membranes were cemented to glass slides with rubber cement and examined by X-ray diffraction. Diffraction patterns indicated well-crystallized material having the three strongest lines for $CaF_{2\ c}$ (3.16 A, 1.93 A, and 1.65 A). The lines were present in the diffractograms for samples 2095, 2097, and 2099. Sample 2100 was not examined, because of the lack of evidence that precipitation had taken place (no visible precipitate, and no change in Ca^{2+} concentration or in F^- activity).

SOLUBILITY OF FLUORITE

The activity products, log $[Ca^{2+}][F^-]^2$, for the three solutions from which synthetic fluorite precipitated were -9.76, -9.61, and -9.89 (table 3). These are close to the thermodynamic activity product constant log K_{S0} = -9.77 calculated from Latimer's (1952) free energy data. More negative values, generally around $10^{-10.4}$, for this constant are quoted by Sillén and Martell (1964, p. 258), and data in the more recent literature seem to indicate that the solubility product for fluorite is not well known. It is possible a somewhat more negative value would have been reached in our solutions after longer aging. The results do show, however, that precipitation of fluorite can occur readily at 25°C from moderately supersaturated solutions.

IMPLICATIONS

That certain thermal water sources in the Snake River basin are near saturation with respect to fluorite appears reasonably assured. This despite the fact that pressure and temperature effects and thermodynamic data are not known well enough to place rigorous boundaries for fluorite precipitation in the ground-water environment.

As a good first approximation, for a water source having a calcium activity of 400 mg/l, a fluoride activity of 2.5 mg/l is permitted before saturation with respect to $CaF_{2\ c}$ is attained (log K_{S0} = -9.77, 25°C). The degree of supersaturation required to cause the onset of precipitation of $CaF_{2\ c}$ is not known to us, but it would probably be influenced by nucleating surfaces in the ground-water environment. That is, mineral surfaces would probably lower the activation energy for the precipitation reaction. Therefore, because precipitation of $CaF_{2\ c}$ did occur in filtered solutions whose fluoride concentrations were increased by factors of only 4, 5, and 3 in samples 2095, 2097, and 2099, respectively, it appears quite likely that fluorite could precipitate at least as readily under conditions in the ground-water aquifer. In that ground-water environment, plenty of nucleating sites are obviously available, and lower degrees of supersaturation are probably required; lower perhaps than those of the spiked solutions (table 3) before precipitation. It would be of interest to look for fluorite in the mineral assemblages related to certain thermal water samples.

The probable source of fluoride in thermal waters of the Snake River basin is the dissolution of volcanic glass in extensive siliceous volcanic rocks as well as hydrolysis of fluorapatite from the Phosphoria Formation (Schoen, 1972). Mixing of water from different lithologic assemblages could occur as water moves toward a thermal spring orifice and possibly supersaturation with respect to $CaF_{2\ c}$ could result in the mixture. If other conditions were favorable, precipitation could occur at the mixing point or beyond it in the flow path, especially if the temperature of the water decreased significantly. For example, at 1 atmosphere pressure and neglecting ionic strength effects, a solution which is saturated at 100°C ($K_{S0} = 10^{-9.29}$) would be supersaturated by a factor of 3 if the solution were cooled to 25°C. This is a somewhat lower degree of supersaturation than that of our solutions, in which sodium fluoride addition had induced precipitation of fluorite. However, a factor of 3 may be sufficient to induce precipitation, particularly in the natural environment.

The calcium and fluoride specific-ion electrodes provide a means of studying chemical equilibrium under field conditions and can be substantial aids toward improving our understanding of natural systems.

REFERENCES CITED

Brown, Eugene, Skougstad, M. W., and Fishman, M. J., 1970, Methods for collection and analysis of water samples for dissolved minerals and gases: U.S. Geol. Survey Techniques Water-Resources Inv., Book 5, Chap. A-1, 160 p.

Klotz, I. M., 1964, Chemical thermodynamics: New York, W. A. Benjamin, Inc., 468 p.

Latimer, W. M., 1952, Oxidation potentials: Englewood Cliffs, N.J., Prentice-Hall, 392 p.

Schoen, Robert, 1972, Hydrochemical study of the National Reactor Testing Station, Idaho: Internat. Geol. Cong., 24th, Montreal 1972, Hydrogeology, sec. 11, p. 306–314.

Sillén, L. G., and Martell, A. E., 1964, Stability constants of metal-ion complexes: Chemical Soc. [London] Spec. Pub. 17, 754 p.

Jour. Research U.S. Geol. Survey
Vol. 1, No. 3, May-June 1973, p. 371–376

EVALUATING THE RELIABILITY OF SPECIFIC-YIELD DETERMINATIONS

By RONALD L. HANSON, Tucson, Ariz.

Abstract.—The specific yield of the alluvial aquifer in the Gila River flood plain in southeastern Arizona has been determined using two methods of analysis—the time-drawdown method and the soil-moisture-content method. Time-drawdown data measured at 17 observation wells during a 3.5-day aquifer test define an average apparent specific yield of 0.13. Soil-moisture-content data measured at nine access holes during the aquifer test indicate that complete gravity drainage had not been attained in the cone of depression by the end of the drawdown period. The moisture-content data were therefore extrapolated with time to define an average specific yield in the range 0.13 to 0.15. The results obtained by the two methods are in close agreement. However, the significantly lower standard deviation of the results from the moisture-content analysis indicates that extrapolation of the apparent values derived by this method may provide a more reliable estimate of the true specific yield than the apparent values derived by the time-drawdown method. Reliable estimates of specific yield in the zone of seasonal water-level fluctuations are also possible from an evaluation of the soil-moisture change in the spring and summer recession period.

Specific yield (S_y) is the ratio of the volume of water a saturated material will yield by gravity to the volume of the material (Meinzer, 1923, p. 28). This definition generally is restricted to unconfined aquifers and implies complete gravity drainage from the zone of water-level decline (Lohman and others, 1972). Specific yield may be used to evaluate the amount of water stored in an unconfined aquifer or to predict water-level changes in the aquifer owing to recharge or discharge.

The most common method used to determine the specific yield of an unconfined aquifer is the analysis of the time-drawdown data collected while pumping water from the aquifer. In recent years a method has been developed for evaluating S_y by measuring the change in soil-moisture content with a neutron moisture probe during times of pumping or seasonal water-level change. Both of these methods define the storage capacity of the aquifer as a result of gravity drainage from the zone of water-level change. Incomplete gravity drainage from the zone will define an apparent specific yield, which is smaller than the true specific yield; therefore, the magnitude of apparent specific yield is time dependent and approaches the true value asymptotically depending on the duration of pumping or water-level change.

This paper compares the specific-yield values determined by the time-drawdown and soil-moisture-content methods, evaluates their variability, and illustrates the effect that duration of drainage has on the values. The paper includes an evaluation of specific yield derived from the depletion of the soil-moisture content that occurs in the spring and summer water-level recession period.

Meyer (1962) found close agreement between the S_y derived from time-drawdown data and S_y derived from moisture-content data for an unconfined aquifer having a water level about 20 feet below the land surface. Meyer derived his S_y values from time-drawdown data collected at five observation wells during a 6.3-day aquifer test and from moisture-content data collected at one access hole during the first 1.03 days of the test. Jones and Schneider (1969) studied an unconfined aquifer having a water level 150 feet below the land surface and found that the S_y values derived from moisture-content data were 50 percent more than the S_y values obtained from time-drawdown data. Jones and Schneider based their S_y values on time-drawdown data collected at 13 observation wells and on moisture-content data collected at one access hole during an 11-day aquifer test.

The time-drawdown and soil-moisture-content data used for this study were obtained at a test site in the flood-plain alluvium in the Gila River valley in south-central Arizona. The test site is near the upstream end of a 15-mile reach of the Gila River flood plain in the Gila River Phreatophyte Project area (Culler and others, 1970). The alluvium at the test site is composed of a 55-foot layer of lenticular gravel, sand, and silt, which overlies the much less permeable basin-fill deposits (Weist, 1971). The depth to water in the alluvium ranges from 10 to 15 feet below the land surface.

Instrumentation at the test site is on the right bank of the Gila River about 800 feet from the channel. Well C1 (fig. 1), the pumped well, is 6 inches in diameter, screened, and penetrates the entire thickness of the aquifer. The 17 observation wells are unscreened and open ended, partly penetrate the aquifer, and are within 400 feet of the pumped well. The 10 soil-moisture access holes are cased with 2-inch-diameter aluminum tubing, extend several feet below the water level, and are adjacent to observation wells (fig. 1).

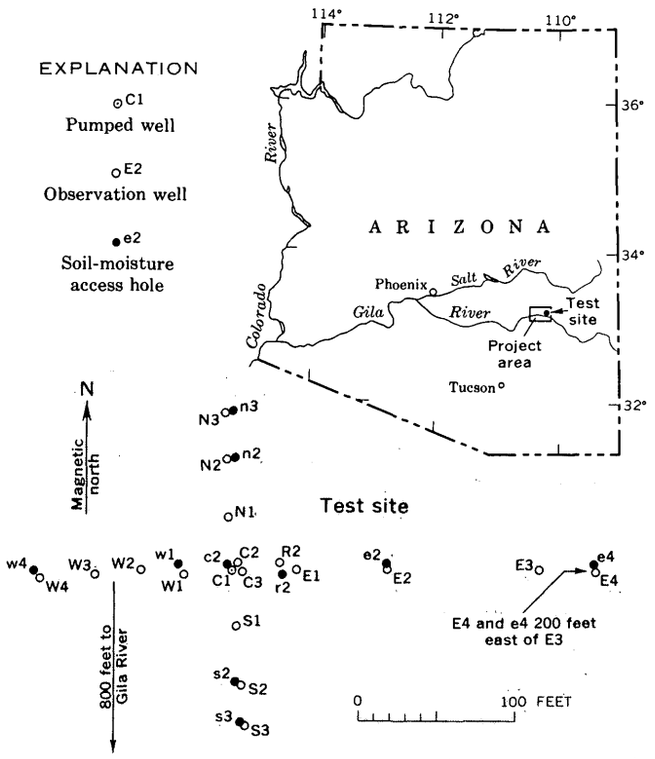

Figure 1.—Map showing the location and type of wells in the test site. The index map of Arizona shows the general location of the test site in the Gila River Phreatophyte Project area.

DETERMINATION OF SPECIFIC YIELD FROM TIME-DRAWDOWN DATA

Estimates of the transmissivity and specific yield of the alluvium were made using data obtained during the aquifer test conducted from April 16 to 20, 1964. Well C1 was pumped at a constant rate of 0.34 $ft^3 sec^{-1}$ or 152 gal min^{-1} for 3.5 days; a longer aquifer test was scheduled, but a leak in the gasline ended the test prematurely. Water levels were measured in the 17 observation wells at regular intervals during the 3.5-day aquifer test and the subsequent 3.6-day recovery period.

A correction for dewatering was applied to the water-level data by subtracting $s^2/2b$ from all measured drawdowns, where s is the drawdown and b is the saturated thickness of the alluvium (Jacob, 1963). The corrected data were then used to prepare time-drawdown plots for each observation well on logarithmic paper. Estimates of transmissivity (T), the instantaneous specific yield (S), and the delayed specific yield (S') were obtained for each observation well by matching the time-drawdown plots to type curves developed by Boulton (1963, fig. 1, p. 472). The early time-drawdown data define S, which represents that water released instantaneously from storage as a result of elastic compaction of the aquifer and expansion of water in response to a reduction in hydrostatic pressure. The later-drawdown data define S', which represents delayed gravity drainage from the interstices above the cone of depression. Table 1 lists the values of T, S, and S' for each well. The average transmissivity for the 17 observation wells is 86,900 gal $day^{-1} ft^{-1}$ with a standard deviation of 18 percent. The average combined specific yield ($S + S'$) for the total period of pumping is 0.13 with a standard deviation of ±0.12 (±92 percent).

Table 1.—*Distance from pumped well to observation wells, r; transmissivity, T; time from start of pumping to negligible delayed gravity drainage, t_0; instantaneous specific yield, S; and delayed specific yield, S'*

Well No.	r (feet)	T (gal $day^{-1} ft^{-1}$)	t_0 (hours)	S	S'
C2	6	51,200	21.5	0.002	0.285
C3	7	102,500	3.7	.005	.326
E1	41	91,700	5.0	0	.020
E2	100	87,100	7.2	.016	.078
E3	200	79,200	15.8	.034	.112
E4	400	87,100	23.9	.025	.081
N1	34	96,800	8.5	.002	.053
N2	70	116,000	3.8	.001	.025
N3	100	82,900	12.1	.010	.089
R2	31	79,200	5.2	.018	.186
S1	37	87,100	7.4	.002	.076
S2	74	79,200	.4	.016	.134
S3	99	87,100	4.3	.010	.082
W1	30	67,100	9.1	.033	.387
W2	60	116,100	.7	.005	.048
W3	90	87,100	1.5	0	.004
W4	125	79,200	16.3	.018	.073
Average		86,900	8.6	0.012	0.121
Standard deviation		±15,800	±7.0	±.011	±.111

Included in table 1 is the time after the start of pumping, t_0, when the effect of delayed gravity drainage ceases to influence drawdown. The values of t_0 were determined from a graph defined by Boulton (1963, fig. 3, p. 477) which relates a given type curve to αt_0 where α is the reciprocal of a delay index. The t_0 values in table 1 suggest that delayed gravity drainage became negligible at all wells within 24 hours after pumping started.

The equations which describe the type curves used in this analysis assume that the aquifer is unconfined, homogeneous, isotropic, and of infinite areal extent with the same saturated thickness throughout. These equations also assume that flow to the pumped well is precisely radial. Because these assumptions are only partly satisfied at the test site, the results of this analysis are questionable.

Part of the large variation in the specific-yield values given in table 1 may be attributed to the uncertainty in the graphical interpretation required for the time-drawdown analysis. The specific-yield values obtained from data for wells near the pumped well may be in error owing to the increase in curvature of the equipotential lines near the pumped well. Some of the variation in specific yield probably is real, however, and reflects the lithologic differences within the aquifer.

Weist (1971, table 2, p. D10) and S. G. Brown (in Hanson, 1972, table 3, p. F10) each made independent determinations

of T and S_y by applying a modification of the nonequilibrium equation (Ferris and others, 1962, p. 100) to the drawdown data measured late in the test. The average T values obtained by Weist and Brown are 79,400 and 73,600 gal day^{-1} ft^{-1}, respectively; and the average S_y values are 0.12 and 0.16, respectively. These values do not differ appreciably from the average transmissivity and combined specific-yield values in table 1; however, the analyses of Weist and Brown indicate that delayed gravity drainage was not complete at all observation wells when pumping ceased.

DETERMINATION OF SPECIFIC YIELD FROM SOIL-MOISTURE-CONTENT DATA

Estimates of specific yield may be obtained from measurements of the change in soil-moisture content as the result of water-level rises or declines. The estimates are computed from the ratio $\Delta c/\Delta h$, where Δc is the change in soil-moisture content, in feet, resulting from a water-level change, and Δh is the water-level change, in feet (Stallman, 1967, p. 183).

Two typical soil-moisture profiles and the corresponding water levels are shown in figure 2; the soil-moisture content and water levels in the profiles were measured in access hole r2 in April and September 1964.

The profiles show the change in soil-moisture content (Δc) in the water-level zone, which extends from about 2 feet above the top of the upper water level to about 1 foot below the lower water level. The part of the zone that is above the water level is considered to be representative of the capillary fringe. The soil-moisture content above the water-level zone is assumed to be unaffected by changes in water level and is not included in the computation of S_y. The difference in the profiles below the lower water level is due to measurement error. In order to obtain reliable estimates of specific yield from the $\Delta c/\Delta h$ ratio, gravity drainage from the capillary fringe must be virtually complete before and after the water-level change.

Soil-moisture measurements were made in 10 access holes at regular intervals during the pumping and recovery periods of the aquifer test; the measurements were made using one of four neutron probes at ¼-foot intervals. Readings were taken at each ¼-foot interval for a duration of 1 minute to minimize the randomness of the count of slow neutrons returning to the probe. Two of the probes have radium-beryllium sources of 5 mCi, one has a radium-beryllium source of 4 mCi, and one has an actinium-beryllium source of 20 mCi. Prior to the aquifer test, each probe was calibrated in barrels containing sand, gravel, and flood-plain alluvium of known moisture content, which was determined from volumetric samples.

Graphs showing the relation between soil-moisture content in the water-level zone and the depth to water in the adjacent observation well were made for each access hole. An example of this relation is shown in figure 3 for access hole r2. The solid line shows the average water level and soil-moisture

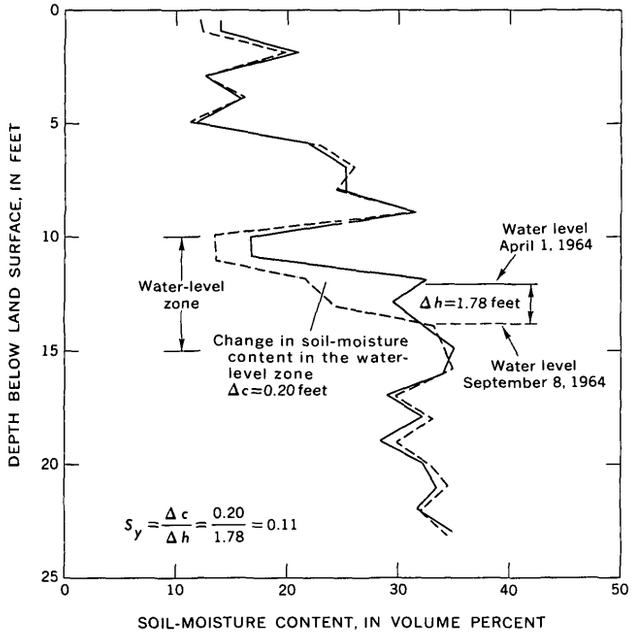

Figure 2.—Profiles showing water-level declines and depletion of soil-moisture content in the water-level zone in access hole r2.

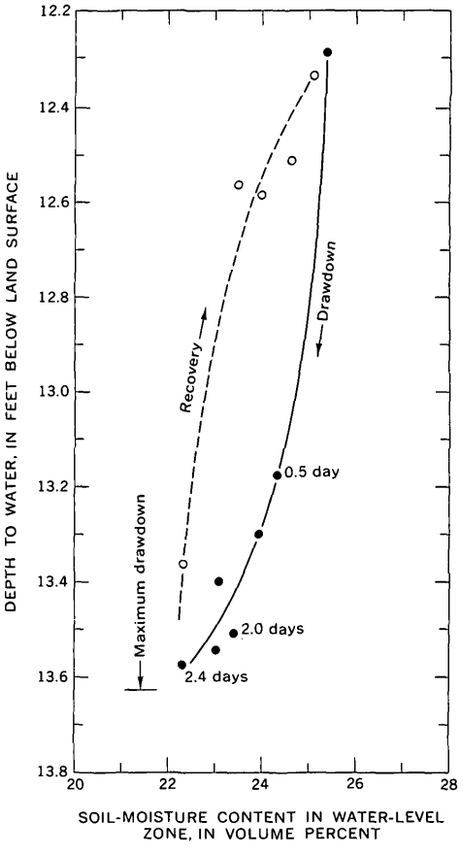

Figure 3.—Graph showing the relation between water-level change and soil-moisture content at access hole r2 during the pumping and recovery periods.

content measured during the 3.5-day pumping period, and the dashed line shows the average water level and soil-moisture content measured during the 3.6-day recovery period. The number of days since pumping started is shown at selected points on the drawdown curve. The hysteresis of soil moisture shows that there is less moisture in the water-level zone during the recovery period than during the drawdown period. The scatter of points along the drawdown and recovery curves is about ±0.5 percent by volume, which indicates an average error of measurement of ±2 percent in the soil-moisture content. This error is attributed to inconsistent depth settings of the probe, misreading of the scaler, water-level changes during the measurement, inaccurate water-level readings, and instrument variability. Although the probes were calibrated prior to the test, calibration inaccuracies also may have contributed to the error because different probes were used in the same access hole.

The extent to which gravity drainage from the water-level zone was complete at the end of the pumping period is unknown, but the data points indicate that about 90 percent of the drawdown and about 75 percent of the soil-moisture depletion occurred during the first 2 days of the pumping test (fig. 3). Similar trends were noted during the recovery period; however, the water level and the soil-moisture content had not reached full recovery 3.6 days after pumping was stopped.

The apparent specific yield at different times after pumping began was computed for each access hole using the ratio of the change in soil-moisture content to the change in water level. Figure 4 shows the relation between apparent specific yield and duration of pumping at the 10 access holes with a line of best fit drawn through the data points in each plot. Little weight was given to those points occurring within the first 12 hours of pumping because of the relatively rapid rate of change in water level during this period. Although the data points for some of the holes suggest a curvilinear rather than a linear relation (for example, hole n2), scatter of the data points does not justify this refinement. The lines through the data points for access holes s2 and c2 indicate virtually no change in apparent S_y during the last 3 days and 2 days of the test, respectively. The estimates of apparent S_y for access hole e4, which is the most distant hole from the pumped well, are not considered reliable because of the very small changes in water level and soil-moisture content measured during the test, and, therefore, the data for this hole are not included in the analysis. The data for the other seven access holes indicate an increase in apparent specific yield with the duration of pumping. Table 2 gives the drawdown and corresponding apparent specific-yield values for the access holes at the end of the 3.5-day aquifer test.

The data from most of the access holes indicate that delayed gravity drainage from the zone of water-level change was not complete at the end of the aquifer test (fig. 4). These results are contrary to the results shown by the t_0 values in table 1 which indicate no significant delayed yield after the first 24 hours of pumping. The reliability of the t_0 values is

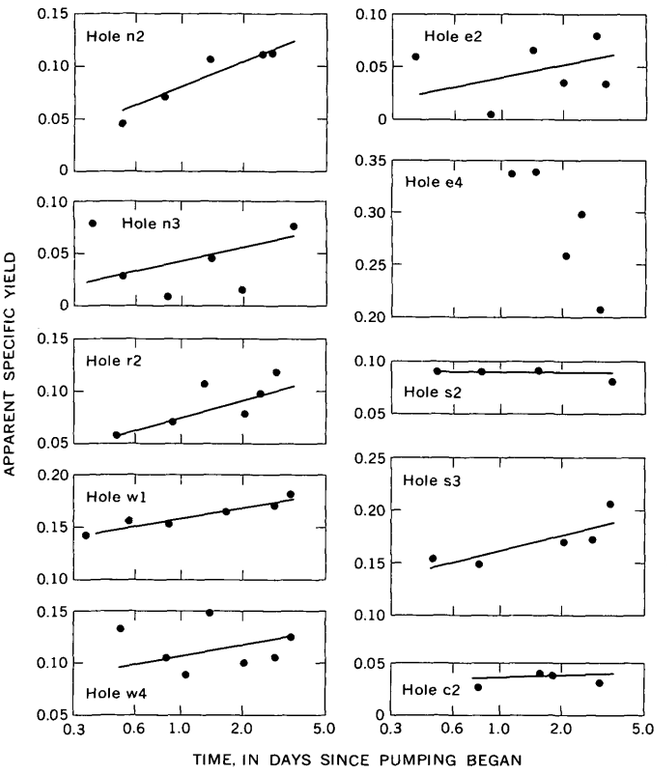

Figure 4.—Graphs showing the relation between apparent specific yield and duration of pumping at 10 soil-moisture access holes.

questionable, however, because of their large deviation (±81 percent) and the many constraints associated with their determination. The average apparent specific yield of 0.11 in table 2 is therefore assumed to represent only partial drainage and is considered to be a minimum value. Distance from the pumped well and the amount of drawdown that occurred in the access holes during the aquifer test do not appear to have significant effects on the apparent specific yield. The standard deviation of ±0.05 (±45 percent) probably reflects soil-moisture content and water-level measurement errors but may

Table 2.—*Drawdown and corresponding apparent specific-yield values computed from the change in soil-moisture content measured at the access holes during the aquifer test*

Access hole No.	Depth of water-level zone (feet)	Distance from pumped well (feet)	Drawdown (feet)	Apparent specific yield
n2	6.75–11.75	71	1.13	0.12
n3	7.25–12.25	101	.92	.07
c2	11.00–17.00	5	2.93	.04
r2	10.00–15.00	32	1.33	.11
e2	10.00–14.00	100	.99	.06
e4	9.50–12.50	400	.39	....
s2	9.75–14.75	72	1.03	.09
s3	9.50–14.50	98	.98	.19
w1	11.75–15.75	34	1.34	.18
w4	10.75–15.75	127	.92	.13
Average				.11
Standard deviation				±.05

include real variations in the extent of delayed gravity drainage at the end of the aquifer test owing to lithologic differences in the aquifer.

In an analysis of the rate of drainage from a column of saturated medium-grained Fresno sand, Prill and others (1965) showed that 90 percent of the moisture in the column was removed after 25 hours of drainage and that sufficient depletion for practical estimates of S_y was attained after 4 days of drainage; they concluded, however, that complete gravity drainage would require several months. Jones and Schneider (1969) showed that 90 percent of the specific yield in the fine sand, caliche, and clay of the Ogallala Formation occurred in the first 6 days of an 11-day aquifer test. The flood-plain alluvium in the Gila River valley is stratified and poorly sorted, and its permeability is probably less than that for the Fresno sand but may be similar to that for the Ogallala Formation. The drainage time for the flood-plain alluvium may, therefore, approximate that for the Ogallala Formation.

The degree to which gravity drainage from the zone of water-level change was complete at the end of the aquifer test is not apparent in figure 4. However, if gravity drainage is assumed to be 90 percent complete after 6 days of pumping, a straight-line extrapolation of the data gives an average apparent specific yield of 0.12 at the end of the 6 days; extrapolation to 10 days increases this value to 0.13, and extrapolation of the data to 30 days increases this value to 0.15. The true specific yield representing complete gravity drainage is highly conjectural, but the small rate of change in the extrapolated values indicates that a specific yield within the range of 0.13 to 0.15 may be more representative than the apparent value of 0.11. Any value within this range also compares favorably with the average S_y of 0.13 derived from the time-drawdown analysis. The significantly lower standard deviation of the average S_y obtained from the moisture-content analysis suggests that the extrapolated apparent values derived by this method define a more reliable estimate of the true S_y than the apparent values derived by the time-drawdown method.

Figure 5 shows the apparent specific-yield values for data from access hole r2 computed from the change in soil-moisture content during the seasonal 160-day water-level recession period from April 1, 1964, to September 8, 1964. The soil-moisture content in the capillary fringe was assumed to be stable at the beginning and end of the recession period because the water level was nearly static for 24 days before April 1 and for 15 days before September 8. These data define an apparent specific yield of 0.13 at the end of the seasonal recession period. Because the data points in figure 5 indicate little change in apparent specific yield during the last 40 days of the recession period, the data were not extrapolated, and the value of 0.13 is considered to represent complete gravity drainage from the water-level zone. Good agreement exists between this value and the apparent S_y of 0.11 for access hole r2 (table 2) derived from the moisture-content data obtained during the aquifer test; even closer agreement could be obtained if the

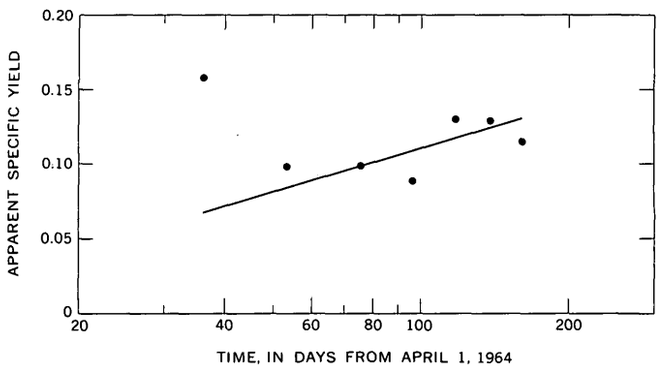

Figure 5.—Graph showing the relation between apparent specific yield and duration of the seasonal recession period at access hole r2.

apparent values for hole r2 in figure 4 are extrapolated to account for delayed gravity drainage. The water-level declines for both the 3.5-day aquifer test and the seasonal 160-day recession period were of about the same magnitude (1.3 and 1.8 feet, respectively) and both declines occurred between 12 and 14 feet below the land surface.

Determinations of S_y from a seasonal change in soil-moisture content may give erroneous results if plant activity or subsurface temperature fluctuations cause a redistribution of moisture in the unsaturated zone during the season. The effects of plant activity are not a factor in this analysis as no vegetation exists within several hundred feet of the test site. The effects of subsurface temperature fluctuations on the seasonal determination of S_y at hole r2 are unknown, but are probably negligible as indicated in figure 2 by the agreement in the April and September moisture profiles above the water-level zone.

CONCLUSIONS

Estimates of specific yield obtained from a typical short-term aquifer test are generally low because complete gravity drainage in the zone of water-level change is seldom achieved during the test. A more reliable estimate of the true specific yield may be obtained by graphical extrapolation of the relation of apparent specific yield versus time. Extrapolation of apparent specific-yield values determined from changes in soil-moisture content at nine access holes during a 3.5-day aquifer test suggests that the average apparent specific yield of 0.11 should be increased to a value between 0.13 and 0.15.

The specific-yield values determined from the time-drawdown analysis are not considered reliable because of the large standard deviation of the values and the subjectivity associated with the method of analysis. The substantially smaller deviation of the apparent specific-yield values obtained from the moisture-content analysis suggests that this method may provide a more reliable estimate of the true specific yield when the apparent values are extrapolated to account for delayed gravity drainage.

A specific yield in the range 0.13 to 0.15 is considered representative of the storage capacity at depths ranging from about 10 to 15 feet below the land surface and may be applied when estimating water-level changes caused by pumping from this depth zone.

Estimates of specific yield in the zone of natural seasonal water-level fluctuations are possible from an evaluation of the soil-moisture change in the spring and summer recession period. In order to obtain reliable estimates, however, the moisture content in the water-level zone must be stable at the beginning and at the end of the recession period, and the redistribution of moisture in the zone due to subsurface temperature fluctuations and plant activity must be minimal during the period.

REFERENCES CITED

Boulton, N. S., 1963, Analysis of data from non-equilibrium pumping tests allowing for delayed yield from storage: Inst. Civil Engineers Proc. v. 26, p. 469–482.

Culler, R. C., and others, 1970, Objectives, methods, and environment–Gila River Phreatophyte Project, Graham County, Arizona: U.S. Geol. Survey Prof. Paper 655-A, 25 p.

Ferris, J. G., Knowles, D. B., Brown, R. H., and Stallman, R. W., 1962, Theory of aquifer tests: U.S. Geol. Survey Water-Supply Paper 1536-E, p. 69–174.

Hanson, R. L., 1972, Subsurface hydraulics in the area of the Gila River Phreatophyte Project, Graham County, Arizona: U.S. Geol. Survey Prof. Paper 655-F, 27 p.

Jacob, C. E., 1963, Determining the permeability of water-table aquifers, *in* Bentall, Ray, compiler, Methods of determining permeability, transmissibility, and drawdown: U.S. Geol. Survey Water-Supply Paper 1536-I, p. 243–341.

Jones, O. R., and Schneider, A. D., 1969, Determining specific yield of the Ogallala aquifer by the neutron method: Water Resources Research, v. 5, no. 6, p. 1267–1272.

Lohman, S. W., and others, 1972, Definitions of selected ground-water terms–Revisions and conceptual refinements: U.S. Geol. Survey Water-Supply Paper 1988, 21 p.

Meinzer, O. E., 1923, Outline of ground-water hydrology, with definitions: U.S. Geol. Survey Water-Supply Paper 494, 71 p.

Meyer, W. R., 1962, Use of a neutron moisture probe to determine the storage coefficient of an unconfined aquifer: Art. 235 *in* U.S. Geol. Survey Prof. Paper 450-E, p. E174–E176.

Prill, R. C., Johnson, A. I., and Morris, D. A., 1965, Specific yield–Laboratory experiments showing the effect of time on column drainage: U.S. Geol. Survey Water-Supply Paper 1662-B, 55 p.

Stallman, R. W., 1967, Flow in the zone of aeration, *in* Chow, Van Te, ed., Advances in hydroscience: New York, Academic Press, v. 4, 428 p.

Weist, W. G., Jr., 1971, Geology and the ground-water system in the Gila River Phreatophyte Project area, Graham County, Arizona: U.S. Geol. Survey Prof. Paper 655-D, 22 p.

RECENT PUBLICATIONS OF THE U.S. GEOLOGICAL SURVEY

(Books may be ordered from the Superintendent of Documents, Government Printing Office, Washington, D.C., 20402, to whom remittances should be sent by check or money order. Give title, series No., stock No. (shown in parentheses in this list), and catalog No. [shown in brackets])

Professional Papers

420-C. Geology and oil resources of the western Puente Hills area, southern California, by R. F. Yerkes. 1972 (1973). p. C1–C63; plates in pocket. $3.10. (2401-2100) [I 19:16:420-C]

585-C. Ground-water hydrology of prairie potholes in North Dakota, by C. E. Sloan. 1972 (1973). p. C1–C28; plate in pocket. 70c. (2401-2157) [I 19:16:585-C]

645. Stratigraphy and ammonite fauna of the Graneros Shale and Greenhorn Limestone near Pueblo, Colo., by W. A. Cobban and G. R. Scott. 1972 (1973). 108 p.; 39 plates showing fossils; plates in pocket. $4.25. (2401-00257) [I 19:16:645]

655-G. Channel changes of the Gila River in Safford Valley, Ariz., 1846–1970, by D. E. Burkham. 1972 (1973). p. G1–G24; plates in pocket. $2. (2401-2065) [I 19:16:655-G]

726-C. Gravity and magnetic features as related to geology in the Leadville 30-minute quadrangle, Colorado, by Ogden Tweto and J. E. Case. 1972 (1973). p. C1–C31; plates in pocket. $1.75. (2401-2145) [I 19:16:726-C]

734-B. Sedimentary petrology and paleocurrents of the Harebell Formation, Pinyon Conglomerate, and associated coarse clastic deposits, northwestern Wyoming, by D. A. Lindsey. 1972 (1973). p. B1–B68. $1.50. (2401-00249) [I 19:16:734-B]

747. Pennsylvanian carbonates, paleoecology, and rugose colonial corals, north flank, eastern Brooks Range, arctic Alaska, by A. K. Armstrong. 1972 (1973). 21 p.; 8 plates showing fossils. $1. (2401-2150) [I 19:16:747]

771. Chemical composition of sedimentary rocks in Alaska, Idaho, Oregon, and Washington, compiled by T. P. Hill and M. A. Werner. 1972 (1973). 319 p. $4.50. (2401-00254) [I 19:16:771]

787. The Borrego Mountain earthquake of April 9, 1968. 1972 (1973). 207 p.; plates in pocket. $6.25. (2401-00218) [I 19:16:787]

790. Stratigraphy, morphology, and paleoecology of a fossil peccary herd from western Kentucky, by W. I. Finch, F. C. Whitmore, Jr., and J. D. Sims. 1972 (1973). 25 p. 70c. (2401-00248) [I 19:16:790]

800-A. Geological Survey Research 1972, Chapter A. 1972 (1973). p. A1–A320. $3.45. (2401-00278) [I 19:16:800-A]

817. Summary petroleum and selected mineral statistics for 120 countries, including offshore areas, by J. P. Albers, M. D. Carter, A. L. Clark, A. B. Coury, and S. P. Schweinfurth. 1973. 149 p. $2.10. (2401-00279) [I 19:16:817]

Bulletins

1314-G. Cadmium in plants, by H. T. Shacklette. 1972 (1973). p. G1–G28. 40c. (2401-00251) [I 19:3:1314-G]

1331-D. Stratigraphy of the Glenns Ferry Formation from Hammett to Hagerman, Idaho, by H. E. Malde. 1972 (1973). p. D1–D19; plates in pocket. $1.25. (2401-02206) [I 19:3:1331-D]

1348. Placer gold deposits of New Mexico, by M. G. Johnson. 1972 (1973). 46 p.; plate in pocket. $1.25. (2401-2162) [I 19:3:1348]

1356. Placer gold deposits of Nevada, by M. G. Johnson. 1973. 118 p.; plate in pocket. $2. (2401-02211) [I 19:3:1356]

1359. Geology and mineral resources of the northern part of the North Cascades National Park, Wash., by M. H. Staatz, R. W. Tabor, P. L. Weis, J. F. Robertson, R. M. Van Noy, and E. C. Pattee. 1972 (1973). 132 p.; plates in pocket. $2. (2401-2135) [I 19:3:1359]

1362. Neogene marine mollusks of the Pacific coast of North America: An annotated bibliography, 1797–1969, by W. O. Addicott. 1973. 201 p. $1.50. (2401-2164) [I 19:3:1362]

1372-C. Strodes Creek Member (Upper Ordovician)—A new map unit in the Lexington Limestone of north-central Kentucky, by D. F. B. Black and N. P. Cuppels. 1973. p. C1–C16. 30c. (2401-00290) [I 19:3:1372-C]

1372-F. The upper Paleozoic Madera Group in the Manzano Mountains, N. Mex., by D. A. Myers. 1973. p. F1–F13. 25c. (2401-00287) [I 19:3:1372-F]

Water-Supply Papers

1757-M. Significance of ground-water chemistry in performance of North Sahara tube wells in Algeria and Tunisia, by F. E. Clarke and B. F. Jones. 1972 (1973). p. M1–M39. 55c. (2401-00256) [I 19:13:1757-M]

1940. Effects of coal mining on the water resources of the Tradewater River basin, Kentucky, by H. F. Grubb and P. D. Ryder. 1972 (1973). 83 p.; plates in pocket. $2.10. (2401-2158) [I 19:13:1940]

1970-B. Summary of floods in the United States during 1968, by J. O. Rostvedt and others. 1972 (1973). p. B1–B73. 60c. (Includes title page and contents for volume, Floods of 1968 in the United States.) (2401-2171) [I 19:13:1970-B]

2099. Quality of surface waters of the United States, 1968–Part 11, Pacific slope basins in California. 1972 (1973). 359 p. $2.75. (2401-00268) [I 19:13:2099]

2119. Surface water supply of the United States, 1966-70–Part 6, Missouri River basin–Volume 4, Missouri River basin below Nebraska City, Nebr. 1972 (1973). 901 p. $5.75. (2401-00267) [I 19:13:2119]